Organic Electronic and Optoelectronic Devices Based on Diphenylamine End-group Polymers

by

Yunfeng Li

A dissertation submitted to the Graduate Faculty of
Auburn University
in partial fulfillment of the
requirements for the Degree of
Doctor of Philosophy

Auburn, Alabama
December 13, 2010

Key Words: Electrochemistry, Modified Electrodes, *p-n* Heterojunction, Organic Diodes, Organic Photovoltaic Cells, Conducting Polymers, High Performance Fiber Metallization

Approved by

Vince Cammarata, Chair, Associate Professor of Chemistry and Biochemistry
Curtis Shannon, Professor of Chemistry and Biochemistry
Rik Blumenthal, Associate Professor of Chemistry and Biochemistry
German Mills, Associate Professor of Chemistry and Biochemistry
Chin-Che Tin, Professor of Physics

Abstract

This work mainly focuses on making a series of organic diodes and photovoltaic devices based on electroconducting polymers with diphenylamine end-groups for their monomers. Most of them are with structural motif of R-X-R. Bilayer electrochemistry and spectroelectrochemistry results show the electron blocking and electron trapping in these bilayers. Solid-state electronic devices were fabricated with oxidatively electropolymerizing polymeric bilayers on gold covered or transparent electroconductive ITO (Indium Tin Oxide) glass slides, followed by Ga/In eutectic liquid droplet, soft contacts by gold leaf, or thermal evaporation of Ag to make an electrical contact. The final part of this work also investigated the surface metallization of high performance commercial fibers, as well as its effect on fiber mechanical properties.

Modified electrodes with current rectification were assembled and investigated by electrochemical methods. The modification materials include poly(FD), a naturally monopolar material (p-type) and poly(DNTD), poly(DPTD), poly(Cl_4DPTD), bipolar organic materials. All these materials are easily grown on each other from their monomer solutions. When one of these bipolar materials was grown on poly(FD) modified Au electrode, the out-layer will be electrochemically isolated from poly(FD) and bilayers show different current responses in positive and negative potentials. *p-n* junction semiconductors with these structures are also characterized and analysized by current-voltage responses and Shockley diode equation. Changing the assembly order of bilayer will switch the device bias direction.

Spectroelectrochemistry experiments on these bilayers were performed in a home-made electrochemical cell coupled with a UV-Vis. spectrometer. The purpose is to understand the

electron transfer behavior in different bilayers. The electron blocking was verified by applying different potentials to these bilayers with poly(FD) as inner, which poly(FD) is directly grown on ITO. Electron trapping behavior was charaterized in those bipolar materials with different reduction potentials.

Four different electropolymerizable monomers with perylene diimide core and their solid state polymers were investigated by different spectral methods. *P-n* heterojunction organic photovoltaic cells were fabricated followed by the thermal evaporation of CuPc and Ag back electrode. Results show that the chlorination of perylene bay area could improve the ability of electron conduction and a device with this compound gave better performance than the others. Gold nanoparticles were incorperated between *p-n* junction to improve the photovoltaic performance since metallic nanoparticles transfer absorbed incident light to enhance plasmonic resonance at the interface of metal and organic dielectric materials.

Acknowledgments

This work would not have been possible without the support of many people. First and foremost, I would like to thank my advisor, Dr. Vince Cammarata, for his intellectual supervision and endless patience throughout my graduate studies. Also, I am very thankful to my committee members: Dr. Curtis Shannon, Dr. Rik Blumenthal, and Dr. German Mills and outside reader Dr. Chin-Che Tin for their comments, suggestions and the guidance they provided me.

I am very grateful to Drs. Chin-Che Tin, Minseo Park, Ayayi Claude Ahyi in Physics Department and Dr. David Stanbury, Dr. Wei Zhan, Mr. Thomas Carrington, as well as Dr. Michael Miller in Biological Sciences for their help, convenience and discussion for my work.

Appreciation also goes to my collaborator, Mr. Brian Little and former lab members: Drs. Lin Wang, Jie Liang, Ms. Qingqing Wang and Mr. Ning Hao. All of my work is based on their research achievements. I have greatly benefited from their results.

My thanks extend to Mses. Carol Nixon, Lynn Walker, Kiley Coan, and Bebe MacDougall for their administrative help and support. I would also like to express my gratitude to all my friends and colleagues in Auburn for their encouragement and invaluable scientific discussions and other supports, as well as Chemistry and Biochemistry Department for the support.

Finally, my special thanks go to my family. I am deeply and forever indebted to my parents for their everlasting love, support and encouragement, for giving of themselves beyond the call of duty. Especially, I want to thank my father for his unconditional love. I would like to dedicate this work to my beloved family.

Table of Contents

List of Tables

List of Schemes

List of Figures

CHAPTER 1

INTRODUCTION AND BACKGROUND

1.1 INTRODUCTION OF CONDUCTING POLYMERS

Materials for electronic devices at the beginning of the 21st century are still dominated by traditional inorganic semiconductors, metals and ceramics.[1] However, in the last 20 years, and especially the last decade, enormous efforts have been dedicated to use of organic materials that can process electric charges or photons. Organic molecules such as polymers, proteins and pigments are being considered as alternatives for carrying out the same functions that are performed by inorganic materials. Polymers have been used extensively as passive components in electronic devices since the early 1950s,[2-5] due to their light weight, flexibility, corrosion resistance, high chemical inertness, electrical insulation and ease of processing. This century will undoubtedly see the use of polymers from passive to active materials with useful optical, electronic and mechanical properties.[6,7] Indeed, this development has already begun with the discovery and systemic studies of conducting polymers.

Among those polymers, conducting polymers (also conjugated polymers, CPs) are considered highly promising for organic electronic devices and emerge as one of the most important materials.[8-10] Conducting polymers are the polymers with spatially extended π-conjugated systems that have delocalized *p*-orbitals in the backbone, through which electrons

can move from one end of a molecule to the other. An important breakthrough of conducting polymers can be dated back to 1977,[11] when Heeger, MacDiarmid and Shirakawa showed that polyacetylene, which is the simplest polyconjugated system, can be rendered conductive by the reaction with bromine or iodine vapors. After this discovery, systematic research has been focused on this area. Following the research on polyacetlene (PA), many other polymers such as polypyrrole (PPy), polythiophene (PT), polyaniline (PANI) and poly(p-phenylene) (PPP) as well as their derivatives have been reported as π-conjugated conducting polymers. Figure 1-1 shows some important types of conducting polymers. Many monographs and reviews of the knowledge accumulated regarding the development of conducting polymers, polymer film electrodes and their application have been published. Those include surveys of polymer synthesis with specific groups,[12,13] methods of characterization[14-16] and areas of application.[17,18]

Conducting polymers can be prepared by using chemical and/or electrochemical techniques, which was described and reviewed by many monographs and references.[12,13,19-23] The principal advantage of chemical synthesis is that it offers the possibility of mass production at low cost. On the other hand, electrochemical methods offer materials with better conducting properties in a form of thin film for some designated applications such as polymer film electrode, thin-layer sensor, micro-technology. Electrochemical techniques are especially well-suited for the controlled synthesis of conducting polymers and for the tuning of a well-defined oxidation state. Also, electrochemical polymerization can be simply carried out in a single compartment cell by adopting a standard three-electrode (working, counter and reference) setup that is immersed in an electrochemical solution.

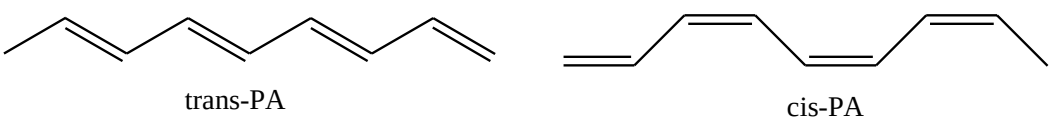

Polyacetylene, PA

Polyparaphenylene, PPP

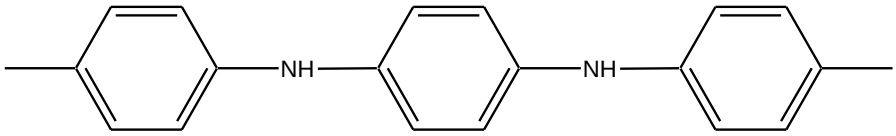

Polyaniline, PANI

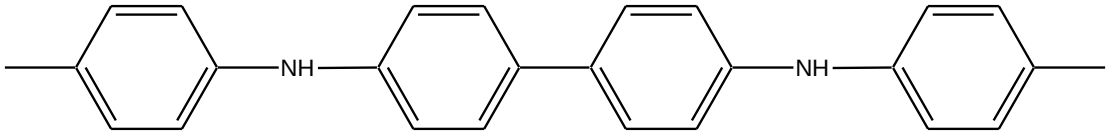

Diphenylamine, DPA

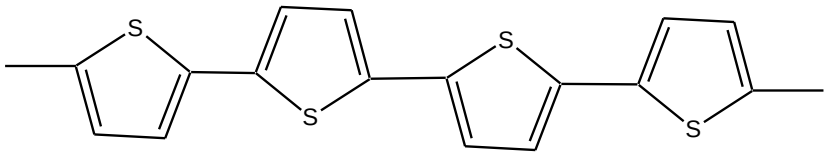

Polythiophene, PT

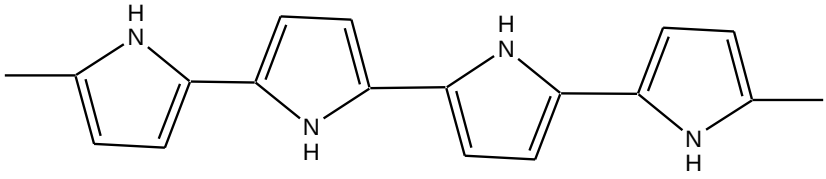

Polypyrrole, PPy

Figure 1-1. Well-known conducting polymers

Conducting polymers have been studied by using the whole arsenal of analytical methods available to chemists. Electrical properties and their controllability by a doping/dedoping process of π-conjugated polymers have been one of the most important issues. For this reason, electrochemical techniques emerged first as a major tool for studying CPs and their electrical, as well as electrochemical properties. Electrochemical techniques include dynamic methods such as cyclic voltammetry (CV), chronoamperometry (CA) and chronocoulometry (CC), and other than playing a significant role in the preparation and deposition of polymers, are also the primary tools to characterize those materials as well as to investigate the kinetics of their charge transport processes.[24] Meanwhile, the combination of electrochemical methods with others analytical tools, especially with spectroscopy such as ultraviolet-visible (UV-Vis), Fourier transform infrared (FTIR), electron spin resonance (ESR), Raman, electrochemical quartz crystal microbalance (EQCM) ,[15,25,26] various microscopies (STM, AFM, SECM), and radiotracer methods, probe beam deflection (PBD) have also enhanced our understanding of the nature of charge transport and transfer processes, surface structure and structure properties. Electrochemical impedance spectroscopy (EIS) has become the most powerful technique used to obtain kinetic parameters such as the rate of charge transfer, diffusion coefficients and double layer capacitance in polymeric electronic devices.[27]

The most interesting property of conducting polymers is their semiconducting properties; some materials exhibit high conductivity and behave almost metallic properties after chemical/ electrochemical modifications. This property can be changed by simple doping, oxidatively or reductively, and also by bringing the material into contact with different compounds. The

chemical, optical, electrical, mechanical properties in CPs can be changed through redox processes combined with the intercalation of anions or cations. To date, CPs had been reported in current rectifier with modified electrodes, chemical and biosensors, field-effect transistors, corrosion protection and control, electrochromic devices, charge-storage devices, light emitting diodes (LEDs), p-n organic diodes and photovoltaic cells (PVs).[28] There has been an increased interest towards the possible applications of conducting polymers as the active elements in electronics. Semiconducting polymers such as PA, PPy, PANI and PPV have been used for the fabrication of Schottky barrier diodes and/or p-n junction diodes.[29-33] Poly(2-methoxy-5-(2'-ethyl-hexyloxy)-1,4-phenylene vinylene) (MEH-PPV)[34] and Poly(3-alkylthiophene)s (P3ATs)[35,36] are widely used as donors in polymeric solar cells.

In this work, we mainly focus on the fabrication of organic diodes and solar cells based on conducting polymers which were electropolymerized by a solution process. All of these monomers contain diphenylamine end groups. From this point of view, the following parts in this chapter will mainly discuss the current research trends about conducting polymers on modified electrodes for current rectification, organic diodes and photovoltaic cells.

1.2 CURRENT RECTIFICATION ON POLYMER MODIFIED ELECTRODES AND ORGANIC DIODES

One basic function of a molecular electronic device is current rectification. A current rectifier is a simple electronic device which allows charge flow in one direction. Since Aviram and Ratner proposed a molecular rectifier based on an asymmetric molecular tunneling junction

in 1974,[37] many small molecule- and/or polymer-based rectifying devices have been reported using advanced design tools in modern molecular electronics, these tools include electropolymerization,[38-40] Langmuir- Blodgett (L-B) films,[41,42] and self-assembly monolayer (SAMs) techniques.[43,44]

In the early 1980s, Murray and co-workers[38-40,45-50] were the first to propose electrochemical rectifiers by modifying electrode surface with a electroactive polymeric bilayer of Ru, Fe and Os complex derivatives, such as poly($(bpy)_2Os(vpy)_2$) and poly-$Ru(VB)_3$ ion complex, where bpy = 2,2-bipyridine, vpy = 4-vinylpyridine and VB = 4-methyl-4'-vinyl-2,2'-bipyridine. These bilayer electrodes, specifically called "double redox couple systems", were made of two discrete, sequentially deposited films of two different redox polymers on electrodes. They demonstrated that oxidation of redox moieties present in the outer polymer layer was constrained to occur via electron transfer mediation through the inner layer due to a different electron energy level which is decided by formal potential, $E^{0'}$ of polymers. In such an arrangement, electron transfer through the bilayer polymer film was found to be unidirectional, acting similar to a diode device in solid state electronics. Wrighton and coworkers reported many types of conjugated polymer-based microelectrode diode and transistor-like devices.[51-56] These molecular microstructure devices were applied in molecular-based diodes, microsensor arrays, microelectrochemical transistors. Polymer materials here included poly(*N*-methyl pyrrole)[51] and polypyrrole,[52] polyaniline,[55] poly(3-methyl-thiopene) ,[56] poly(vinylferrocene), $PVFc^{+/0}$ and N-N'-didibenzyl-4-4'- Bipyridinium ($BPQ^{2+/+}$).[53] Electrochemical devices showing pH-dependent rectifying behavior have also been demonstrated

by Wrighton and coworkers[57-62], this example of polymer-based electrochemical rectifier involved redox polymers containing quinone and viologen subunits, which demonstrated the principle of pH-dependent electrochemical rectification and charge-trapping phenomena.

Microscale rectifers and molecular devices with layers of redox polymer films or deposition of single component film onto electrodes have also been reported. The electrochemical responses of metal tris(bipyridyl) complexes, $M(bpy)_3^{2+}$ and a metallocene cation, or metalloporphyrins and viologens at zeolite as modified electrodes showed that molecular-level microstrutures organized by zeolites conveyed electrons unidirectionally.[63,64] Moreover, a polymer based bilayer composed of inner layer with Methylene Blue (MB) redox species covered with very thin insulating poly(OPD) (poly(*Ortho*-phenylene diamine)) film and outer layered with ferrocene trapped in Nafion® film also shows electrochemical rectification characteristics.[65] Unidirectional current flow is exhibited in the same structure with ferrocene monocarboxylic acid and poly(acrylic acid) (PAA) system,[66,67] Prussian blue and poly[4,4'-bis-(butylsulphanyl)-2,2'-bithiophene] system.[68] Recently, a new strategy for constructing a monolayer modified electrode with n-alkanethiol self-assembly modification also showed electrochemical rectification, those monolayer materials include, ferrocene carboxamide,[69] redox-active ferrocene-functionalized poly(propylene imine) dendrimers[44], and thiophenol and thioctic acid system,[67,70] even using only branched short alkanethiol.[43] Further development of these systems has also been extended to microstructures, such as a unimolecular rectifier of amphiphilic molecules.[42,71-75] The materials of molecular devices also extended to biomolecules. For example, biorectifiers of nano-dimensions with metalloproteins on Au electrodes were

reported[76] and a pH-dependent electrochemical rectification was displayed by a protein ion channel reconstituted in a planar phospholipid membrane controlled by electrostatic interactions between channel ionizable residues and permeating ions.[77]

Based on unidirectional current flow working principle and some aforementioned microscale current rectifiers on electrodes, macroscopic p-n diodes based on conducting polymers were designed. Macroscale organic rectifying devices were reported earlier than microscale current rectifying electrodes, when Meinhard reported a solid state p-n junction in 1964 with chloranil/*p*-phenylenediamine (p-type) and phenazine (n-type) prepared by vacuum deposition.[78] Due to the bipolar nature of conducting polymers, mixed non-doped conductor polymeric materials are rarely used for rectifying devices. Most of these devices are fabricated by doping with cations or anions in the fabrication procedure. With the discovery of highly conductive p-type and n-type doping of poly(acetylene), building p-n junction with these PAs has been a target. Limitations in the doping chemistry of PA have resulted in few examples of p-n junctions based on these materials. In these limited studies, chemical doping and mechanical press contacting,[29] photochemical doping[79] and ion implantation,[80-82] internal ion compensation[83] have been explored. However, the air and moisture sensitivity of doped poly(acetylene) based devices, as well as their low rectification ratio tempered their practical applications.

Electrochemical polymerization provides another way to fabricate air and humidity stable p-n junction diodes. Koezuka et al.[32] reported the first organic heterojunction by utilizing two conducting polymers: poly(acetylene) and poly(*N*-methyl pyrrole) (PNP). It was found that its characteristics were shown to be strongly dependent on the oxidation state of PNP. A Pt|PPy

(anion-doped)|PT (cation-doped) |In p-n junction diode was electrochemically fabricated by Aizawa and Shirakawa, followed by controlled-potential electrochemical doping to make the PPy layer anion-doped and the PT layer cation-doped.[84] They built this device by making a dense microstructure in an the outer PT film to prevent anion dedoping of the inner PPy layer. Uehara, et al.[85] studied the electron transfer between poly(3-methylthiophene) and 5,10-dihydrophenazine derivatives in a series of bilayer devices Au|P3MT|dihydrophenazines|Al. The rectification ratio from +2.0V to -2.0V is 40-500 depending on different dihydrophenazine derivatives. These devices did not only show current rectification in the dark but also showed photovoltaic effects under illumination. Zener-type p-n junction diodes were also fabricated by Kudo, et al.[86] The p-n junction diodes consisting of a p-type phthalocyanine (Pc) sublimed film and a n-type perylene derivative (N, N'- 4-hydroxyphenyl- 3,4,9,10-perylene-tetracarboxylic-diimide, hph-PTC) electrodeposited film doped with metal ions exhibited Zener-type breakdown and photocurrent enhancement. The rectification and photocurrent enhancement were also observed in the electro-codeposited film consisting of phthlocyanine- and perylene-derivatives.[87] Moreover, the p-n homojunction has been also investigated. Srivastava, et al.[88] reported the formation of such a junction on a single PANI film which is chemically cation-doped on one side and anion-doped on the other side by ion implantation and Yamashita et al.[79] produced similar structures in P3MT film by chemically cation-doping and photosensitized anion-doping on the film.

Overall, modified-electrode current rectifiers and p-n junction organic diodes were widely researched at the micro- and macro-scales. The explored materials include doped or undoped

conducting polymers PA, PANI, PPy, PT and redox metallopolymers. With UV-Vis excitation for most of those materials, many of these devices, in which those active organic layers were sandwiched between two metal electrodes or ITO coated glass slides, also showed photovoltaic effects. This leads those semiconductor organic molecules and CPs to another application, which is to fabricate organic solar cells. In next part, the research of organic solar cells will be reviewed.

1.3 ORGANIC PHOTOVOLTAIC CELLS (OPVs)

Currently, close to 85% of the energy supply worldwide is based on fossil fuels like coal, oil and natural gas, which are not renewable sources.[89,90] The biggest problem with this energy structure is that the price of oil and gas will be skyrocketing, while reserves of fossil fuel are declining and energy demand is steadily increasing. Moreover, although it is still controversial, the estimated atmospheric carbon dioxide concentration in the next several decades will lie in the range of 540 to 970 ppm (part per million), which could result in the global climate warming by 1~6 ℃.[91-93] When searching for an alternative source of energy, the vast amount of energy the earth receives from the sun (1.75×10^{17} W) has drawn attention. With the total world energy usage in 2008 being 4.74×10^{20} J, less than one hour is need to fulfill this demand[89,90]. However, harnessing this source of energy in a cost-effective way is not easy. Several technologies can be employed. First of all, sunlight can be converted to thermal energy directly which can subsequently be used for hot water, heating or conversion into electrical energy.[94] Alternatively, sunlight can be directly converted to electrical energy using the photovoltaic effect. The current

situation is that, the field of photovoltaics (PV) is dominated by inorganic materials. Silicon based solar cells have a 90% market share due to the large material availability and extensive derived knowledge from the microelectronics industry.[95] The main drawback of this type of device is the high purity needed for proper device operation. The energy and also the costs needed in the fabrication process limits its usefulness as an alternative energy sources.

Organic photovoltaic cells (also organic solar cells, OPVs) are a relatively new route towards achieving flexible, large area, low cost electrical energy conversion devices. Organic materials can be solution-processable, allowing for low cost deposition techniques such as spin-coating, inkjet printing, electrochemical polymerization and roll to roll fabrication. Another advantage is there are numerous modifications that can tune the chemical and physical properties of these organic materials that will also allow great flexibility in design. The high absorption coefficient of organic materials allows organic solar cells to absorb most of the light in extremely thin (~100nm) layers, which significantly reduce material usage. There are multiple approaches which are all being actively pursued within the research area of organic solar cells, these various approaches can be roughly divided into 3 types: dye-sensitized, small molecular and polymer based heterojunction (HJ) devices.

The dye-sensitized solar cell (DSSC) was first introduced by O'Reagan and Grätzel in 1991 and consists of a nanoporous titanium oxide (TiO_2) layer.[96] The TiO_2 material is covered with a ruthenium dye which, after the absorption of light, injects an electron into the TiO_2 that can be collected at an electrode. An electrolyte regenerates the dye and is responsible for the hole transport to a counter electrode. The main disadvantage of DSSC is the use of the liquid

electrolyte, which causes stability problems,[97] although it currently has higher power conversion efficiency than the other two.

On the other hand, solid state OPVs based on a HJ between small molecules and polymeric materials have gained a broad interest today.[98] The concept of organic photovoltaic cell first appeared in the middle of 1970s and the first published result about OPV consisted of an organic dye monolayer sandwiched between two metal electrodes.[99,100] The performance of this kind of OPV cell is dependent on three main factors: material selection, material growth technique and device architecture. The materials that form a complete device are the transparent conducting electrode substrate, organic active layers and also a reflective metallic electrode. Materials of active organic layers are the most important part for improving cell performance. Both small molecular and polymeric OPVs are normally fabricated by thermal evaporation or spin-coating of a donor and acceptor material in either a double layer structure or a bulk-heterojunction (BHJ). Indium-tin- oxide (ITO) coated glass is the most commonly used transparent conducting electrodes and substrate in device fabrication. Since the first reports on such devices more than 30 years ago, their power conversion efficiencies (PCE, η_P) have increased considerably from 0.01% in 1974[99] to 1 % in 1986[101] and more recently to 6.5% in 2007,[102] the highest reported η_P so far for a single OPV is 6.77%[103] and it is still under improvement. Figure 1- 2 gives the timeline development of OPV with related publication papers per year and power efficiency improvement. As we can see, with much interest gained in recent years, the number of published papers is exportially increasing, and the power conversion efficiency, especially for polymeric solar cells, is improving steadily.

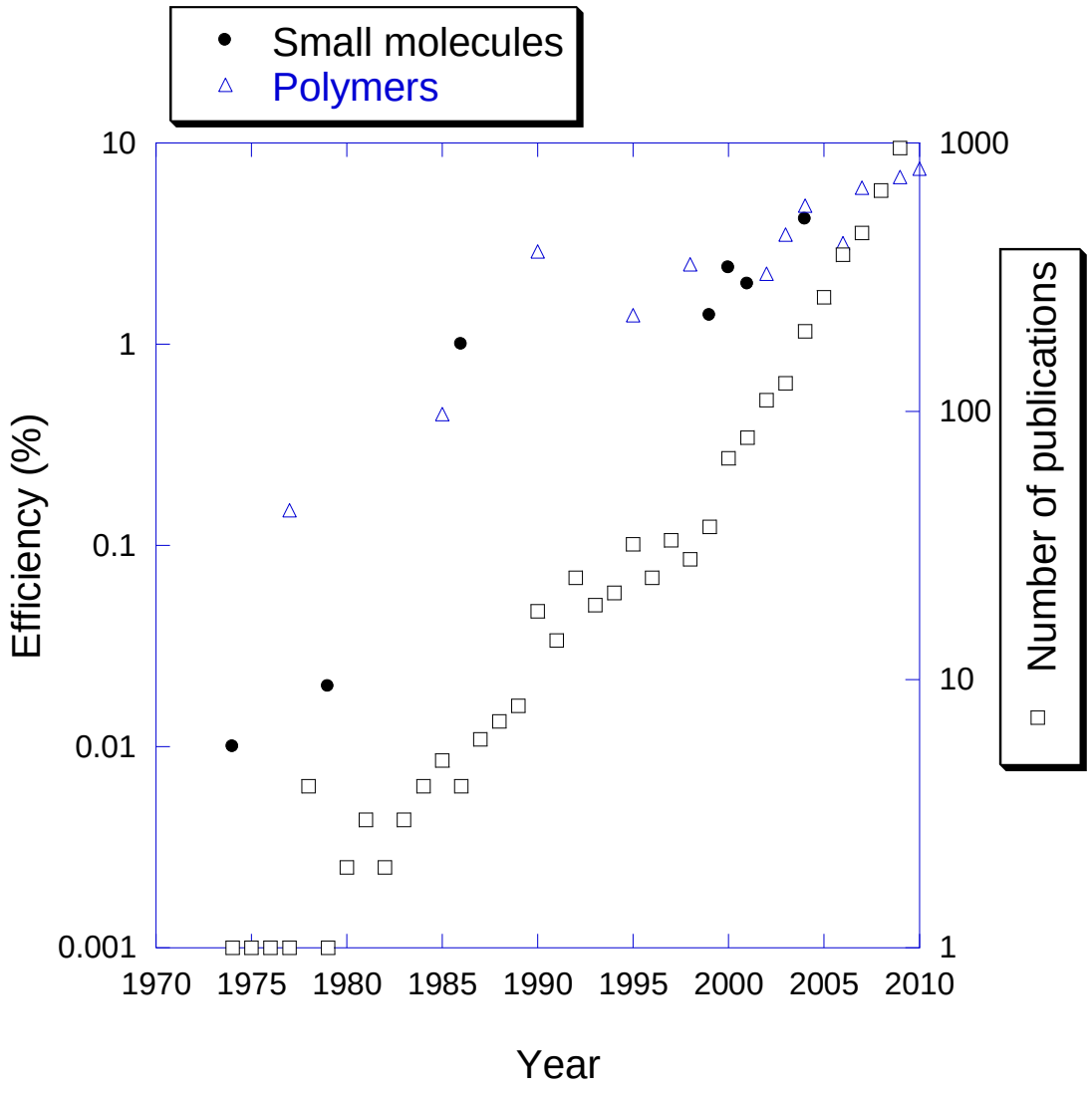

Figure 1-2. Timeline of small molecule and polymer based OPV development

1.3.1 Photovoltaic fundamentals and theory

Power generation by a PV cell is a process to convert solar energy into electricity. This section discusses how a PV cell works and how to calculate its power efficiency. The optical-to-electrical energy conversion process for a donor/acceptor OPV can be roughly considered as four steps:[104]

1) Light absorption and exciton generation with efficiency η_A; 2) exciton diffusion, where the fraction of excitons reaching the D/A interface is η_{ED}; 3) the charge-transfer reaction with efficiency η_{CT}; 4) collection of carriers at the electrodes with efficiency η_{CC}. The internal quantum efficiency η_{IQE} is the product of four efficiencies:

$$\eta_{IQE} = \eta_A \cdot \eta_{ED} \cdot \eta_{CT} \cdot \eta_{CC} \qquad (1\text{-}1)$$

The general way to characterize a PV cell is showing its current density curve (J-V) under illuminations and finding its incident photon-to-current conversion efficiency (IPCE) at a various irradiation light wavelengths.

Current density-voltage (*J*-*V*) characteristics for a typical PV cell in the dark and under incident illumination are shown in Figure 1-3. The figure also shows the short-circuit current density, J_{SC}, and open circuit voltage, V_{OC}, under illumination. The operating range of the solar cell is therefore $0 < V < V_{OC}$, where the device generates power. The fill factor (FF), which is defined as the ratio of the actual maximum obtainable power to the theoretical power, is calculated as

$$FF = \frac{J_m V_m}{J_{SC} V_{OC}} \qquad (1\text{-}2)$$

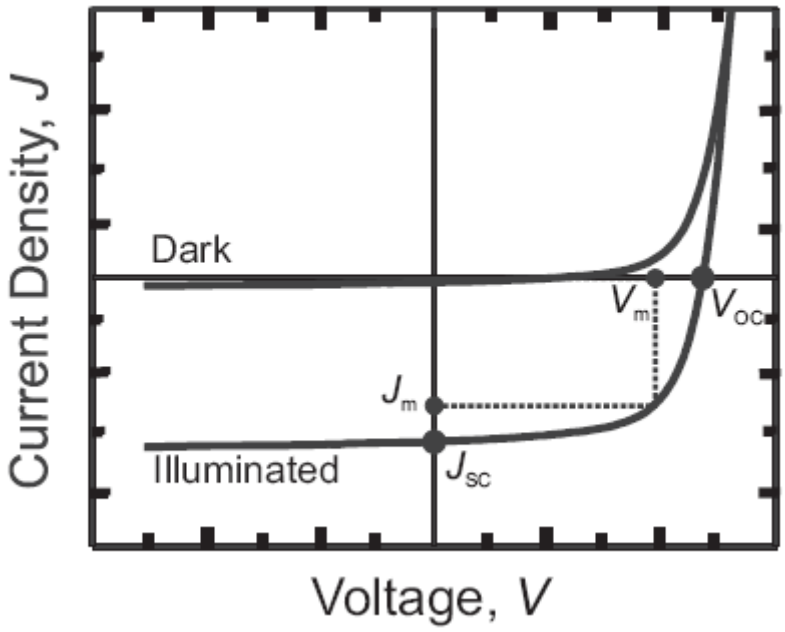

Figure 1-3. Typical current-voltage (J-V) curves of a solar cell in the dark and under illumination.

where the product $J_m V_m$ corresponds to the maximum power point. Then, the power conversion efficiency, η_P, is

$$\eta_P = \frac{J_m V_m}{P_0} = \frac{J_{SC} V_{OC}}{P_0} \times FF \qquad (1\text{-}3)$$

where P_0 is the incident light intensity. The incident photo-to-current efficiency (IPCE) at a particular wavelength can be obtained by the following expression:

$$(\text{IPCE})\% = \frac{1240(eV \bullet nm) \times J_{SC}(\frac{mA}{cm^2})}{\lambda(nm) \times \Phi(\frac{mW}{cm^2})} \times 100 \qquad (1\text{-}4)$$

where Φ is the monochromatic light intensity.

1.3.2 PDIs-based small molecular OPVs

Small molecular OPVs are normally fabricated by thermal evaporation or spin coating of a donor and acceptor small molecular materials in either a double layer or a bulk heterojunction structure. Currently, the donor materials mainly include metal phthalocyanines (MePc) and polyacenes, such as pentacene and tetracene. For acceptors, perylene compounds like 3,4,9,10-perylene tetracarboxylic bis-benzimidazole (PTCBI or PV) or other perylene diimides derivatives (PDIs) as well as fullerene (C_{60}) and its soluble derivatives, e.g. [6, 6]-phenyl-C_{61}-butyric acid methyl ester (PCBM), are commonly used, see Figure 1-4. Some new materials have been reported, such as HBC-PhC_{12} working as donor[105]. Both Fullerene family and PDIs have suitable LUMO and HOMO energies as n-type materials and relatively high electron mobility. Compared to fullerene, one advantage of PDIs is that, they have a very strong absorption between 400-600nm, which can improve the light-absorption efficiency when

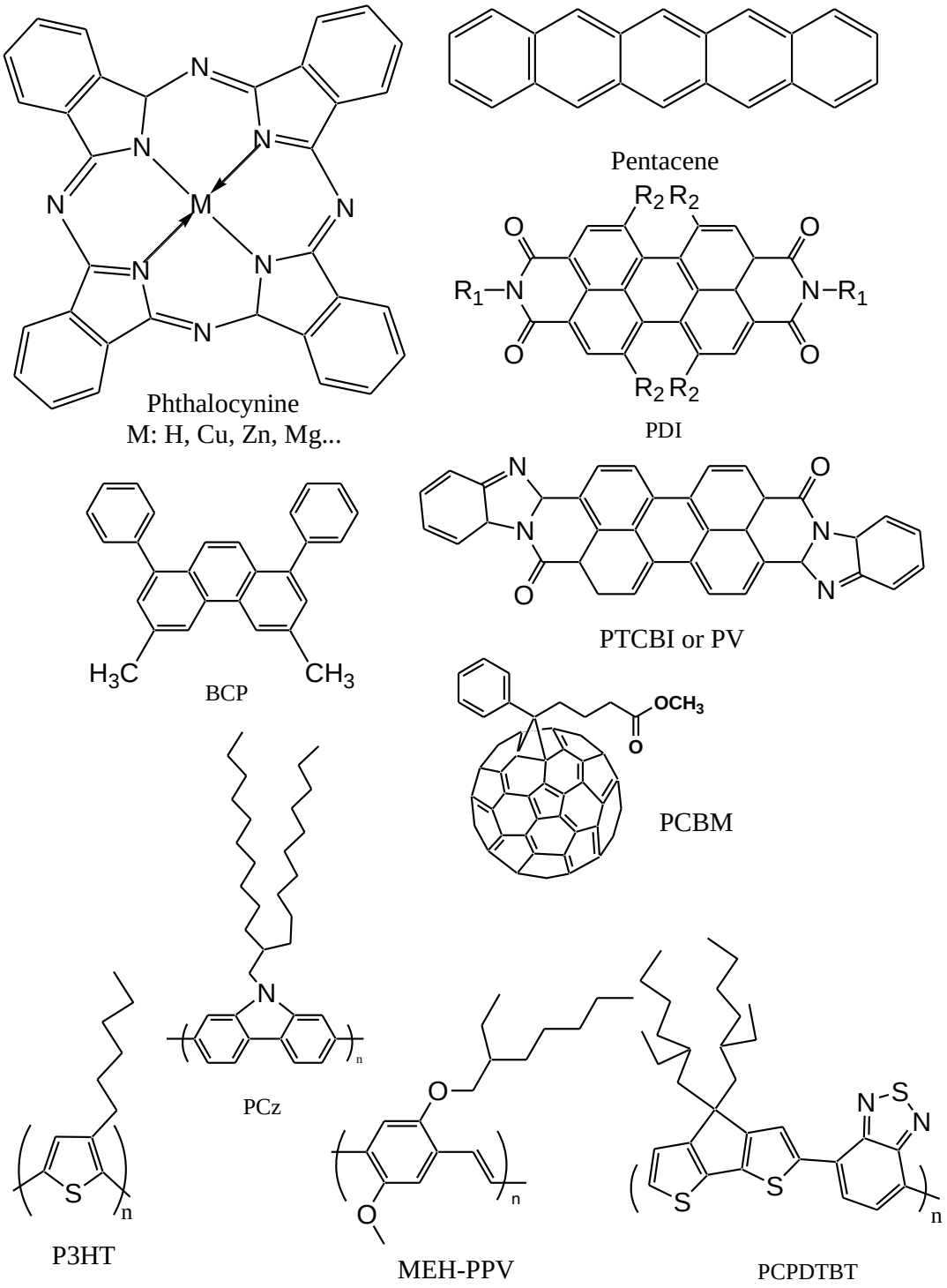

Figure 1-4. Materials for organic photovoltaic cells

used in a solar cell. The following chapters will focus on the perylene-core based materials and their devices, we mainly discuss these PDIs-based small molecule OPVs. More information about perylene can be found in Chapter 4.

As mentioned before, the first efforts to fabricate organic photovoltaic devices based on small molecules can date back to the middle of 1970s.[99,100,106,107] However, the efficiencies at that time did not reach more than 0.01%. The cell structure normally consisted of one single organic dye active layer sandwiched between two metal electrodes. Around 1980, Tang[108,109] patented the first p-n junction bilayer OPV with a 40 nm copper phthalocyanine (CuPc) layer and a 40 nm perylene derivative layer where the efficiency was at least about 0.1%. An early milestone in OPV design by Tang[101] in 1986 used CuPc as p-type material (electron donor) and PTCBI as n-type material (electron acceptor) in a simple p-n heterojunction (HJ) bilayer structure. A high power conversion efficiency of 0.95% was reported, with 0.45V as the open-circuit voltage and 65% fill factor, indicating excellent charge transport. After this, the p-n junction OPVs based on these two or related materials were widely investigated,[63,110-127] including PDI material modifications, solar cell structure design. But most of the efficiencies were still less than 1% and the V_{oc} was about 0.5 V, see Table 1-1.

The original Tang solar cell was improved by adding a bathocuproine (BCP) as an exciton-blocking layer (EBL) with similar *p-n* semiconductor materials,[128] a chemical with large optical energy gap to block electrons as well as holes and the efficiency reached to 2.4 ±0.3 %. The structure of incorporating BCP blocking layer was reported as ITO|CuPc(30nm)|-PTCBI(30nm)|BCP(10nm)|Ag. Another high efficiency (η=1.5%) was obtained by cosublimation

of CuPc and PTCBI leading to a blend structure followed by an annealing step,[129] in which the cell structure was changed from p-n HJ to p-n bulk-heterojunction (BHJ) with an improved interfacial area. Later in 2005, a novel deposition method called vapor phase deposition (VPE) helped to increase the efficiency for this system further since a highly intermixed donor-acceptor interface could be obtained. The interfacial area was increased by a factor of four as compared to a bilayer structure while still maintaining n-type and p-type percolating pathways, and a power conversion efficiency of 2.2% was reported.[130,131]

Like p-n structure OPVs, ones with inverted n-p structure composed of PDIs were investigated by many researchers and some of them were listed in Table 1-1. Tang showed that the reversed structure of ITO|CuPc|PTCBI|Au changes the photovoltage polarity and reduces the V_{oc} somewhat.[101] The Yokoyama group reported the same structure with similar *p-n* doped/undoped materials and they also assembled a tandem cell composed of two n-p inverted structure cells, which were separated by a very thin Au film.[110] Later they modified this *n-p* HJ into ITO|n|i|p|Au three layer (detailed structure as ITO|PTCBI|PTCBI:H_2Pc| H_2Pc|Au or ITO|DMP|DMP:H_2Pc| H_2Pc|Au), and cell efficiency was 0.63% with J_{sc}=2.14 mA/cm^2, V_{oc}=0.51 V and fill factor of 48%.[136] Here DMP is dimethyl PDI. Whitlock, et al.[132] showed for the cell structure ITO|DMP|ClAlPc|Ag a fill factor as high as 42%. Tsuzuki, et al.[119] also fabricated similar two types of n-p HJ devices as Hiramoto's but with a p type material of titanyl phthalocyanine. Breeze, et al.[133,137] compared the p-n and n-p structure with PTCBI and p-type polymer, M3EH-PPV, and showed that the n-p structure had higher cell performance (η_p=0.71%). Nakamura, et al.[134,138] investigated a series of n-p cells consisting of n-type perylene pigment

penetrated by p-type conjugated polymers (MEH-PPV, PPAV-HH-PPV and P3HT) and an Indium-modified ITO.

Table 1-1 Photovoltaic properties of p-n heterojunction solar cells based on perylene and phthalocyanine derivatives under illumination with 100 mW/cm^2 (1 SUN)

Structure	V_{OC} (V)	J_{SC} mA/cm^2	*FF*	η_P (%)	Reference
ITO|CuPc|PTCBI|Ag	0.45	2.3	0.65	0.95	[101]
ITO|Me-PTCDI|co-layer|CuPc|Au	0.51	2.14	0.48	0.63	[114]
ITO|PTCBI|CuPc|Au	0.53	1.61	0.42	0.43	[114]
ITO| Me-PTCDI|ClAlPc|Ag	0.23	0.35	0.42	---	[132]
ITO|CuPc|PTCDA|In	0.55	2.0	0.35	0.77	[110]
ITO|Me-PTCDI|H_2Pc|Au	0.44	2.87	0.56	0.76	[111]
ITO|PTCBI|Me-PTCDI|H_2Pc| Au	0.35	1.27	0.40	0.24	[117]
ITO|CuPc:PTCBI|Ag*	0.44	0.88	0.31	1.5	[129]
ITO|CuPc|PTCBI|BCP|Ag	0.48	4.2	0.55	2.4	[128]
ITO|PTCBI|M3EH-PPV| Au	0.56	1.96	0.63	0.71	[133]
ITO|In|PTCBI|P3AT|Au	0.42	4.4~6.5	0.38~0.56	1.0	[134]
ITO|In|PTCBI|MEH-PPv|PEDOT|Au	0.52~0.66	2.4~3.2	0.27~0.5	0.4~1.5	[135]
ITO|In|PTCBI|PPAV-HH-PPV|PEDOT|Au	0.5~0.64	2.5~6.5	0.3~0.5	0.3~1.9	[135]

*The illumination source is a 7.8 mW/cm^2 tungsten-halogen lamp.

1.3.3 Polymeric OPVs

Polymer photovoltaic cells are based on π conjugated conducting polymers as electron donors. Polythiophene and polyphenylenevinylene are two common p-type conducting polymers for OPV, such as poly(3-hexylthiophene) (P3HT)[139] and poly(2-methoxy-5- (2'-ethylhexoxy)-

1,4-phenylenevinylene) (MEH-PPV)[34], and polycarbazoles (PCz) have been reported as p-type material[140] but this material is much less commonly than P3HT. The n-type polymers have been investigated less. A fullerene derivative, PCBM, has been widely used in polymer/small molecules systems. Detailed studies by many groups in the past several years have identified P3HT as the most attractive polymer donor material. Power conversion efficiencies reached about 5% using P3HT/PCBM. After an exhaustive research, it appears that the P3HT/PCBM system is approaching its limits due to the absorption range limitation of the materials. Recently, polythiophenes with conjugated side chains exhibiting a broader response range to solar radiation have been synthesized. Liang and Yu et al.[141,142] synthesized new semiconductor polymers with alternating thieno [3,4-b]thiophene and benzodithiophene units which showed a cell η_P as high as 5.6%. The low band-gap benzo(1,2-b:4,5-b')dithiophene (BDT) based materials exhibited very promising properties for OPVs and the η_P value of a single BHJ cell was improved to 5.4% in 2008 and 6.77% was achieved in 2009, which is the highest literature reported power efficiency for a single OPV so far.

1.3.4 Tandem structures

Danziger et al[143,144] investigated the electrochemistry and photochemistry of bilayer and multilayer structures composed by PDI and metal phthalocyanine. They found that most of the photo-current was produced at the very narrow interface region. The transient photocurrent was directly proportional to the number of M-Pc/PTCDA interfaces, which was confirmed through the characterization of multilayer assemblies. This provided critical momentum for moving OPV research from single p-n junction to multiple hetero-junctions.

Cell performance was improved further by a stacked tandem type structure, especially to realize high open-circuit voltage. Another advantage is that tandem structures broaden the absorption spectra because it is not feasible to absorb the entire solar spectrum using a single D/A pair forming the OPV cell. Tandem structures can be formed by stacking semitransparent HJ components with an ultra thin metal layer in between as an internal floating electrode which acts as a charge recombination site. In 1990, Hiramoto et al.[111] reported a tandem type solar cell comprised of two stacked, series connected sub-cells based on evaporated small molecules where each cell was an organic p-n junction composed of 50 nm of metal free phtholocyanine (H_2Pc) and 70 nm of perylene tetracarboxylic acid derivatives. The V_{oc} of tandem cell was almost twice the one of single HJ cell. Xue et al.[145] described a high-efficiency CuPc/C_{60}, two-element tandem cell tuned to optimize efficiency in the blue and red spectral regions. It employed a silver nanoparticles charge recombination layer and a pair of double-HJ cell. The output voltage of the tandem cell is doubled compared to a single cell element in the stack and achieved a 5.7% at 1 Sun (AM 1.5 illumination) due to its increased thickness over a single planar-mixed element. Another breakthrough in solution-processed tandem cells was reported by Kim et al., demonstrating a high efficiency of 6.5%.[102] This tandem device was entirely solution-processed except for the top evaporated electrode. For the bottom BHJ cell a 130 nm thick layer of poly[2,6-(4,4-bis-(2-ethyl-hexyl)-4H- cyclopenta[2,1-b;3,4-b']- dithiophene)-alt-4,7-(2,1,3-benzo-thiadiazole)] (PCPDTBT):PCBM was cast from their chlorobenzene solution and the top cell was made of a blend of P3HT:$PC_{70}BM$ processed from chloroform with a thickness 170 nm. The absorption bands of PCPDTBT and P3HT complemented each other and these two

materials cover the spectral region from 400 to near 900 nm.

1.4 SUMMARY

Conducting polymers combine mechanical properties of plastics with high electron conductivity. Due to the high processability, their chemical and physical properties can be fine-tuned by organic synthesis and electrochemical synthesis. The number of papers dedicated to topics related to CPs is large, including CP synthesis, analysis and application. CPs possess a variety of properties related to their electrochemical behavior, therefore electrochemistry and its coupling methods are the main tools to explore CP. It has been known for more than 30 years that conducting polymers may be used for electrode modification, for current rectification and polymeric electronic diodes. Their most recent applications include organic light emitting diodes and organic polymer solar cell. So far, in the field of organic solar cells, a vast variation in designs which combines materials selection and cell architecture, as well as fabrication methods have been considered, from small molecule evaporated materials to fully solution-processed polymer approaches.

1.5 BACKGROUNDS AND AIM OF THIS WORK

One of our group's research interests is to synthesize and characterize new conducting polymer materials and apply these polymer materials in electrochromic and electronic devices. Over the years, a series of monomers with a structural motif R-X-R have been synthesized in our lab, see Figure 1-5. Here R is the diphenylamine (DPA) endgroup and X is an electroactive functional unit. Polymeric films on electrode surfaces can be obtained by electrochemical

oxidative polymerization of monomers resulting in an alternating polymer of diphenylbenzidine (two para- linked diphenylamine groups) and the X unit. Generally, these conductive polymers contain conjugated *4n+2* Hückel aromatic rings. The big aromatic systems make it possible for the polymer films to have unusual electrical and optical properties. Depending on the X units they are promising materials for electrochromic applications, organic diodes and materials for organic photovoltaic cells. These polymer single thin films deposited on metal electrodes or indium tin oxide (ITO) have been investigated and characterized by cyclic voltammetry, Langmuir-Schaefer techniques, grazing angle FTIR, UV-Vis. spectroelectrochemistry and electrochemical quartz crystal microbalance (EQCM). Most of them are also promising as electrochromic materials and have been systematically investigated in our lab.

Among these monomers, the one with X= naphthalene diimide group (**DNTD**, full name is N,N'- Di[p-phenylamino(phenyl)]-1,4,5,8-naphthalene tetracarboxylic diimide) and ferrocenedicarboxamido group (**FD**, 1,1'-bis[[p- phenylamino-(phenyl)]amido]-ferrocene), are easily soluble in common organic solvents such as methylene chloride, and were originally synthesized by Wang L. et al. Cyclic voltammetric studies of DNTD and its corresponding polymers were performed.[146,147] Wang found that voltammetry of the polymer has a $1e^-$ and $2e^-$/monomer unit oxidation consistent with the oxidation of the diphenyl benzidine unit that is formed during dimerization and polymerization. However, the material with X= perylene diimide group (**DPTD**, N,N'-Di[p-phenylamino (phenyl)]-perylene-3,4,9,10-tetracarboxylic diimide) that are unsubstituted at the imide nitrogens have been found to be less soluble due to their tendency to self-assemble and self-aggregate. It was found that substituting the PDI

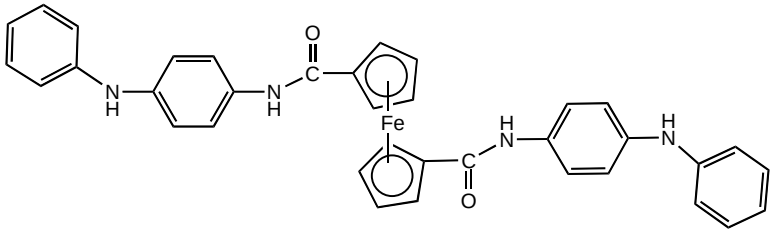

FD

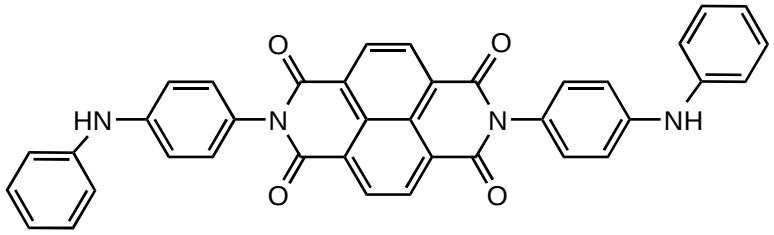

DNTD

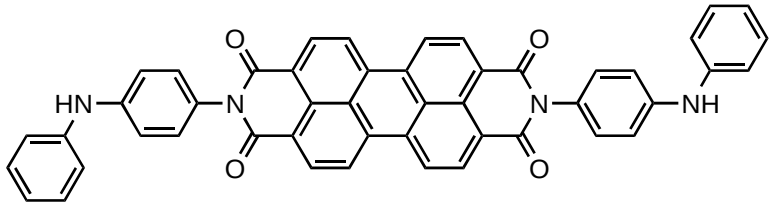

DPTD

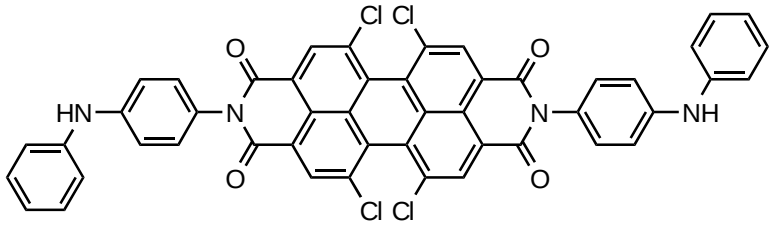

Cl_4DPTD

Figure 1-5 A series of monomers synthesized in our lab with structure motif of R-X-R, R=diphenylamine (DPA) group and electroactive unit X.

imide positions with aromatic amines increases the solubility dramatically.[148] Further substitutions at the bay positions of PDI molecules have been shown to change the rigidity of the perylene core to a more twisted conformation, which consequently increase the solubility as well. By modification of perylene rings and diphenylamine endgroups, the monomers with perylene core synthesized by Liang have better solubilities in methylene chloride.[149] Liang synthesized a monomer (**Cl_4DPTD**, (N,N'-Di[p-phenylamino (phenyl)]-perylene-1,6,7,12 tetrachloro-3,4,9,10-tetracarboxylic diimide)) with four Cl atoms bond to the perylene ring bay area which decreases the reduction potential and makes the polymer films more stable in reduced states.[149] All of the chemical structures of the monomers are listed in Figure 1-5. In order to improve the natural solubility of monomers with a perylene core, Liang synthesized **(*t*-BuPhO)$_4$DPTD**, (N,N'-di[p-phenylamino(phenyl)]-1,6,7,12-tetrakis (4-tert-butylphenoxy-3,4,9,10-tetracarboxilylic diimide) by replacing the chlorine group by *t*-BuPhO group at the perylene bay region. He also synthesized a monomer with a cyclohexyl-group connecting to the diimide ends and the perylene 1,7 positions were replaced by p-anilino-phenoxy groups, (**cyclohexyl-DPTD**, N,N'-dicyclohexyl-1,7-di-p-anilino- phenoxyperylene-3,4,9,10- tetracarboxilylic diimide). Based on these monomers, electrochromic devices with improved stability, high transmittance ratio and fast response time were developed.[149] The chemical structures of **(*t*-BuPhO)$_4$DPTD** and **Cyclohexyl-DPTD** are shown in Figure 1-6.

1.5.1 Polymers synthesized from monomer solutions

The electropolymerization mechanism of FD, DNTD, DPTD and Cl_4DPTD in organic solvents such as CH_2Cl_2 with the electrolyte tetrabutylammonium hexafluorophospate ($TBAPF_6$)

was widely researched and well elucidated. During the first positive scan all compounds in organic solvents show an irreversible oxidation at around + 1.1 V vs. Ag/AgCl, which is assigned to the irreversible oxidation of the diphenylamine end groups. However, on the second and subsequent scans a new oxidation peak at +0.75 V appears and increases in intensity. This is consistent with the diphenylbenzidene (DPB) linkage being formed.[146,150] For the electropolymerzation of FD, there is an overlap of the redox of DPB unit and ferrocene unit (+0.75~0.85V), which makes the second peak much larger than the first one (+0.55V).[150]

Since all the polymerization processes in this dissertation are related to diphenylamine (DPA) end groups, it is necessary to introduce the DPA polymerization mechanism. DPA was first studied by Knop,[151] and can be dimerized or polymerized chemically or electrochemically through a radical cation mechanism via fast reactions. Hayat et al[152] reported that poly(DPA) was precipitated at a Pt electrode to form a conductive film. There are many reports of oxidative electropolymerization of diphenylamine in acid media.[153-155] Yang and Bard[156] studied the polymerization of DPA with microelectrodes, and proposed the two possible radical cation coupling mechanisms, ECEC and EECC. Scheme 1-1 shows these two processes. Hao[26] and Wang[150] gave a detailed explanation of the electropolymerization mechanism of DNTD and FD. Further, Hao[26] showed that the DNTD polymerization process was dominated by an ECEC mechanism using the method of EQCM. Hao and others found out in both cases that the passed charges of each cycle is linear to voltammetric cycles, indicating the thin film had uniformed growth on the electrode surface.[26,157]

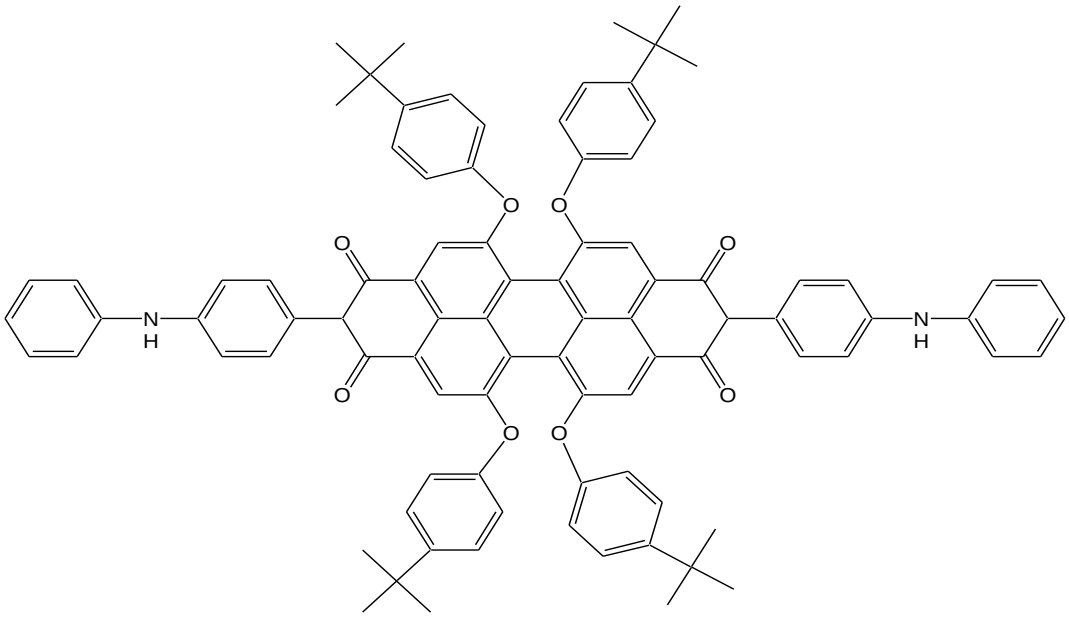

N,N'-di[*p*-phenylamino(phenyl)]-1,6,7,12-tetrakis (4-*tert*-butylphenoxy-3,4,9,10-tetracarboxilylic diimide

$(t\text{-BuPhO})_4$DPTD

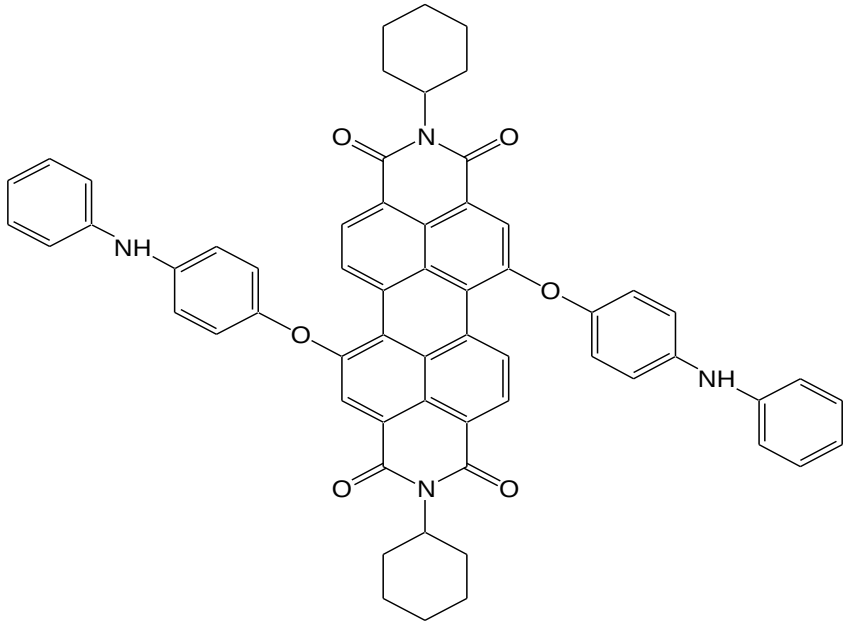

N,N'-dicyclohexyl-1,7-di-*p*-anilino-phenoxyperylene-3,4,9,10-tetracarboxilylic diimide

Cyclohexyl-DPTD

Figure 1-6 Chemical structures of $(t\text{-BuPhO})_4$DPTD and Cyclohexyl-DPTD

1.5.2 Single polymeric film in solution

Figure 1-7 shows the cyclic voltammograms of FD, DNTD, DPTD andCl_4DPTD polymer films in CH_2Cl_2 containing 0.1 M $TBAPF_6$ supporting electrolyte with scan range from 0.0 V to +1.4 V at a scan rate of 200 mV/s on a 0.018 cm^2 Au electrode. From Figure 1-7, we can see that in the positive scan (voltage >0 vs. Ag/AgCl), there are two separate redox species, in which the first corresponds to DPB/DPB^+ and second to DPB^+/DPB^{2+} for all four polymers. DPB/DPB^+ formal potential (E^0) is found at around +0.72 V and DPB^+/DPB^{2+} formal potential is at the value of +0.94 V. These two oxidation peaks in the graph show equal amounts of passed charge. At the negative-voltage direction scan, there are other redox species which are assigned to X/X^- (X is naphthalene diimide for DNTD and perylene tetracarboxylic diimide (PTCDI) for DPTD and Cl_4DPTD) and X^-/X^{2-}. Further, the peak currents for the reduction and oxidation of the surface coated polymers vary linearly with the sweep rate, confirming the behavior expected for the surface-immobilized redox species for electroactive polymers on Au electrode. Importantly, for those very thin films at low scan rates, when the charge transfer at the interface and charge transport processes with the film are fast, the

peak current I_p is linear to the corresponding scan rate, υ, with following relationship[24]:

$$I_p=n^2F^2/(4RT)*A\Gamma\upsilon \qquad (1\text{-}5)$$

here n is the number of electrons in the process, F means Faraday constant, R is the gas constant, T is temperature, and A represents electrode area.

The Figure 1-7 (A), cyclic voltammogram of poly(FD) also shows that it has two uneven area redox peaks when scanned in positive voltage vs. Ag/AgCl. They correspond to DPB/DPB^+

EECC process:

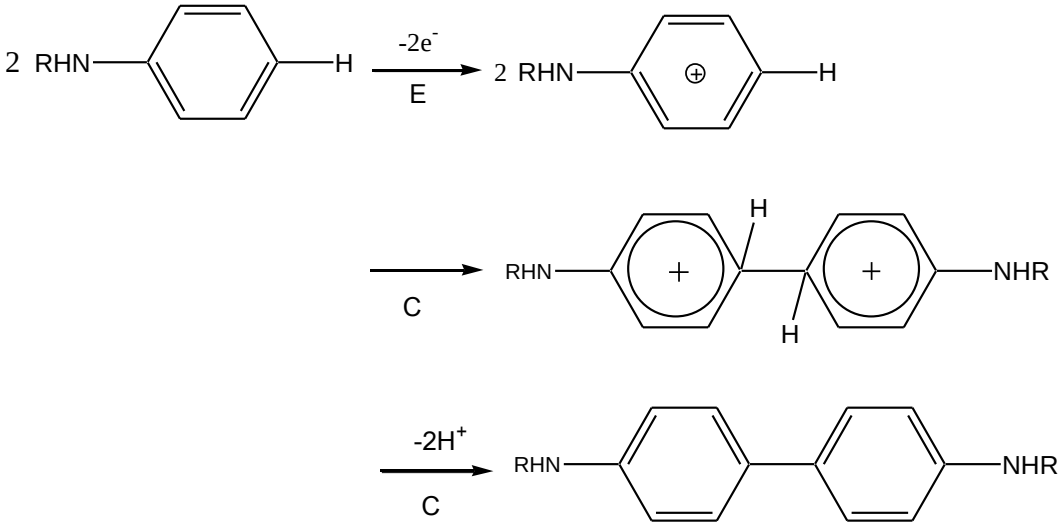

ECEC process:

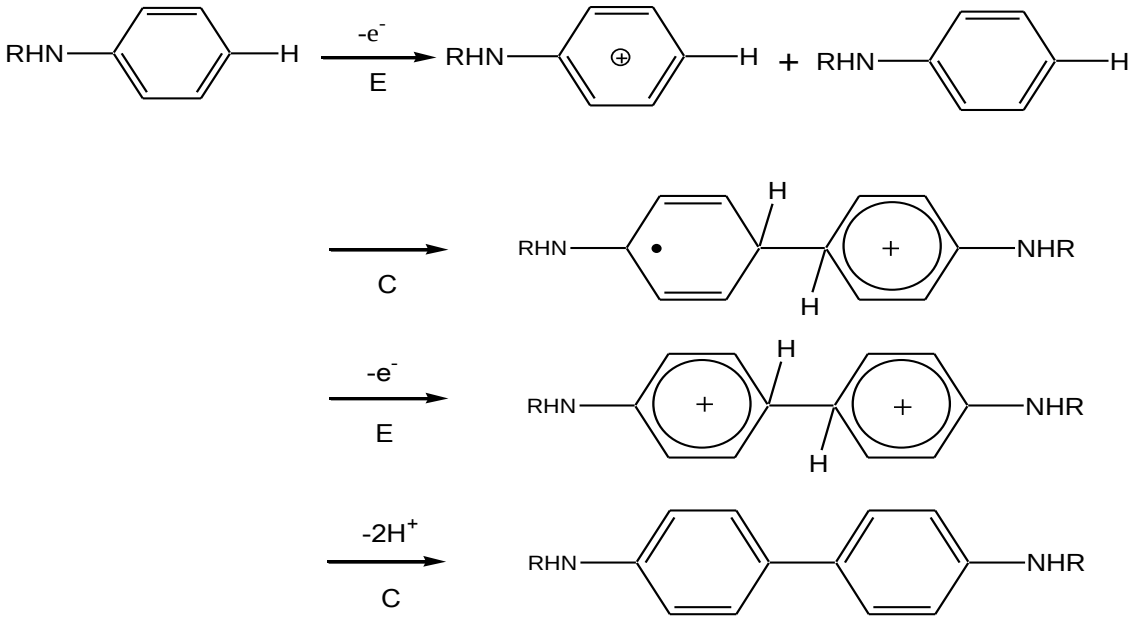

Scheme 1-1 EECC and ECEC Mechanism[156]

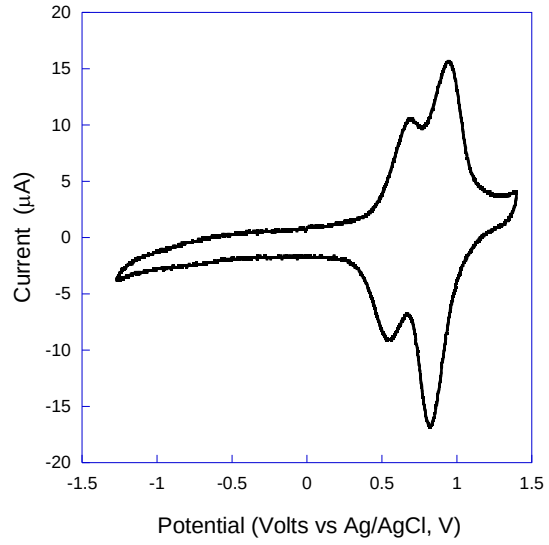

A: Poly(FD)

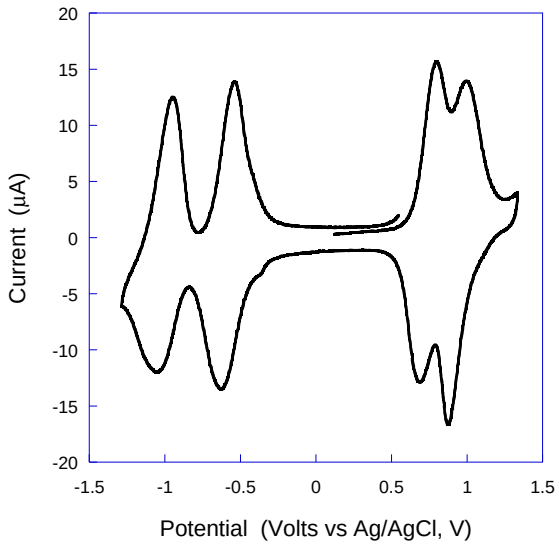

B: Poly(DNTD)

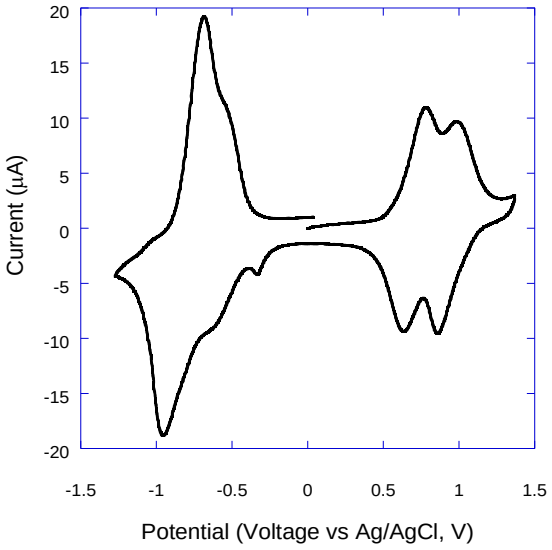

C: Poly(DPTD)

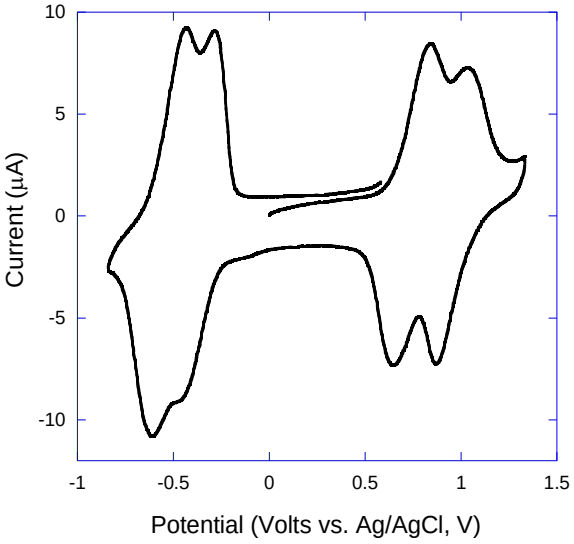

D: Poly(Cl_4DPTD)

Figure 1-7. R-X-R polymeric single film electrochemistry on 0.018 cm^2 Au electrode in CH_2Cl_2 with 0.1 M $TBAPF_6$ under scan rate of 200 mV/s at room temperature.

for the small peak, DPB^{+}/DPB^{2+} and Fc/Fc^{+} overlapping peaks for the more positive wave, which has doubled the charge to the DPB/DPB^{+} peak. However, when poly(FD) was scanned to negative voltages vs. Ag/AgCl up to -1.2 V, we cannot find any reduction peak. In the electrochemical window of methylene chloride solvent, we cannot find the reduced form of FD. This confirms that the poly(FD) thin film is electro-inactive at negative potentials and is a unipolar material (p-type).

Poly(DPTD) and poly(Cl_4DPTD) were also easily made by the oxidative electropolymerization from their monomer solutions and single layer films were emersed from the deposition solution, rinsed with copious amounts of CH_2Cl_2 and immersed into a fresh electrolyte solution of 0.1M $TBAPF_6$. It shows two well-separated reversible oxidative waves in the cyclic voltammetry consistent with previous work on the surface-confine diphenyl benzidine cation and dication (shown in Figure 1-7 C and D, respectively). [146,158] The negative scan, shows a multiple electron reduction with a smaller wave at more positive potential then a larger overlapping wave for poly(DPTD) between -0.5V and -1.0 V. Based on previous research,[26] one e^- reduces each imide ring and a third e^- reduces the perylene ring. Two pair of reversible reductive peaks of poly(Cl_4DPTD) are associated with diimide structures.[149] Since they are electroactive in either positive or negative potentials, both films are bipolar materials, similar to poly(DNTD).

The cyclic voltammograms of poly(cyclohexyl-DPTD) and poly(t-BuPhO)$_4$DPTD are presented in Figure 1-8 A and 1-8 B. Poly(cyclohexyl-DPTD), exhibits only one redox couple at

negative potentials, the first half-wave reduction potential, $E_{1/2}^{-1}$, is about -0.783 V vs. Ag/AgCl. In contrast, poly(t-BuPhO)$_4$DPTD exhibits two redox couples at negative potentials and 3 redox couples at positive potentials. Its first $E_{1/2}^{-1}$ is about -0.703 V and, the first half-wave oxidation potential, $E_{1/2}^{+1}$ is about 0.805 V vs. Ag/AgCl. This is evidence of a greater electron density at the perylene core for (t-BuPhO)$_4$DPTD and cyclohexyl-DPTD than for DPTD, but Cl$_4$DPTD is more electron deficient than DPTD.

Based on the previous research in our lab, we attempted to make a series of polymeric electronic devices with these R-X-R structured monomers. The main interest of this work focused on electrochemically polymerizing those compounds in a bilayer manner and exploring their potential as organic electronic diodes and solar cells. With evidence of bilayer current rectification in electrolyte solution, solid state polymeric p-n type diodes were made. This will be discussed in more detail in the following chapter 2. Spectroelectrochemistry was used to explore the electron blocking and trapping behavior in different polymeric bilayers based on above-discussed monomers. This technique can provide not only powerful evidence of the electron-blocking in bilayers with poly(FD), but can also be used to investigate the electron transfer within those layers that could be employed in photovoltaic cells. We also constructed p-n heterojunction organic solar cells by thermally evaporating p-type small molecular layers followed by electrochemical synthesis of different n-type polymeric layers. The cell performance of such devices were characterized from the current-voltage curves.

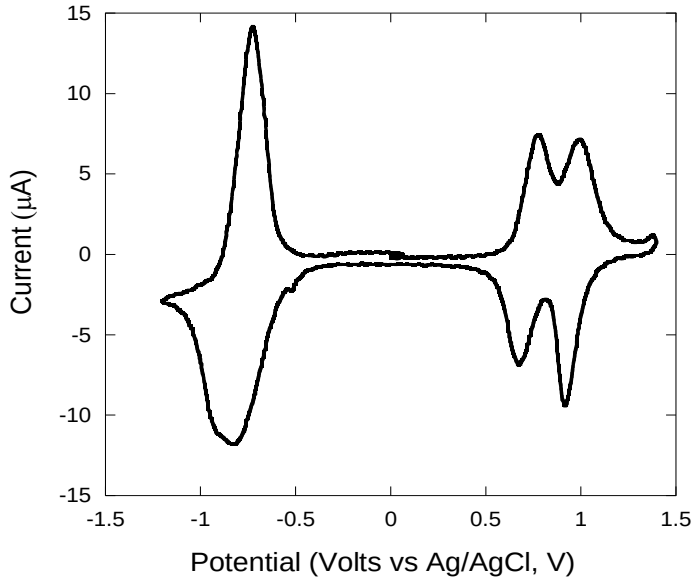

A. poly(Cyclohexyl-DPTD)

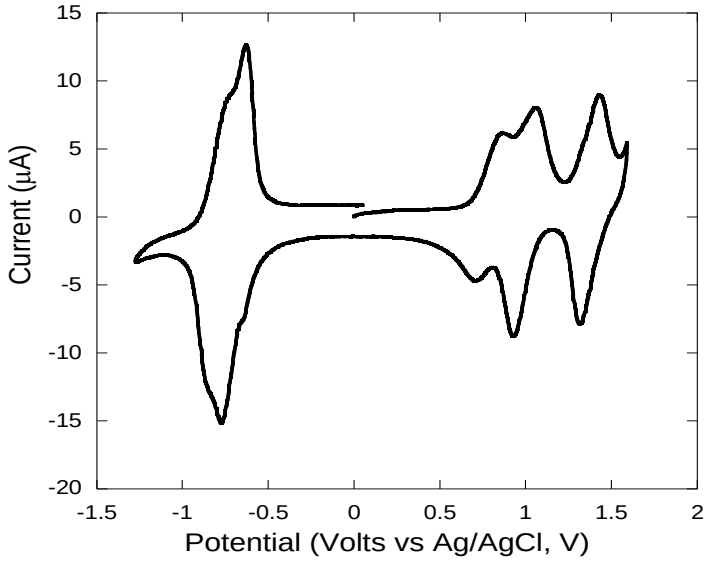

B. poly((t-BuPhO)$_4$DPTD)

Figure 1-8. Poly(Cyclohexyl-DPTD) and poly((t-BuPhO)$_4$DPTD) single film electrochemistry on 0.018 cm^2 Au electrode in CH_2Cl_2 with 0.1 M $TBAPF_6$ under scan rate of 200 mV/s at room temperature.

REFERENCES

1. Streetman, B. G.; Banerjee, S. K. *Solid State Electronic Devices, 6th Ed.*; Prentice Hall, 2009.

2. Cassidy, H. G. *Proc. Natl. Acad. Sci. U. S. A.* **1952**, *38*, 934-7.

3. Cassidy, H. G.; Ezrin, M.; Updegraff, I. H. *J. Am. Chem. Soc.* **1953**, *75*, 1615-17.

4. Ezrin, M.; Updegraff, I. H.; Cassidy, H. G. *J. Am. Chem. Soc.* **1953**, *75*, 1610-14.

5. Atchison, G. J. *J. Polym. Sci.* **1959**, *35*, 557-8.

6. *Organic Electronics: Materials, Manufacturing and Applications*; Klauk, H., Ed.; Wiley-VCH: Weinheim, Germany, 2006.

7. *Organic Electronics*; Meller, G.; Grassor, T., Eds.; Springer: Berlin Heidelberg, 2010; Vol. 223.

8. Heeger, A. J. *Angew. Chem., Int. Ed.* **2001**, *40*, 2591-2611.

9. MacDiarmid, A. G. *Angew. Chem., Int. Ed.* **2001**, *40*, 2581-2590.

10. Shirakawa, H. *Angew. Chem., Int. Ed.* **2001**, *40*, 2575-2580.

11. Shirakawa, H.; Louis, E. J.; MacDiarmid, A. G.; Chiang, C. K.; Heeger, A. J. *J. Chem. Soc., Chem. Commun.* **1977**, 578-80.

12. Genies, E. M.; Boyle, A.; Lapkowski, M.; Tsintavis, C. *Synth. Met.* **1990**, *36*, 139-82.

13. Roncali, J. *Chem. Rev.* **1992**, *92*, 711-38.

14. Buttry, D. A. *Applications of the quartz crystal microbalance to electrochemistry*; Marcel Dekker: New York, 1991; Vol. 17.

15. Ward, M. D. In *Physical electrochemistry*; Rubinstein, I., Ed.; Marcel Dekker: New York,

1995 p293-283.

16. Barbero Cesar, A. *Phys Chem Chem Phys* **2005**, *7*, 1885-99.

17. Rosseinsky, D. R.; Mortimer, R. J. *Adv. Mater. (Weinheim, Ger.)* **2001**, *13*, 783-793.

18. Gerard, M.; Chaubey, A.; Malhotra, B. D. *Biosens. Bioelectron.* **2002**, *17*, 345-359.

19. Gilch, H. G.; Wheelwright, W. L. *J. Polym. Sci., Part A-1: Polym. Chem.* **1966**, *4*, 1337-49.

20. Rudin, A. *The Elements of Polymer Science and Engineering: An Introductory text for engineers and chemists*; Academic Press, 1982.

21. Genies, E. M.; Penneau, J. F.; Lapkowski, M.; Boyle, A. *J. Electroanal. Chem. Interfacial Electrochem.* **1989**, *269*, 63-75.

22. John, R.; Wallace, G. G. *J. Electroanal. Chem.* **1991**, *306*, 157-67.

23. Vivier, V.; Cachet-Vivier, C.; Michel, D.; Nedelec, J. Y.; Yu, L. T. *Synth. Met.* **2002**, *126*, 253-262.

24. Bard, A. J.; Faulkner, L. R. *Electrochemical Methods: Fundamentals and Applicaitons*; 2nd Ed. ed.; John Wiley&Sons, 2001.

25. Hepel, M. In *Interfacial electrochemistry*; Wieczkowski, A., Ed.; Marcel Dekker: New York, 1999.

26. Hao, N., M.S. Thesis, Auburn University, 2001.

27. Orazem, M. E.; Tribollet, B. *Electrochemical Impedance Spectroscopy*; John Wiley & Sons: Hoboken, New Jersey, 2008.

28. *Handbook of Conducting Polymers, 2 Vol. Set*; 3rd ed.; Reynolds, J.; Skoheim, T. A., Eds.; CRC Press, 2007.

29. Chiang, C. K.; Gau, S. C.; Fincher, C. R., Jr.; Park, Y. W.; MacDiarmid, A. G.; Heeger, A. J. *Appl. Phys. Lett.* **1978**, *33*, 18-20.

30. Abruna, H. D.; Denisevich, P.; Umana, M.; Meyer, T. J.; Murray, R. W. *J. Am. Chem. Soc.* **1981**, *103*, 1-5.

31. Aizawa, M.; Watanabe, S.; Shinohara, H.; Shirakawa, H. *J. Chem. Soc., Chem. Commun.* **1985**, 264-5.

32. Koezuka, H.; Hyodo, K.; MacDiarmid, A. G. *J. Appl. Phys.* **1985**, *58*, 1279-84.

33. Cheng, C. H. W.; Boettcher, S. W.; Johnston, D. H.; Lonergan, M. C. *J. Am. Chem. Soc.* **2004**, *126*, 8666-8667.

34. Yu, G.; Gao, J.; Hummelen, J. C.; Wudl, F.; Heeger, A. J. *Science (Washington, D. C.)* **1995**, *270*, 1789-91.

35. Shaheen, S. E.; Brabec, C. J.; Sariciftci, N. S.; Padinger, F.; Fromherz, T.; Hummelen, J. C. *Appl. Phys. Lett.* **2001**, *78*, 841-843.

36. Al-Ibrahim, M.; Roth, H. K.; Schroedner, M.; Konkin, A.; Zhokhavets, U.; Gobsch, G.; Scharff, P.; Sensfuss, S. *Org. Electron.* **2005**, *6*, 65-77.

37. Aviram, A.; Ratner, M. A. *Chem. Phys. Lett.* **1974**, *29*, 277-83.

38. Abruna, H. D.; Denisevich, P.; Umana, M.; Meyer, T. J.; Murray, R. W. *J. Am. Chem. Soc.* **1981**, *103*, 1-5.

39. Denisevich, P.; Willman, K. W.; Murray, R. W. *J. Am. Chem. Soc.* **1981**, *103*, 4727-37.

40. Leidner, C. R.; Sullivan, B. P.; Reed, R. A.; White, B. A.; Crimmins, M. T.; Murray, R. W.; Meyer, T. J. *Inorg. Chem.* **1987**, *26*, 882-91.

41. Baldwin, J. W.; Amaresh, R. R.; Peterson, I. R.; Shumate, W. J.; Cava, M. P.; Amiri, M. A.; Hamilton, R.; Ashwell, G. J.; Metzger, R. M. *J. Phys. Chem. B* **2002**, *106*, 12158-12164.

42. Metzger, R. M. *Synth. Met.* **2003**, *137*, 1499-1501.

43. Chi, Q.; Zhang, J.; Ulstrup, J. *J. Phys. Chem. B* **2006**, *110*, 1102-1106.

44. Ju, X.; Feng, W.; Kittichungchit, V.; Hori, T.; Moritou, H.; Fujii, A.; Ozaki, M. *Thin Solid Films* **2009**, *518*, 786-790.

45. Leidner, C. R.; Murray, R. W. *J. Am. Chem. Soc.* **1985**, *107*, 551-6.

46. Leidner, C. R.; Denisevich, P.; Willman, K. W.; Murray, R. W. *J. Electroanal. Chem. Interfacial Electrochem.* **1984**, *164*, 63-78.

47. Pickup, P. G.; Leidner, C. R.; Denisevich, P.; Murray, R. W. *J. Electroanal. Chem. Interfacial Electrochem.* **1984**, *164*, 39-61.

48. Pickup, P. G.; Murray, R. W. *J. Electrochem. Soc.* **1984**, *131*, 833-9.

49. Pickup, P. G.; Kutner, W.; Leidner, C. R.; Murray, R. W. *J. Am. Chem. Soc.* **1984**, *106*, 1991-8.

50. Willman, K. W.; Murray, R. W. *J. Electroanal. Chem. Interfacial Electrochem.* **1982**, *133*, 211-31.

51. Kittlesen, G. P.; White, H. S.; Wrighton, M. S. *J. Am. Chem. Soc.* **1984**, *106*, 7389-96.

52. White, M. S.; Olson, D. C.; Shaheen, S. E.; Kopidakis, N.; Ginley, D. S. *Appl. Phys. Lett.* **2006**, *89*, 143517/1-143517/3.

53. Kittlesen, G. P.; White, H. S.; Wrighton, M. S. *J. Am. Chem. Soc.* **1985**, *107*, 7373-80.

54. Kittlesen, G. P.; Wrighton, M. S. *J. Mol. Electron.* **1986**, *2*, 23-33.

55. Paul, E. W.; Ricco, A. J.; Wrighton, M. S. *J. Phys. Chem.* **1985**, *89*, 1441-7.

56. Thackeray, J. W.; White, H. S.; Wrighton, M. S. *J. Phys. Chem.* **1985**, *89*, 5133-40.

57. Palmore, G. T. R.; Smith, D. K.; Wrighton, M. S. *J. Phys. Chem. B* **1997**, *101*, 2437-2450.

58. Smith, D. K.; Tender, L. M.; Lane, G. A.; Licht, S.; Wrighton, M. S. *J. Am. Chem. Soc.* **1989**, *111*, 1099-105.

59. Smith, D. K.; Lane, G. A.; Wrighton, M. S. *J. Phys. Chem.* **1988**, *92*, 2616-28.

60. Smith, D. K.; Lane, G. A.; Wrighton, M. S. *J. Am. Chem. Soc.* **1986**, *108*, 3522-5.

61. Hable, C. T.; Crooks, R. M.; Valentine, J. R.; Giasson, R.; Wrighton, M. S. *J. Phys. Chem.* **1993**, *97*, 6060-5.

62. Hable, C. T.; Crooks, R. M.; Wrighton, M. S. *J. Phys. Chem.* **1989**, *93*, 1190-2.

63. Li, Z.; Wang, C. M.; Persaud, L.; Mallouk, T. E. *J. Phys. Chem.* **1988**, *92*, 2592-7.

64. Li, Z.; Mallouk, T. E. *J. Phys. Chem.* **1987**, *91*, 643-8.

65. Berchmans, S.; Usha, S.; Ramalechume, C.; Yegnaraman, V. *J. Solid State Electrochem.* **2005**, *9*, 595-600.

66. Ramalechume, C.; Yegnaraman, V.; Mandal, A. B. *J. Solid State Electrochem.* **2006**, *10*, 499-505.

67. Ramalechume, C.; Berchmans, S.; Yegnaraman, V.; Mandal, A. B. *J. Electroanal. Chem.* **2005**, *580*, 122-127.

68. Lupu, S.; Mihailciuc, C.; Pigani, L.; Seeber, R.; Totir, N.; Zanardi, C. *Electrochem. Commun.* **2002**, *4*, 753-758.

69. Alleman, K. S.; Weber, K.; Creager, S. E. *J. Phys. Chem.* **1996**, *100*, 17050-17058.

70. Berchmans, S.; Ramalechume, C.; Lakshmi, V.; Yegnaraman, V. *J. Mater. Chem.* **2002**, *12*, 2538-2542.

71. Metzger, R. M. *Chem. Rev. (Washington, DC, U. S.)* **2003**, *103*, 3803-3834.

72. Metzger, R. M. *Chem. Phys.* **2006**, *326*, 176-187.

73. Weibel, N.; Grunder, S.; Mayor, M. *Org. Biomol. Chem.* **2007**, *5*, 2343-53.

74. Metzger, R. M. *J. Mater. Chem.* **2008**, *18*, 4364-4396.

75. Metzger, R. M. *Synth. Met.* **2009**, *159*, 2277-2281.

76. Rinaldi, R.; Biasco, A.; Maruccio, G.; Cingolani, R.; Alliata, D.; Andolfi, L.; Facci, P.; De Rienzo, F.; Di Felice, R.; Molinari, E. *Adv. Mater. (Weinheim, Ger.)* **2002**, *14*, 1453-1457.

77. Alcaraz, A.; Ramirez, P.; Garcia-Gimenez, E.; Lopez, M. L.; Andrio, A.; Aguilella, V. M. *J. Phys. Chem. B* **2006**, *110*, 21205-21209.

78. Meinhard, J. E. *J. Appl. Phys.* **1964**, *35*, 3059-60.

79. Yamashita, K.; Kunugi, Y.; Harima, Y.; Chowdhury, A.-N. *Jpn. J. Appl. Phys., Part 1* **1995**, *34*, 3794-7.

80. Koshida, N.; Wachi, Y. *Appl. Phys. Lett.* **1984**, *45*, 436-7.

81. Slaoui, A.; Collins, R. T. *MRS bulletin* **2007**, *32*, 211-218.

82. Wang, W. M.; Wan, H. H.; Rong, T. W.; Bao, J. R.; Lin, S. H. *Nucl. Instrum. Methods Phys. Res., Sect. B* **1991**, *B61*, 466-71.

83. Cheng, C. H. W.; Lonergan, M. C. *J. Am. Chem. Soc.* **2004**, *126*, 10536-10537.

84. Aizawa, M.; Shinohara, H.; Yamada, T.; Akagi, K.; Shirakawa, H. *Synth. Met.* **1987**, *18*, 711-14.

85. Uehara, K.; Ichikawa, T.; Matsumoto, K.; Sugimoto, A.; Tsunooka, M.; Inoue, H. *J. Electroanal. Chem.* **1997**, *438*, 85-89.

86. Kudo, T.; Kimura, M.; Hanabusa, K.; Shirai, H. *J. Porphyrins Phthalocyanines* **1998**, *2*, 231-235.

87. Kudo, T.; Kimura, M.; Hanabusa, K.; Shirai, H. *J. Porphyrins Phthalocyanines* **1999**, *3*, 310-315.

88. Srivastava, M. P.; Mohanty, S. R.; Annapoorni, S.; Rawat, R. S. *Phys. Lett. A* **1996**, *215*, 63-68.

89. Lewis, N. S.; Nocera, D. G. *Proc. Natl. Acad. Sci. U. S. A.* **2007**, *103*, 15729-15735.

90. Lewis, N. S. *MRS bulletin* **2007**, *32*, 808-820.

91. Wigley, T. M. *Science (Washington, DC, U. S.)* **2007**, *316*, 829-830.

92. Wigley, T. M. L. *Science (Washington, DC, U. S.)* **2005**, *307*, 1766-1769.

93. Wigley, T. M. L. *Nature (London)* **1997**, *390*, 267-270.

94. Petrasch, J. *Tomography-based Methods for Reactive Flows in Porous Media: Applied to Solar Thermal Reforming of Hydrocarbons*; VDM Verlag 2009.

95. Slaoui, A.; Collins, R. T. *MRS Bull.* **2007**, *32*, 211-218.

96. O'Regan, B.; Graetzel, M. *Nature (London)* **1991**, *353*, 737-40.

97. Meng, Q. B.; Takahashi, K.; Zhang, X. T.; Sutanto, I.; Rao, T. N.; Sato, O.; Fujishima, A.; Watanabe, H.; Nakamori, T.; Uragami, M. *Langmuir* **2003**, *19*, 3572-3574.

98. *Organic Photovoltaics, Mechanism, Materials and Devices*; Sun, S.-S.; Saricifti, N. S., Eds.; CRC Press (Taylor&Francis): Boca Raton, FL, 2005.

99. Ghosh, A. K.; Morel, D. L.; Feng, T.; Shaw, R. F.; Rowe, C. A., Jr. *J. Appl. Phys.* **1974**, *45*, 230-6.

100. Tang, C. W.; Albrecht, A. C. *J. Chem. Phys.* **1975**, *62*, 2139-49.

101. Tang, C. W. *Appl. Phys. Lett.* **1986**, *48*, 183-5.

102. Kim, J. Y.; Lee, K.; Coates, N. E.; Moses, D.; Nguyen, T.-Q.; Dante, M.; Heeger, A. J. *Science (Washington, DC, U. S.)* **2007**, *317*, 222-225.

103. Chen, H.-Y.; Hou, J.; Zhang, S.; Liang, Y.; Yang, G.; Yang, Y.; Yu, L.; Wu, Y.; Li, G. *Nat. Photonics* **2009**, *3*, 649-653.

104. Forrest, S. R. *MRS Bull.* **2005**, *30*, 28-32.

105. Schmidt-Mende, L.; Fechtenkotter, A.; Mullen, K.; Moons, E.; Friend, R. H.; MacKenzie, J. D. *Science (Washington, DC, U. S.)* **2001**, *293*, 1119-1122.

106. Reucroft, P. J.; Takahashi, K.; Ullal, H. *Appl. Phys. Lett.* **1974**, *25*, 664-666.

107. Reucroft, P. J.; Takahashi, K.; Ullal, H. *J. Appl. Phys.* **1975**, *46*, 5218-23.

108. Tang, C. W. *Patent US 4164431* **1979**.

109. Tang, C. W. *Patent US 4281053* **1981**.

110. Hiramoto, M.; Kishigami, Y.; Yokoyama, M. *Chem. Lett.* **1990**, 119-22.

111. Hiramoto, M.; Suezaki, M.; Yokoyama, M. *Chem. Lett.* **1990**, 327-30.

112. Morikawa, T.; Adachi, C.; Tsutsui, T.; Saito, S. *Nippon Kagaku Kaishi FIELD Full Journal Title:Nippon Kagaku Kaishi* **1990**, 962-7.

113. Hiramoto, M.; Fujiwara, H.; Yokoyama, M. *Appl. Phys. Lett.* **1991**, *58*, 1062-4.

114.Hiramoto, M.; Fujiwara, H.; Yokoyama, M. *J. Appl. Phys.* **1992**, *72*, 3781-7.

115. Hiramoto, M.; Fukusumi, H.; Yokoyama, M. *Appl. Phys. Lett.* **1992**, *61*, 2580-2.

116. Zhou, S.; Liu, Y.; Qiu, W.; Xu, Y.; Huang, X.; Li, Y.; Jiang, L.; Zhu, D. *Adv. Funct. Mater.* **2002**, *12*, 65-69.

117. Shichiri, T.; Suezaki, M.; Inoue, T. *Chem. Lett.* **1992**, 1717-20.

118. Yanagi, H.; Tamura, N.; Taira, S.; Furuta, H.; Douko, S.; Schnurpfeil, G.; Woehrle, D. *Mol. Cryst. Liq. Cryst. Sci. Technol., Sect. A* **1995**, *267*, 435-40.

119. Tsuzuki, T.; Hirota, N.; Noma, N.; Shirota, Y. *Thin Solid Films* **1996**, *273*, 177-80.

120. Feng, W.; Fujii, A.; Lee, S.; Wu, H.; Yoshino, K. *J. Appl. Phys.* **2000**, *88*, 7120-7123.

121. Tsuzuki, T.; Shirota, Y.; Rostalski, J.; Meissner, D. *Sol. Energy Mater. Sol. Cells* **2000**, *61*, 1-8.

122. Nagai, K.; Morishita, K. i.; Yoshida, H.; Norimatsu, T.; Miyanaga, N.; Izawa, Y.; Yamanaka, T. *Synth. Met.* **2001**, *121*, 1445-1446.

123. Wang, H.; Peng, B.; Wei, W. *Huaxue Jinzhan (Progress in Chemistry)* **2008**, *20*, 1751-1760.

124. Kim, I.; Haverinen, H. M.; Wang, Z.; Madakuni, S.; Kim, Y.; Li, J.; Jabbour, G. E. *Chem. Mater.* **2009**, *21*, 4256-4260.

125. Kim, I.; Haverinen, H. M.; Wang, Z.; Madakuni, S.; Li, J.; Jabbour, G. E. *Appl. Phys. Lett.* **2009**, *95*, 023305/1-023305/3.

126. Shibano, Y.; Imahori, H.; Adachi, C. *J. Phys. Chem. C* **2009**, *113*, 15454-15466.

127. Kim, J. Y.; Bard, A. J. *Chem. Phys. Lett.* **2004**, *383*, 11-15.

128. Peumans, P.; Bulovic, V.; Forrest, S. R. *Appl. Phys. Lett.* **2000**, *76*, 2650-2652.

129. Peumans, P.; Uchida, S.; Forrest Stephen, R. *Nature (London, U. K.)* **2003**, *425*, 158-62.

130. Ma, W.; Yang, C.; Gong, X.; Lee, K.; Heeger, A. J. *Adv. Funct. Mater.* **2005**, *15*, 1617-1622.

131. Yang, F.; Shtein, M.; Forrest, S. R. *Nat. Mater.* **2005**, *4*, 37-41.

132. Whitlock, J. B.; Panayotatos, P.; Sharma, G. D.; Cox, M. D.; Sauers, R. R.; Bird, G. R. *Opt. Eng. (Bellingham, Wash.)* **1993**, *32*, 1921-34.

133. Breeze, A. J.; Salomon, A.; Ginley, D. S.; Gregg, B. A.; Tillmann, H.; Horhold, H. H. *Appl. Phys. Lett.* **2002**, *81*, 3085-3087.

134. Nakamura, J.-i.; Suzuki, S.; Takahashi, K.; Yokoe, C.; Murata, K. *Bull. Chem. Soc. Jpn.* **2004**, *77*, 2185-2188.

135. Nakamura, J.-I.; Yokoe, C.; Murata, K.; Takahashi, K. *J. Appl. Phys.* **2004**, *96*, 6878-6883.

136. Hiramoto, M.; Fujiwara, H.; Yokoyama, M. *J. Appl. Phys.* **1992**, *72*, 3781-7.

137. Breeze, A. J.; Salomon, A.; Ginley, D. S.; Tillmann, H.; Horhold, H.-H.; Gregg, B. A. *Proc. SPIE-Int. Soc. Opt. Eng.* **2003**, *4801*, 34-39.

138. Nakamura, J.-I.; Yokoe, C.; Murata, K.; Takahashi, K. *J. Appl. Phys.* **2004**, *96*, 6878-6883.

139. Reyes-Reyes, M.; Kim, K.; Carroll, D. L. *Appl. Phys. Lett.* **2005**, *87*, 083506/1-083506/3.

140. Li, J.; Dierschke, F.; Wu, J.; Grimsdale, A. C.; Muellen, K. *J. Mater. Chem.* **2006**, *16*, 96-100.

141. Liang, Y.; Feng, D.; Wu, Y.; Tsai, S.-T.; Li, G.; Ray, C.; Yu, L. *J. Am. Chem. Soc.* **2009**, *131*, 7792-7799.

142. Liang, Y.; Wu, Y.; Feng, D.; Tsai, S.-T.; Son, H.-J.; Li, G.; Yu, L. *J. Am. Chem. Soc.* **2009**, *131*, 56-57.

143. Danziger, J.; Dodelet, J. P.; Armstrong, N. R. *Chem. Mater.* **1991**, *3*, 812-20.

144. Danziger, J.; Dodelet, J. P.; Lee, P.; Nebesny, K. W.; Armstrong, N. R. *Chem. Mater.* **1991**, *3*, 821-9.

145. Xue, J.; Uchida, S.; Rand, B. P.; Forrest, S. R. *Appl. Phys. Lett.* **2004**, *84*, 3013-3015.

146. Wang, L.; Goodloe, G. W.; Stallman, B. J.; Cammarata, V. *Chem. Mater.* **1996**, *8*, 1175-1181.

147. Wang, L., Ph.D. Dissertation, Auburn University, 1997.

148. Langhals, H. *Heterocycles* **1995**, *40*, 477-500.

149. Liang, J., Ph.D. Dissertation, Auburn University, 2003.

150. Wang, L.; Cammarata, V. *Thin Solid Films* **1996**, *284-285*, 297-300.

151. Knop, J. *J. Am. Chem. Soc.* **1924**, *46*, 263-9.

152. Hayat, U.; Bartlett, P. N.; Dodd, G. H.; Barker, J. *J. Electroanal. Chem. Interfacial Electrochem.* **1987**, *220*, 287-94.

153. Zotti, G.; Cattarin, S.; Comisso, N. *J. Electroanal. Chem. Interfacial Electrochem.* **1988**, *239*, 387-96.

154. Inzelt, G. *J. Solid State Electrochem.* **2002**, *6*, 265-271.

155. Huo, L.; He, C.; Han, M.; Zhou, E.; Li, Y. *J. Polym. Sci., Part A: Polym. Chem.* **2007**,

45, 3861-3871.

156. Lin, S. H.; Sheng, K. L.; Rong, T. W.; Bao, J. R.; Wang, W. M.; Wan, H. H.; Zhou, Z. Y.; Zhu, X. F.; Yang, F. J. *Nucl. Instrum. Methods Phys. Res., Sect. B* **1991**, *B59-60, Pt. 2*, 1257-62.

157. Wang, Q.Q., M.S. Thesis, Auburn University, 1999.

158. Wang, L.; Wang, Q. Q.; Cammarata, V. *J. Electrochem. Soc.* **1998**, *145*, 2648-2654.

CHAPTER 2

BILAYER MODIFIED ELECTRODES WITH CURRENT RECTIFICATION AND ORGANIC DIODES BASED ON DIPHENYLAMINE POLYMERS

2.1 INTRODUCTION

At present, there is considerable interest in developing electronic and photonic devices with organic materials as active components.[1] These photonic and electronic devices could be achieved through chemical modification of surfaces.[2-5] One simple function of such molecular electronic devices is current rectification, where current flows only in one direction. Unidirectional electron flow within an ordered structure is a fundamental phenomenon, highly exploited in electronic technologies and by living organisms. To realize an electrochemical interface with rectification characteristics, it is desirable to modify the electrode surface with very thin films possessing good electron blocking properties and capable of exhibiting the desirable redox conductivity. As mentioned in Chapter 1, Murray and coworkers were the first to report an electrochemical approach to construct current rectification electrodes.[6,7] Their rectification interface was based on an electrode modified with two different, spatially segregated polymers containing Ru , Os, and Fe complexes with different redox potentials. These bilayer electrodes were made up of two discrete sequentially deposited films of two different redox polymers. For example, the linear potential sweep voltammetric response of the bilayer Pt/poly-$[Ru(4\text{-vinylpridine})_3]^{3+}$/poly-$[Fe(vbpy)_3]^{2+}$ in solution with electrolyte showed electron

transfer and charge trapping.[8] Another example of polymer-based electrochemical rectification involved redox polymers containing quinone and viologen subunits, which demonstrated pH-dependent rectification.[9-11] Other approaches towards building such thin films include self-assembly[4] and Langmuir-Blodgett techniques[12,13] that form monolayers. These monolayers could be further functionalized by using appropriate linking strategies to yield bilayer assemblies.

Polymer bilayers sandwiched between two electrodes, or side by side construction of two connected polymers grown on submicrometer-spaced conducting electrodes, allow the direct measurement of current-voltage characteristics. Such a construction is called a solid-state organic p-n junction diode. With the discovery of highly conductive p-type and n-type poly(acetylene) (PA) ,[14] building a p-n junction with PA has been a target. Several ways of doping PA to construct a p-n junction diode have been explored, including chemical doping and mechanical press contacting,[15] photochemical doping,[16,17] ion implantation[18,19] internal ion compensation,[20,21] and polyelectrolyte mediated electrochemical fabrication.[22]

Electrochemical polymerization provides another way to fabricate air and humidity stable p-n junction diodes. A Pt|poly(pyrrole), PPy (anion-doped)|poly(thiophene), PT (cation-doped) |In p-n junction diode was electrochemically fabricated by Aizawa and Shirakawa,[23] followed by controlled-potential electrochemical doping to make the PPy layer anion-doped and the PT layer cation-doped. Uehara et al.[24] studied the electron transfer between electropolymerized poly(3-methylthiophene) (P3MT) on a gold-sputtered glass slide and thermally sublimed dihydrophenazine derivatives, in a series of bilayer devices of Au|P3MT|dihydrophenazines|Al.

The typical rectification ratio from +2.0V to -2.0V is 7-500 depending on different diyhydrophenazine derivatives. Some of these devices not only showed current rectification in the dark but also showed photovoltaic effects under illumination.

In organic electronics, the construction of the contact between the metal electrode layer and organic active materials is critical for device design because the quality of the contact decides the performance of a device. There are currently three general techniques for forming top contacts for large area (i.e. more than several molecules) electrical measurements on organic molecules: 1) physical deposition of metals, 2) chemical or electrochemical installation of a metal layer, or 3) use of a liquid metal. Physical direct deposition of metals is a general way that uses thermal evaporation or sputtering (electron-beam) of metals and it ensures atomic-level contact but gives low yields of devices owing to damage to the organic monolayer by reaction with hot metal vapors or in the formation of metal filaments that short the junctions. Chemical or electrochemical preparation of a metal layer relies on electroless deposition of metal on insulating surfaces of fibers and polymers under redox reaction to reduce the target metal chemically by seeding some catalysts, normally a noble metal. Another step follows that turns the surface more conductive by electrochemical methods. However, the rectification performance of polymer-based rectifiers is limited by current leakage through imperfect polymers interfaces and through pinholes present within the polymers, especially when these molecular rectifiers were scaled up to macrosize solid-state diodes. More seriously, due to the formation of pinholes induced by all deposition processes, it is very easy to form electrical shorts between two electrodes when the top metallic electrode is coated on top of polymeric films with regular

methods such as sputtering, thermal evaporation or electroless deposition. A report claims that evaporation of metal top contacts on thin films results in about 50~90% short-circuited devices.[25] Thicker polymer films can minimize this problem, but may compromise the speed and lower rectification efficiency of such devices because the speed is also related to the rate of electron hopping between redox moieties in the polymer layers. Hg forms a more ideal electrode contact for physical-organic studies since this liquid metal (at room temperature) allows formation of conformal contacts. However, Hg is toxic, amalgamates with metals and measurements with Hg must be performed under a solvent bath to minimize vaporization.

In this chapter we used different "soft", ready-made methods to achieve metallic contacts with organic films. Specifically, we used conformal electrodes from the liquid metal eutectic, Ga-In, with 75% Ga and 25% In by weight, and a melting point=15.5 ℃.[26] There are several advantages of eutectic Ga-In; 1) it is a liquid and can be formed into metastable, nonspherical structures at room temperature without any complex instruments or masks and does not spontaneously reflow into the shape with the lowest interfacial free energy as normal liquids such as water and Hg; 2) it has high electrical conductivity (3.4×10^4 S cm^{-1}) and, 3) it tends to make low contact-resistance interfaces with a variety of materials. These advantages make liquid Ga-In eutectic useful for forming electrodes for thin-film devices. A second soft approach for making contacts between metallic layers and organic thin films combines wafer bonding with capillary interactions to develop and control, the lift-off float-on (LOFO) process. This method relies on capillary interactions, introduced by the liquid-solid interfaces between two solids and a common liquid for transferring thin solid metallic films onto a solid support.[25,27] The details of

this process can be summarized as following, 1) evaporation or sputtering of a metal film (gold, silver) onto a solid glass slide substrate; 2) detaching the metallic layer from the glass substrate in a dilute HF acid solution and floating it on a sub-phase liquid as a metal leaf (lift off); 3) adsorbing a molecular layer onto the metal leaf to add molecular functionality to the interface; 4) attaching the metal leaf to the target substrate, in a liquid mediated process (float-on).

At the same time, we also reported that a series of polymer bilayer-film modified electrodes show electrochemical rectification in both electrolyte solution and the solid-state. These polymeric thin bilayer films, poly(DNTD), poly(DPTD), poly(Cl_4DPTD) and poly(FD) were electropolymerized on the surface of another polymer through their monomer solutions. The chemical structure of these monomers are shown in Figure 2-1. Based on previous research in our group, they are different kinds of monomers applied as electrochromic materials synthesized in our group.[28-30] All these bilayer systems show current rectification characteristics because they contain a unipolar material, poly(FD), which yields an asymmetric electrochemical response in different scan directions. With the same bilayer structures grown on Au coated glass slides, followed by making contacts with a small drop of eutectic Ga-In liquid metal or metal leaf by the method of LOFO on the surface of bilayer films, we could successfully construct new types of organic p-n junction diode in the solid-state. The current-voltage curves of these bilayers are asymmetric and nonlinear, exhibiting typical diode characteristics. An electron trapping diagram is shown here to explain the phenomena of current rectification on bilayer modified electrodes in solution. The working mechanism of this type of organic diode was also explained by electron trapping diagrams.

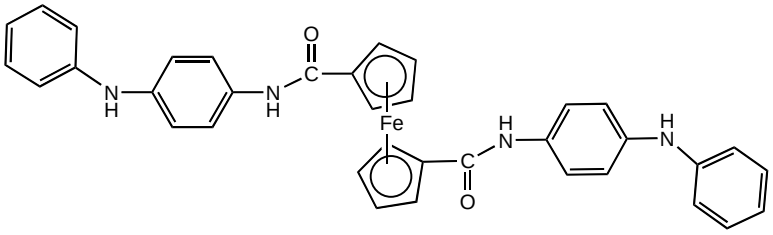

FD

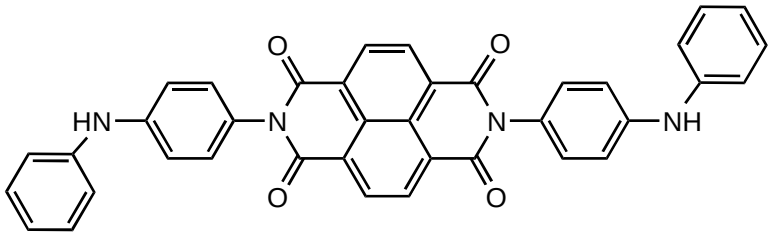

DNTD

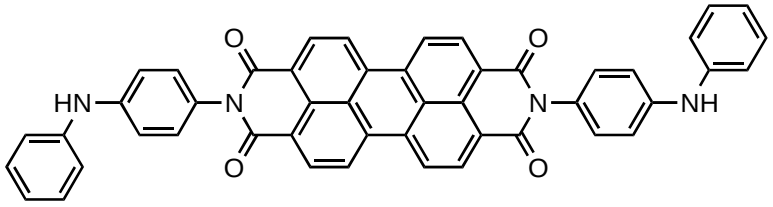

DPTD

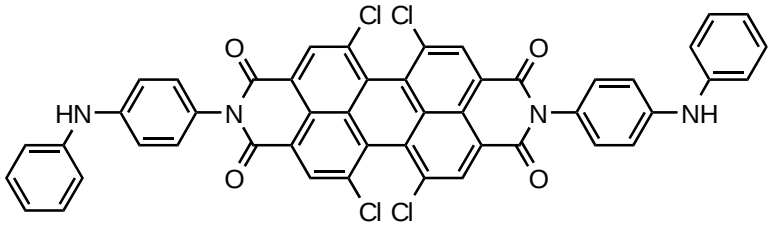

Cl_4DPTD

Figure 2-1 A series of monomers synthesized in our lab with structure motif of R-X-R, R=diphenylamine (DPA) group and electroactive unit X.

2.2 EXPERIMENTAL

2.2.1 Reagents and materials.

Methylene chloride (CH_2Cl_2, 99.9% Fisher) was freshly distilled from calcium hydride (CaH_2, Aldrich). Tetrabutylammonium hexafluorophospate, $TBAPF_6$ (Aldrich, 98%) was dried under vacuum at 100 ℃ for at least 48 hrs. The syntheses of DNTD, DPTD, Cl_4DPTD and FD are described in the literature.[31-33] Microscope glass slides (Fisherbrand) were cut into 8×25 mm pieces and coated with Au or Ag by sputter coating (EMS 550X). The resistance of these glass slides was 5-8 Ω/cm as detected by a two-probe ohmmeter. Liquid metal, Ga/In eutectic (Indium and Gallium were purchased from Aldrich) was used to form the circuit without destroying the polymeric layer. For gold and silver LOFO, 10-15 drops of HF (Fisher, 49%) were placed in a plastic cup with 50 ml de-ionized water. After metal leaves were floated on water surface, transfer these leaves to a clean bath with 5-8 drops of ethanol solution with 0.2 mM hexanethiol were added into 50ml the water. After 4-5 hrs, carefully place these leaves on bilayer modified glass slides.

2.2.2 Bilayer electropolymerization and thin film electrochemistry.

Cyclic voltammetry was performed on an electrochemistry working station with a modified AFRDE4 Bi-Potentiostat (Pine Instrument Co.) and a Universal Programmer (EG&G Model 175). A three-electrode cell was degassed with Argon, see Figure 2-2. Voltammograms were recorded on a computer equipped with a National Instrument data collector. The reference electrode was Ag/AgCl saturated with KCl, the counter electrode was a spiral Pt wire, and the

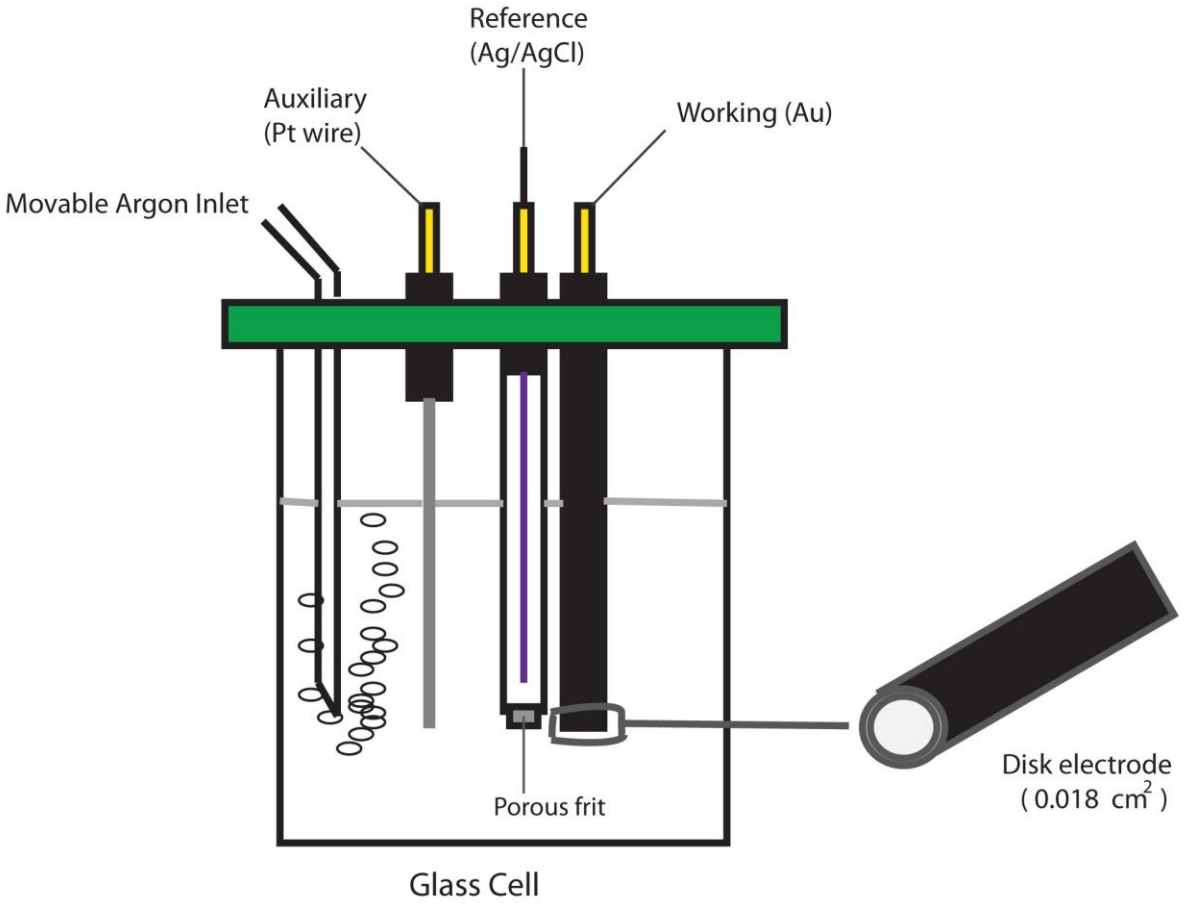

Figure 2-2 Three-electrode electrochemical cell with Argon degassing inlet

working electrodes were typically either a 1.5 mm diameter (0.018 cm^2) Au disk or a sputter-coated glass slide described above.

DNTD oxidative electropolymerization was performed in a CH_2Cl_2 solution with 0.1 M $TBAPF_6$ and DNTD monomer. The FD polymerization process was analogous to the DNTD method. DPTD and Cl_4DPTD are less soluble than DNTD in CH_2Cl_2. They were found to be soluble and electro-polymerizable from CH_2Cl_2 with small amounts (~5% V:V) of trifluoroacetic acid (TFA) and triethylamine (TEA, 2.5% V:V).[29] All of the polymeric thin film electrochemistry was performed with a scan rate of 200 mV/s.

2.2.3 Electrical contact.

This step was used to finish the circuit when measuring an I-V curve. As discussed previously, two methods were tried. A droplet of a Ga/In eutectic with diameter of approximately 1.0 mm was applied to the surface of bilayer thin films. The needle probes with a diameter approximately 0.1 mm were gently positioned onto the sputter coated Au film at one side and dipped into a Ga/In droplet gently under a microscope. This arrangement is shown in Figure 2-3. LOFO method was used to assemble gold or silver leaves on bilayer films and its procedure has been described in the literature.[27]

2.2.4 I-V Characteristics.

Two-point probe system (Signatone Model S-725) was used to acquire current-voltage (J-V) curves via connection to a Keithley 2400 Sourcemeter and a computer equipped with Labview® code programs for acquiring data. The potential moved normally as a step of 0.1 V or 0.2 V controlled by the program and the current-voltage data was recorded by the computer.

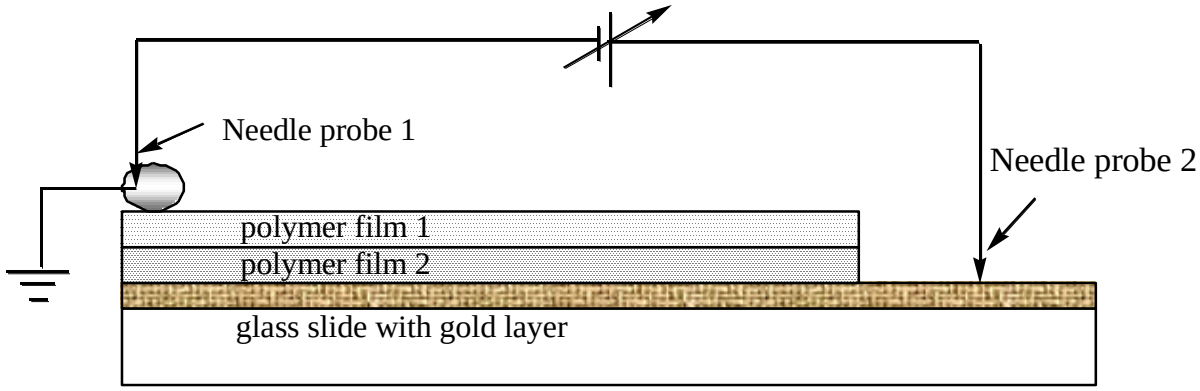

Figure 2-3. Diagram for measuring current-voltage characteristics of organic diodes

2.3 RESULTS AND DISCUSSION

The structures of monomers are shown in Figure 2-1, with a structural motif of R-X-R. DNTD contains two types of electroactive groups, a naphthalenetetracarboxylic diimide group and two flanking diphenylamine groups (R). FD is a monomer containing a ferrocene group and two flanking diphenylamine groups linked by an amide bond. Both of these monomers have been synthesized and used as electrochromic materials in our group.[31,32] DPTD was first synthesized by L.Wang [28] and further investigated by Q.Wang [29] and Hao.[34] Cl_4DPTD was synthesized and electropolymerized as an air-stable electrochromic material by Liang.[30] All of these monomers are easily polymerized/copolymerized in their solutions and detailed research was performed by L.Wang ,[31] Q.Wang, [29] and Liang.[30]

2.3.1 Single film growth on gold electrode

Since FD and DNTD show good solubility in CH_2Cl_2, they are used to investigate single film growth kinetics on a gold electrode. Both FD and DNTD growth rates are concentration dependent and there is roughly a linear relationship based on monomer solutions with different concentration varying from 0.1 mM to 0.6 mM; this is consistent with Q.Wang's results.[29] The relationship between each growth cycle on a 0.018 cm^2 Au electrode and its corresponding charge of 0.3 mM DNTD and 0.3 mM FD are also shown in Figure 2-4 and 2-5, respectively. Their typical growth cyclic voltammograms are also inserted in their deposition plots. For each monomer, 5 runs were performed and the average of the integrated cathodic and anodic current regions was used to evaluate the charge. The standard deviation is shown for the 5 runs. The plot

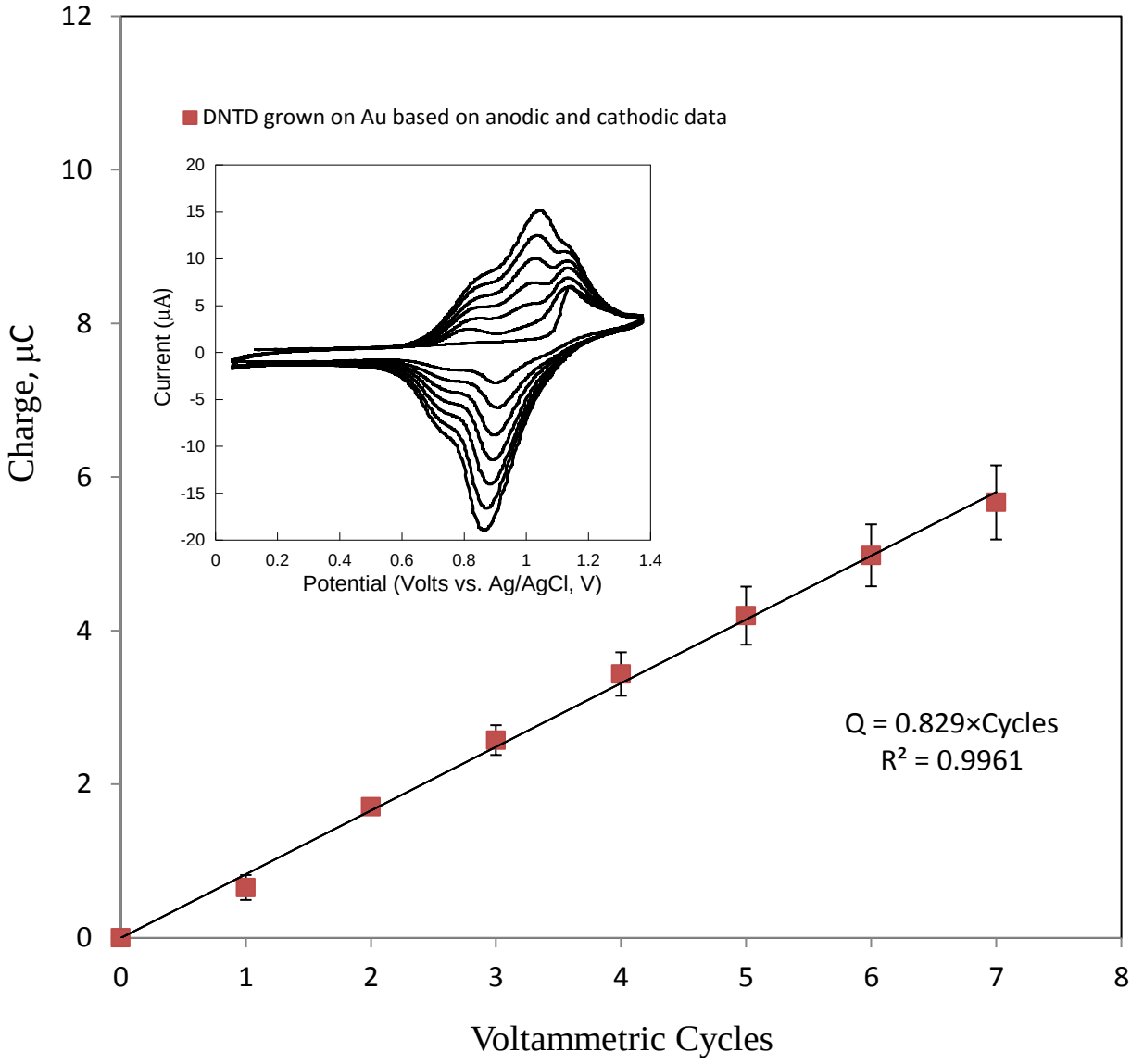

Figure 2-4 Charge vs. voltammetric cycles for the oxidative electropolymerization on a 0.018 cm^2 Au electrode at room temperature, with 0.1 M $TBAPF_6$ in 0.3 mM DNTD CH_2Cl_2 and a scan rate of 200 mV/s, charge was integrated from 0.5 V to 1.2V(±0.05V).

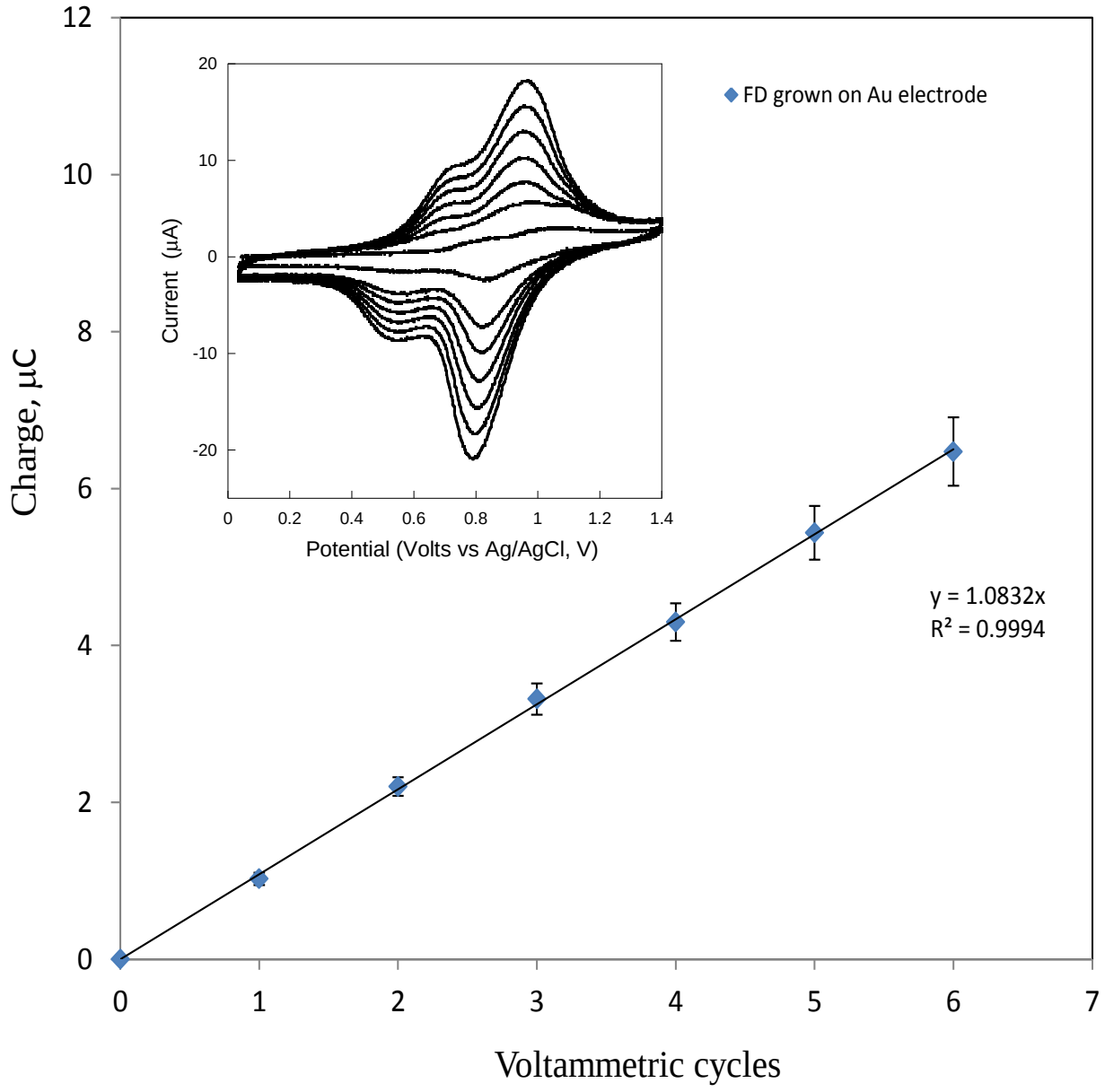

Figure 2-5 Charge vs. voltammetric cycles for FD oxidative electropolymerization on a 0.018 cm^2 Au electrode at room temperature, with 0.1 M $TBAPF_6$ in 0.3 mM FD CH_2Cl_2 and a scan rate of 200 mV/s, charge was integrated from 0.5 V to 1.2V(±0.05V).

shows that 0.829 μC of charge passed for each cycle for 0.3 mM DNTD. This is equal to 1.19×10^{-9} mol/cm^2 DNTD grown for each voltammetric cycle. For 0.3 mM FD, the charge for each cycle is about 1.08 μC, corresponding 1.03×10^{-9} mol/cm^2 FD deposited. From the growth data, we can see that DNTD has slightly higher electronic conductivity than FD. FD has three redox species in oxidation,[31] DPB^0/DPB^+, DPB^+/DPB^{2+} and Fc/Fc^+, but DNTD has only two DPB cation species for each electrochemical cycle.[32]

2.3.2 Formation of polymeric bilayers

Figure 2-6 and 2-8 describe cyclic voltammograms of poly(FD) grown on poly(DNTD) (also shown as poly(FD)|poly(DNTD)) and poly(DNTD) grown on poly(FD) (poly(DNTD)|poly(FD)), respectively. For poly(FD)|poly(DNTD), the first scan shows two separated diphenyl benzidine (DPB) redox peaks, which are similar to the peaks of poly(DNTD) single layers, which was shown in Chapter 1. Later scans show these two peaks overlap and become a big peak. The peak current increases upon scanning showing increasing amounts of the second layer grown on the surface of first layer. The growth of poly(DNTD) on poly(FD) (Figure 2-8) also shows the same phenomenon as poly(DNTD)|poly(FD) (see in Figure 2-6). Moreover, as the calculated charge in each cycle shows the polymer thin film growth on top of another is still linear, as shown on Figure 2-7 and 2-9. This experiment was performed 5 times on each bilayer and the average and standard deviation of cathodic and anodic charge were used as the value of charge and error bar for each run. From the bilayer growth data, we can see that for each cycle, 8.9×10^{-10} mol/cm^2 FD is grown on the poly(DNTD) modified electrode in 0.3 mM FD

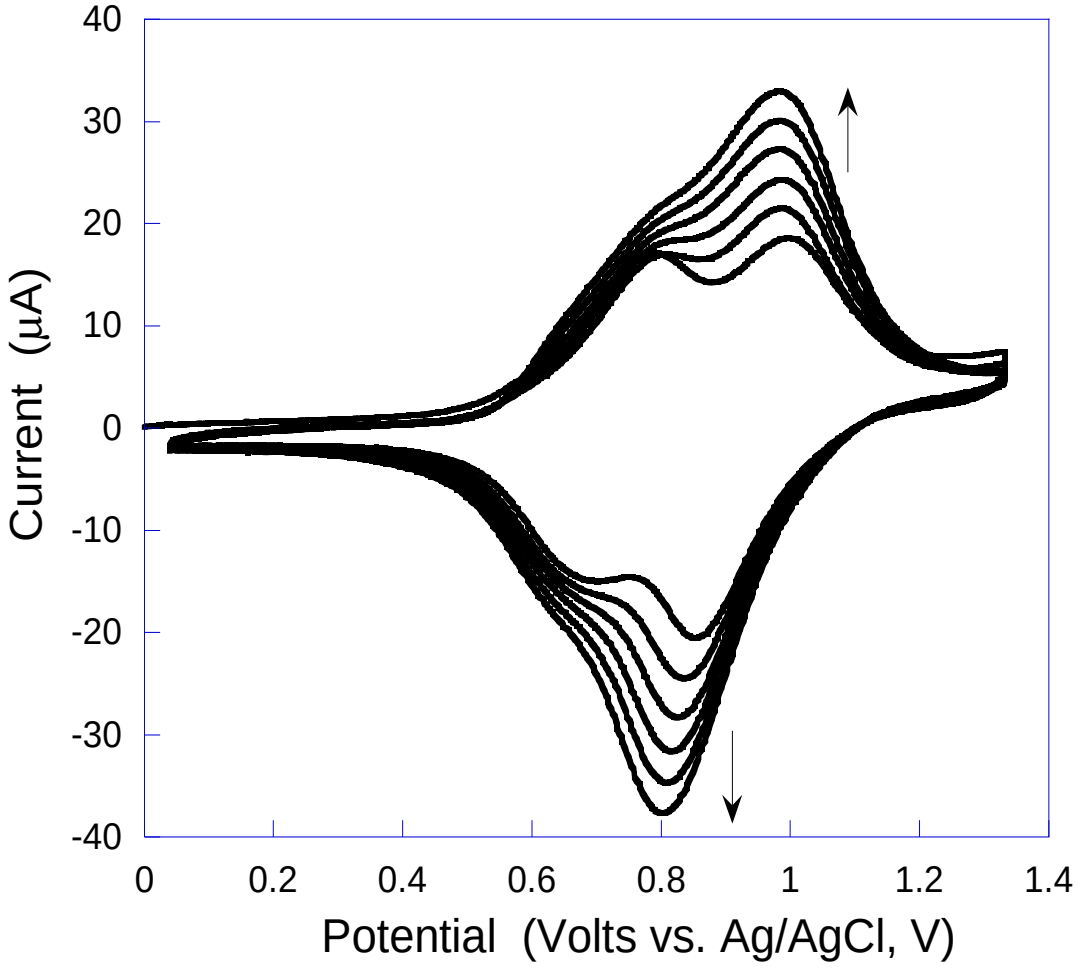

Figure 2-6 Cyclic voltammogram of poly(FD) grown on poly(DNTD) on a 0.018 cm^2 Au electrode at room temperature, with 0.3 mM FD and 0.1 M $TBAPF_6$ in CH_2Cl_2 and a scan rate of 200 mV/s.

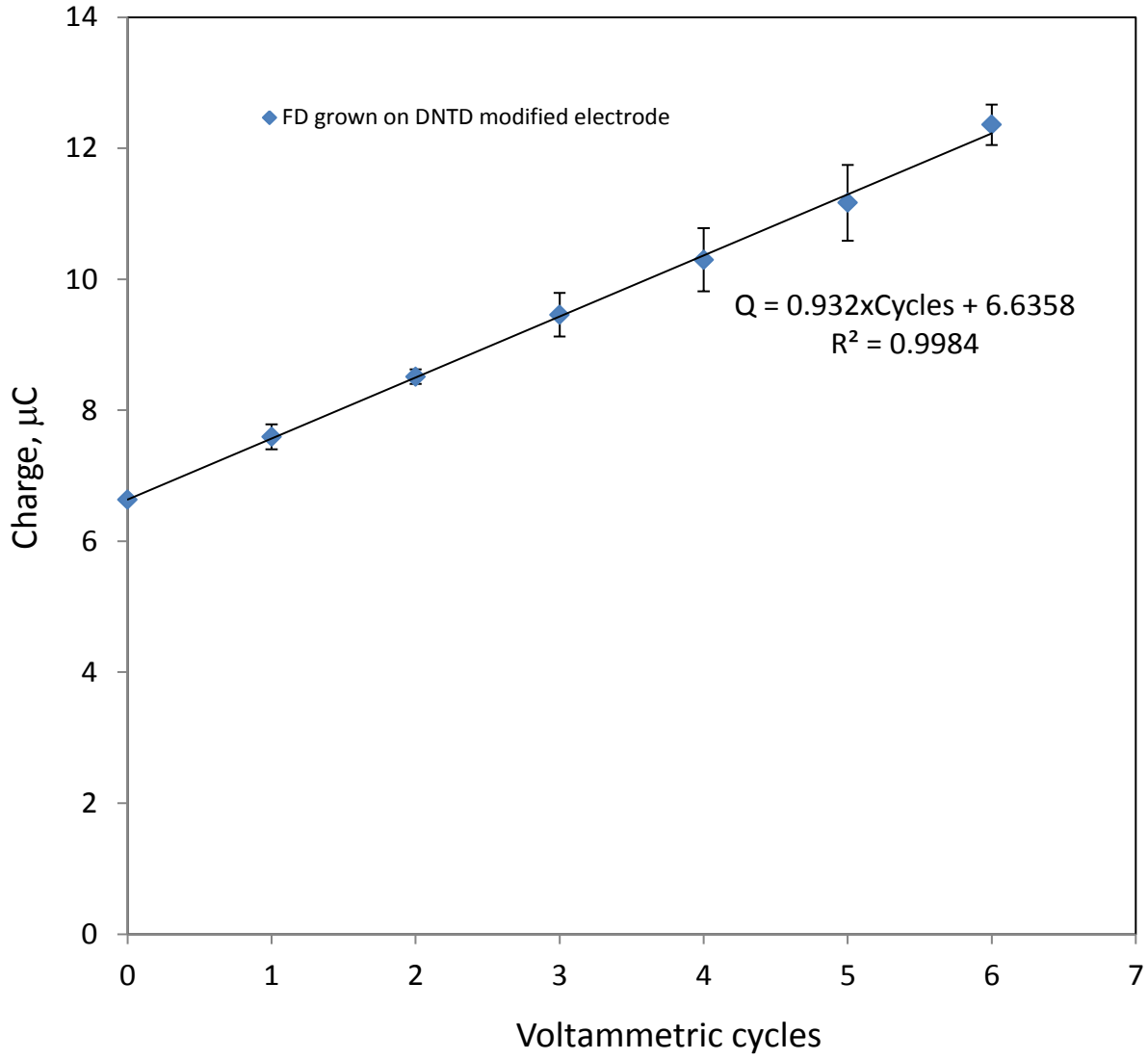

Figure 2-7. Charge vs. voltammetric cycles in poly(FD) grown on poly(DNTD) on a 0.018 cm^2 Au electrode at room temperature, with 0.3 mM FD and 0.1 M $TBAPF_6$ in CH_2Cl_2 and a scan rate of 200 mV/s, charge was integrated from 0.5 V~1.2V(±0.05V).

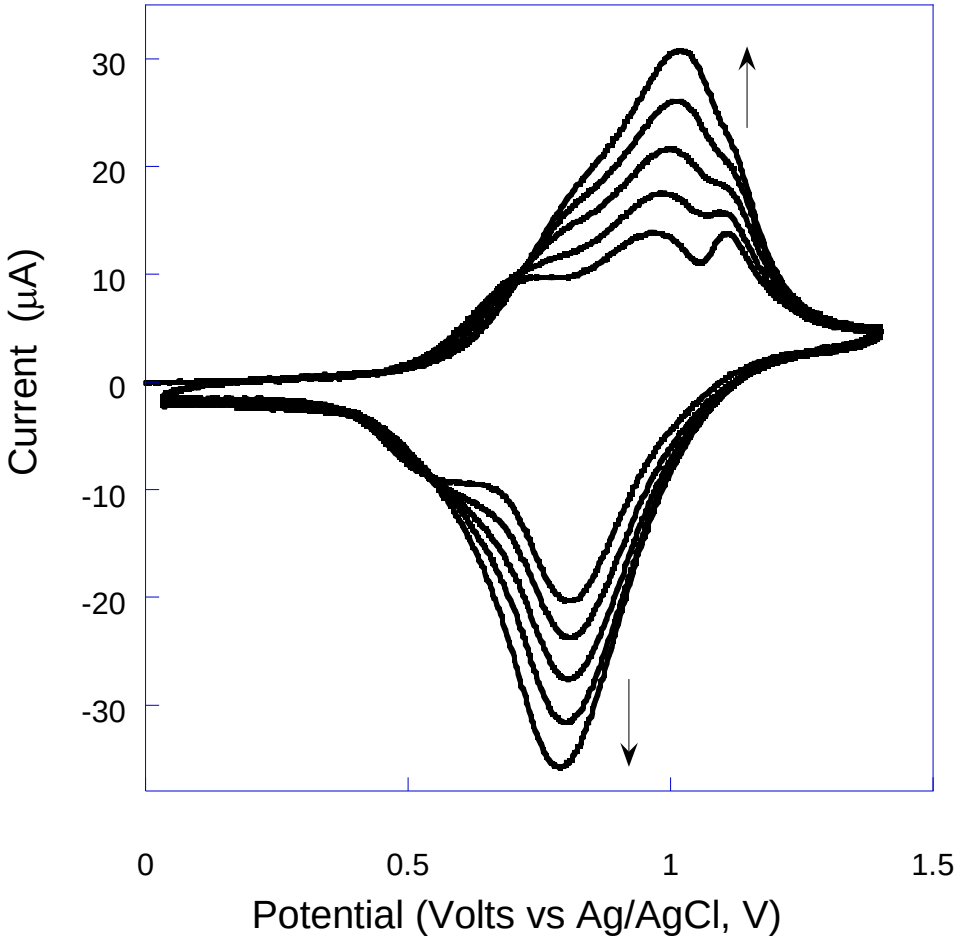

Figure 2-8 Cyclic voltammogram of poly(DNTD) grown on poly(FD) on a 0.018 cm^2 Au electrode at room temperature, with 0.3 mM DNTD and 0.1 M $TBAPF_6$ in CH_2Cl_2 and a scan rate of 200 mV/s.

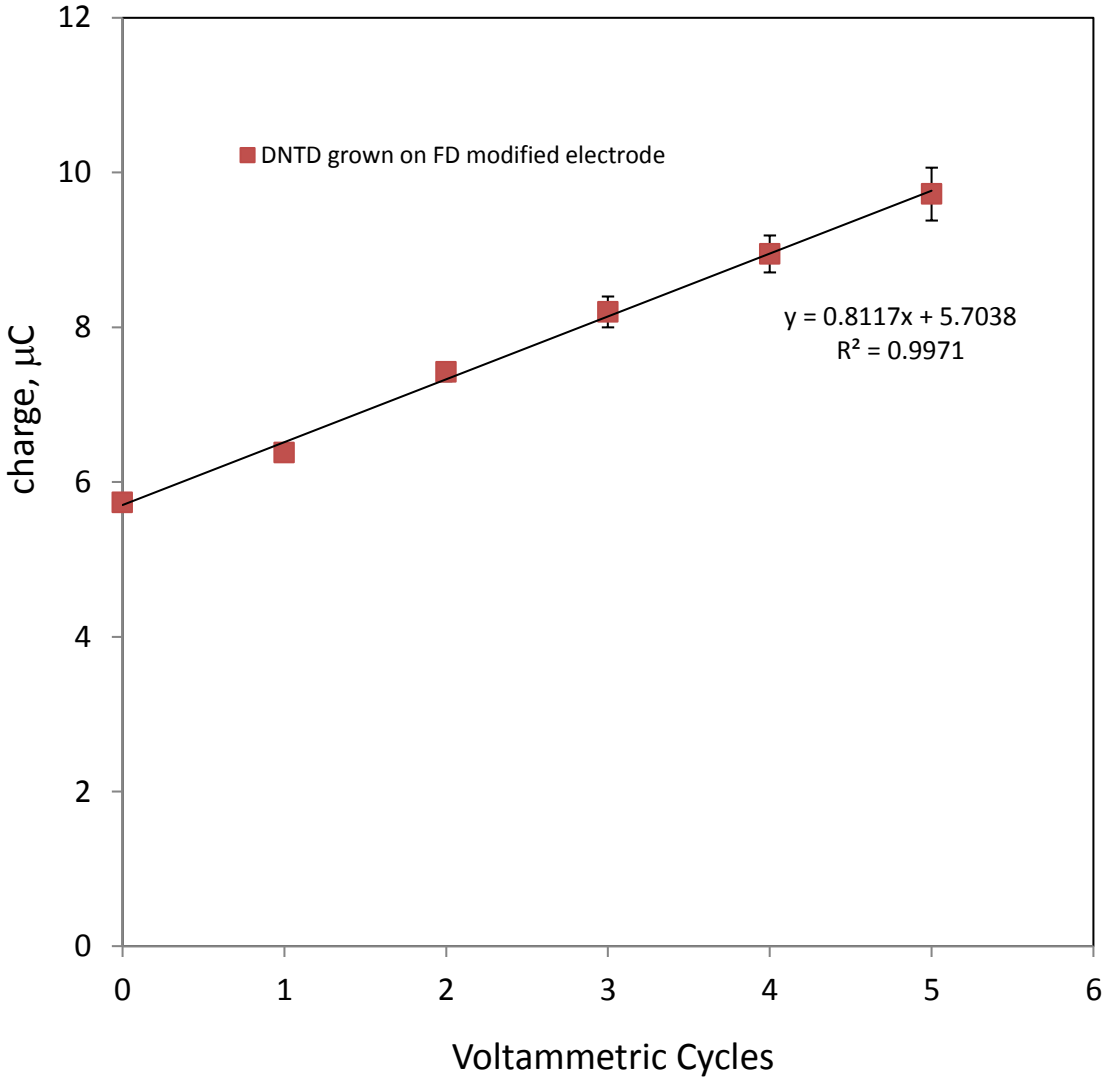

Figure 2-9 Charge vs. voltammetric cycles in poly(DNTD) grown on poly(FD) with the same growing conditions of Figure 2-8, charge was integrated from 0.5 V to 1.2V(±0.05V).

solution and 1.14×10^{-9} mol/cm^2 DNTD is grown on poly(FD) in 0.3 mM DNTD, which both have slightly slower growing rate as compared to the one grown on an Au electrode surface.

2.3.3 Bilayer polymer films in solution

Figure 2-10 compares the voltammograms for the same Au electrode, modified with a single layer of poly(DNTD) (dash line) and then FD was deposited on top to form poly(DNTD)|poly(FD) bilayer (solid line) scanned in CH_2Cl_2 with 0.1 M $TBAPF_6$. For the Au|poly(DNTD)|poly(FD) bilayer, there are two redox peaks at positive and negative potentials, respectively. The significant increase of the redox current in the positive potential region corresponds that a FD film formed on a DNTD film. However, in the negative potential region the area of the diimide redox is almost the same as the single poly(DNTD) film. This can also be verified from the integrated current at positive potentials, which is much higher than that at negative potentials. The Au|poly(DNTD)|poly(FD) bilayer has around 1.47×10^{-8} mol/cm^2 of poly(DNTD) and 8.65×10^{-9} mol/cm^2 of poly(FD) (the charge is about 12.50×10^{-6} C) compared to 1.47×10^{-8} mol/cm^2 of poly(DNTD) single layer (6.64×10^{-6} C of charge), but at negative potentials, the charge of the bilayer is almost the same as single poly(DNTD) layer. Figure 2-11 also demonstrates the relationship between peak current and scan rates of this kind of bilayer. For poly(DNTD) and poly(DNTD)|poly(FD), the peak currents for the reduction and oxidation of the surface coated single or bilayer vary linearly under different sweep rates. This confirms the behavior expected for the surface-immobilized redox species for both, which was discussed in Chapter 1 and the peak current and sweep rates obey the relationship described in equation 1-5.

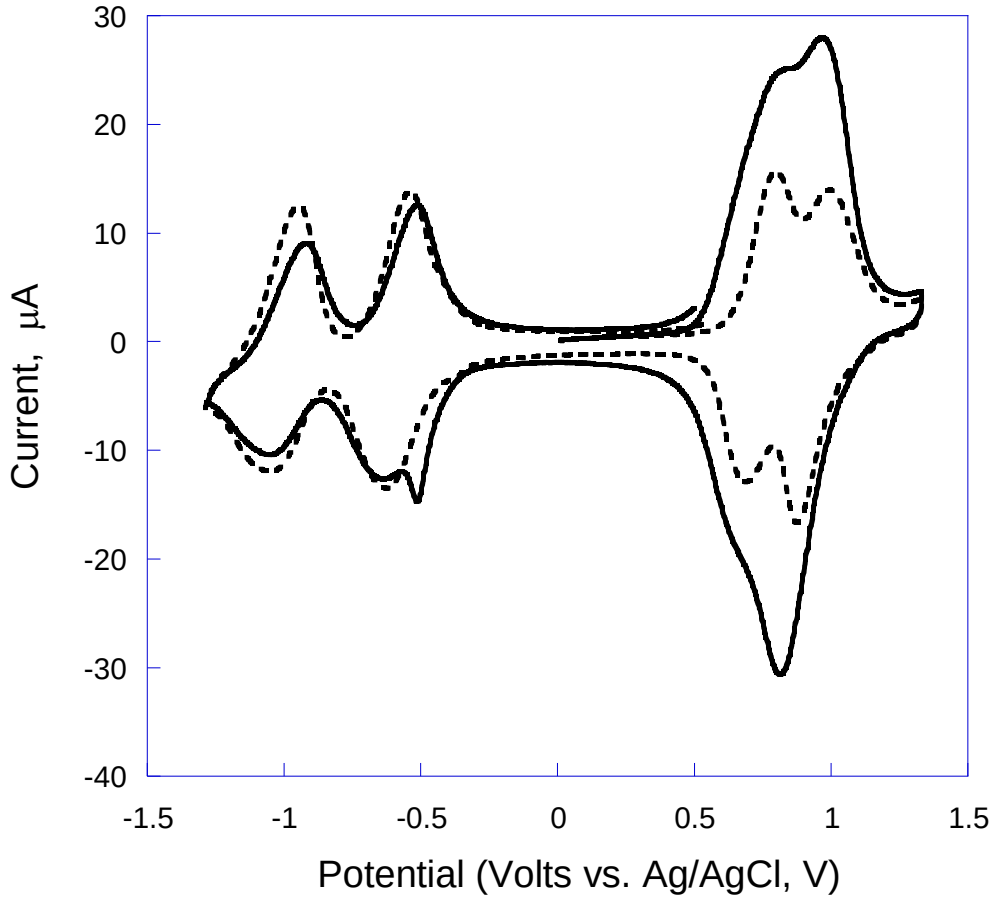

Figure 2-10 Electrochemistry of a bilayer (solid line) with Au|poly(DNTD)|poly(FD) vs. the underlying single layer Au|poly(DNTD) (dash line) scanned in 0.1 M $TBAPF_6$ CH_2Cl_2 solution at room temperature and a scan rate of 200 mV/s.

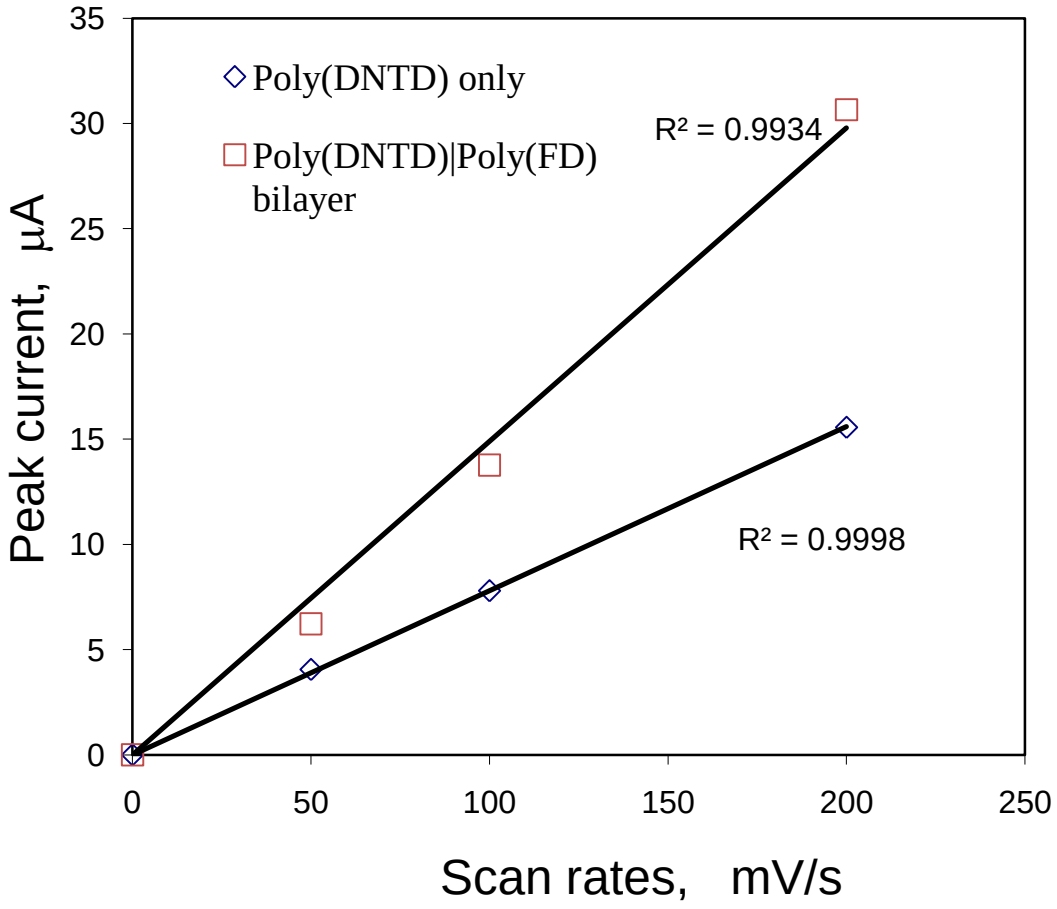

Figure 2-11. Linear relationship between peak current vs. scan rates based on poly(DNTD) and poly(DNTD)|poly(FD) bilayer in 0.1 M $TBAPF_6$ CH_2Cl_2 with $\Gamma_{poly(DNTD)} = 1.47 \times 10^{-8}$ mol/cm^2 and $\Gamma_{poly(FD)} = 8.65 \times 10^{-9}$ mol/cm^2, data shown here is from the first oxidative peak.

An inverted bilayer arrangment was also studied. The voltammograms for a bilayer of poly(FD) as inner layer and poly(DNTD) as the outer layer and the underlying poly(FD) was recorded and compared in Figure 2-12. When the bilayer modified Au electrode was scanned from -1.2 V to +1.4 V vs. Ag/AgCl, in the positive potential region, both anodic and cathodic peaks of the bilayer film are much larger than those of the pure poly(FD) film. The two separated peaks correspond to DPB^0/DPB^+ and on overlapping peak of DPB^+/DPB^{2+} and Fc^0/Fc^+. This indicates that a significant amount of poly(DNTD) film (1.05×10^{-8} mol/cm^2) was formed on the poly(FD) film (1.13×10^{-8} mol/cm^2). At negative potentials, the diimide peaks of the DNTD film are not observed. This phenomenon shows that the outer layer of poly(DNTD) was insulated by the inner poly(FD) layer at negative potentials, since the FD film is electroactive in the positive potential region but electrochemical inactive at the negative scan. Transport of electrons from the electrode to poly(DNTD) were blocked by the poly(FD) film and finally the reduction of naphthalene diimide groups cannot occur at negative potentials.

The charge transfer in bilayer film systems is illustrated in Scheme 2-1 for bilayer Au|poly(DNTD|poly(FD). In Scheme 2-1A, where positive potentials are applied to the bilayer of Au|poly(DNTD|poly(FD), when the voltage arrives near the first formal potential (~+0.81 V) or more, DPB^0 will be oxidized into DPB^+. The charge from DPB^0 unit in poly(DNTD) will easily transfer to Au. DPB^0 units of poly(FD) can then reduce DPB^+ in poly(DNTD), resulting in one electron transfer to the layer of poly(DNTD). This shows that, at positive potentials, both layers give electrochemical responses and the charge in the whole process is the sum of both layers. However, as showed in Scheme 2-1B if the bilayer was scanned to negative potentials

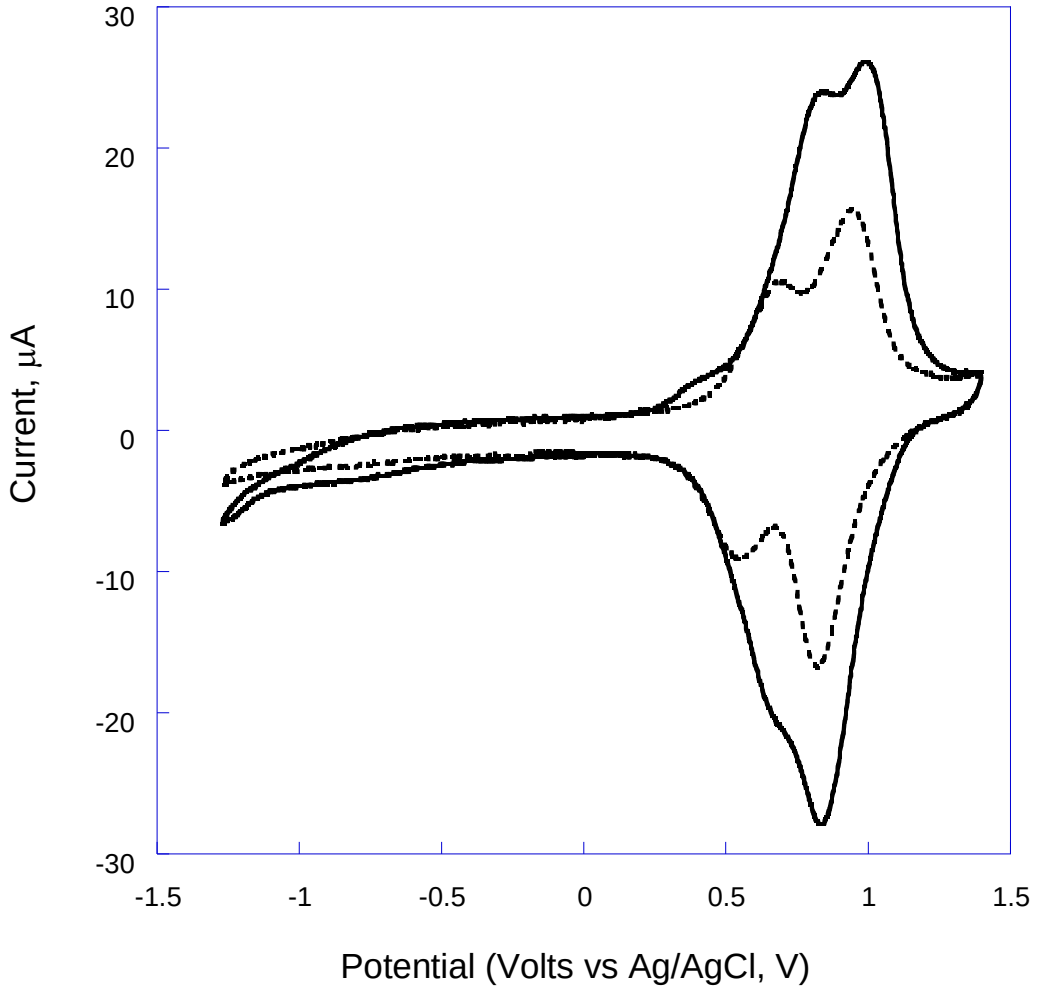

Figure 2-12. Electrochemistry of Au|poly(FD)|poly(DNTD) bilayer (solid line) vs. the underlying single layer Au|poly(FD) (dash line) scanned in 0.1 M $TBAPF_6$ CH_2Cl_2 solution at room temperature and a scan rate of 200 mV/s.

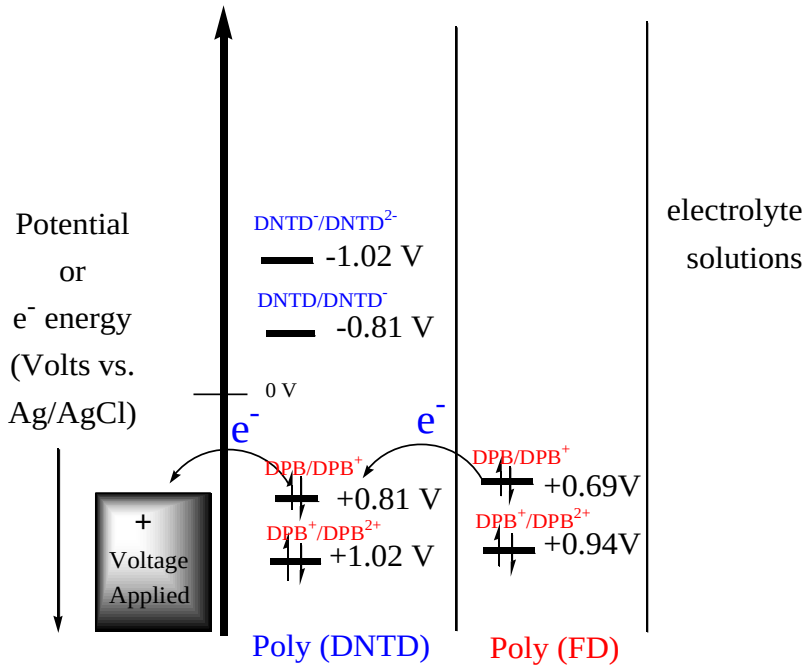

A: Positive potentials applied

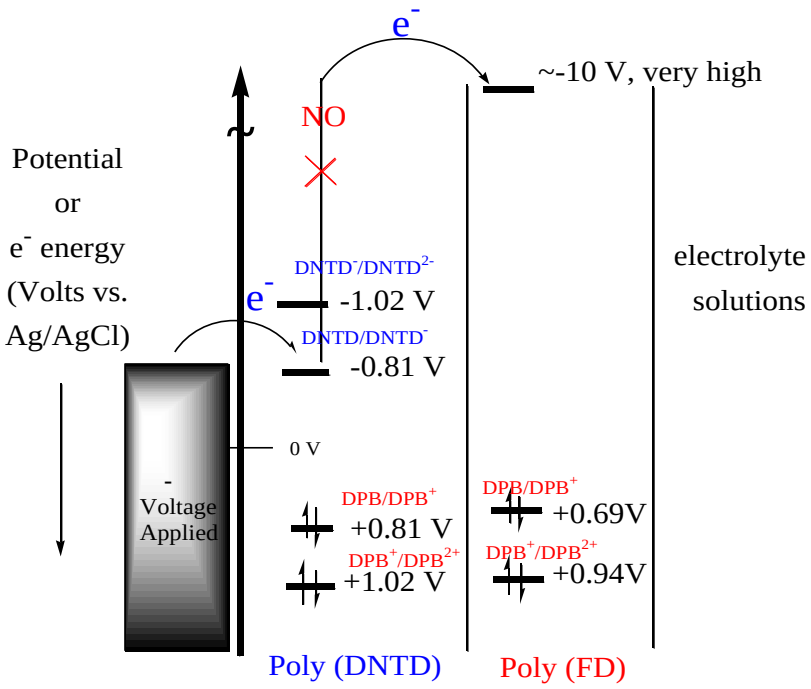

B: Negative potentials applied

Scheme 2-1 Electron transfer in bilayer Au|poly(DNTD)|poly(FD) scanned in solution with $TBAPF_6$.

vs. Ag/AgCl, when the potential is changed to ~-0.81 V or more negative, the electrons in Au have enough energy to fill poly(DNTD) LUMO and form $DNTD^-$ unit (first reduced form). Since poly(FD) has no reducible units at this potential, poly(FD) will not have any electrochemical response and will be an insulator at negative potentials. The passed charge at negative potentials for bilayer is the same as the single poly(DNTD).

Scheme 2-2 depicts charge transfer for Au|poly(FD)|poly(DNTD). At the positive potentials shown in Scheme 2-2 A, since both poly(DNTD) and poly(FD) have DPB redox couples, and DPB^+/DPB^{2+} and Fc^0/Fc^+ have closely matched oxidation potentials, those redox species are all electro-active, which yields a bilayer peak current higher than that of a single layer and acts similarly to Au|poly(DNTD)|poly(FD). However, when poly(FD) film as inner bilayer was scanned to negative potentials, due to the electro-inactivity of poly(FD), there is no reduction peak until -1.2 V. As Scheme 2-2 B shows, the electron energy is insufficient to transfer electrons into the LUMO energy level of poly(FD) at potential of -1.2 V. Since no electrons transfer from the Au electrode to the poly(FD) film, the outer poly(DNTD) layer will be blocked from reduction to $DNTD^-$. The outer poly(DNTD) layer is isolated by poly(FD) at negative potential scans.

Overall, only a unidirectional current flow is observed, showing rectifying behavior at the Au electrode|poly(FD) interface in electrolyte solution. Also, that current flow through Au|poly(DNTD)|poly(FD) at positive applied potentials is much higher than that at negative potentials, giving the characteristics of current rectification at same positive/negative voltage value. The bilayers of poly(FD)/poly(DPTD) and poly(FD)/poly(Cl_4DPTD) also show the same

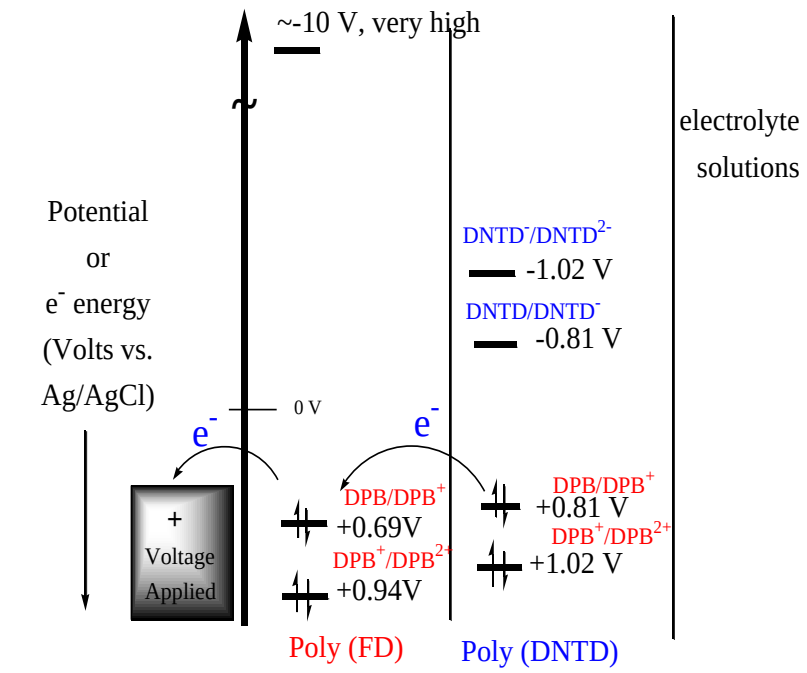

A: Positive applied potentials, electron transferred

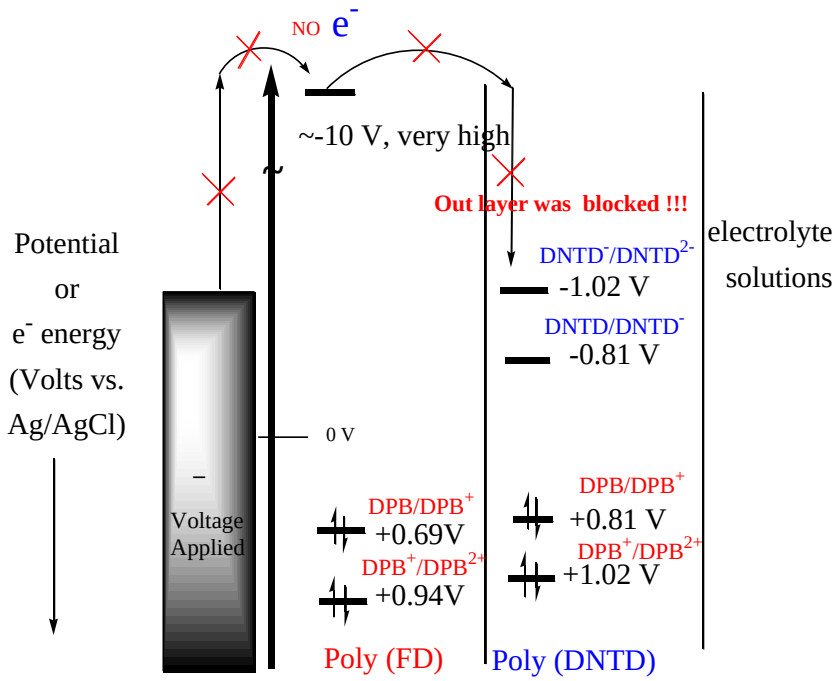

B: Negative applied potentials, electron blocked

Scheme 2-2 Electron transfer and blocking in bilayer Au|poly(FD)|poly(DNTD) vs. Ag/AgCl scanned in solution with $TBAPF_6$.

properties as poly(FD)/poly(DPTD). Their voltammograms are shown in Figure 2-13 and 2-14, which was recorded the bilayer voltammograms of poly(FD)/poly(DPTD) and poly(FD)/poly(Cl_4DPTD), respectively. They also show the same characteristics as poly(FD)/poly(DNTD) bilayer films as compared to the poly(DPTD) and poly(Cl_4DPTD) monolayer electro-responses described in Chapter 1 (see section 1.5.2).

2.3.4 Organic diodes based on polymeric bilayer films

Bilayers similar to those in section 2.3.3 were contacted with a droplet of Ga/In eutectic instead of an electrolyte solution to form solid state devices. Electrical characterization shows that the device can actually pass more steady-state current upon application of potential in one direction than in the other. Typical current-voltage (*J*-*V*) characteristics for bilayers consisting of poly(FD) grown on poly(DNTD) and poly(DNTD) grown on poly(FD) are presented in Figure 2-15 and 2-16, respectively. The poly(DPTD)/poly(FD) bilayers also show the similar *J*-*V* characteristics at the same structure arrangement of bilayer as poly(DNTD)/poly(FD) system, their *J*-*V* curves are shown in Figure 2-17 and Figure 2-18. Rectification of current was observed in films made from these polymer bilayers. The system of Au|poly(DNTD)|poly(FD)|GaIn exhibits a positive turn-on voltage at around +0.53 V where a negative turn on voltage (forward bias) of -2.5 V is detected for Au|poly(FD)|poly(DNTD)|GaIn. Both organic diodes have high break-down voltages (reverse bias), of around +9.2 V for Au|poly(DNTD)|poly(FD)|GaIn and around -6.4 V for Au|poly(FD)|poly(DNTD)|GaIn. The rectification ratio ($RR=I_{forward}/I_{reverse}$) is as high as 260 at ±4.8 V for poly(DNTD) as inner layer and 650 for poly(FD) as inner layer at ±1.5 V, respectively, see Figure 2-19. Here, poly(FD) plays a role of p-type semiconductor and

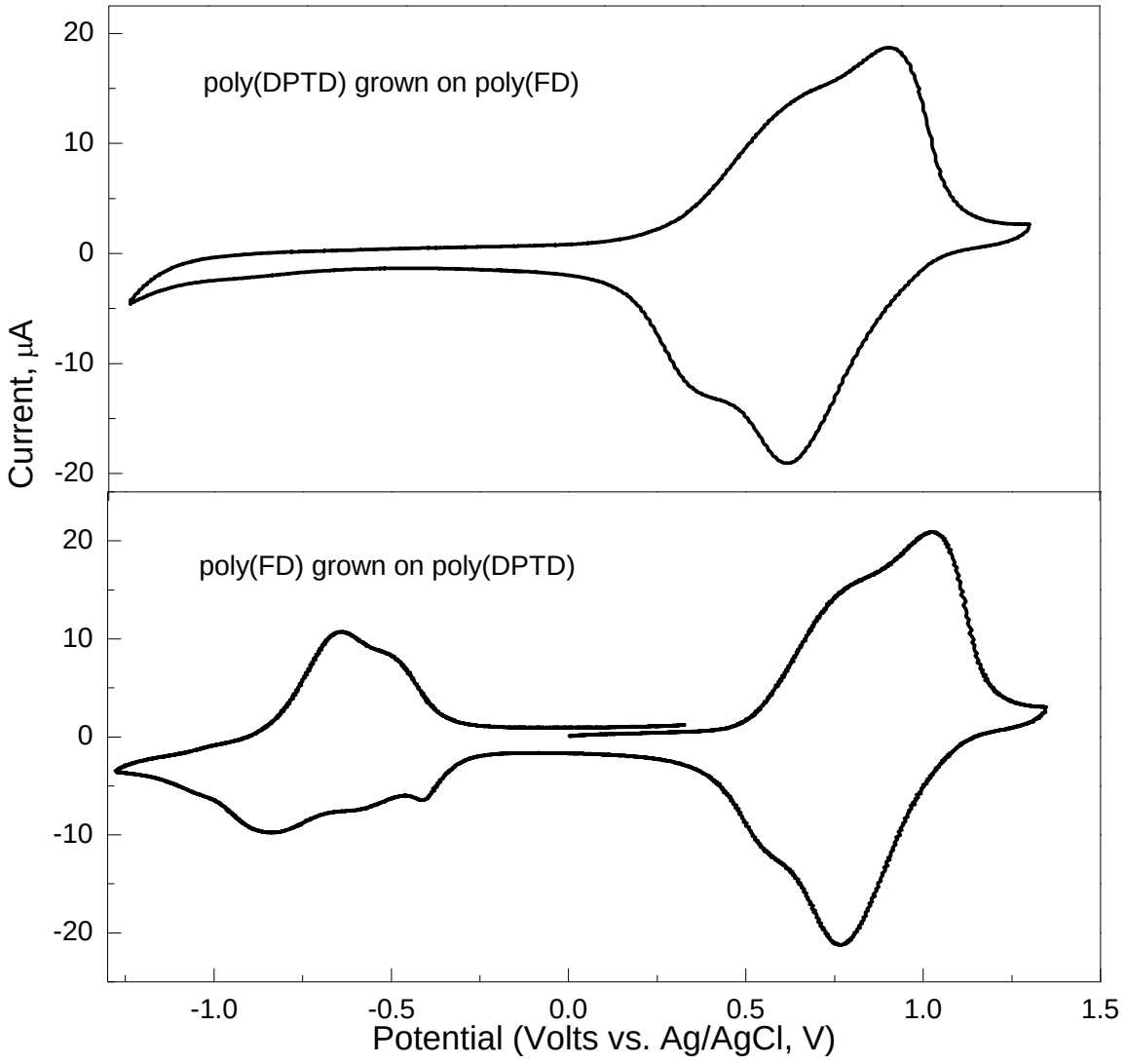

Figure 2-13. The cyclic voltammograms of poly(FD)/poly(DPTD) bilayers on 0.018 cm^2 Au electrode, performed in CH_2Cl_2 with 0.1 M $TBAPF_6$ at room temperature and a scan rate of 200 mV/s.

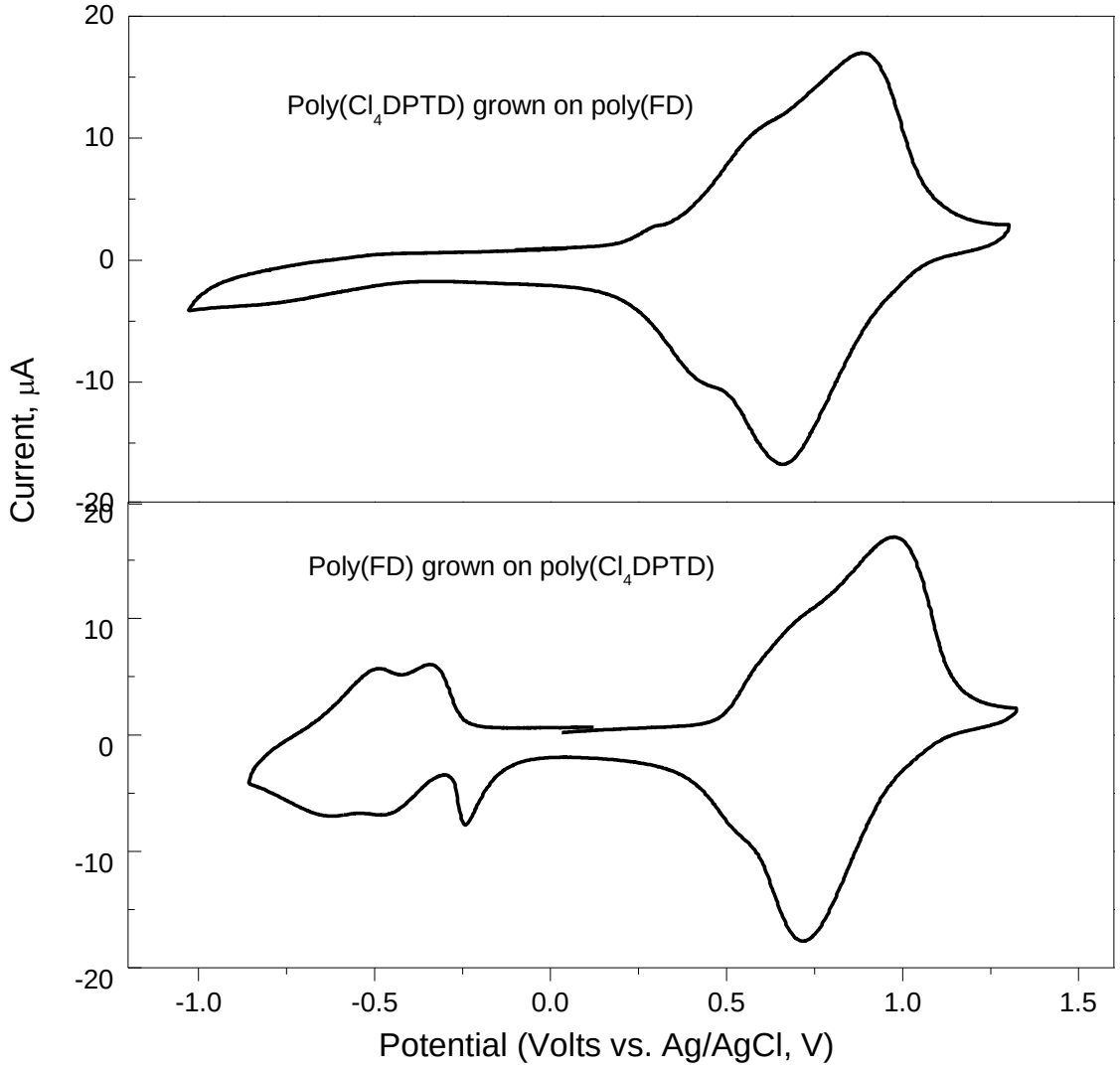

Figure 2-14. The cyclic voltammograms of poly(FD)/poly(Cl_4DPTD) bilayers on a 0.018 cm^2 Au electrode, performed in CH_2Cl_2 with 0.1 M $TBAPF_6$ at room temperature and a scan rate of 200 mV/s.

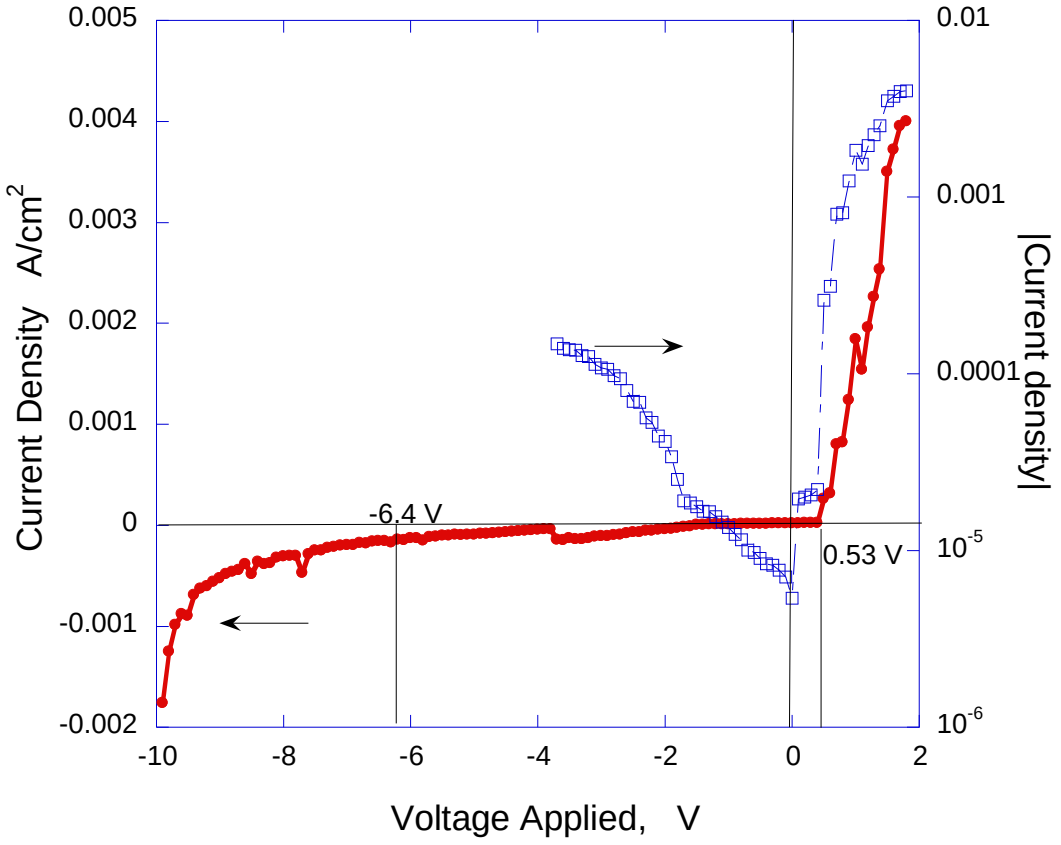

Figure 2-15. I-V characteristics of a Au|poly(FD)|poly(DNTD)|Ga-In organic diode with $\Gamma_{poly(DNTD)}=6.19\times10^{-9}$ mol/cm^2 and $\Gamma_{poly(FD)}=3.65\times10^{-9}$ mol/cm^2 under air and at room temperature.

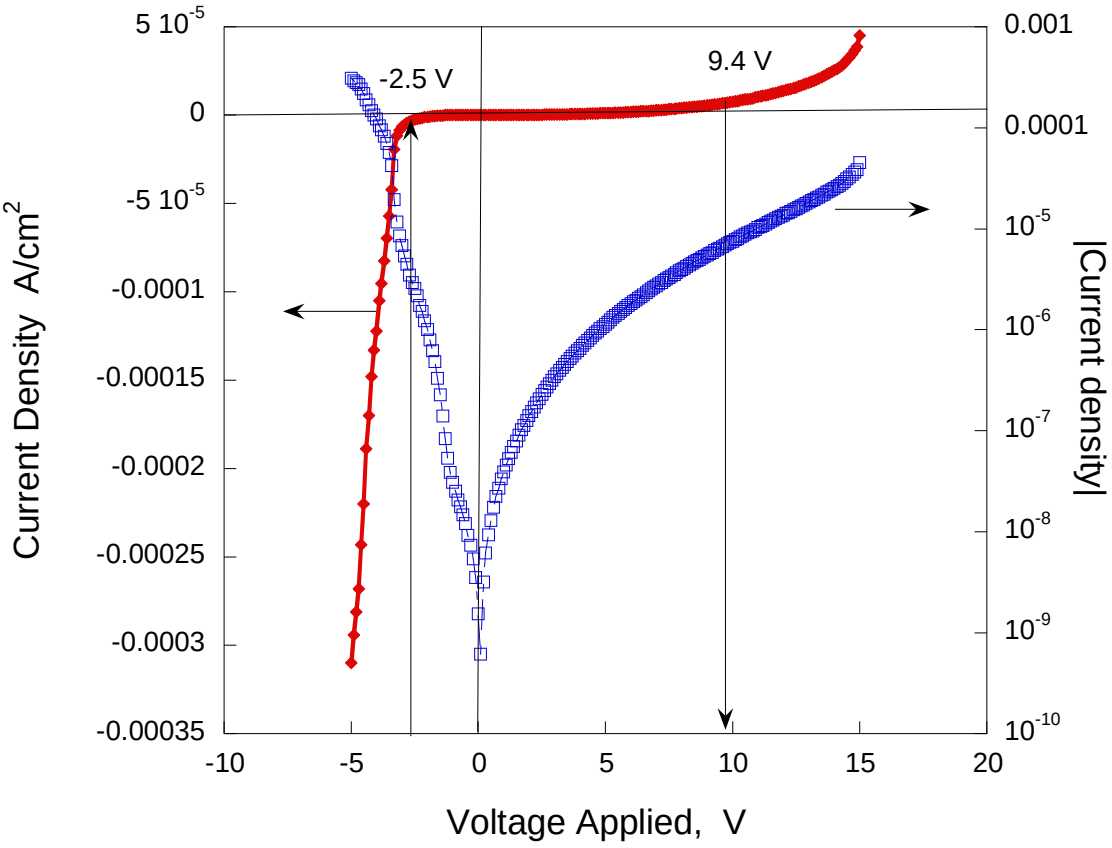

Figure 2-16. I-V characteristics of an Au| poly(DNTD)|poly(FD)|Ga-In organic diode with $\Gamma_{poly(DNTD)}=8.5\times10^{-9}$ mol/cm^2 and $\Gamma_{poly(FD)}=4.82\times10^{-9}$ mol/cm^2 under air and at room temperature.

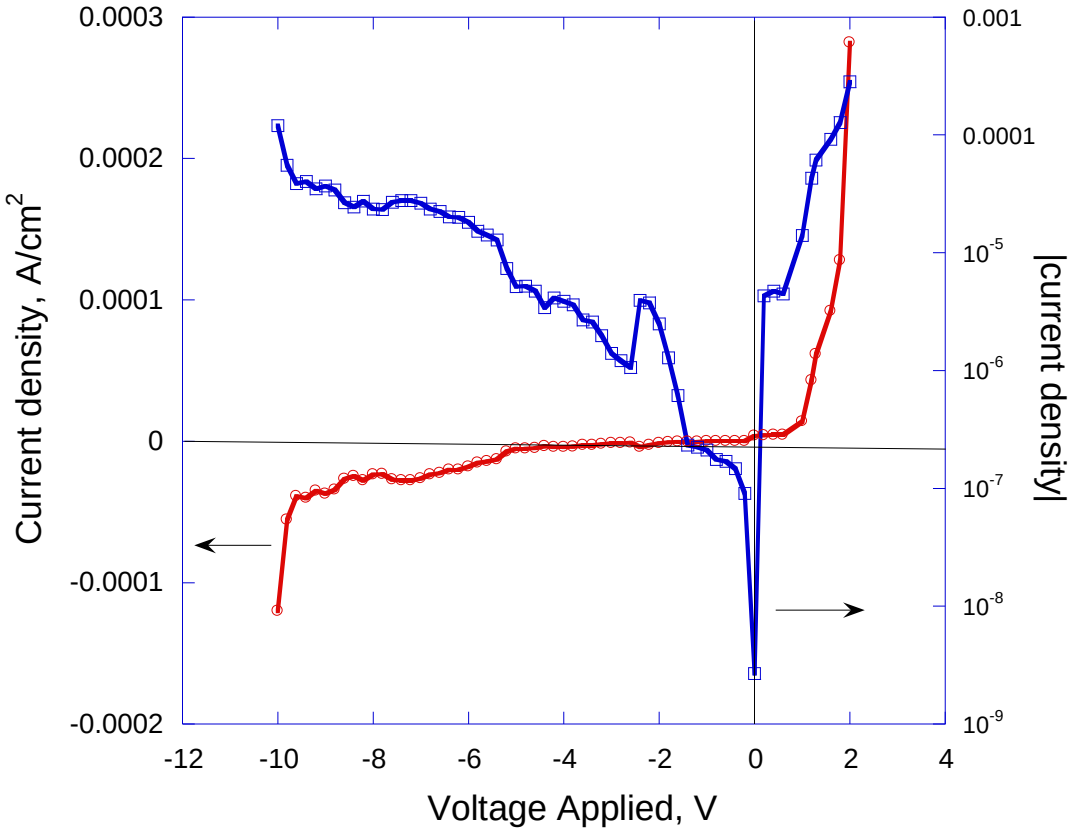

Figure 2-17. I-V characteristics of an Au|poly(FD)|poly(DPTD)|Ga-In organic diode with $\Gamma_{poly(DPTD)}=2.43\times10^{-9}$ mol/cm^2 and $\Gamma_{poly(FD)}=3.22\times10^{-9}$ mol/cm^2 under air and at room temperature.

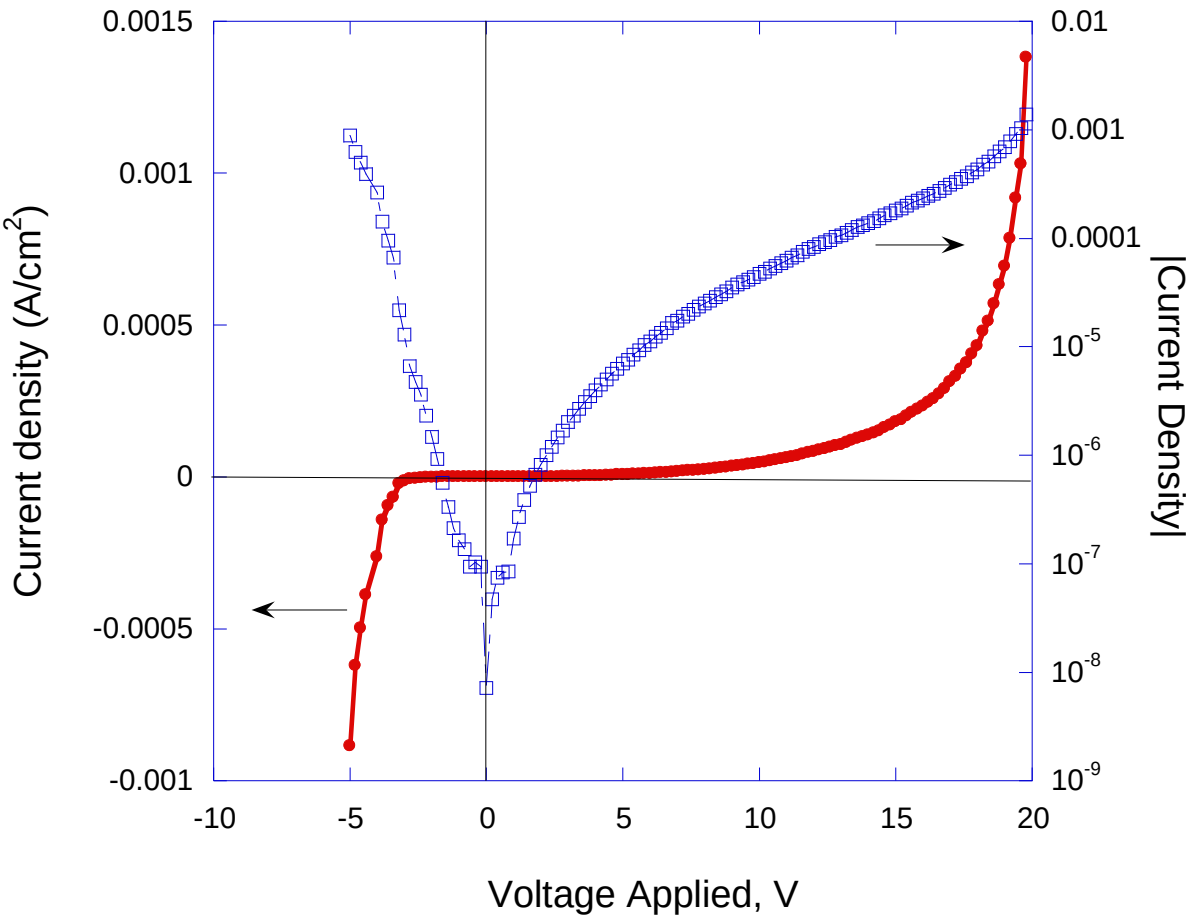

Figure 2-18. I-V characteristics of an Au|DPTD|FD|Ga-In organic diode with $\Gamma_{poly(DPTD)}=2.22\times10^{-9}$ mol/cm^2 and $\Gamma_{poly(FD)}=3.76\times10^{-9}$ mol/cm^2 under air and at room temperature.

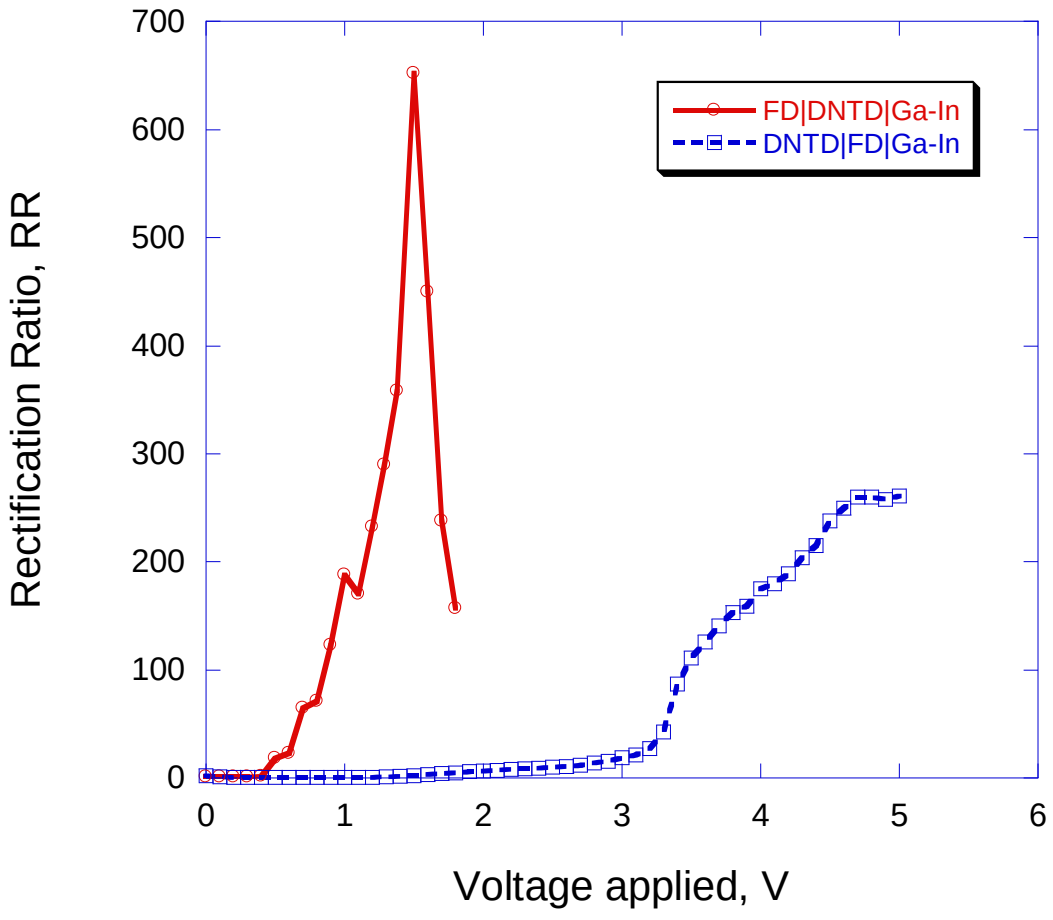

Figure 2-19 Rectification ratio of poly(DNTD)/poly(FD) diodes

the other polymer, poly(DNTD), poly(DPTD) or poly(Cl_4DPTD) works as n-type material.

Here, we use the Au|poly(DNTD)|poly(FD)|GaIn structure as an example, shown in Scheme 2-3 to explain the electron blocking process of these organic diodes in the solid-state. As shown in Scheme 2-3A, when a negative voltage was applied to the Au-coated side and positive voltage applied to poly(FD) side, a relatively small negative potential can reduce poly(DNTD) (low reduction formal potential of poly(DNTD)) and an electron will fill the LUMO. At the same time, the poly(FD) also exhibits a low oxidation formal potential, which induces the HOMO of poly(FD) to lose an electron. The energy difference between LUMO of poly(DNTD) and HOMO of poly(FD) allows electrons to transfer from the LUMO of poly(DNTD) and fill the HOMO of oxidized poly(FD). The electrons move forward (current flows) at the small voltage difference between poly(DNTD) and poly(FD), which produces a small forward bias in the diode. Scheme 2-3B shows the opposite situation for the same diode structure. When a positive voltage was applied to the poly(DNTD) side and a negative voltage applied to poly(FD), only a small positive voltage to oxidize the poly(DNTD). Due to the high energy level LUMO of poly(FD), a large negative potential is required to provide an electron with enough energy to fill LUMO of poly(FD), then transfer to the empty LUMO of poly(DNTD). Here, only a large voltage difference between poly(DNTD) and poly(FD) can make electron move from poly(FD) to poly(DNTD), resulting in a large reverse bias.

Upon further investigation of the *J*-*V* curves of these diodes, it is found that the current density flowing through the structure of Au|poly(FD)|poly(DNTD)|GaIn is much higher,

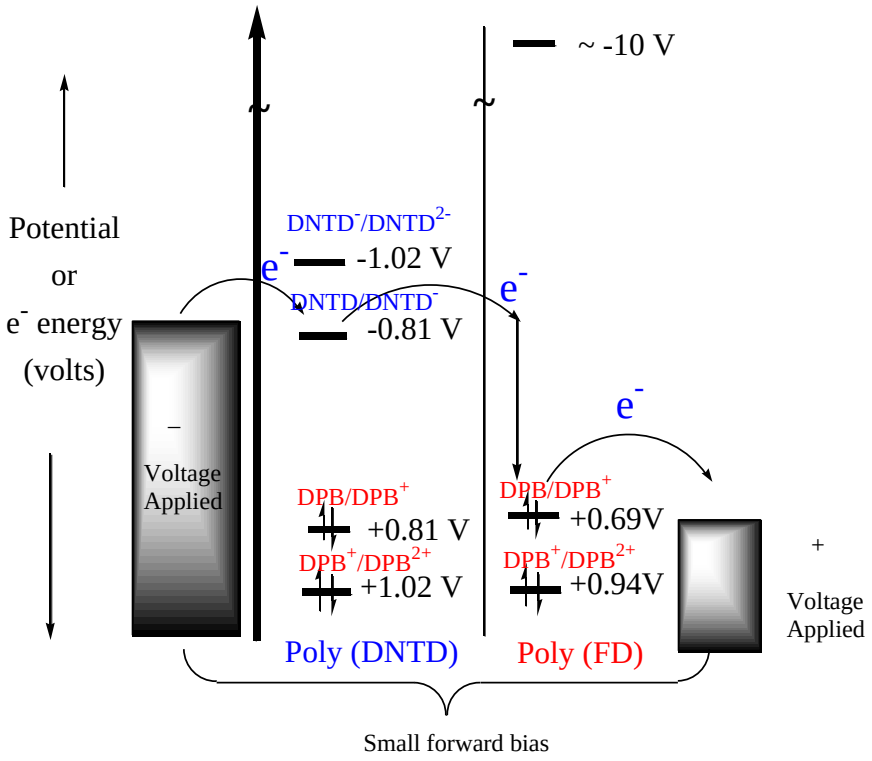

A: Forward bias

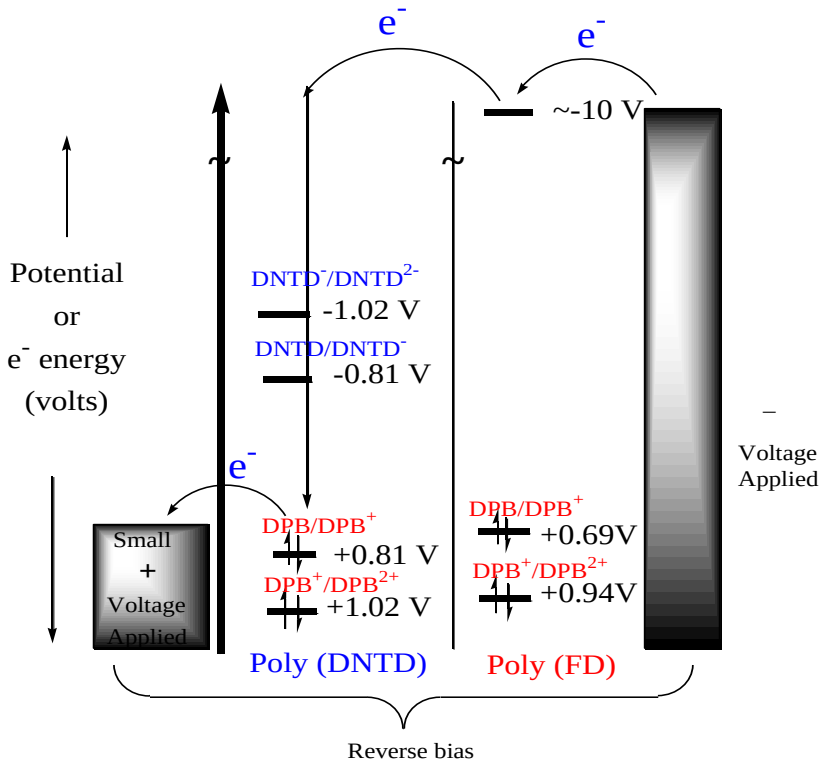

B: Reverse bias

Scheme 2-3. Electron transfer in bilayer Au|poly(DNTD)|poly(FD)|Ga-In in the solid state.

(around 300~500 times) than the one of Au|poly(DNTD)|poly(FD)|GaIn, we believe this is because of the conductivity difference between the two polymers and the small contact area between the Ga/In droplet and the surface of the polymers. Figure 2-20 depicts measured current density flowing through single layers of poly(DNTD) and poly(FD) sandwiched betweena Au/GaIn electrodes. The poly(FD) device in current density is several hundred times less than that of poly(DNTD), which is consistent with the differences of the bilayer devices. These single layer devices also show current rectification consistent with those of metal-semicondutor-metal Schottky diode. As poly(DNTD) is a bipolar material, it shows high current flow once applied voltages larger than ± 4 V are applied and where poly(FD) exhibits the same phenomenon at this voltage. Another reason may be that the surface density Γ of Au|DNTD|FD is about 30% higher than the one of Au|FD|DNTD (see Table 2-1), which makes the later bilayer much thicker. Thinner organic film are characterized by a lower resistance and faster electronic switching, which is also consistent with the observed current density data.

According to the Shockley theory of diodes,[35] a p-n junction occurs when a piece of n-type Ge or Si is in contact with a p-type material so that a transition from p-type to n-type occurs in a continuous solid specimen. In such a p-n junction, the total current I flowing across the junction barrier can be expressed via the general Shockley equation as follows:

$$I = I_s \left[\exp(\frac{qV_a}{nkT}) - 1 \right] \qquad (2\text{-}1)$$

Here I_s, the saturation current, is the current flowing in reverse bias, V_a is the applied voltage (positive value of V_a being forward) across the junction itself, q is the electric charge, n is

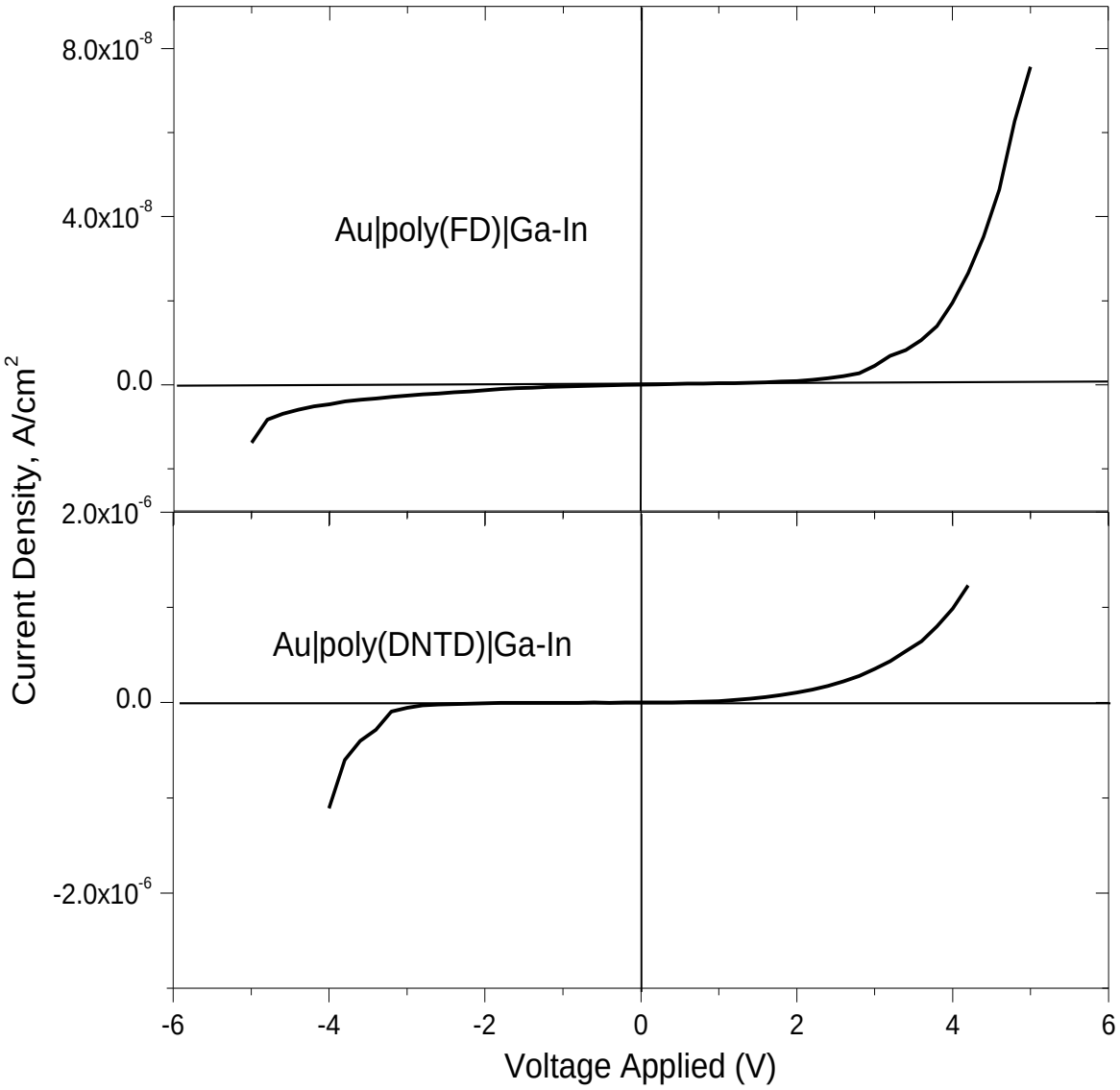

Figure 2-20 Current-voltage responses of a single layer device at room temperature with $\Gamma_{poly(DNTD)}=9.14\times10^{-9}$ mol/cm^2 and $\Gamma_{poly(FD)}=4.24\times10^{-9}$ mol/cm^2.

the ideality factor and kT is the thermal energy, k is the Boltzmann constant and T is the temperature. In the Shockley theory for p-n junctions, n is unity in the absence of recombination. By plotting ln I vs. V_a , the ideality factor and the saturation current can be obtained from the slope and intercept, where n is equal to $\frac{kT}{q}\frac{\partial \ln I}{\partial V_a}$ for $qV_a \gg nkT$ and the $\ln I_s$ is the intercept. We used the data for each diode device in conjunction with the above relationships, the results are summarized in Table 2-1.

It is somewhat challenging to compare the diode quality of junctions fabricated with different active materials, approaches, electrode materials and geometric configurations. The saturated current of our devices typically ranges from 0.8-40 μA/cm^2, which are much larger than those of doped p-n junction devices made via thermal evaporation[36] but closer to those of devices based on polymers.[24] The ideality factor, n of these devices is about 10-16, which is much larger than silicon-based inorganic *p-n* junction (n=1-2),[35] doped organic *p-n* junction (n=2-4)[36] and polyacetylene p-n junctions fabricated from polyelectrolyte-mediated electrochemistry (PMEC) (n=5.5).[22] The rectification ratio (RR) of different devices is also different, but typical maximum RR at 80-600, which is comparable to others.[22-24,36] The *J-V* behavior of these devices shows two general deviations from the ideal diode behavior. The first is the inevitable deviation from an exponential behavior at large forward bias due to the finite resistance of the materials, which is also very different from the doped *p,n* materials. The second is the common existence of electrical shunt that prevents the reverse current from saturating. The origin of this shunt appears to be related to imperfections in fabrication, such as the pin-holes

existing in these polymers, which also makes the reverse bias behavior not as reproducible as the forward bias behavior.

Table 2-1 Summary of organic diode devices characteristics

Device	$\Gamma_{n\text{-type}}$ /$\times 10^{-9}$ mol/cm^2	$\Gamma_{p\text{-type}}$ /$\times 10^{-9}$ mol/cm^2	Ideality factor(*n*)	Saturation current (A/cm^2)	Diode drop (*V*)	Rectification ratio
Au|DNTD|FD|Ga-In	8.5	4.82	15.53	1.4×10^{-7}	2.8(-), 14.1(+)	260 (±4.8*V*)
Au|FD|DNTD|Ga-In	6.19	3.65	15.90	4.1×10^{-5}	0.5(+), 7.5(-)	650(±1.5*V*)
Au|DPTD|FD|Ga-In	4.35	3.71	17.92	8.2×10^{-7}	3.1(-), 16.5(+)	99 (±4.8*V*)
Au|FD|DPTD|Ga-In	2.22	3.43	16.88	1.3×10^{-6}	1.1(+), 7.0(-)	411 (±2.0*V*)
Au|FD|DPTD|Au	2.76	3.22	10.07	2.5×10^{-5}	1.8(+), 5.6(-)	84.6 (±2.4*V*)
Au| FD|DPTD |Ag	2.27	3.46	13.22	7.5×10^{-7}	1.0(+), 6.9(-)	151 (±1.0 *V*)

Devices obtained using different methods for establishing the back electrode contacts to organic materials were also fabricated and compared in Table 2-1. Here, the Ga-In eutectic liquid drop, Au and Ag metallic leaves were assembled on the surface of Au|FD|DPTD bilayer devices. All of these devices showed I-V characteristics similar to that of Au|FD|DNTD|Ga-In (compare Figure 2-17, Figure 2-21 and Figure 2-22). With similar surface concentration (Γ) of organic active layers, the data in Table 2-1 show that the device with an Au leaf electrode exhibits better conductivity although the rectification ratio is similar. This result could be due to the fact that both Ag and Ga-In exhibit lower work functions, which leads to a metal-to-organic charge

transfer and formation of covalent-bond-like states at the DPTD-on-metal interface.[37] The rectification ratio (RR) of each device is also plotted in Figure 2-23. It shows very different responses RR for of *p*-*n* type devices as compared with those of *n*-*p* type ones. A large current was observed when a positive potential was applied to the FD layer even at around +1 *V*. A possible reason is that DPTD and metal establish a better resistance contact than FD layer and metal. This may be due to the electropolymerization process forming a less resistive contact to poly(FD) compared to the physical deposition process. Since this contact shows lower current density, it appears to be the limiting factor in these devices.

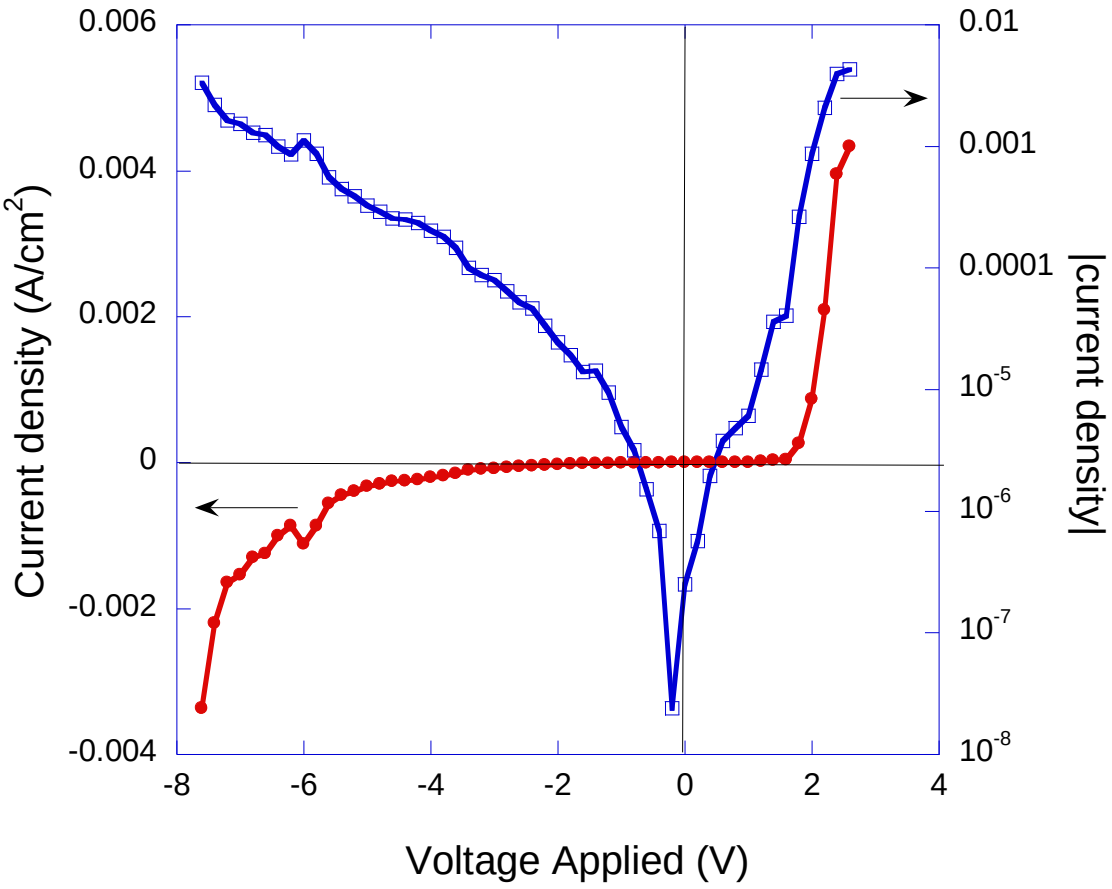

Figure 2-21. I-V characteristics of Au|poly(FD)|poly(DPTD)|Au organic diode with $\Gamma_{poly(DPTD)}=2.43\times10^{-9}$ mol/cm^2 and $\Gamma_{poly(FD)}=3.22\times10^{-9}$ mol/cm^2 under air and at room temperature.

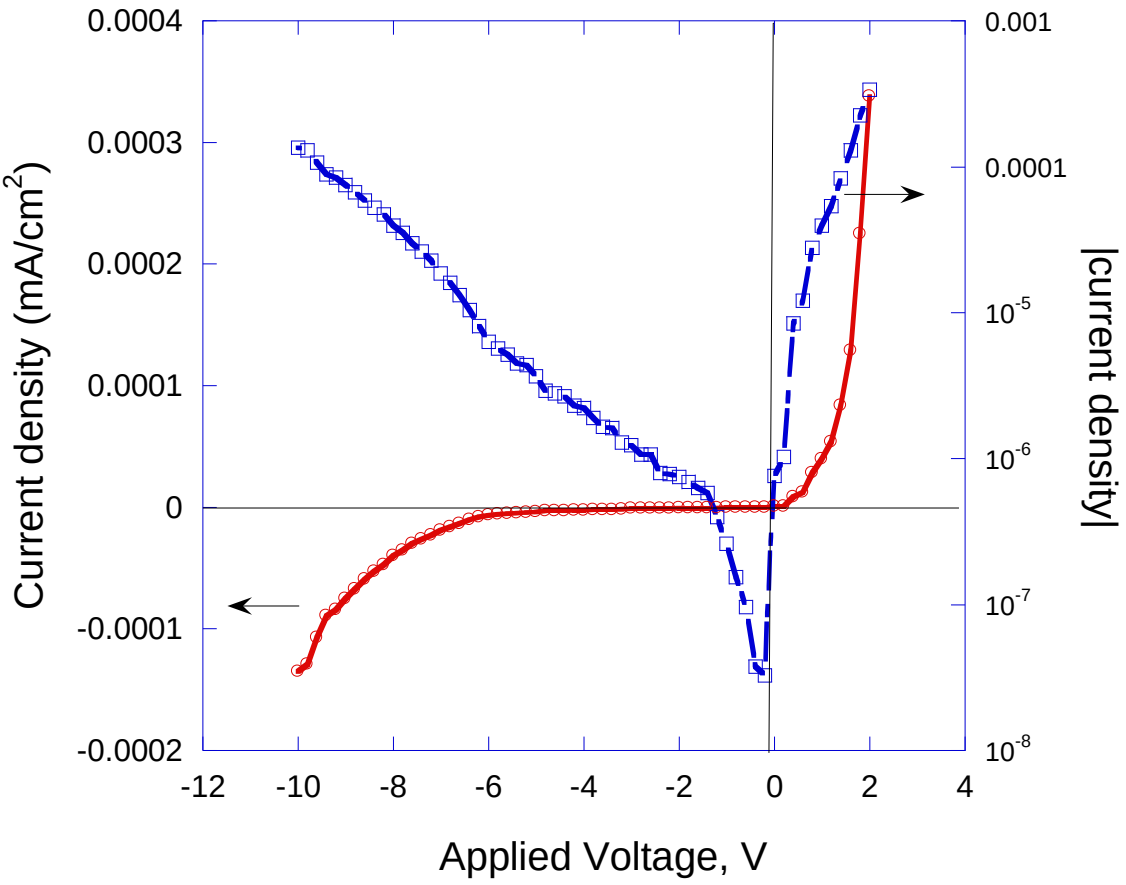

Figure 2-22. I-V characteristics of Au|FD|DPTD|Ag organic diode with $\Gamma_{poly(DPTD)}=2.27\times10^{-9}$ mol/cm^2 and $\Gamma_{poly(FD)}=3.46\times10^{-9}$ mol/cm^2 under air and at room temperature.

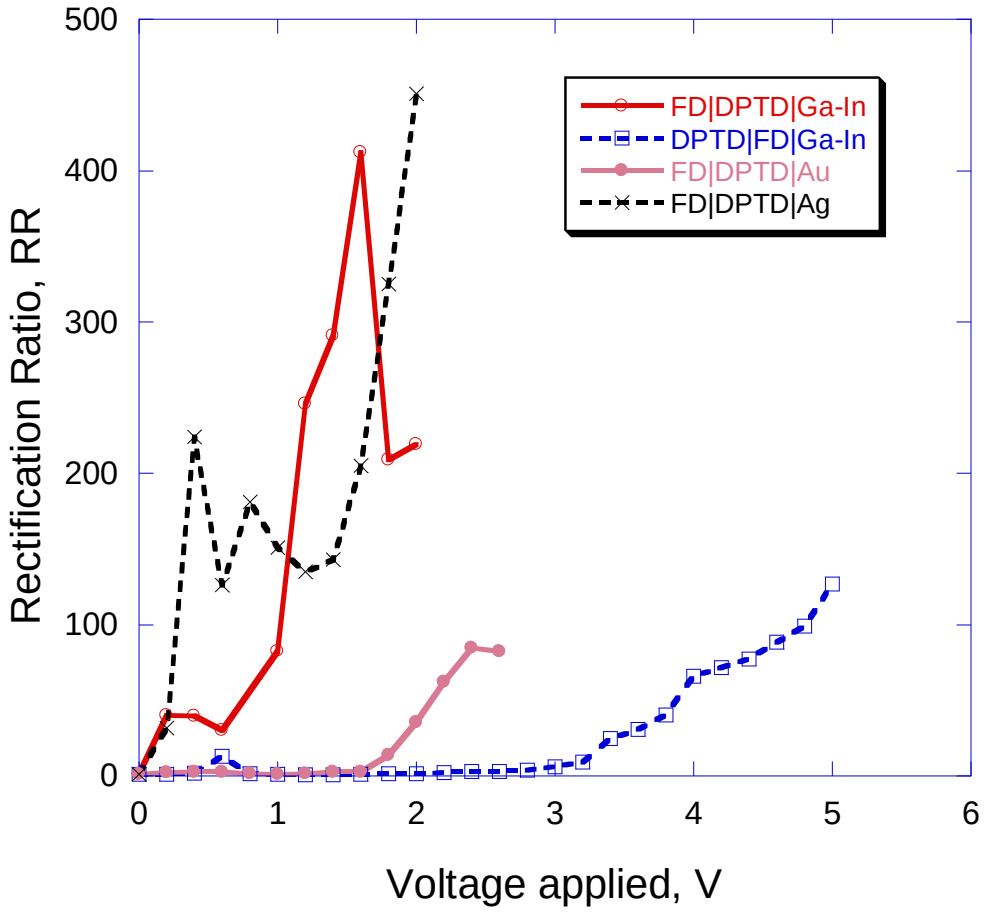

Figure 2-23 Rectificaiton ratio plot of poly(DPTD)/poly(FD) devices

2.4 CONCLUSIONS

Bilayer modified electrodes were prepared and characterized, using thin film polymers that were successfully electropolymerized from DNTD, DPTD, Cl_4DPTD and FD monomer solutions. These bilayers showed current rectification characteristics in solutions containing supporting electrolyte. The current rectification of bilayer modified electrodes were consisted of poly(FD) —a natural p-type material and a bipolar material, poly(DNTD), poly(DPTD) or poly(Cl_4DPTD). Poly(DNTD)/poly(FD) and poly(DPTD)/poly(FD) bilayer systems were also fabricated electrochemically on macroscopic electrodes and act as organic diodes when Ga/In eutectic and LOFO metallic leaf establish soft contacts on their surfaces. The typical maximum rectification ratio is between 80~650 at a certain voltage. Reversing the bilayer order changes the direction of rectification.

REFERENCES

1. *Handbook of Conducting Polymers, 2 Vol. Set*; 3rd ed.; Reynolds, J.; Skoheim, T. A., Eds.; CRC Press, 2007.

2. Kudo, T.; Kimura, M.; Hanabusa, K.; Shirai, H. *J. Porphyrins Phthalocyanines* **1998**, *2*, 231-235.

3. Kudo, T.; Kimura, M.; Hanabusa, K.; Shirai, H. *J. Porphyrins Phthalocyanines* **1999**, *3*, 310-315.

4. Oh, S.-K.; Baker, L. A.; Crooks, R. M. *Langmuir* **2002**, *18*, 6981-6987.

5. Berchmans, S.; Usha, S.; Ramalechume, C.; Yegnaraman, V. *J. Solid State Electrochem.* **2005**, *9*, 595-600.

6. Abruna, H. D.; Denisevich, P.; Umana, M.; Meyer, T. J.; Murray, R. W. *J. Am. Chem. Soc.* **1981**, *103*, 1-5.

7. Denisevich, P.; Willman, K. W.; Murray, R. W. *J. Am. Chem. Soc.* **1981**, *103*, 4727-37.

8. Pickup, P. G.; Murray, R. W. *J. Electroanal. Chem.* **1984**, *164*, 39-61.

9. Kittlesen, G. P.; White, H. S.; Wrighton, M. S. *J. Am. Chem. Soc.* **1984**, *106*, 7389-96.

10. Kittlesen, G. P.; White, H. S.; Wrighton, M. S. *J. Am. Chem. Soc.* **1985**, *107*, 7373-80.

11. Kittlesen, G. P.; Wrighton, M. S. *J. Mol. Electron.* **1986**, *2*, 23-33.

12. Martin, A. S.; Sambles, J. R.; Ashwell, G. J. *Thin Solid Films* **1992**, *210-211*, 313-16.

13. Martin, A. S.; Sambles, J. R.; Ashwell, G. J. *Phys. Rev. Lett.* **1993**, *70*, 218-21.

14. Shirakawa, H.; Louis, E. J.; MacDiarmid, A. G.; Chiang, C. K.; Heeger, A. J. *J. Chem. Soc., Chem. Commun.* **1977**, 578-80.

15. Chiang, C. K.; Gau, S. C.; Fincher, C. R., Jr.; Park, Y. W.; MacDiarmid, A. G.; Heeger, A. J. *Appl. Phys. Lett.* **1978**, *33*, 18-20.

16. Yamashita, K.; Kunugi, Y.; Harima, Y.; Chowdhury, A.-N. *Jpn. J. Appl. Phys., Part 1* **1995**, *34*, 3794-7.

17. Lin, F.; Walker, E. M.; Lonergan, M. C. *J. Phys. Chem. Lett.* **2010**, *1*, 720-723.

18. Koshida, N.; Wachi, Y. *Appl. Phys. Lett.* **1984**, *45*, 436-7.

19. Wang, W. M.; Wan, H. H.; Rong, T. W.; Bao, J. R.; Lin, S. H. *Nucl. Instrum. Methods Phys. Res., Sect. B* **1991**, *B61*, 466-71.

20. Cheng, C. H. W.; Lonergan, M. C. *J. Am. Chem. Soc.* **2004**, *126*, 10536-10537.

21. Cheng, C. H. W.; Boettcher, S. W.; Johnston, D. H.; Lonergan, M. C. *J. Am. Chem. Soc.* **2004**, *126*, 8666-8667.

22. Robinson, S. G.; Johnston, D. H.; Weber, C. D.; Lonergan, M. C. *Chem. Mater.* **2010**, *22*, 241-246.

23. Aizawa, M.; Shinohara, H.; Yamada, T.; Akagi, K.; Shirakawa, H. *Synth. Met.* **1987**, *18*, 711-14.

24. Uehara, K.; Ichikawa, T.; Matsumoto, K.; Sugimoto, A.; Tsunooka, M.; Inoue, H. *J. Electroanal. Chem.* **1997**, *438*, 85-89.

25. Haick, H.; Cahen, D. *Acc Chem Res* **2008**, *41*, 359-66.

26. Chiechi, R. C.; Weiss, E. A.; Dickey, M. D.; Whitesides, G. M. *Angew. Chem.* **2008**, *47*, 142-144.

27. Vilan, A.; Cahen, D. *Adv. Funct. Mater.* **2002**, *12*, 795-807.

28. Wang, L., Ph.D. Dissertation, Auburn University, 1997.

29. Wang, Q., M.S. Thesis, Auburn University, 1999.

30. Liang, J., Ph.D. Dissertation, Auburn University, 2003.

31. Wang, L.; Cammarata, V. *Thin Solid Films* **1996**, *284-285*, 297-300.

32. Wang, L.; Goodloe, G. W.; Stallman, B. J.; Cammarata, V. *Chem. Mater.* **1996**, *8*, 1175-1181.

33. Wang, L.; Wang, Q. Q.; Cammarata, V. *J. Electrochem. Soc.* **1998**, *145*, 2648-2654.

34. Hao, N., M.S. Thesis, Auburn University, 2001.

35. Shockley, W. *Electronics and Holes in Semiconductors*; Van Nostrand: New York, 1950.

36. Harada, K.; Werner, A. G.; Pfeiffer, M.; Bloom, C. J.; Elliott, C. M.; Leo, K. *Phys. Rev. Lett.* **2005**, *94*, 036601/1-036601/4.

37. Hill, I. G.; Schwartz, J.; Kahn, A. *Org. Electron.* **2000**, *1*, 5-13.

CHAPTER 3

VISIBLE SPECTROELECTROCHEMICAL STUDY ON ELECTRON BLOCKING AND TRAPPING BEHAVIOURS IN DIFFERENT BILAYERS

3.1 INTRODUCTION

Mixed conductor polymeric materials are rarely used for rectifying devices.[1,2] By virtue of their bipolar nature, dominance by electron transport or hole transport depends on the connecting electrode material and the applied potential. When these materials are in contact with a unipolar material, the potential for rectification exists depending on the charge state of all the materials. Electrical properties of conducting polymers and their controllability by a doping/dedoping process have been an important issue in the field of organic electronics. For this reason, electrochemical techniques emerged first as a major tool for studying conducting polymers and their electrical, as well as electrochemical properties. However, these techniques are not by themselves suitable to identify unknown species that are formed as intermediates or as products in a redox reaction. The combination of electrochemistry with some other techniques can solve this problem and allow for a more complete analysis of electron transfer processes and complicated redox reaction.

The coupling of electrochemical and spectroscopic techniques is intensively used in the characterization of electroactive films.[3,4] Spectroelectrochemistry (SEC) has been a powerful

technique in following the spectral changes of conducting polymer films during their electrochemical growth and doping/dedoping processes for determining energy levels since the late 1960s.[5] Several spectroscopic techniques such as UV-Visible and near-infrared absorption (UV-Vis-NIR) or reflection spectroscopy, infrared spectroscopy (IR), Raman spectroscopy and X-ray absorption or scattering, have been combined with electrochemical methods for study of redox processes that occur within thin layers on electrode surfaces and in solution.[6] UV-Vis-NIR spectrometries have become routine methods for investigations of conducting polymer films, where they are used to monitor the chemical changes occurring in the surface film. Optically transparent electrodes (OTEs) are usually employed, which are normally either indium–tin oxide (ITO) or a very thin (less than 100 nm) layer of gold or platinum on a glass or quartz substrate.

Our group also designed a spectroelectrochemical cell (see Figure 3-1) for UV-Vis-NIR spectroelectrochemical experiments. Teflon was used to build the cell body. There are two windows (front and rear window) in this cell. Three small holes on the top were made so that counter and reference electrodes could be set up inside the cell, the third hole is for Argon degassing and is relatively small. The glass that was chosen to cover the rear window is partially transparent to UV radiation, as well as transparent to visible and near IR radiation. ITO coated transparent glass slides were used as working electrode and covered the front window. Both aqueous and non-aqueous solution can be used in this cell system, offering a wide potential range. This cell system can be set up in the sample compartment of a UV-Vis. spectrophotometer and is connected to a potentiostat, enabling detection of species absorbing in UV-Vis-NIR regions of the spectrum following the oxidation or reduction of an electroactive material on the surface of

the working electrode.

As mentioned in Chapter 1, a series of monomers with a structural motif R-X-R have been synthesized in our lab over the years.[7-10] Polymeric films on electrode surfaces can be obtained by electrochemical polymerization of monomers resulting in an alternating polymer of diphenylbenzidine (two para- linked diphenylamine groups) and the X unit. The spectroelectrochemistry of single thin films on ITO has been investigated for many of these materials.[10,11] For convenient comparisons of the bilayer spectra data, monolayer electrospectra especially from the reduced form of poly(FD), poly(DNTD), poly(DPTD) and poly(Cl4DPTD) are shown in Figures 3-2 to 3-5.

In this chapter, we study the electron blocking and trapping behavior of bilayers, which are sequentially electrochemically polymerized in the same manner as single layered materials. Figure 1-5 depicts the chemical structures of the monomers from which we synthesized our bilayer materials: DNTD, FD, DPTD, and Cl_4DPTD. Because of their intense absorption bands in the UV-Visible region, poly(DPTD) and poly(Cl_4DPTD) have the potential to be used in photovoltaic cell devices.[12] Due to the natural unipolar native of poly(FD), which can only be oxidized at a certain potential, electron blocking is anticipated to happen when poly(FD) is placed between the ITO and another bipolar polymeric film such as poly (DNTD) or poly(DPTD). Trapping of carriers is expected to take place when two films with different reductive potentials are contacted.

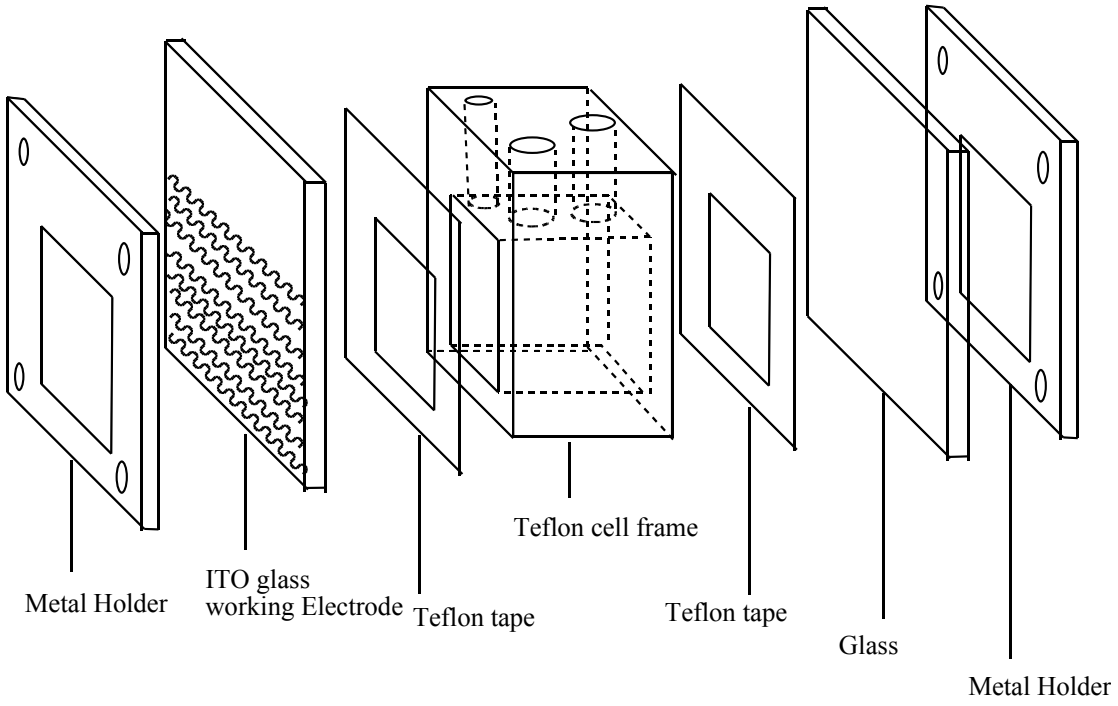

A: Separated cell view

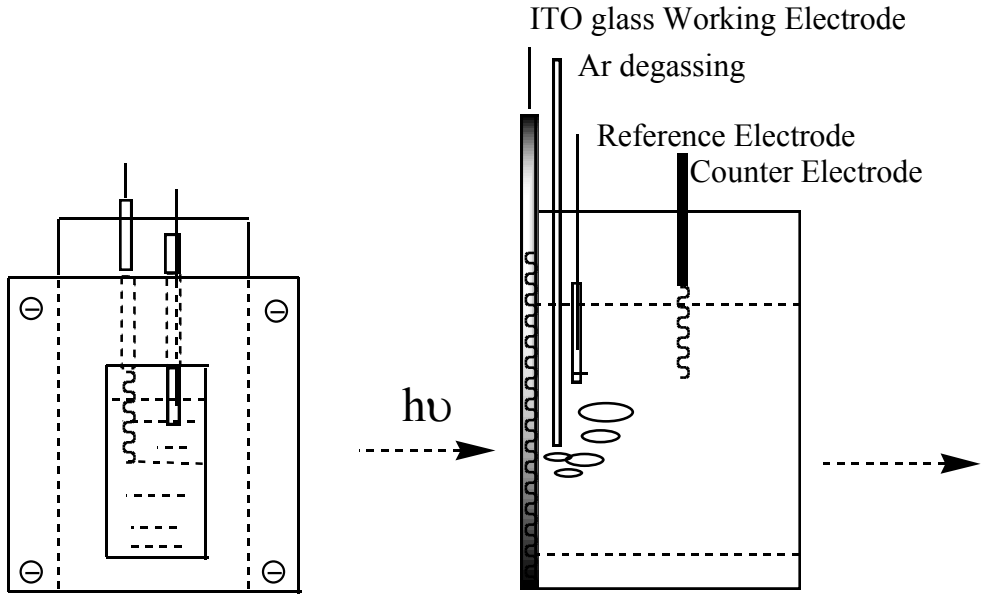

B: Assembled cell view

Figure 3-1 The diagram of spectroelectrochemical cell

3.2 EXPERIMENTAL

The synthesis of diphenylamine endgroup monomers (DNTD, DPTD, Cl_4DPTD and FD, see Figure 1-5) have been previously described in the literature.[7-11,13] Methylene chloride (CH_2Cl_2, 99.9% Fisher) was freshly distilled from CaH_2 (Aldrich Chemical Co.). Tetrabutylammonium hexafluorophosphate, $TBAPF_6$ (Aldrich, 98%) was dried prior to use *in vacuo* at 100 °C for at least 48 hrs. Cyclic voltammetry in solution was performed under the same conditions as described in Chapter one. Indium tin oxide (ITO, Delta Technologies, Ltd.) 70Ω/□ coated glass slides were used as working electrodes to electrooxidatively polymerize different monomers onto the front windows of the SEC cell. The procedures for the electrochemical polymerization of the monomers has been described elsewhere.[10,11] Microscope glaslides (Fisherbrand) were chosen to cover the rear window of SEC cell. The reference electrode was Ag/AgCl in saturated KCl and Pt mesh was used for the counter electrode. The long pathlength spectroelectrochemical cell has been described elsewhere.[10] The UV-Vis measurements were performed on an Agilent 8453 UV-Visible spectrophotometer coupled with a CV-27 potentiostat for applying electrochemical potentials. Solutions in the electrochemical cell were bubbled with Ar for at least 15 mins. Each spectrum was taken when the electrochemical cell current decayed to zero and was integrated for 2 seconds. At each applied potential, a minimum of 2 spectra were taken to verify consistency.

3.3 RESULTS AND DISCUSSION

3.3.1 Electrochemistry and spectroelectrochemistry of a single layer

All the compounds, FD, DNTD, DPTD and Cl_4DPTD can be electropolymerized from their monomer solutions in CH_2Cl_2. Cyclic Voltammegrams of poly(FD), poly(DNTD), poly(DPTD) and poly(Cl_4DPTD) thin film on Au electrode in CH_2Cl_2 with 0.1 M $TBAPF_6$ at a scan rate of 200 mV/s were shown in Chapter 2. Poly(DNTD), poly(DPTD) and poly(Cl_4DPTD) show similar voltammograms, all these thin films deposited on electrodes exhibit two redox species either at the positive potential or negative potential regions, which correspond to DPB^0/DPB^+, DPB^+/DPB^{2+} and the X group redox species, respectively. Poly(FD) only exhibits DPB^0/DPB^+, DPB^+/DPB^{2+} two redox species at positive potentials. Table 3-1 shows the oxidation and reduction data of the resulting polymer films. Each material is oxidized at nearly the same positive potential but they have very different reductive potentials. The oxidation wave has been assigned to the diphenylbenzidine linkage which is common to all four polymers.[10,11,13]

The spectroelectrochemistry of poly(DNTD), poly(FD), poly(DPTD) and poly(Cl_4DPTD) single layer films was also investigated and discussed by our former group members. In order to have a better understanding of the bilayer electron behaviors, some spectroelectrochemical results of single layer films are presented in Figures 3-2 to 3-5. Also, some characteristic absorption peaks from several single films are listed in Table 3-2.

We have previously postulated that an important intermediate species in these films is the π-stacking diphenylbenzidium cation dimer.[7] The ability to form this dimer may, in part, be

Table 3-1 Electrochemical data of different polymers [10,11,13]

Polymers		DNTD	DPTD	Cl_4DPTD	FD
$E_{1/2}$ Oxidation	(1st)	0.722 V	0.700 V	0.705 V	0.608 V
	(2nd)	0.938 V	0.904 V	0.899 V	0.880 V
$E_{1/2}$ Reduction	(1st)	-0.596 V	-0.592 V	-0.413 V	N/A
	(2nd)	-1.015 V	-0.825 V	-0.577 V	
Longest wavelength absorbed (nm) at 0.0 V		384	490, 535	522, 488	<350

Potentials vs. Ag/AgCl; 0.1 M $TBAPF_6$, CH_2Cl_2, scan rate=200mV/s.

Table 3-2 Visible absorption bands for reduced polymer films[10,11,13]

Polymer	FD		DNTD	
	Anion	Dianion	Anion	Dianion
Absorbance bands (nm)	-	-	482, 528, 613, 701, 782	762
Polymer	DPTD		Cl_4DPTD	
	Anion	Dianion	Anion	Dianion
Absorbance bands (nm)	490, 529, 722，810，970	490, 526, 577, 654	763，923，1015	485, 523, 688

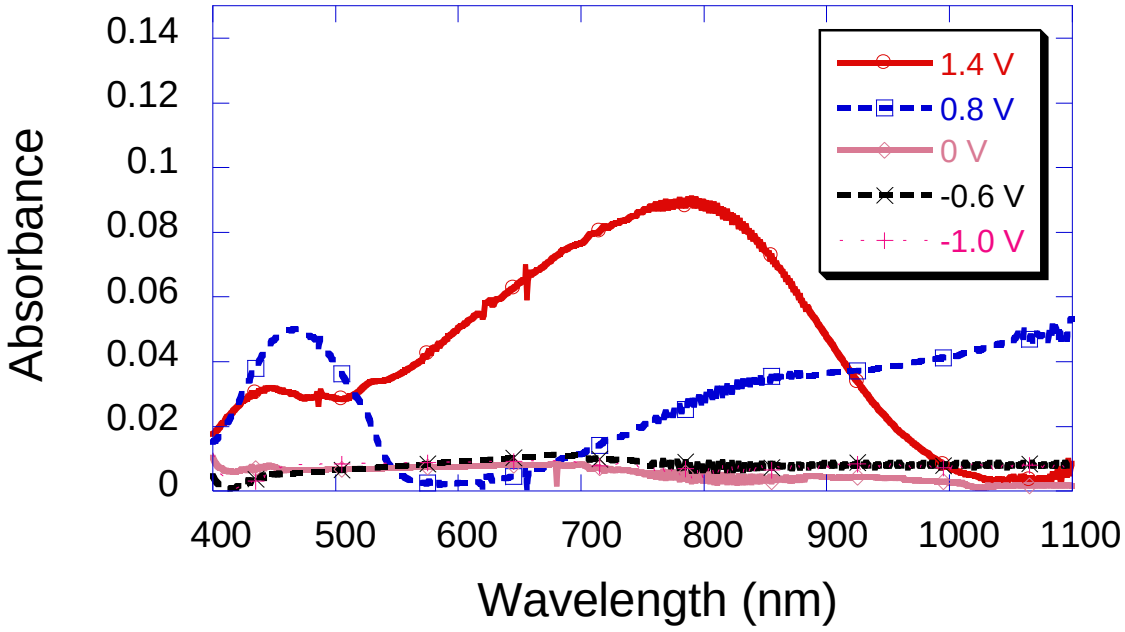

Figure 3-2. Poly (FD) spectroelectrochemistry at potentials vs. Ag/AgCl

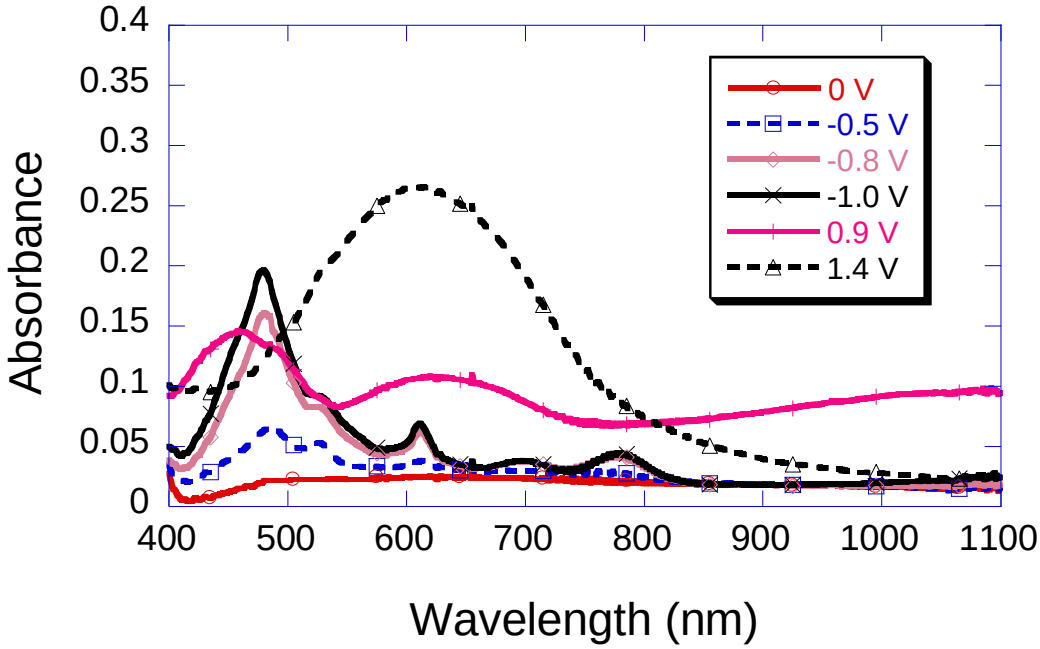

Figure 3-3. Poly(DNTD) spectroelectrochemistry at potentials vs. Ag/AgCl

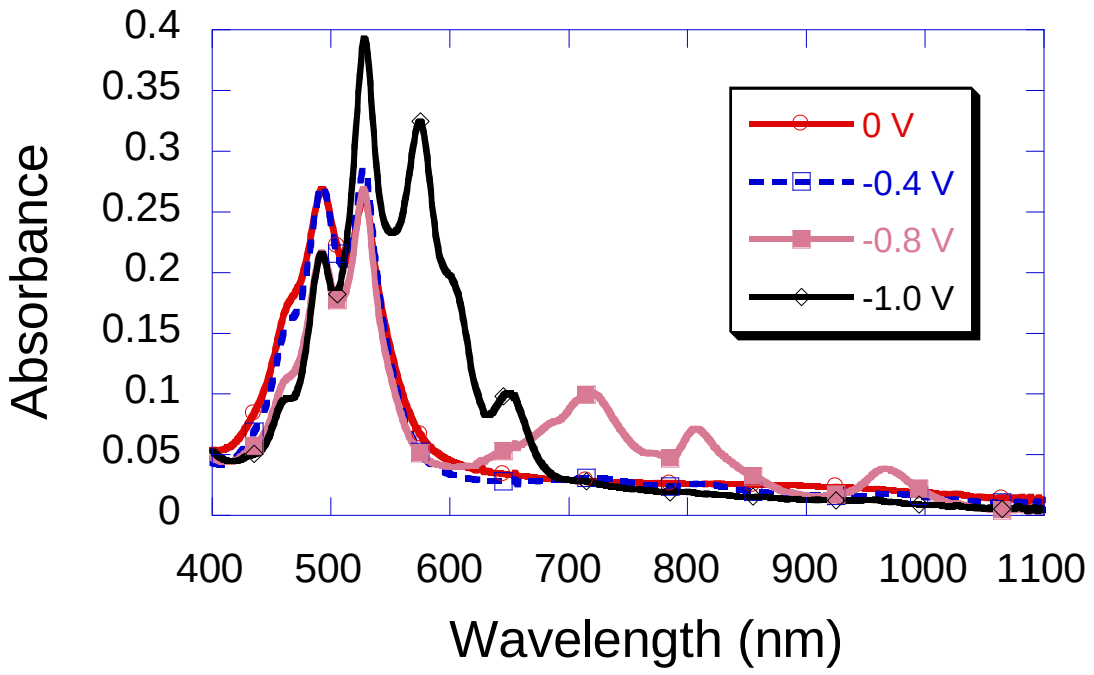

Figure 3-4. Poly(DPTD) spectroelectrochemistry at negative potentials vs. Ag/AgCl

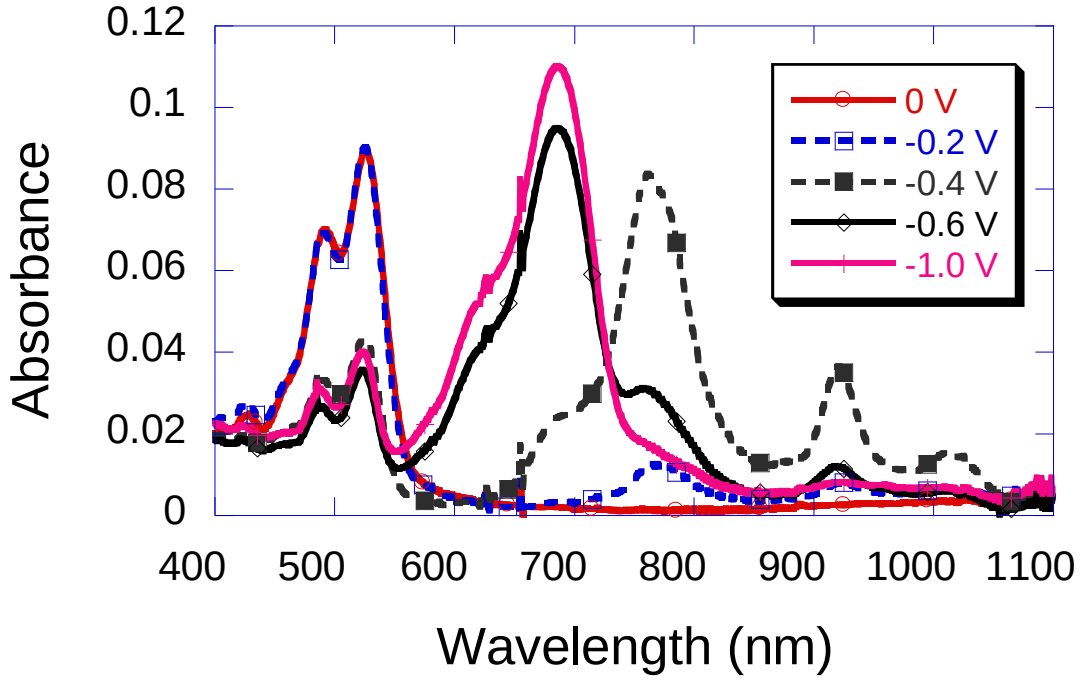

Figure 3-5. Poly(Cl_4DPTD) spectroelectrochemistry at negative potentials vs. Ag/AgCl

determined by the steric bulk of the -X- group as well as by interchain interactions between -X- groups. One important difference is that poly(FD) is based on an amide linked diphenylbenzidine where the other polymers are imide linked. Also poly(FD) contains a dicarboxyferrocenyl group which has a third accessible oxidation based at the Fe center. The result of these two differences is that the first oxidation signal of poly(FD) is ~0.1V more negative as compared to that of the imide based polymers.

3.3.2 Electron blocking in bilayers

We used poly(DNTD)/poly(FD) and poly(DPTD)/poly(FD) bilayers to investigate the electron blocking behavior. Figures 3-6A and 3-8B depict spectroelectrochemical results for both bilayer films of ITO|poly(FD)|poly(DNTD) with $\Gamma_{FD}=1.56\times10^{-9}$ mol/cm^2 and $\Gamma_{DNTD}=1.24\times10^{-9}$ mol/cm^2 and ITO|poly(DNTD)|poly(FD) with $\Gamma_{DNTD}=2.93\times10^{-9}$ mol/cm^2 and $\Gamma_{FD}=0.77\times10^{-9}$ mol/cm^2, respectively. Results for ITO|poly(FD)|poly(DPTD) are shown in Figure 3-7A, Γ_{FD} is 2.29×10^{-9} mol/cm^2 and Γ_{DPTD} is 0.33×10^{-9} mol/cm^2; for bilayer ITO|poly(DPTD)|poly(FD) in Figure 3-7B, Γ_{FD} is 0.72×10^{-9} mol/cm^2 and Γ_{DPTD} is 1.86×10^{-9} mol/cm^2.

Neither poly(DNTD) nor poly(FD) bilayer films show any significant absorbance at wavelengths >400 nm but poly(DPTD)/poly(FD) films exhibit signals at 490 nm and 535 nm (the same as poly(DPTD) single film) at 0.0V vs. Ag/AgCl. When positive potentials are applied, e.g. +0.8V, a broad band which peaks ~1100 nm appears in all bilayers and if a greater potential is applied (+1.2-1.4V), this band disappears, and is replaced by an intense peak between 600-800

nm. This corresponds to the oxidation of diphenylbenzidine group in the polymer units.[7] Individual films of poly(FD), poly(DNTD) and poly(DPTD) cations show intense absorptions at 840 nm,[7] 610 nm[8] and 682 nm,[9] respectively. Since absorptions due to the full oxidation of both films is observed, an oxidized inner film of poly(FD) will oxidize the outer layer of poly(DNTD) and an oxidized inner film of poly(DNTD) will oxidize the outer layer of poly(FD), The same phenomenon also happens in the case of poly(DPTD)/poly(FD) bilayer films. Based on half-wave potentials ($E_{1/2}$) of poly(DPTD)/poly(FD) bilayers, the HOMO energies of these materials are closely matched and facile electron transfer between layers occurs. Upon reduction back to the neutral state the absorption of both bilayers reverses to the original spectra consistent with a complete reduction of the inner and outer layers.

At potentials more negative than 0.0V, the optical and electrochemical behavior of the two orientations of bilayer films is different. Previously, we showed that poly(FD) is electroinactive at negative potentials to at least -1.2V vs. Ag/AgCl; the spectroelectrochemistry of poly(FD) shows the same spectra across this range. For the bilayer of ITO|poly(FD)|poly(DNTD) (Figure 3-6A), the spectra of this bilayer film is similar to that of a single layer of poly(FD) showing the same absorbance from 0.0 to -1.0V, which is similar to the case of ITO|poly(FD)|poly(DPTD), shown in Figure 3-7A. Reversal of the potential to 0.0V results in no changes. However, for the bilayer of ITO|poly(DNTD)|poly(FD) (Figure 3-6B) or ITO|poly(DPTD)|poly(FD) (Figure 3-7B), at potentials more negative of 0.0V a series of absorbance peaks (482, 613, 701, 782 nm for poly(DNTD) and 722, 810, 970 nm for poly(DPTD) or 577, 654 nm appear at more negative potentials e.g. -1.0 V vs. Ag/AgCl and are indicative of the poly(DNTD) and poly (DPTD)

anions (Table 3-2). Upon reversing the potential, the spectrum returns to the original one recorded at 0.0V. It is clear that the inner poly(FD) layer blocks electron transfer to outer poly(DNTD) or poly(DPTD) layers, but when the direction of electron transfer is reversed, the inner poly(FD) does oxidize the outer layer .

3.3.3 Electron trapping in bilayers based on bipolar conducting polymers

For polymer bilayers where both layers are bipolar conductors, differences in their energy levels can lead to interesting charge localizations. For example, an ITO|poly(DNTD)|poly(Cl_4DPTD) bilayer, with $\Gamma_{DNTD}=4.21\times10^{-9}$ mol/cm^2 and $\Gamma_{Cl4DPTD}=1.88\times10^{-9}$ mol/cm^2 , was electrochemically polymerized and investigated using spectroelectrochemistry. Both poly(DNTD) and poly(Cl_4DPTD) show two redox couples at negative potentials and each shows changes in their spectra in response to different potentials. Figure 3-8 shows the reduced form of the bilayer as the potentials increase from -0.9 to 0.3V. At -0.9V, absorbances at 482, 613 and 782 nm are indicative of poly(DNTD) anion[9] and at the same potential, the absorbance peak ~688 nm can be assigned to poly(Cl_4DPTD) dianion.[10] When the potential increases from -0.9V to -0.3V, the peaks for poly(DNTD) anion and poly(Cl_4DPTD) dianion disappear and poly(Cl_4DPTD) anion absorbance peaks at 763 and 923 nm appear. In single layer films of poly(Cl_4DPTD) the oxidation of the poly(Cl_4DPTD) anion occurs at -0.4V, but in the bilayer films, the absorbances assigned to the poly(Cl_4DPTD) anion do not disappear until +0.3V.

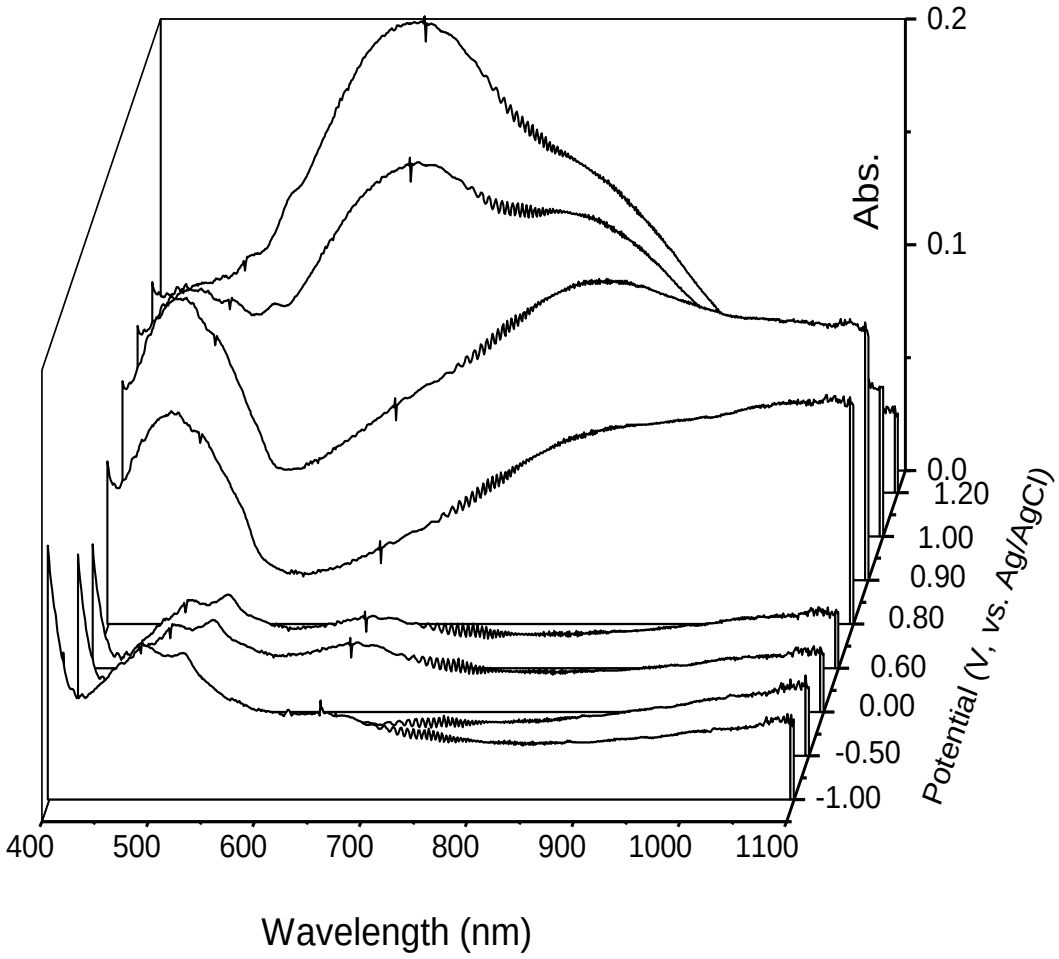

Figure 3-6A Spectroelectrochemistry of ITO|poly(FD)|poly(DNTD).

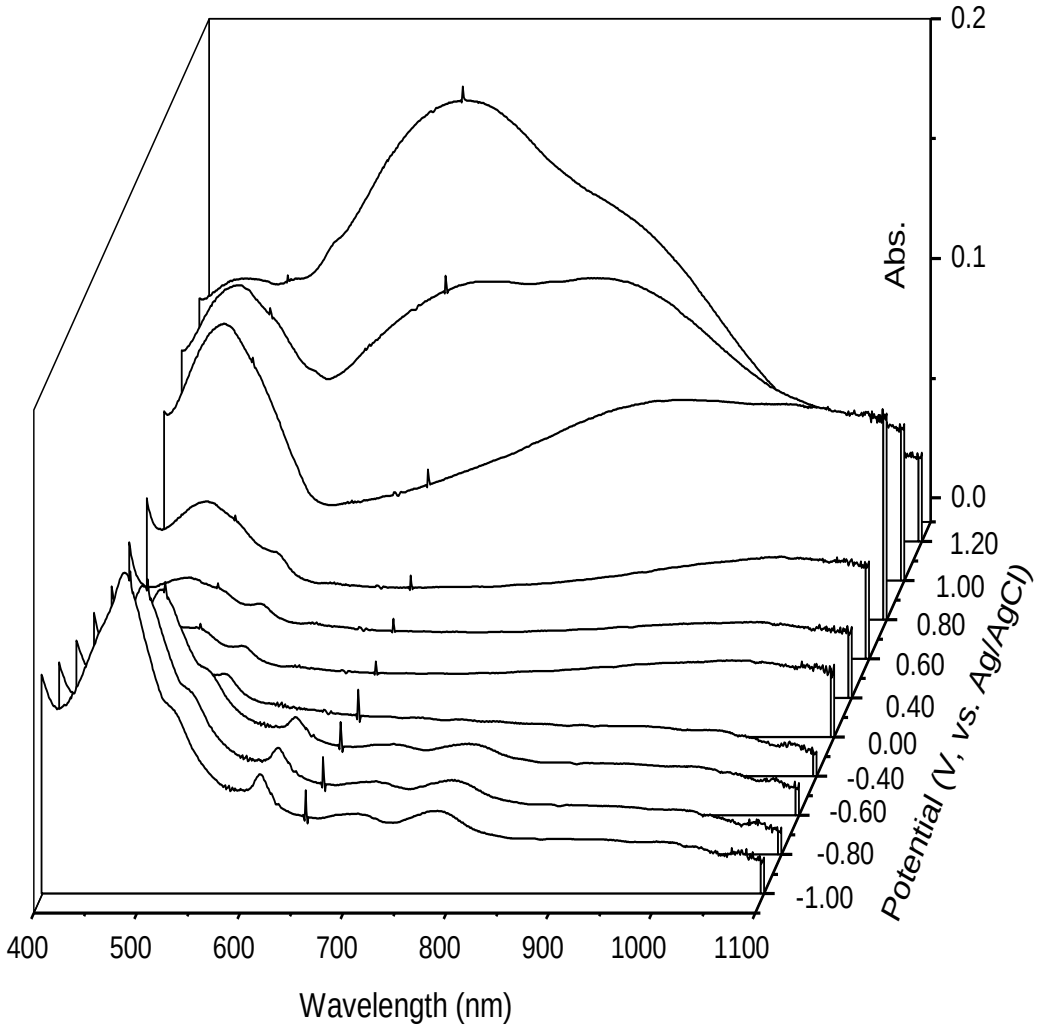

Figure 3-6B. Spectroelectrochemistry of ITO|poly(DNTD)|poly(FD).

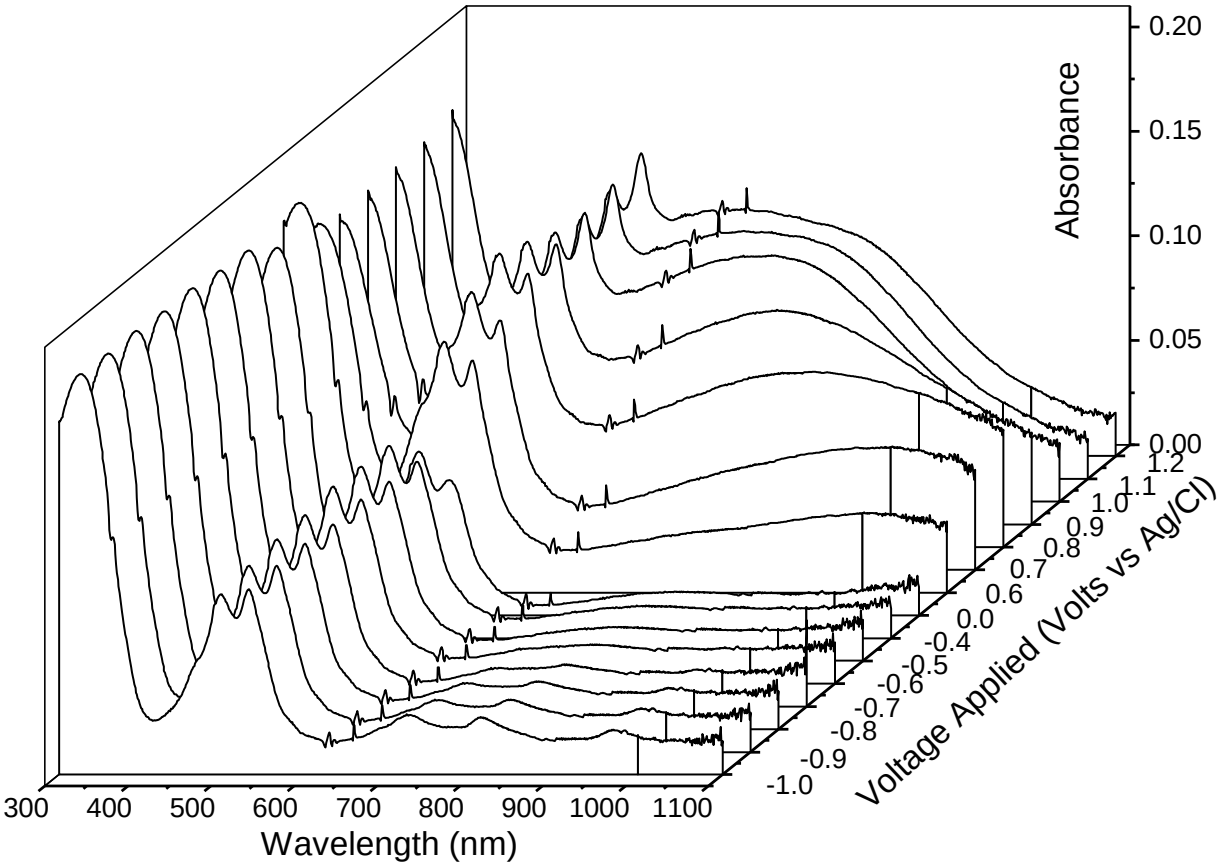

Figure 3-7A Spectroelectrochemistry of bilayers with poly (DPTD) grown on poly (FD).

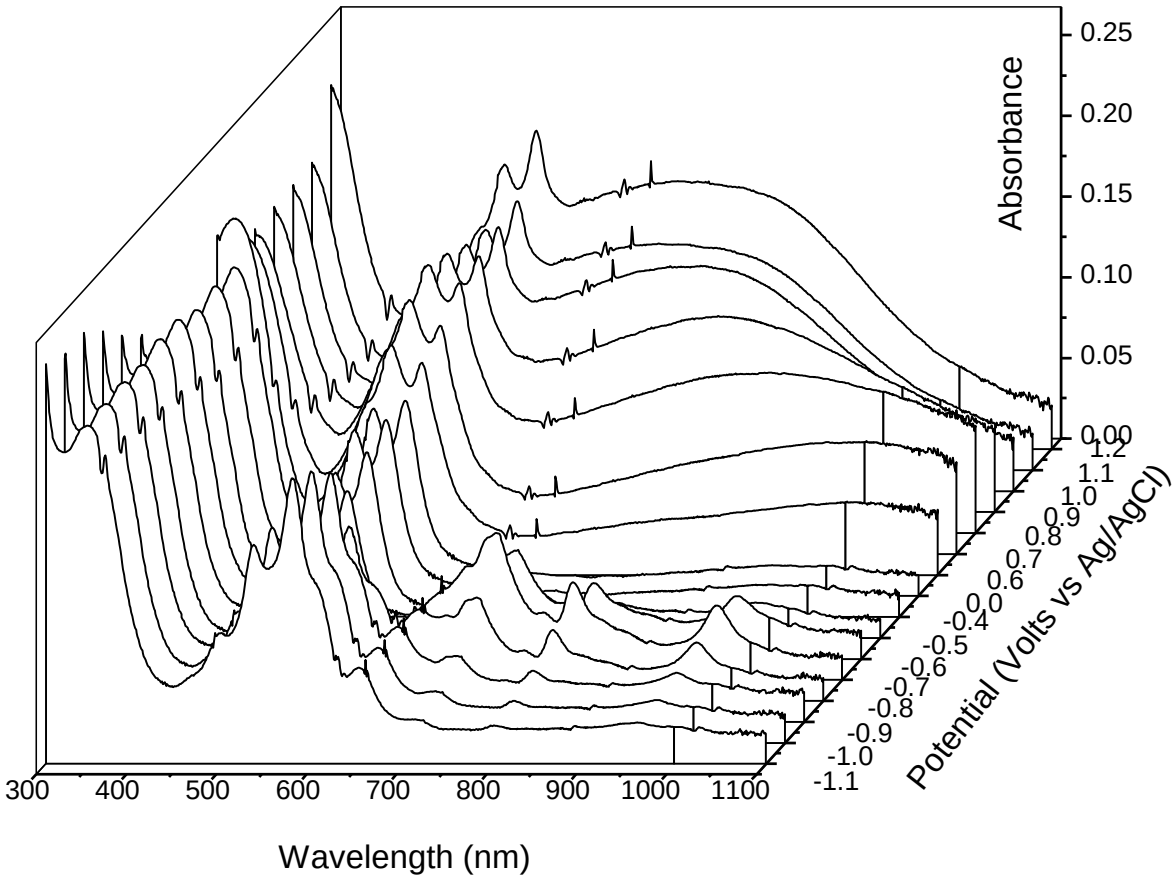

Figure 3-7B Spectroelectrochemistry of bilayers with poly (FD) grown on poly (DPTD).

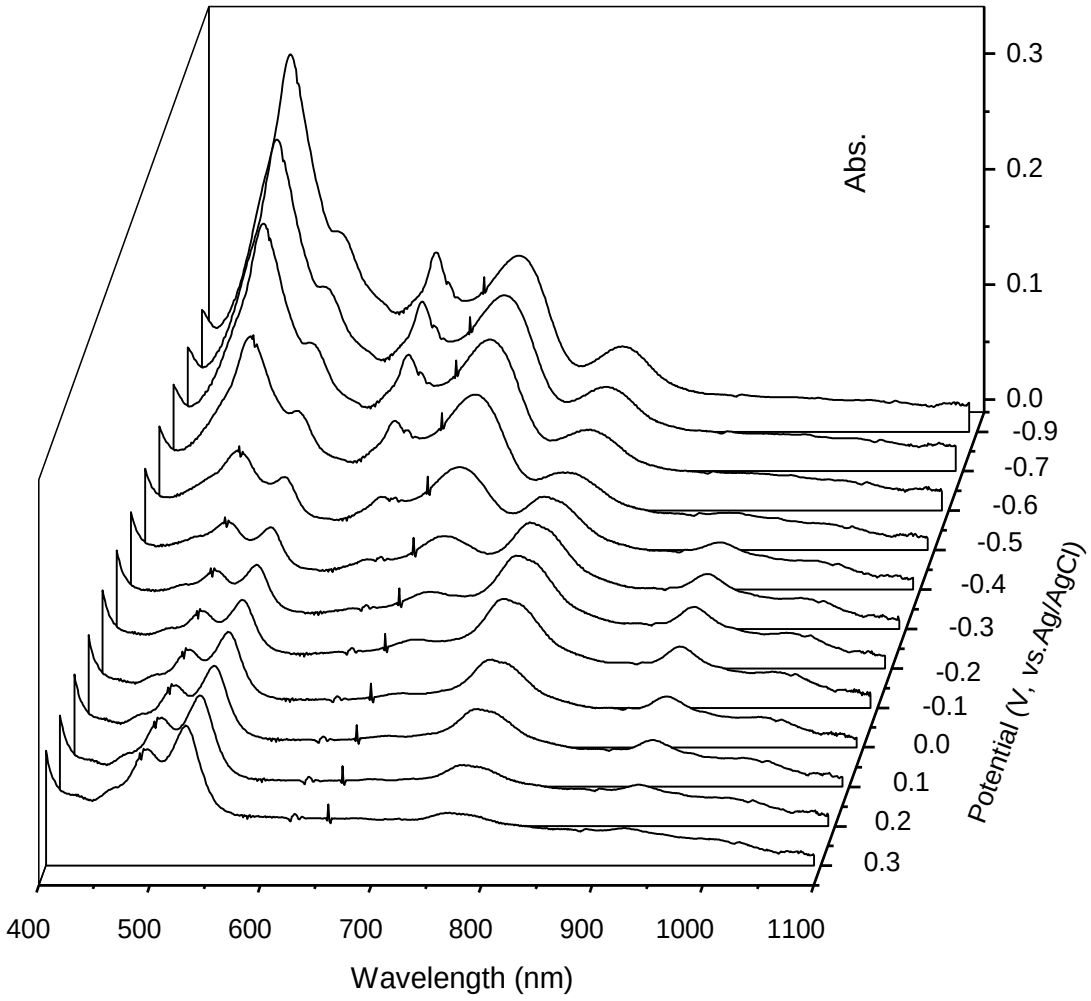

Figure 3-8. Electron trapping shown by spectroelectrochemistry in ITO|poly(DNTD)|poly(Cl_4DPTD) bilayers at negative potentials.

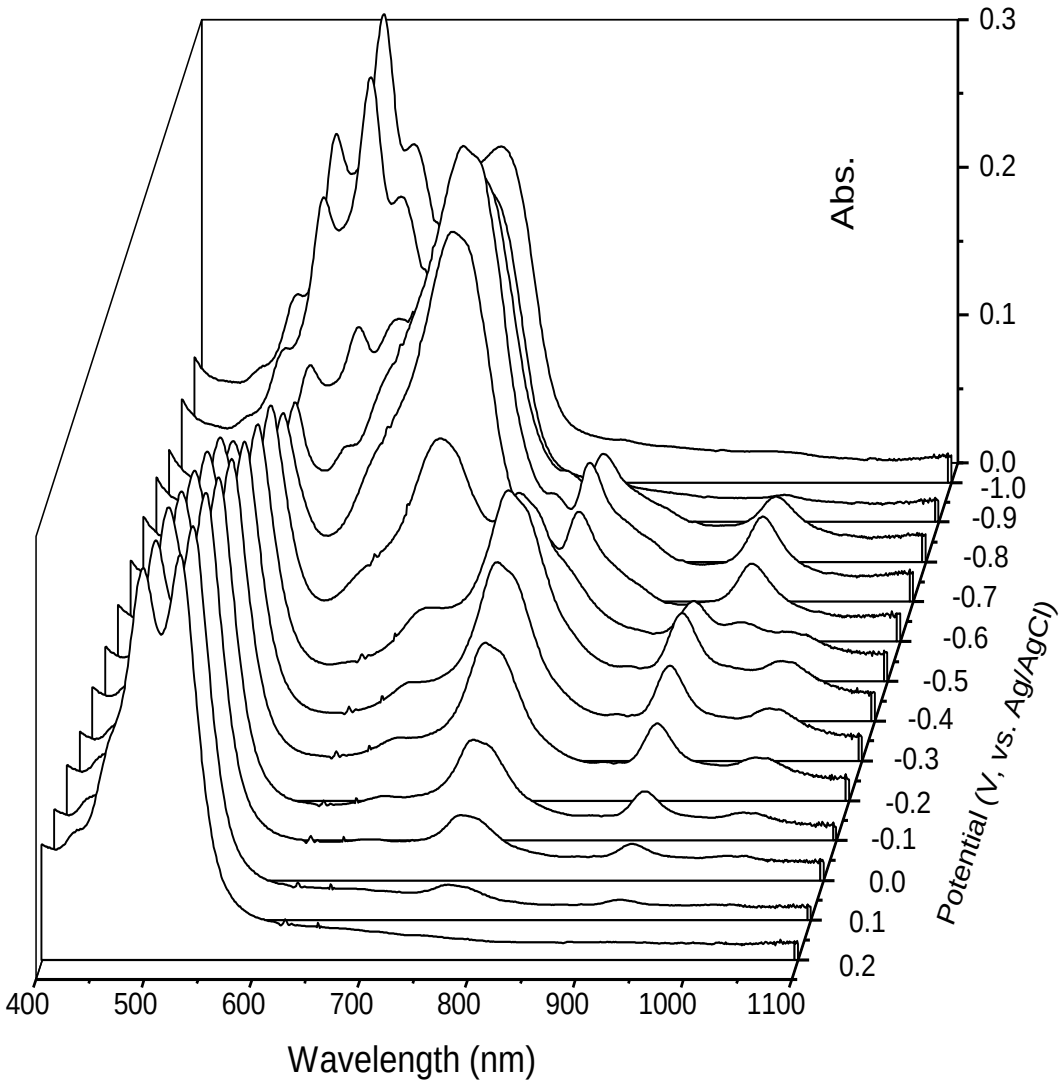

Figure 3-9. Electron trapping shown by spectroelectrochemistry in ITO|poly(DPTD)|poly(Cl_4DPTD) bilayers at negative potentials.

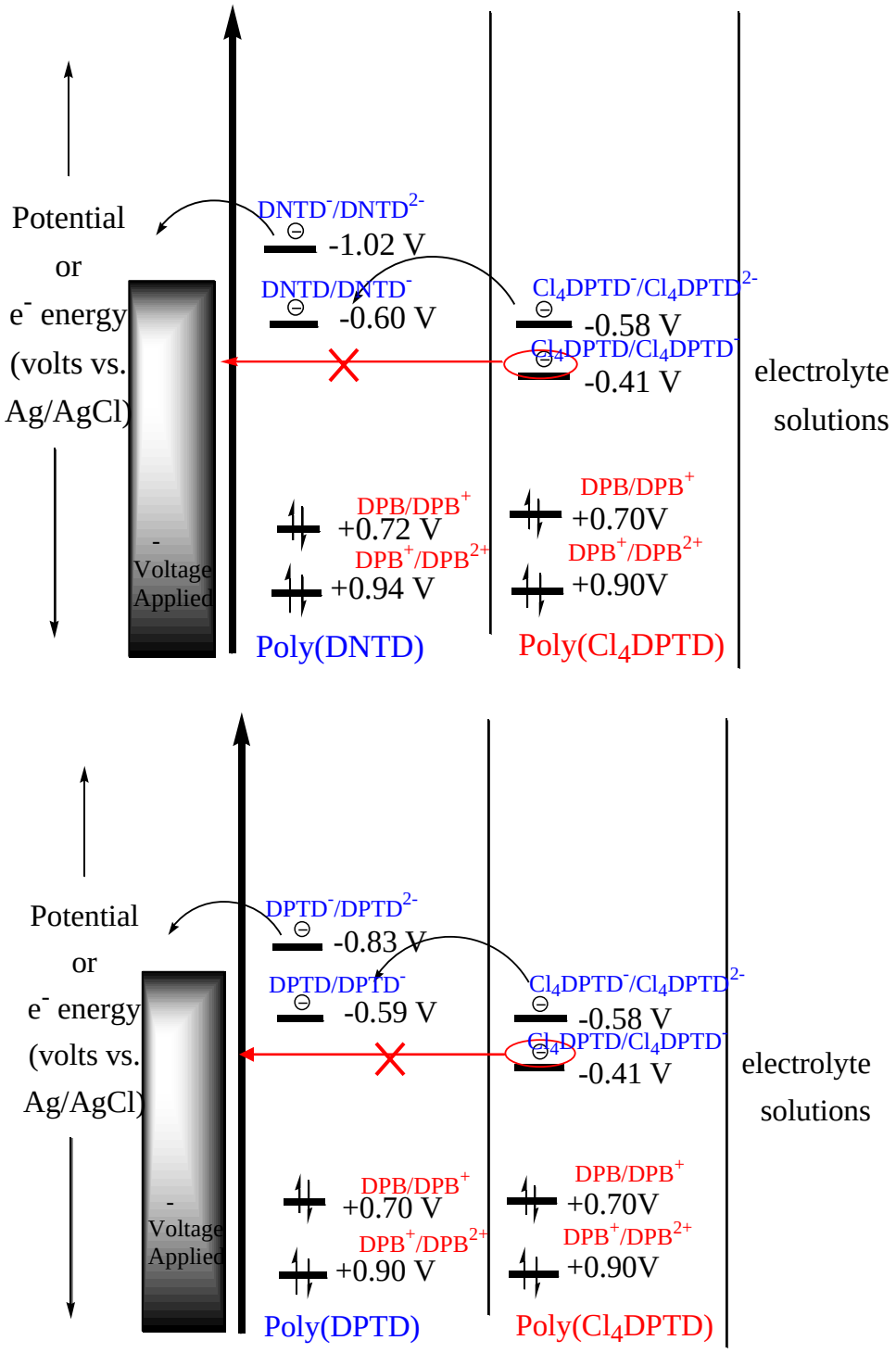

Scheme 3-1. Electron trapping in bilayers of ITO|poly(DNTD)|poly(Cl_4DPTD) and ITO|poly(DPTD)|poly(Cl_4DPTD).

The oxidation occurs as poly(Cl_4DPTD) dianion becomes the poly(Cl_4DPTD) anion at -0.4V, while at the same potential the poly(DNTD) anion transforms into the neutral insulating form. Upon further oxidation up to +0.3V, poly(Cl_4DPTD) anion is trapped between the electrolyte and the neutral poly(DNTD) polymer. Slightly more than +0.6V are needed to overcome this electron barrier. From Table 1, the first reduction potential of poly(Cl_4DPTD) is more positive than poly(DNTD) by +0.18V. This +0.18V uphill barrier requires the application of +0.6V to allow electron transfer. It is important to note that at +0.3V, poly(DNTD) has not accessed the p-doped, oxidized form which starts to occur at +0.6V. This result shows that electrons can be trapped in the poly(Cl_4DPTD) layer at potentials 0.6V more positive of their thermodynamic potential.

From Table 3-1, the first reduction potential of poly(DPTD) is nearly identical to that of poly(DNTD), while the second reduction of poly(DPTD) is more positive than that of poly(DNTD). The implication is that the same +0.18V barrier should exist for electron trapping in a bilayer composed to ITO|poly(DPTD)|poly(Cl_4DPTD) as in ITO|poly(DNTD)|-poly(Cl_4DPTD). The spectroelectrochemical responses for this bilayer for increasing potentials from -1.0V to 0.2V are shown in Figure 3-7B. At a potential of -1.0V, both of polymer films are reduced to their dianion forms and with increasing in potential, the poly(DPTD) dianion is oxidized by one electron becoming the anion, as evidenced by the absorption peak at 577 nm disappearing and peaks at 810 nm and 970 nm appearing while the peak at 688 nm remained unchanged.[9] The absorption peaks of poly(DPTD) anion start decreasing at -0.5V and vanishes at -0.4V. At the same potential, the poly(Cl_4DPTD) dianion spectroelectrochemical response

follows that of the poly(DPTD) anion where the peak at 688 nm starts to decrease at -0.5V and disappears at -0.3V. At a potential of -0.4V, the absorption bands at 763 and 923 nm corresponding to the poly(Cl_4DPTD) anion are most intense.[9] As above, single layer films of poly(Cl_4DPTD) anion are completely reoxidized at -0.4V but poly(Cl_4DPTD) anions exist in the bilayer even at +0.1V. This shows that electron trapping also occurs in the outer bilayer, but the positive potential required to overcome the barrier (0.4V) is less than in the poly(DNTD) case. The reasons for this are unclear. We speculate that either poly(DNTD) is a better insulator with fewer defect sites due to more efficient packing, or that the larger dispersion in energy levels for poly(DPTD) from additional defect sites reduces the barrier. When the inner layer is reoxidized to the neutral form cations are expelled into the outer layer.[14] For the outer layer to reduce the inner layer, energetic contributions from cation exchange must be accounted for. The important conclusion is that while the thermodynamic barrier may be relatively small, the actual barrier to electron transfer between layers can be much larger. The electron trapping diagrams for both bilayers are also shown in Scheme 3-1, in which the energy level of the poly(Cl4DPTD) anion is 0.18 eV smaller than those of the poly(DNTD) or poly(DPTD) anions.

3.4 CONCLUSIONS

The electron blocking and trapping behavior of a series of electrochemically polymerized bilayer materials have been studied by visible spectroelectrochemistry. Electron blocking could be achieved when the inner material of the bilayer has no energetically available electrochemical response. Electron trapping occurs when the bilayer is fully doped (in this case reductively) but the inner material is oxidized to the insulating form before the outer layer and the energetics for electron exchange is not favorable. A larger potential for overcoming that barrier is required than the one predicted by thermodynamics.

REFERENCES

1. Koezuka, H.; Hyodo, K.; MacDiarmid, A. G. *J. Appl. Phys.* **1985**, *58*, 1279-84.

2. Li, Y.; Cammarata, V. *Abstracts, 60th Southeast Regional Meeting of the American Chemical Society, Nashville, TN, United States, November 12-15* **2008**, SERMACS-2008.

3. Holze, R. *Handbook of Advanced Electronic and Photonic Materials and Devices Vol. 8: Conducting polymers*; Academy Press, 2001.

4. Keyes , T. E.; Foster, R. J. In *Handbook of Electrochemistry*; Zoski, C. G., Ed.; Elsevier: Boston, 2007.

5. Gale, R. J. *Spectroelectrochemistry: Theory and Practice*; Plenum Press: New York, 1988.

6. *Spectroelectrochemistry*; Kaim, W.; Klein, A., Eds.; RSC: Cambridge, UK, 2008.

7. Wang, L.; Cammarata, V. *Thin Solid Films* **1996**, *284-285*, 297-300.

8. Wang, L.; Goodloe, G. W.; Stallman, B. J.; Cammarata, V. *Chem. Mater.* **1996**, *8*, 1175-1181.

9. Wang, L.; Wang, Q. Q.; Cammarata, V. *J. Electrochem. Soc.* **1998**, *145*, 2648-2654.

10. Liang, J., Ph.D. Dissertation, Auburn University, 2003.

11. Wang, L., Ph.D. Dissertation, Auburn University, 1997.

12. Li, Y.; Cammarata, V.; Tin, C.-C. *unpublished results*.

13. Wang, Q., M.S. Thesis, Auburn University, 1999.

14. Cammarata, V.; Zhu, W.; Liang, J. *PMSE Prepr.* **2004**, *91*, 975-976.

CHAPTER 4

EFFECT OF STRUCTURAL MODIFICATIONS IN THE SPECTRAL PROPERTIES OF PERYLENE DIIMIDE DERIVATIVES AND P-N JUNCTION ORGANIC SOLAR CELLS BASED ON PERYLENE-CORE POLYMERS

4.1 INTRODUCTION OF PDIs AND THEIR OPVs

Fast progress in the efficiency of OPVs will potentially make them a competitive alternative to inorganic solar cells due to the low-cost of materials and fabrication processes. After more than 30 years of research, different types of materials for OPVs have been reported based on small molecules,[1,2] polymers[3,4] or combinations of both.[5,6] The highest literature reported power conversion efficiency (PCE) reported so far for a single cell is close to 7.4% in the case of poly[4,8-bis-substituted-benzo[1,2-b:4,5-b0]dithiophene-2,6-diyl-alt-4-substituted-thieno[3, 4-b]thiophene-2,6-diyl] (PBDTTT)-derived polymers[4] and p-type semiconducting polymers such as thieno[3,4-b]thiophene and benzodithiophene units.[7,8] The cell concepts here also include different cell structures, including single active layer,[9] p-n heterojunction bilayer,[1] bulk-heterojunction[3] and tandem cells,[10-12] as well as inverted p-n junction with a structure of ITO|n-type|p-type|metal.[5,6,10,13] In order to improve the PCE of OPVs, many aspects should be considered, such as the absorption coefficients of the materials, the exciton dissociation rates and the charge-carrier mobilities. Due to the low electron mobilities of organic materials, the active layer thickness should normally be limited to below 100 nm. Most

of the electron acceptors such as fullerene derivatives and TiO_2 nanoparticles for OPVs have relatively low light absorption coefficients in the visible region and do not π-π stack in any direction. However, perylene diimide (PDIs) deriviatives are a group of very interesting acceptors because they have large molar absorption coefficients, good electron accepting properties, show high electron mobility along the π-π stacking axis as well as being easily made and exhibit chemical and thermal stability.[14]

Perylene tetracarboxylic acid diimides (PDIs), perylene diimides for short, are well-known, widely available, typical n-type organic semiconductor materials. Perylene dyes (PDs) were first discovered and synthesized by Kardos and Weitzenbock in 1913,[15,16] and since then have been extensively studied for a variety of purposes, including pigments,[17] laser dyes,[14,18] electronic devices[19] and more recently solar cells.[1,20] Early uses included vat dyes, primarily because of their resistance to fading after being exposed for a long time to light, as well as for industrial dye pigments. It was not until much later, in 1959, that PDIs were found to be extremely fluorescent.[17] The main reason for this late discovery was a result of their poor solubility in most organic solvents. The parent PDIs give a strong yellow-green luminescence.[14] PDIs are characterized by high fluorescence quantum yields and photo-stabilities that have enabled them to serve as fluorescent standards, sensors,[18] and laser dyes.[21] The advantageous fluorescent properties have also enabled researchers to use these compounds as optical sensors.[22] The use of PDs as laser dyes has also increased substantially over the years because of their greater photostability than most other dyes.[23-25]

The parent structure of PDI is showed as Figure 4-1, exhibiting flat π-systems when R' is

sterically small, as confirmed by X-ray diffraction of several single crystals.[26-29] According to the observed bond lengths, perylene diimide can be thought in terms of two naphthalene half units, connected by two single bonds.[30] PDI structures have been shown to display several distinct properties; ones that affect their solubility,[14] electronic structure,[31] self-aggregation[30] and solid-state color.[32] The molecular structure of a substituted PDI is also shown in Figure 4-1. The rigid, perylene core is made up of benzene rings that act as a stabilizing feature, while the N-R single bond at each end of the molecule is known as the imide position. The bay positions are located on the edges of the benzene rings and are represented by R'. Different substitutions have been made at both the R and R' positions and have lead to the discovery of different characteristic properties of PDI molecules.

Like perylene itself, PDIs that are unsubstituted at the imide nitrogens have been found to be insoluble. Langhals contributed much in the area of PDI solubility[14] and found that substituting the PDI at the imide positions with aromatic amines increases the solubility dramatically. Further substitutions on the N-amide aromatic ring with either *tert*-butyl groups or long chain primary and secondary alkyl groups increases the solubility of the perylene diimide even more.[14,30] Substitutions at the bay positions of the PDI molecule have shown to change the rigidity of the perylene core to a more twisted conformation, which consequently increases the solubility as well. Also, substituents in the bay area have a pronounced effect on the respective redox potentials.[32]

Analysis using electrochemistry and UV-Visible spectroscopy reveals that the PDI parent LUMO and HOMO energies are at -3.8 eV and -6.0 eV,[33] respectively. The LUMO energy

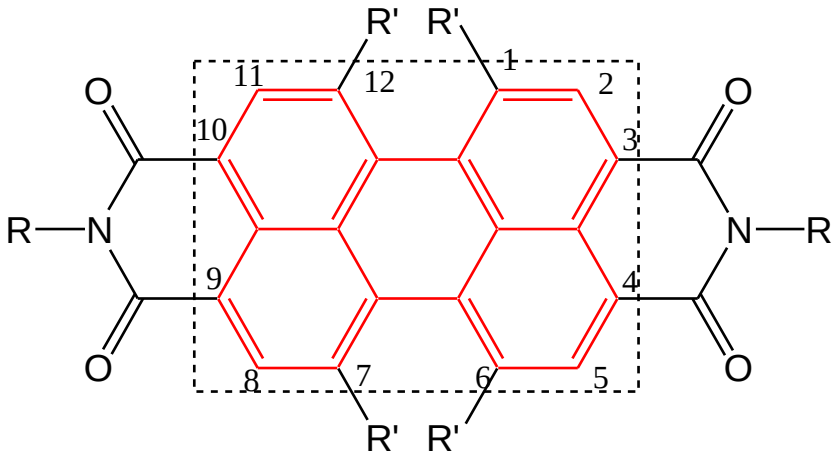

Figure 4-1 The parent structure of perylene diimide, R'=R=H.

is very close to the one of C_{60} and its derivative, PCBM, another n-type material used in photovoltaics. In order to match the energy levels of p-type materials, especially for those materials with higher HOMO and lower LUMO energy levels, it is necessary to modify the HOMO and LUMO energy levels of PDI's. PDIs are very conducive to modifications that change their LUMO and HOMO energy level to fit different p-type semiconductors. Normally, the chemical modifications at 1,6,7,12-perylene bay area positions (as shown in Figure 4-1) or the imide regions can fulfill the purpose. When electron-withdrawing or donating functional groups were added to these positions, the LUMO and HOMO of PDI could be modified. For example, when the 1,6,7,12-perylene bay area H-atoms were replaced by Cl-atoms, the PDI LUMO changes from -3.8 eV to -3.9 eV;[33] on the other hand, when the same positions were replaced by phenoxyl groups, the LUMO increases to -3.7 eV. If stronger electron donors or acceptors were added, both LUMO and HOMO would be affected, e.g. if the perylene bay area 1,7 –positions were replaced by the stronger donor, pyrrolidinyl groups, the PDI's LUMO and HOMO would change to -3.4 eV and -5.0 eV, respectively.[34] If cyano groups were added, which are stronger e^- acceptors than Cl-groups, the LUMO and HOMO energies changed to -5.0 eV and -6.04 eV, respectively.[34]

Along with appropriate energy levels, another important property for good n-type semiconductors is their electron mobility. Due to the high electron density and flat structure of the perylene core, it is very easy for PDIs to form π-π stacks, which contributes to enhanced electron mobility.[30] Also, increasing electron affinity of PDIs can be achieved by introduction of electron-withdrawing functional groups such as halogens or cyano groups in the bay area, which

lowers the LUMO energy.[34,35] As an example, when the 1,6,7,12-perylene bay area positions were replaced by Cl-atom, the electron mobility improves from 0.039 to as high as 0.14 $cm^2 \cdot V^{-1} \cdot s^{-1}$.[33] The replacement with Cl-atoms makes PDIs more electrophilic, which facilitates electron transfer in the solid-state. Currently, the highest reported mobility of a PDI derivative is 0.6 $cm^2 \cdot V^{-1} \cdot s^{-1}$ with N,N'-dioctyl-3,4,9,10-perylene tetracarboxylic diimide (PTCDI-C8H).[36] Higher mobility allows excitons to reach an interface in a shorter time before they are quenched, increasing charge separation efficiency. This is favorable to improving the power efficiency of a solar cell.

The photo-induced charge separation between PDI and metal phthalocyanine has been widely investigated by femtosecond transient spectroscopy. The Wasielewski group found that a donor-acceptor radical will form under laser excitation in a few picoseconds for the dendrimer molecules including PDI and ZnTPP.[37,38] Also $PDI^{-\cdot}$ radicals interact strongly with adjacent PDI molecules in the dendrimer molecular column stack.[37-39] They also found that it takes about 3.2 ps to form the $ZnTPP^{+}$-PDI^{-} radical ion pair resulting in charge separation.[37] The radical recombination time is 3.0~4.8 ns.[38]

The PTCBI-CuPc based OPV was first investigated by Tang and its efficiency was close to 1%.[1] The original Tang OPV efficiency was improved by the Forrest research group. In 2000, they added an exciton-blocking layer, bathocuproine (BCP), to the Tang cell and the efficiency reached 2.4%.[40] They also used PTCBI-CuPc co-sublimation followed by annealing to build a bulk-heterojunction structure, resulting in cell efficiency of about 1.5% in 2003.[20] A new vapor phase deposition (VPE) helped to increase the efficiency for this system further to 2.2 %.[41,42]

In order to improve the efficiency of OPVs, another approach is to yield increased optical absorption and photocurrent generation in the photoactive layer by inducing surface plasmons through careful control of nanoparticle properties. Metallic nanoparticles incorporated in OPVs can exhibit strong scattering of the incident light when the frequency of the incident photon matches the surface plasmon resonance of the metallic nanoparticles.[43-45] Some metallic nanoparticles exhibit a broad absorption spectrum depending on types of metal, particle size and shape, which dictate the corresponding surface plasmon resonances.[43] Kulkarni, et al.[46] also showed that silver nanoparticles can enhance optically produced polaron charge generation three fold over pure 3-hexylthiophene. Silver and gold nanoparticles incorporated with organic photoactive layers have been shown to improve cell performance 20-40% compared to the devices without nanoparticles.[47-50]

To date, most of the applications for OPVs with perylene derivatives were performed with DSSC,[51,52] layered structures through vapor deposition with insoluble PDIs,[1,5,13] as well as spin coating with those soluble ones.[34] The inverted p-n structure with PDI related materials has proven to work as well as normal p-n structures without any further modification of the ITO glass, see Chapter 1, Table 1-1.[1,5,6,10,13,53-57] However, applications of polymers with perylene units are quite limited[58,59] and to the best of our knowledge, here we report OPVs fabricated from the electropolymerization of PDI-core monomers solution for the first time. Thus, in this chapter we have undertaken a systematic study on various PDIs, which have different functional groups in the polymer units, to find a solution fabrication method and the most promising PDI acceptor structure for OPVs. Four different PDI-core monomers were chosen: **DPTD**,

N,N'-Di[p-phenylamino (phenyl)]-perylene-3,4,9,10- tetracarboxylic diimide; **Cl_4DPTD**, (N,N'-Di[p-phenylamino (phenyl)]-perylene-1,6,7,12 tetrachloro-3,4,9,10-tetracarboxylic diimide); **(t-BuPhO)$_4$DPTD**, N,N'-di[p-phenylamino(phenyl)]- 1,6,7,12-tetrakis (4-tert-butylphenoxy-perylene-3,4,9,10-tetracarboxylic diimide; and **cyclohexyl-DPTD**, N,N'-dicyclohexyl-1,7-di-p-anilino- phenoxy-perylene-3,4,9,10- tetracarboxylic diimide. The structures of DPTD, Cl_4DPTD, (t-BuPhO)$_4$DPTD and cyclohexyl-DPTD structures are shown in Figure 4-2. All of these monomers have the same chemical structure motif of R-X-R. Based on previous research, all of them can be electropolymerized on transparent ITO electrodes.[60,61] This leads to an inverted p-n structure with ITO|n-type|p-type|metal when followed by vacuum thermal evaporation of CuPc and then silver metal.

Copper phthalocyanine (**CuPc**, structure shown in Figure 4-3), which is known to show high hole mobility, has been chosen as a electron donor by many researchers.[62-65] Using **CuPc** as a hole transporting layer and varying the electron acceptor PDI-core polymers, we can assume that the observed properties differences in devices are mainly derived from the different structural and physical properties of the PDIs.

4.2 EXPERIMENTAL

4.2.1 Reagents and materials

Methylene chloride (CH_2Cl_2, 99.9% Fisher) was freshly distilled from calcium hydride (CaH_2, Aldrich) and used as a solvent for electropolymerization. Tetrabutylammonium

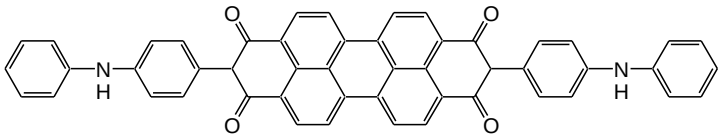

DPTD

N,N'-Di p-phenylamino (phenyl) -perylene-
3,4,9,10- tetracarboxylic diimide

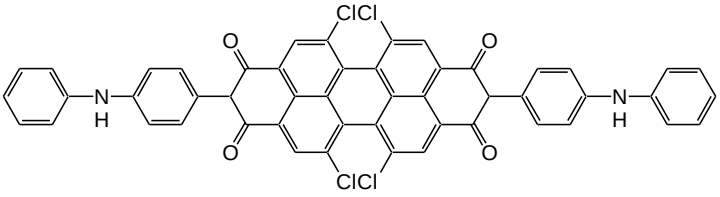

Cl_4DPTD

N,N'-Di p-phenylamino (phenyl) -perylene-
1,6,7,12 tetrachloro-3,4,9,10-tetracarboxylic diimide

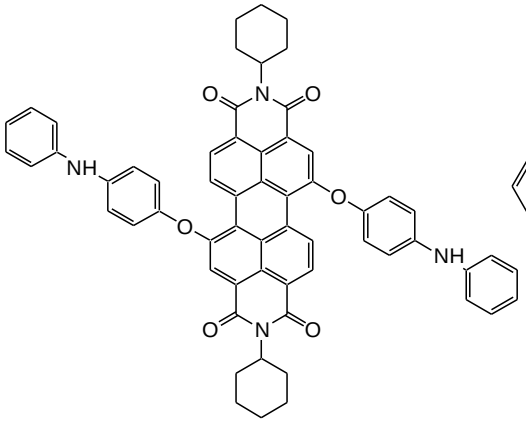

Cyclohexyl-DPTD

N,N'-dicyclohexyl-1,7-di-*p*-anilino-phenoxy-
perylene-3,4,9,10-tetracarboxilylic diimide

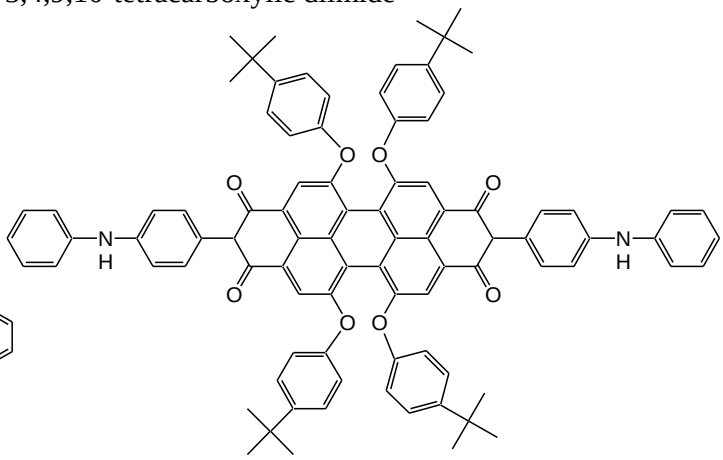

(*t*-BuPhO)$_4$DPTD

N,N'-di[*p*-phenylamino(phenyl)]-1,6,7,12-tetrakis
(4-*tert*-butylphenoxy)- 3,4,9,10-tetracarboxilylic diimide

Figure 4-2 Chemical structures of four different monomers that produce perylene-core polymers.

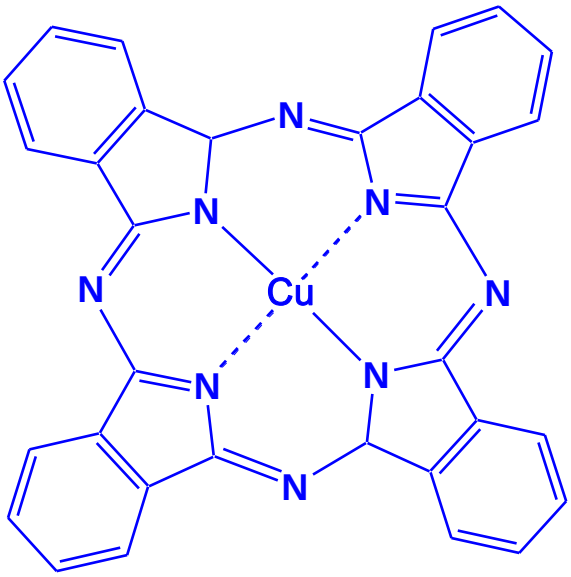

CuPc

Figure 4-3 Chemical structure of copper phthalocyanine.

hexafluorophosphate, $TBAPF_6$ (Aldrich, 98%) was dried under vacuum at 100 °C for at least 48hrs. The PDI-core monomers were previously synthesized in our lab[60,61] and their corresponding polymers were investigated as electrochromic materials. PTCBI was synthesized using published procedures.[66] All polymers were polymerized via electro-oxidation in a standard three-electrode cell in their solutions with 0.2 mM monomer concentration and 0.1 M $TBAPF_6$; details of the electropolymerization process have been published previously.[61] Indium Tin Oxide (ITO) coated glass slides were purchased from Delta Technologies Inc. with a sheet resistance of 70Ω/□. Copper phthalocyanine, CuPc (Aldrich, 99%) was used as p-type material for the OPVs.

4.2.2 Analytical instruments

UV-Visible and fluorescence spectra were measured using a Shimadazu UV-VIS-NIR double beam spectrometer (UV-3600) using 1 nm slit width and Perkin Elmer LS55 Luminescence Spectrometer, respectively. The transmission baseline of the optical spectra were referenced to a blank ITO glass substrate and data was recorded in slow scan mode with a slit width of 2 nm. Diffuse reflection visible spectra were obtained from Shimadazu UV-2501 PC UV-Visible double beam spectrometer with an ISR-240A diffuse reflectance attachment with a 5 nm slit width. The baseline of diffuse reflectance spectra was also based on a blank ITO glass in the 400-800 nm range.

4.2.3 OPV fabrication

All photovoltaic devices were fabricated as sandwich structures with two active layers between ITO and a backside Ag electrode, see Figure 4-4. ITO coated glass was sonicated

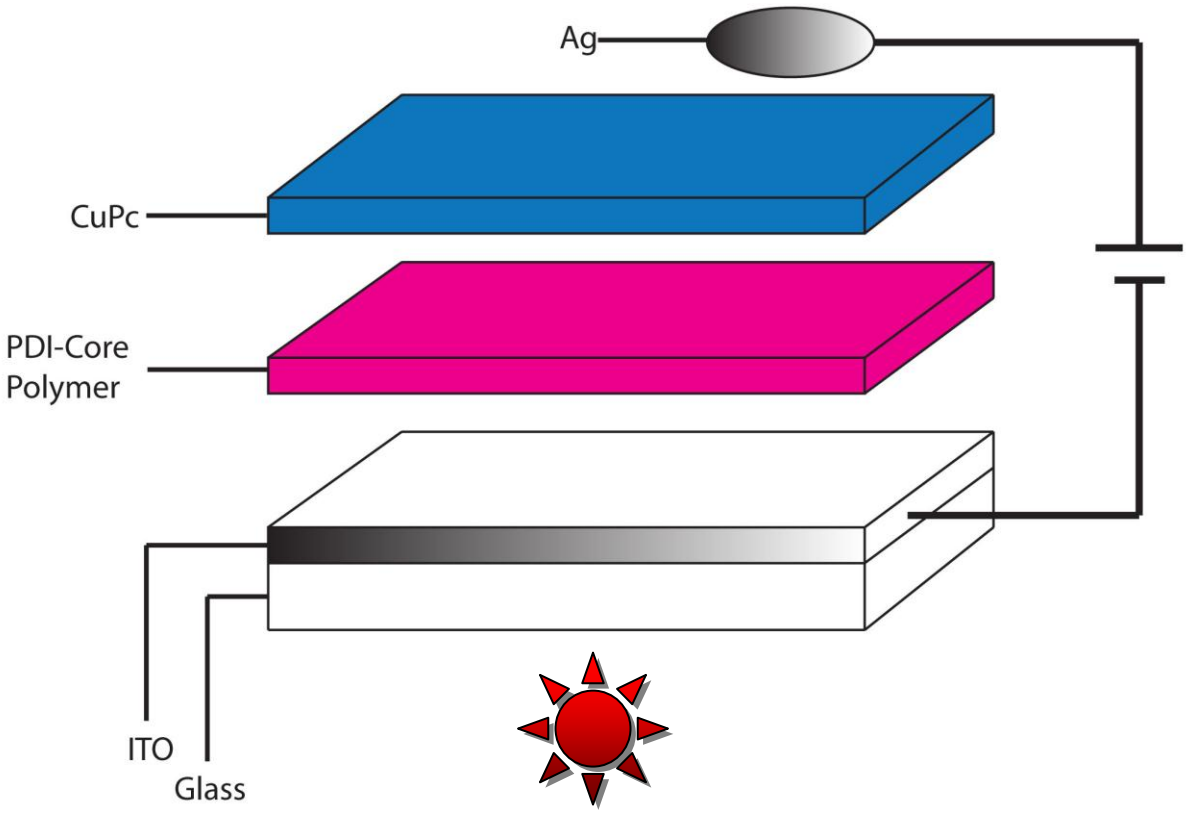

Figure 4-4 PDI-polymers-CuPc photovoltaic devices configuration.

in methanol for 30 mins., then cleaned in a mixture of hydrogen peroxide (H_2O_2, 30.9%, Fisher), ammonium hydroxide (NH_4OH,37% , Fisher) and de-ionized water in volume ratio of 1:1:10.[67] The surface of cleaned ITO glass with size of 11×25 mm was modified by oxidative electropolymerization of different polymers. The modified ITO glass was removed from the monomer solution and rinsed thoroughly with CH_2Cl_2 to remove the electrolyte. CuPc (Aldrich, 99%) was deposited onto dry glass slides modified with PDI-core polymer *in vacuo* (base pressure < 2.0×10^{-5} Torr) using our home-made thermal evaporation system with turbo and mechanical pumps, see Figure 4-5. A typical evaporation process consists of: 1) maintain chamber under vacuum for about 30 mins; 2) turn on the power supply connected to heater and the CuPc-contained basket; 3) set current to 32 A where the voltage will increase slowly to about 3.5 V. The CuPc will sublime and deposit on cold polymer surface in 60 seconds after the heater becomes red. In order to get a CuPc film of proper thickness (20-25 nm), the evaporation time is about 110-120 seconds. After adding a layer of CuPc on the polymer, an Ag top electrode was deposited by the same procedure on top of the organic layers through a shadow mask. The current for Ag sublimation is 110 A and voltage is about 4.8 V. The pixel size as defined by the overlap of ITO and Ag back electrode was 1.1-2.0 mm^2, see Figure 4-5 for the mask size.

4.2.4 Nanoparticle deposition

The Au nanoparticles were purchased from Aldrich Chemicals with a mean particle size of 8-12 nm. The nanoparticles were deposited dropwise on the polymeric film surface and baked in a 90 ºC oven to evaporate the water from the gold nanoparticle solution before deposition of the CuPc layer and the Ag electrode. All other device fabrication and all measurements were

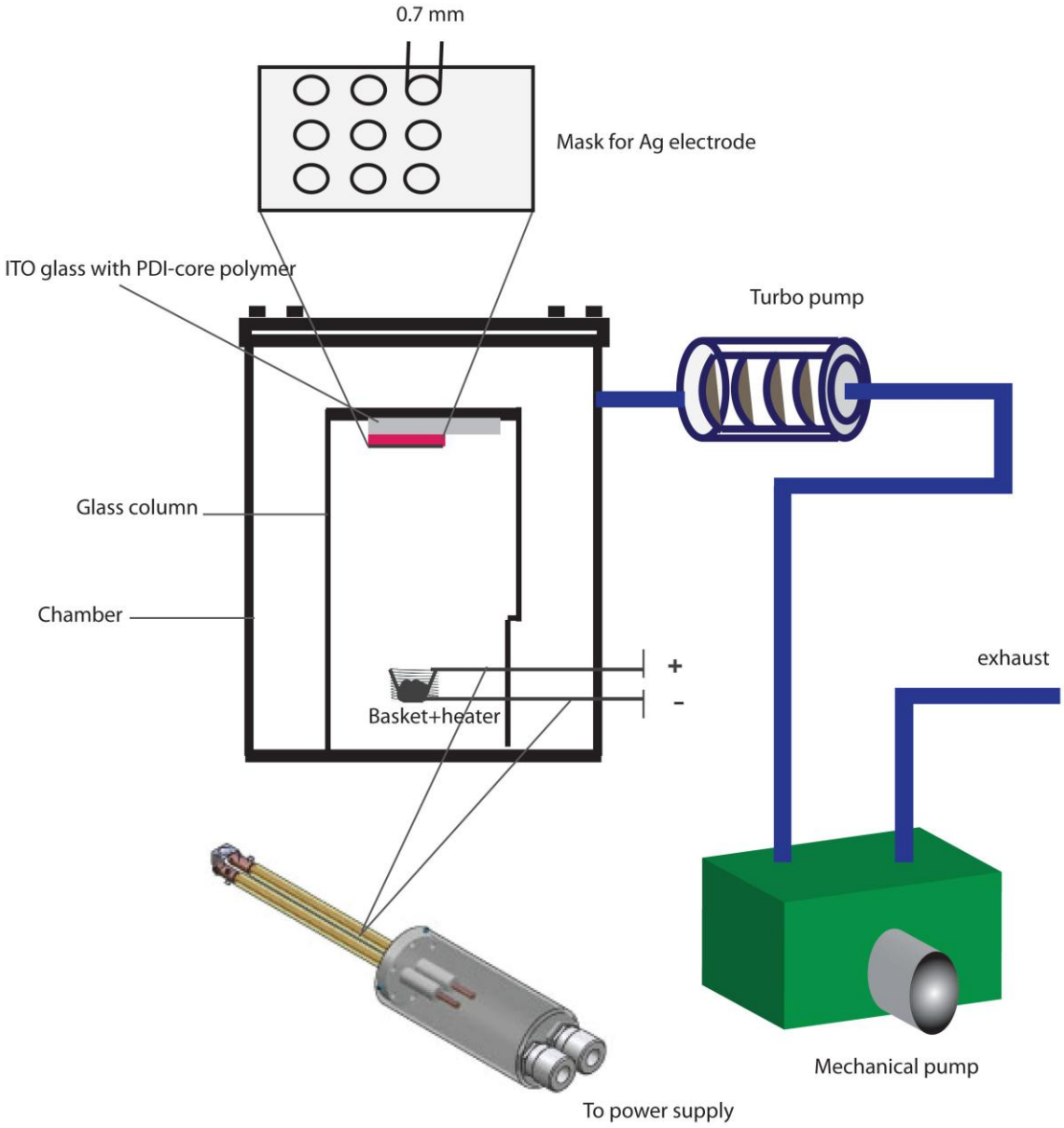

Figure 4-5 Diagram of home-made thermal evaporation system.

performed at ambient atmosphere as using the same procedure as described in part 4.2.3.

4.2.5 OPV characterization

All electrical measurements were performed at ambient atmosphere. The current-voltage curve of the photovoltaic device was measured in dark and under illumination of light with an intensity of ~100 mW/cm^2 (Newport Oriel Apex Illuminator, AM1.5), calibrated by a powermeter (Newport powermeter 1815-C). Electrical data were taken using a Keithley 6487 picoammeter/voltage source unit communicating with a Labview 8® (National Instrument) programmed computer.

4.3 RESULTS AND DISCUSSION

Fabrication of organic photovoltaic cells and electronic devices requires better soluble PDI-core semiconductor materials in order to enable utilization of solution processes, although insoluble and high-melting PDIs like PTCBI are easily obtained by the reaction of perylene tetracarboxylic acid dianhydride with a multitude of aromatic or aliphatic amines.[66] There are two proven, successful approaches to prepare soluble PDIs: introducing of solubilizing substituents at the imide nitrogen, and substitution of such groups into the bay area. In order to make oxidative electropolymerizable PDI monomers, it is necessary to introduce electropolymerizable groups in either imide nitrogen or the bay area. In our case, we introduce diphenylamine groups for DPTD, Cl_4DPTD and (t-BuPhO)$_4$DPTD at the imide nitrogen position. DPTD contains H-atoms in the bay area and to decrease the LUMO energy, four Cl-groups were introduced to generate Cl_4DPTD. To increase the LUMO energy, four *p*-tert-butyl phenoxyl

groups were introduced into the same bay area positions to form (t-BuPhO)$_4$DPTD. Cyclohexyl groups have been shown to increase solubility of macromolecules. In order to provide an electropolymizable linkage, two *p*-anilino-phenoxyl groups replaced the H-atoms at the bay area to make the product electropolymerizable, see Figure 4-2. Among these four monomers, (t-BuPhO)$_4$DPTD and cyclohexyl-DPTD have much better solubility in CH_2Cl_2 than the other two. The steric bulk of the t-butyl phenoxy group introduced to the bay region and the steric strain in the bay area can lead to twisting of the two naphthalene half units of the parent PDI core from the flat π-system, and the cyclohexyl group at the imide position also minimizes π-π aggregation in solution.[32]

4.3.1 Work function of PDI-core polymeric films

The electrochemical properties of PDIs have been investigated by many researchers.[33,68] Their data show that PDIs are fairly electron deficient dyes, which are easily reduced and rather difficult to oxidize, leading to enhanced air stability. For the parent PDI, two reversible reduction waves are found via cyclic voltammetry. The first reduction potential is very comparable to that of C_{60}. The redox properties of the electroactive PDI-core polymers and molecules were determined by cyclic voltammetry measurements at room temperature in CH_2Cl_2. In Liang's work,[61] as well as depicted in Figure 1-8 A, poly(cyclohexyl-DPTD)'s CV exhibits only one redox couple at negative potentials, the first half wave reduction potential, $E_{1/2}^{-1}$, is about -0.783 V vs. Ag/AgCl. Figure 1-8 B shows that poly(t-BuPhO)$_4$DPTD displays 2 redox couples at negative potentials and 3 couples at positive potentials. The first half-wave reduction potential

$E_{1/2}^{-1}$ is at about -0.703 V and, the first half wave oxidation potential, $E_{1/2}^{+1}$ is at about 0.805 V vs. Ag/AgCl. This shows the greater electron density at the perylene core for (t-BuPhO)$_4$DPTD and cyclohexyl-DPTD than for DPTD, but Cl$_4$DPTD is more electron deficient than DPTD.

With the information of redox properties of each compound, the relative LUMO energy levels could be evaluated. In order to estimate the absolute energies of LUMO levels, the redox data are standardized to the ferrocene-ferricenium couple, which is calculated at an absolute energy of -4.8 eV.[69] Here, Ag/AgCl vs. Fc/Fc$^+$ is about -0.35 V.[34] The LUMO energy levels then can be calculated using equation (4-1). In the same manner, the HOMO energy levels of all four polymers can be also estimated by their first half-wave oxidative potentials with equation (4-2). The LUMO and HOMO energy levels of these compounds obtained from equation (4-1) and (4-2) are listed in Table 4-1:

Table 4-1. Electroactive data and work function of different polymers/compounds

Polymers/ Compounds	DPTD	Cl$_4$DPTD	(t-BuPhO)$_4$ DPTD	Cyclohexyl-DPTD	CuPc
1st Half-wave Oxidative data $E_{1/2}^{+1}$ (V)	0.700	0.705	0.771	0.717	N/A
1st Half-wave Reductive data $E_{1/2}^{-1}$ (V)	-0.592	-0.413	-0.708	-0.775	N/A
Longest wavelength absorbed (nm) at 0 V	530 (2.340 eV)	524 (2.366 eV)	581 (2.134 eV)	552 (2.246 eV)	695
HOMO (eV)	-5.150	-5.155	-5.221	-5.167	-2.65[70]
LUMO (eV)	-3.858	-4.037	-3.742	-3.675	-4.85[70]

Note: All electrochemical potentials derived from CV in CH_2Cl_2 with 0.1M $TBAPF_6$ at a scan rate of 200 mV/s and at room temperature.

Φ_{LUMO} = - first reduction voltage (vs. Ag/AgCl) – (4.8-0.35) eV (4-1).

Φ_{HOMO} = - first oxidation voltage (vs. Ag/AgCl) – (4.8-0.35) eV (4-2).

The work function of each PDI-polymer and CuPc is illustrated in Figure 4-6.

4.3.2 Spectral studies in solution and solid-state films

UV-Visible spectroscopy experiments were performed on the organic materials DPTD, Cl_4DPTD, cyclohexyl-DPTD, and (t-BuPhO)$_4$DPTD in CH_2Cl_2 solutions and solid state films. Figure 4-7 presents the absorption spectra of these perylene-core monomers in solution. Several authors have studied the absorption and fluorescence properties of the perylene derivative films in detail.[14,21,30,32,34] These monomers, similar to other PDIs, have intense absorption bands in the 400-600 nm region. In our case, the maximum absorption of DPTD, Cl_4DPTD, cyclohexyl-DPTD and (t-BuPhO)$_4$DPTD are 530, 524, 552 and 581 nm, respectively. For the unsubstituted PDI-core compound—DPTD, an absorption at 530 nm with a strongly pronounced vibronic fine structure is observed which has been assigned to the electronic S_0-S_1 transition, with a transition dipole moment along the long molecular axis.[30] Pronounced changes in the absorption and emission bands take place if the parent PDIs are substituted at the aromatic core in the bay area. With two phenoxy groups attached at positions 1 and 7, the maximum shifts to longer wavelengths by about 20 nm (cyclohexyl-DPTD at 552 nm) and with four phenoxy groups the peak shifts by almost 50 nm ((t-BuPhO)$_4$DPTD) as compared to the unsubstituted parent PDI. This is in a good agreement with previous results.[71-73] According to AM1 calculations and the crystal structure of a related dye, two phenoxy substituents induce a

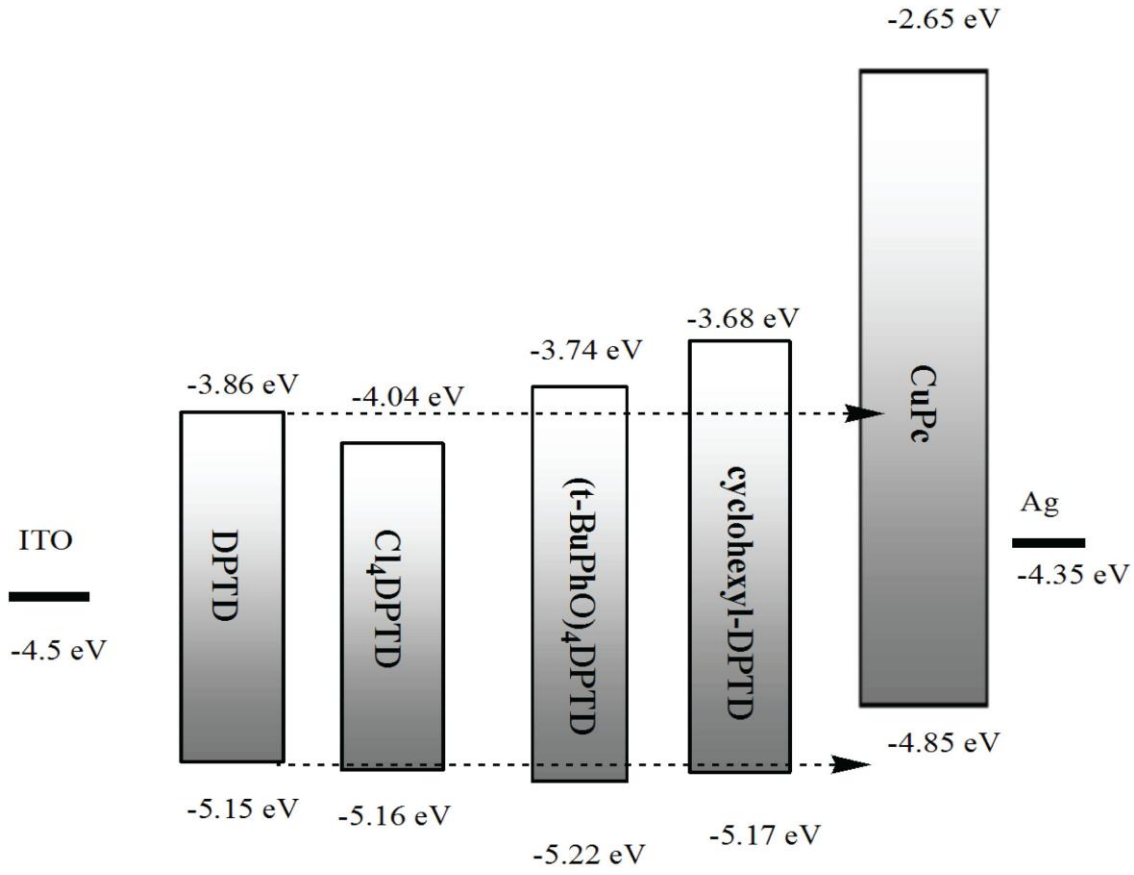

Figure 4-6 Energy level diagrams of ITO|PDI-core polymer|CuPc|Ag devices, the ITO and silver work functions were obtained from references.[74,75]

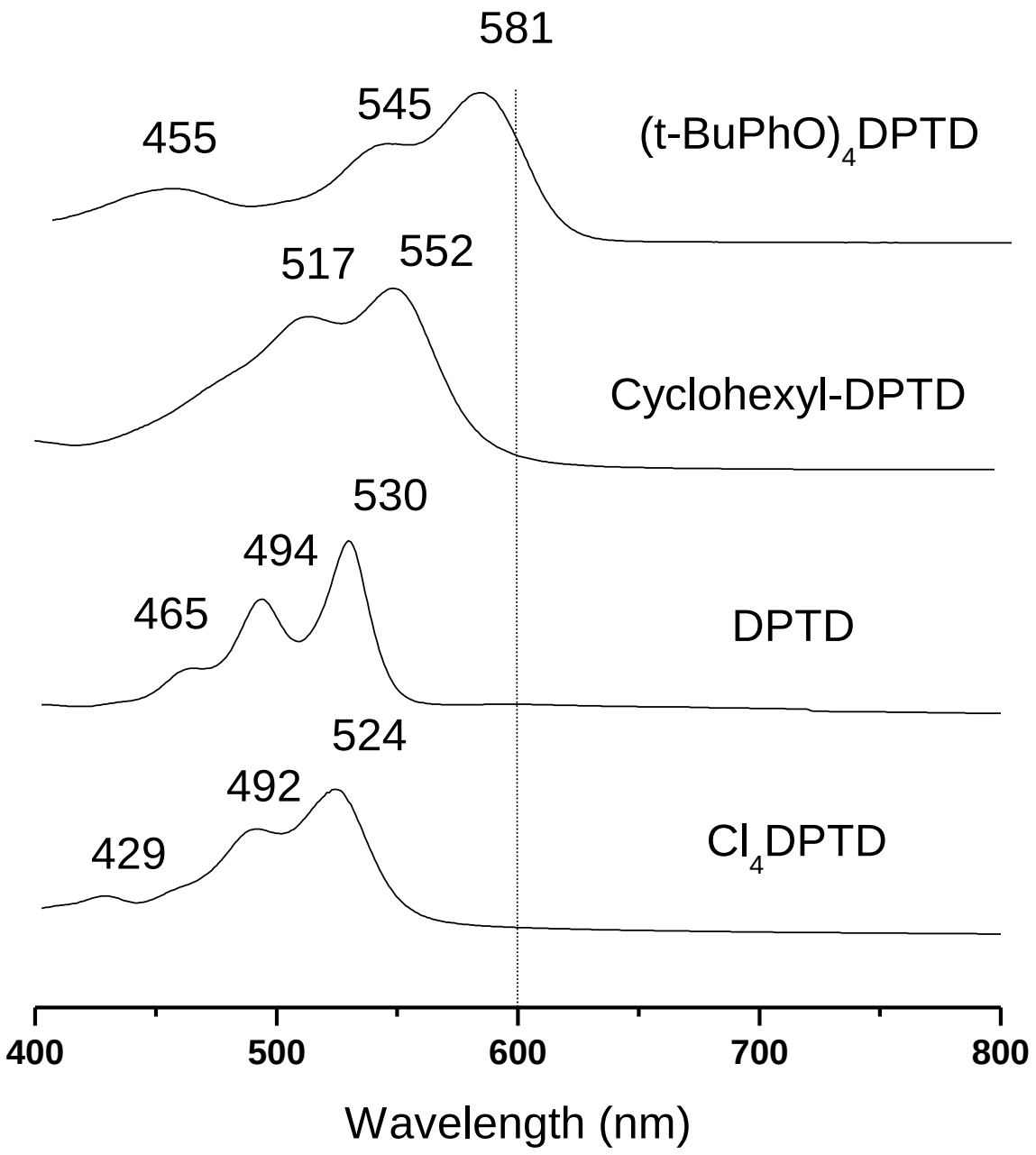

Figure 4-7 UV-Visible spectra of different PDI-core monomers in dichloromethane,

(Concentration of DPTD is 4×10^{-6} M and other three are 6×10^{-6} M).

twisting of the two naphthalene subunits in the perylene core by about 15º, and a 25º twisting results for four substituents.[30] The resulting loss of planarity and rigidity of the PDI core causes considerable absorption band broadening. In our case, the absorption spectra of Cl_4DPTD, (t-BuPhO)$_4$DPTD and cyclohexyl-DPTD are all broadened as compared to that of DPTD.

The optical properties of these four monomers in CH_2Cl_2 are also summarized in Table 4-2. Because of the rigidity of the perylene core in DPTD, this molecule exhibits a higher absorption coefficient than the other monomers and its quantum yield of fluorescence is close to 1, which is higher than the others too. The wavelength of maximum fluorescence intensity for each compound in solution is also listed in Table 4-2.

Table 4-2 Optical properties of perylene-core monomers in CH_2Cl_2

Compounds	λ_{abs}/nm	$\varepsilon/M^{-1}\cdot cm^{-1}$	λ_{em}/nm
DPTD	530	6.55×10^4	537
Cl_4DPTD	524	4.66×10^4	550
Cyclohexyl-DPTD	552	4.38×10^4	576
(t-BuPhO)$_4$DPTD	581	4.67×10^4	602

Note: λ_{abs}: maximum absorption wavelength; λ_{em}: maximum emission wavelength

Solid state polymeric films of these compounds were also characterized and their visible spectra are shown in Figure 4-8. From these results, it is evident that when PDI films were electropolymerized from dichloromethane solution to form solid state films, the full width of at

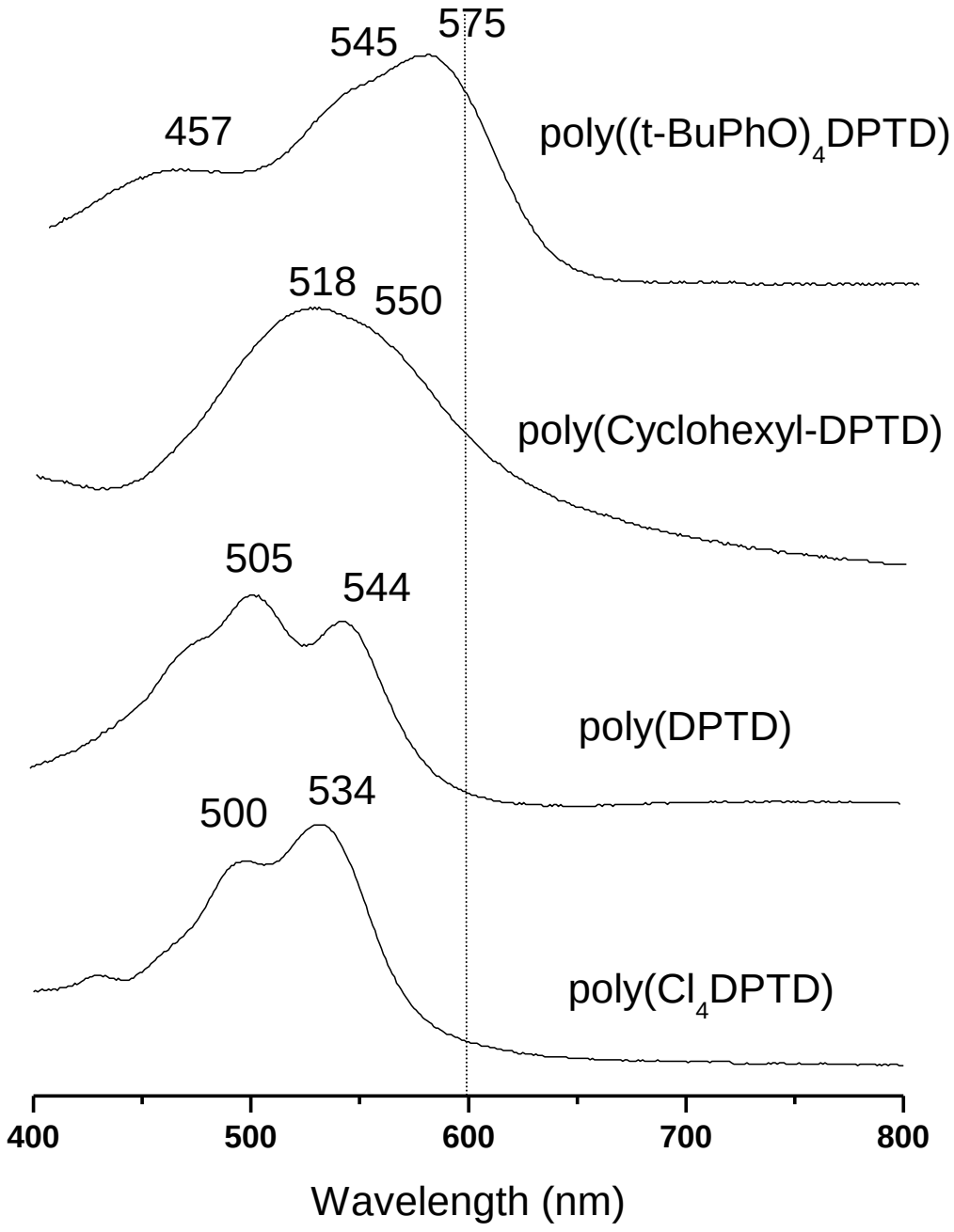

Figure 4-8 UV-Visible spectra of different PDI-core polymeric thin films on ITO.

half maximum absorption of solid films becomes much broader than in solution. The maximum absorption peaks of poly(DPTD) and poly(Cl_4DPTD) in solid films show a bathochromic shift (a change in band position to a longer wavelength) relative to those of the monomers after electropolymerization. This red shift is believed to be caused by the H-aggregation of perylene moiety, consistent with face to face aggregation.[37] The extended H-aggregation in the acceptor polymers could give rise to a charge transport channel along the π-π stacking axis. However, the transmission visible spectra of cyclohexyl-DPTD and (t-BuPhO)$_4$DPTD polymeric thin films shows the same absorption maximum, which implies that they do not form extended aggregates as much as poly(DPTD) and poly(Cl_4DPTD) undergo in the solid state. The reason, at least partially, could be that the steric hindrance of the phenoxy groups in the bay area twists the perylene core, preventing a close approach of the two rings.

Transmission visible spectra of PDI-core polymer/CuPc solid-state bilayers are presented in Figure 4-9. As shown in this Figure, the peaks at 690 nm and 617 nm are assigned to CuPc absorptions. Spectra for DPTD-CuPc, Cl_4DPTD-CuPc and Cyclohexyl-DPTD-CuPc cover the region from 490~700 nm. The Cl_4DPTD-CuPc spectrum shows a weaker absorption at about 570±20 nm but depicts a sharp absorption at 536 nm. However, because of the red shift in the absorption of (t-BuPhO)$_4$DPTD relative to that of DPTD, the PDI signal partially overlaps the CuPc's absorption at 619 nm. The spectrum of a (t-BuPhO)$_4$DPTD-CuPc bilayer shows a very strong absorption peak at 590 nm but with a smaller absorption coefficient than the other three polymers in other regions. The visible diffuse reflectance spectra of single layers and bilayers containing CuPc are also depicted and compared with their respective visible absorption spectra

in Figure 4-10. As we can see, the reflectance and absorption spectra are similar but the reflectance spectra shows less scattering, narrower absorption bands and they resemble closely to the spectra of these compounds obtained in CH_2Cl_2 solutions.

Table 4-3 summarizes the optical properties of solid state perylene-core polymer films on ITO. The absorbance coefficient of the solid films is somewhat lower than that of to the monomers in solution. Fluorescence of the solid films was not detected when examined with a fluorescence microscope; most likely the fluorescence of solid film being quenched by the ITO layer present on the glass, or self-quenching.

Table 4-3 Visible properties of solid state perylene-core polymer film

Compounds	λ_{abs}/nm	Absorbance coefficient ($/M^{-1}\cdot cm^{-1}$)	Surface density Γ, ($\times 10^{-9} mol/cm^2$)
DPTD	544	5.33×10^4	2.14
Cl_4DPTD	534	3.75×10^4	2.46
Cyclohexyl-DPTD	550	3.41×10^4	3.18
(t-BuPhO)$_4$DPTD	575	3.87×10^4	3.05

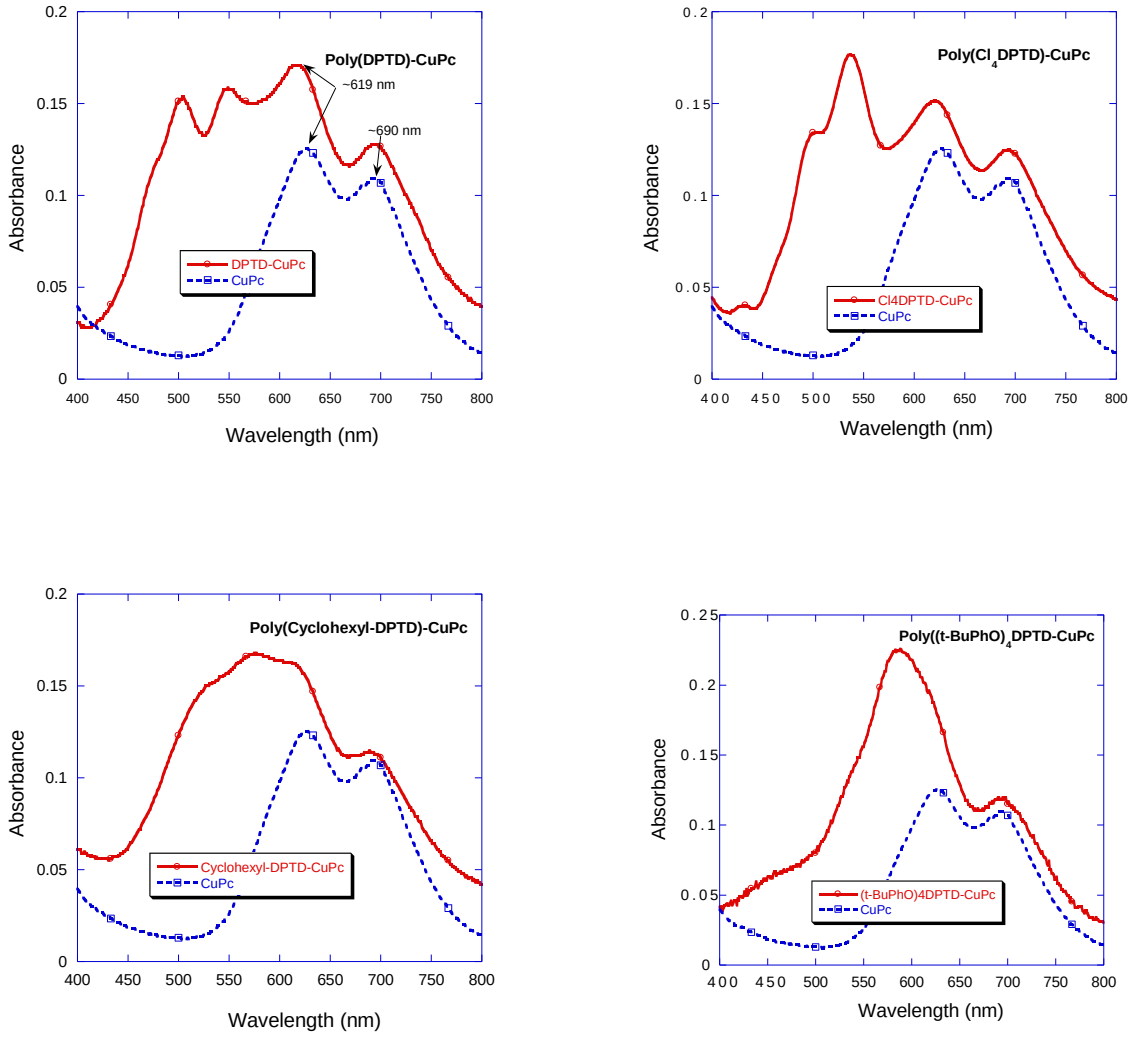

Figure 4-9 Visible Spectra of different PDI-core polymer-CuPc bilayers on ITO glass, the peaks at ~619 nm and 690 nm are assigned to CuPc absorption.

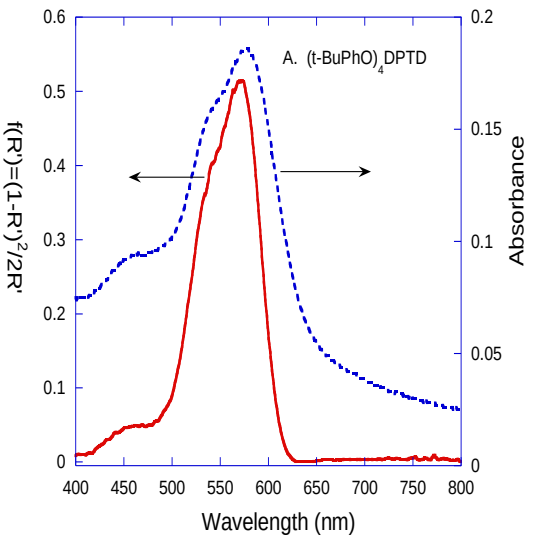

A: poly((t-BuPhO)$_4$ DPTD)

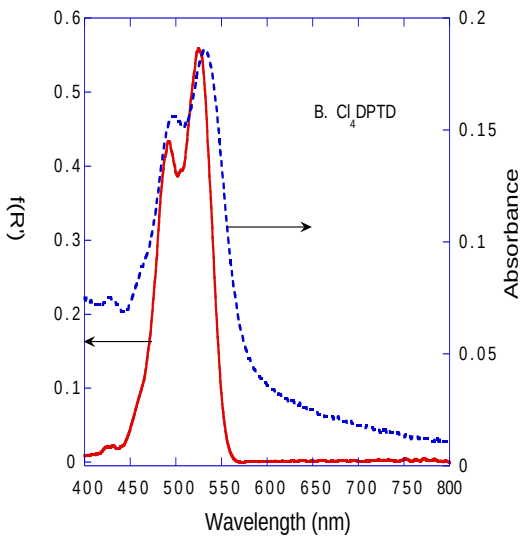

B: poly(Cl$_4$ DPTD)

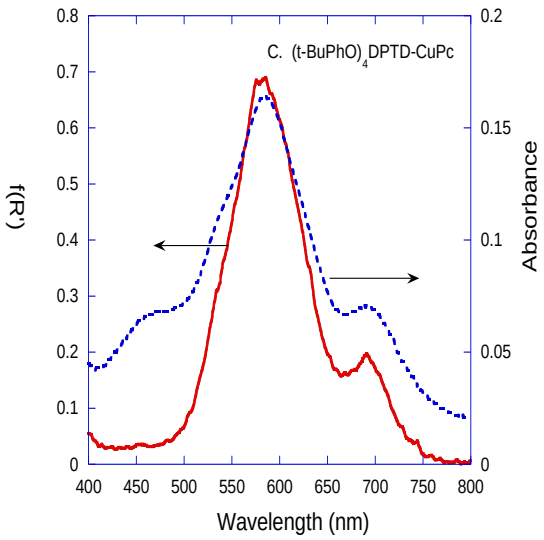

C: poly((t-BuPhO)$_4$ DPTD)-CuPc

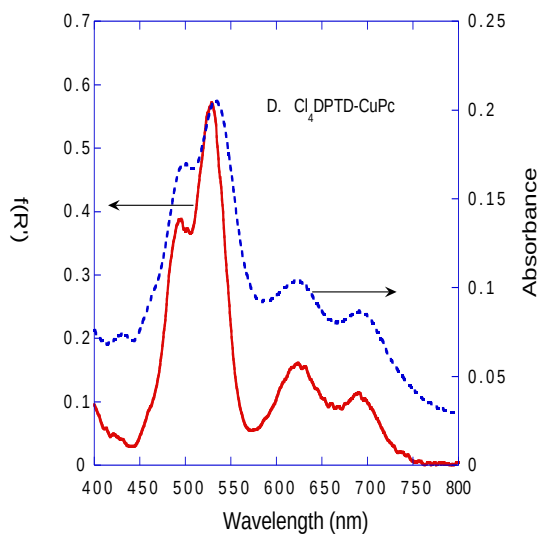

D: poly(Cl$_4$ DPTD)-CuPc

Figure 4-10 Diffuse reflectance spectra of polymeric single layers (A,B) and bilayers with CuPc (C, D).

4.3.3 Thickness determination of CuPc

The thickness of the CuPc film cannot be directly determined in the process of thermal evaporation with our vacuum chamber system. As CuPc forms soft organic thin films, it is difficult to measure the exact thickness using profilometry. An alternate approach is to measure the CuPc films absorbance intensity and use the Beer's law to determine the thickness,

$$A=\varepsilon\cdot\Gamma \qquad (4\text{-}3)$$

Absorbance is linear with film thickness over a certain range. Table 4-4 lists literature results of thickness of CuPc films and their corresponding transmission value at ~617 nm. Figure 4-11 gives the plot of these data. The data from Tang and Kim will not be considered as their results are inconsistent with others measurements.[1,65]

Table 4-4 List of CuPc thin films thickness and their corresponding absorbance at 617 nm

Thickness of CuPc	Absorbance at 617 nm (or converted from ε)	Reference
20 nm	0.36	65[65]
20 nm	0.17	76[76]
25 nm	0.52	1[1]
50 nm	0.48	54[54]
50 nm	0.42	76[77]
70 nm	0.54	78[78]
100 nm	0.75	79[79]

Using the above data, we derive the relationship between the CuPc thickness and visible absorption as:

$$A=0.0079(\text{nm}^{-1})\cdot\text{CuPc thickness (nm)} \qquad (4\text{-}4)$$

where 0.0079 nm^{-1} is the slope of the straight line shown in Figure 4-11. Thus, the CuPc thickness can be estimated as:

$$\text{CuPc thickness (nm)} = 125\ \text{nm}\cdot A \qquad (4\text{-}5)$$

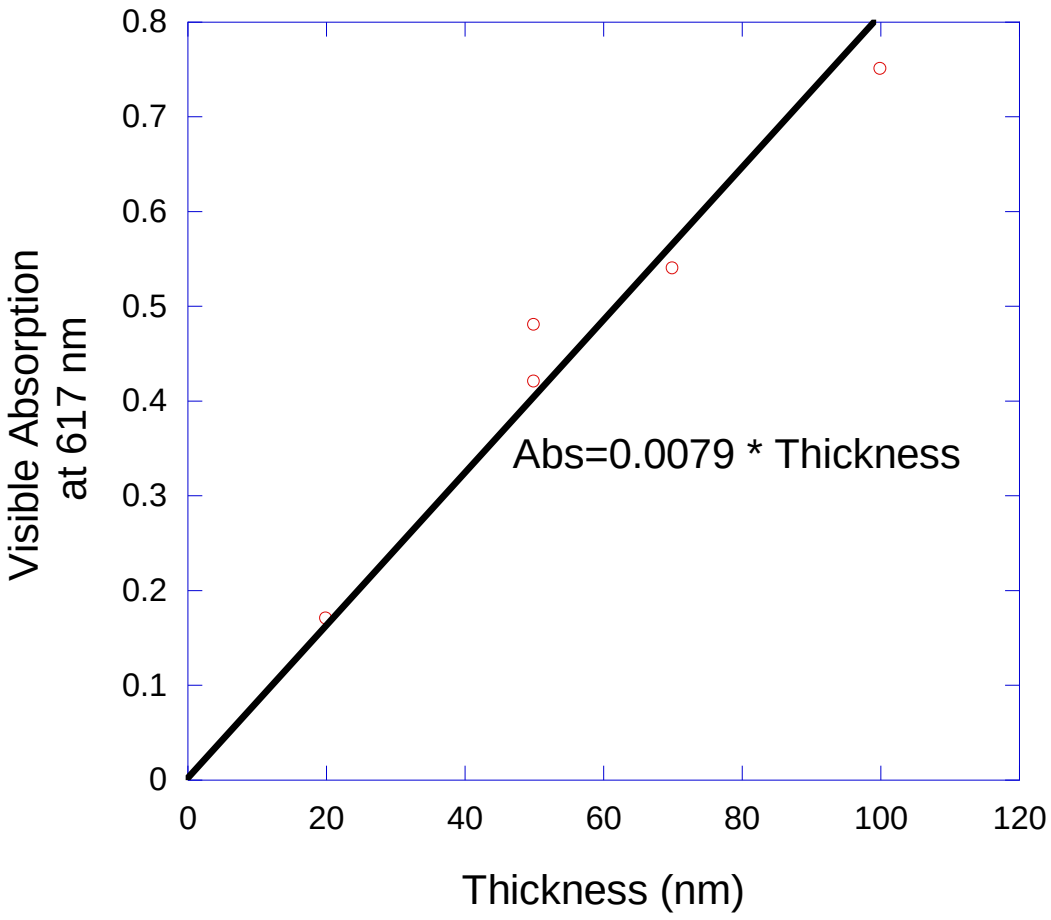

Figure 4-11 The relationship between the transmission absorption at 617 nm of CuPc films and their thickness based on literature values.

4.3.3 Solar cell characterization

Photovoltaic measurements of cells from bilayer films were performed using an AM 1.5 solar simulator where the incident light intensity was 100 mW/cm^2. The polymeric PDI thin layers were 15-20 nm thick and for CuPc layer, the selected thickness was 20-25 nm, based on UV-Vis absorption and profilometry measurements, as well as published results.[1,54,65,80]

The typical dark and illuminated I-V characteristics for our devices are shown in Figure 4-12, here the ITO|poly(t-BuPhO)$_4$DPTD)|CuPc|Ag device is used as an example. From the I-V characteristics, the device shows significant photo current under illumination. For this particular device, the short circuit current density J_{sc} is 1.13 mA/cm^2 and open circuit voltage V_{oc} is about 0.50 V. The forward bias direction corresponds to a positive voltage on the Ag backside electrode. The dark *J*-*V* curve (dashed line) in the forward bias can be described by the general Shockley equation as follows:

$$I = I_s\left[\exp(\frac{qV_a}{nkT}) - 1\right] \qquad (4\text{-}5)$$

The values of the reversed saturation current I_s and ideality factor *n* are ~3×10^{-7} A/cm^2 and ~5, respectively.

Results of the device performance under illumination for the different PDI-core polymers and CuPc are presented in Figure 4-13. The fill factor (FF) and PCE of the solar cell device were also calculated from the values of V_{oc} and J_{sc} using the equation (1-2) and (1-3) and summarized in Table 4-5. All four of different monomers can be used as n-type materials in OPV. However, there are significant differences in their cell performance. Poly(DPTD) is characterized by the

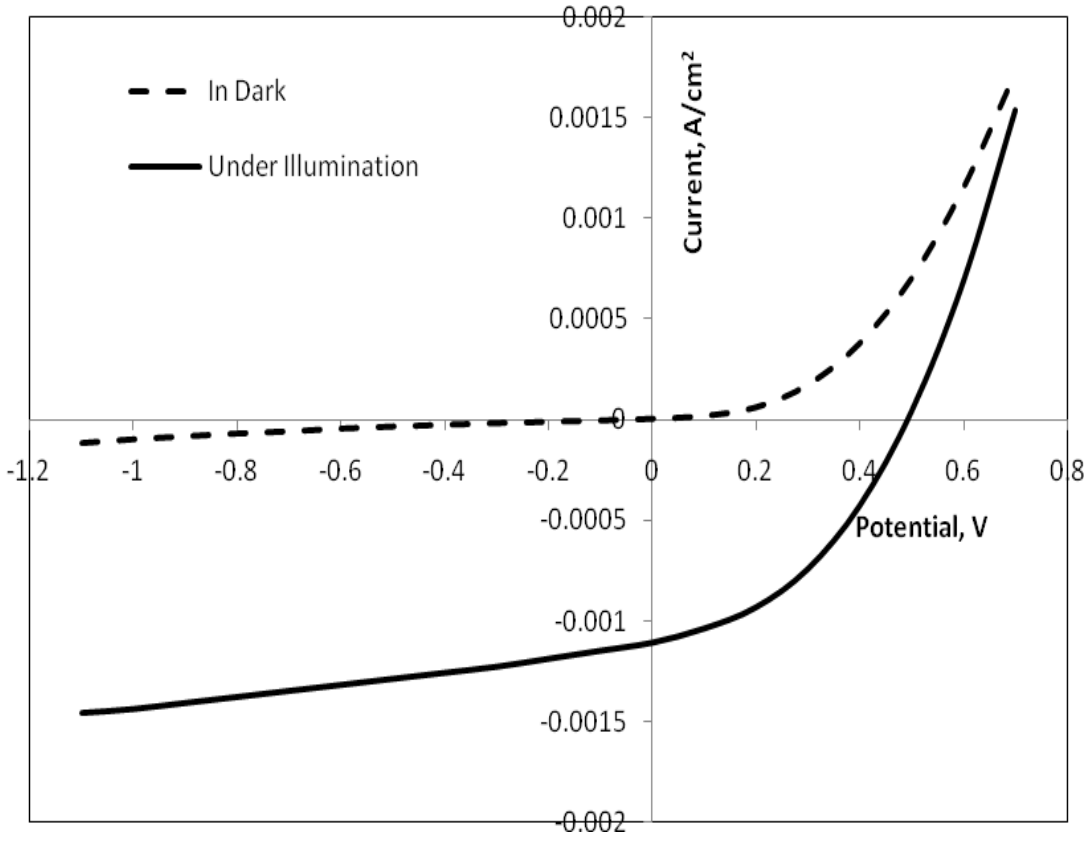

Figure 4-12 The I-V characteristics of an ITO|poly((t-BuPhO)$_4$DPTD)|CuPc|Ag device in the dark and under illumination.

lowest surface coverage (Γ) and correspondingly these films are the thinnest ones due to relatively poor monomer solubility in CH_2Cl_2. Thinner film thickness causes a larger leakage current which is known to decrease the fill factor and to lower V_{oc} .[81] The cell with poly(DPTD) has the lowest V_{oc} in these four devices, although poly(DPTD) has a larger HOMO-LUMO difference than poly(Cl_4DPTD). We can see from the Figure 4-13, there is a large increase in current at reverse bias for the poly(DPTD) device. Both poly(cyclohexyl-DPTD) and poly((t-BuPhO)$_4$DPTD) devices show larger V_{oc} but smaller short-circuit currents than poly(Cl_4DPTD) devices. The reason is at least partially related to the energy difference (ΔE) between LUMO of n-type and HOMO of p-type materials. Literature results suggest that the V_{oc} is linearly correlated to ΔE with offset (V_{oc} = ΔE -0.3)[82] or without an offset.[83] Cl_4DPTD exhibits the lowest ΔE among the four polymers and its device correspondingly has the second lowest V_{oc}, but still higher than the device made with poly(DPTD). The reason might be that the thickness of the poly(Cl_4DPTD) film is higher than that of the poly(DPTD) film, leading to less current leakage. As discussed in the introduction and in Liang's work,[61] chlorinated molecules behave better in terms of electron mobility and ambient stability than the parent compound. Also from Figure 4-6, based on the LUMO-HOMO energy levels of these different polymers, we can see the chlorination of PDI core results in lower LUMOs and HOMOs for the PDI-core, increasing the electron mobility and facilitating electron conduction. The *J-V* curve of poly(Cl_4DPTD)-CuPc cell shows that J_{sc} and PCE almost double as compared to values for poly(DPTD)-CuPc's. The typical cell resistance ranges between 5-10 kΩ for a film area of 0.0113 cm^2. The specific series resistance (R_sA), defined by

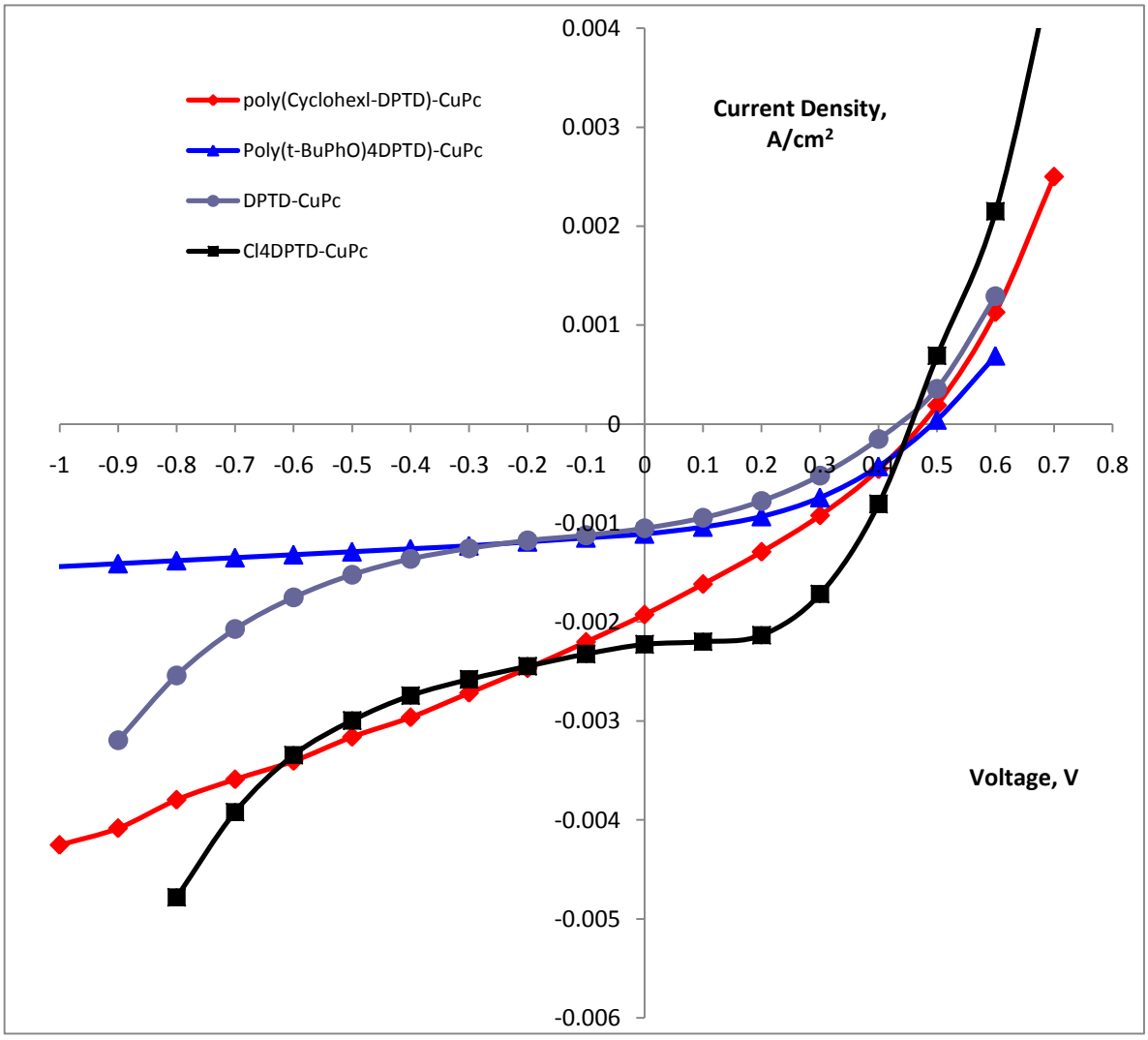

Figure 4-13 The I-V characteristics of different PV devices based on PDI-core polymer and CuPc under illumination.

the slope of the *J*-*V* curve at *J*= 0 mA/cm^2 is estimated to be about 128 Ωcm^2, 76 Ωcm^2, 143 Ωcm^2 and 174 Ωcm^2 for the cells based on poly(DPTD), poly(Cl_4DPTD), poly(cyclohexyl-DPTD) and poly(t-BuPhO)$_4$DPTD, respectively. The cell with poly(Cl_4DPTD) has the lowest series resistance and corresponding to best cell performance. The specific sheet resistance (R_{sh}A), defined by the slope of the *J*-*V* curve at *V*=0 V, of these cells based on poly(DPTD), poly(Cl_4DPTD), poly(cyclohexyl-DPTD) and poly(t-BuPhO)$_4$DPTD amount to 1100 Ωcm^2, 1650 Ωcm^2, 345 Ωcm^2, and 2000 Ωcm^2, respectively. The smallest sheet resistance of poly(cyclohexyl-DPTD) resulted in the lowest fill factor.

One point to be noted is that, as is evident from Figure 4-9, the average absorbance value between 450-700 nm for each polymer-CuPc bilayers is about 0.135. This implies that almost 73% incident light has not been absorbed by these bilayers. If a device could be made to absorb all the incident light (for example, by using vertical alignment of films), then the real energy efficiency will be tripled or quadrupled more than the cell PCE, as calculated in Table 4-5.

Table 4-5 Photovoltaic cell performance results for ITO|PDIs-polymer|CuPc|Ag devices.

Compounds	$\Gamma_{\text{n-type}}$ ′(mol/cm^2)	J_{sc}/mA. cm^{-2}	V_{oc}/ V	R_{series} Ωcm^2	R_{sheet} Ωcm^2	FF (%)	PCE (%)	η(%) =PCE/$P_{light\ absorbed}$
Poly(DPTD)	2.76×10^{-9}	1.05	0.42	128	1100	38.1	0.168	0.62
Poly(Cl_4DPTD)	3.05×10^{-9}	2.23	0.45	76	1650	51.3	0.515	1.91
Poly(cyclohexyl-DPTD)	3.46×10^{-9}	1.92	0.48	143	345	30.1	0.277	1.03
Poly((t-BuPhO)$_4$DPTD)	3.18×10^{-9}	1.13	0.50	174	2000	39.5	0.223	0.83

4.3.4 Gold nanoparticle effects on cell performance

Recent progress in manipulating nanoparticles has boosted the effectiveness of organic solar cells. The power conversion efficiency of organic solar cells has been enhanced by around 2 percent in cell efficiency through the use of quantum dots (CdSe)[84] and the use of nanoclusters doubled the PCE.[85] Also, by adding 20 nm gold nanoparticles on ITO, followed by casting a PEDOT:PSS layer, an MEHPPV and fullerene bulk heterojunction layer, the cell power efficiency was improved 40%[48] and bigger nanoparticles showed more effects than the smaller ones in the range of 5-20 nm.[49] Metallic nanoparticles change the optical properties, resulting from electrodynamics effects and modification of the dielectric environment. The plasmon resonance or surface plasmon resonance (SPR) is localized near the boundary between the metal nanostructure and surrounding dielectric and electromagnetic field at the interface.[43] In larger nanoparticles, the surface plasmon peak is red-shifted and in the case of extremely small nanoparticles (for gold, <25 nm), this shift is small but a broadening of the plasmon peak is observed.[86-88] So, addition of gold nanoparticles between the polymer and CuPc layers should increase the light absorption at short wavelengths and improve the cell performance. Also, these particles will produce plasmon resonance on surface with irradiation. Figure 4-14 shows the absorption spectra of bilayer with and without incorporation of Au nanoparticles. As we can see from Figure 4-14, the spectral results show that maximum absorption of Au nanoparticles in the solid-state is red-shifted as compared to the signal of Au particles in solution. The reason for choosing gold nanoparticles is they are not easily oxidized in air and also due to its

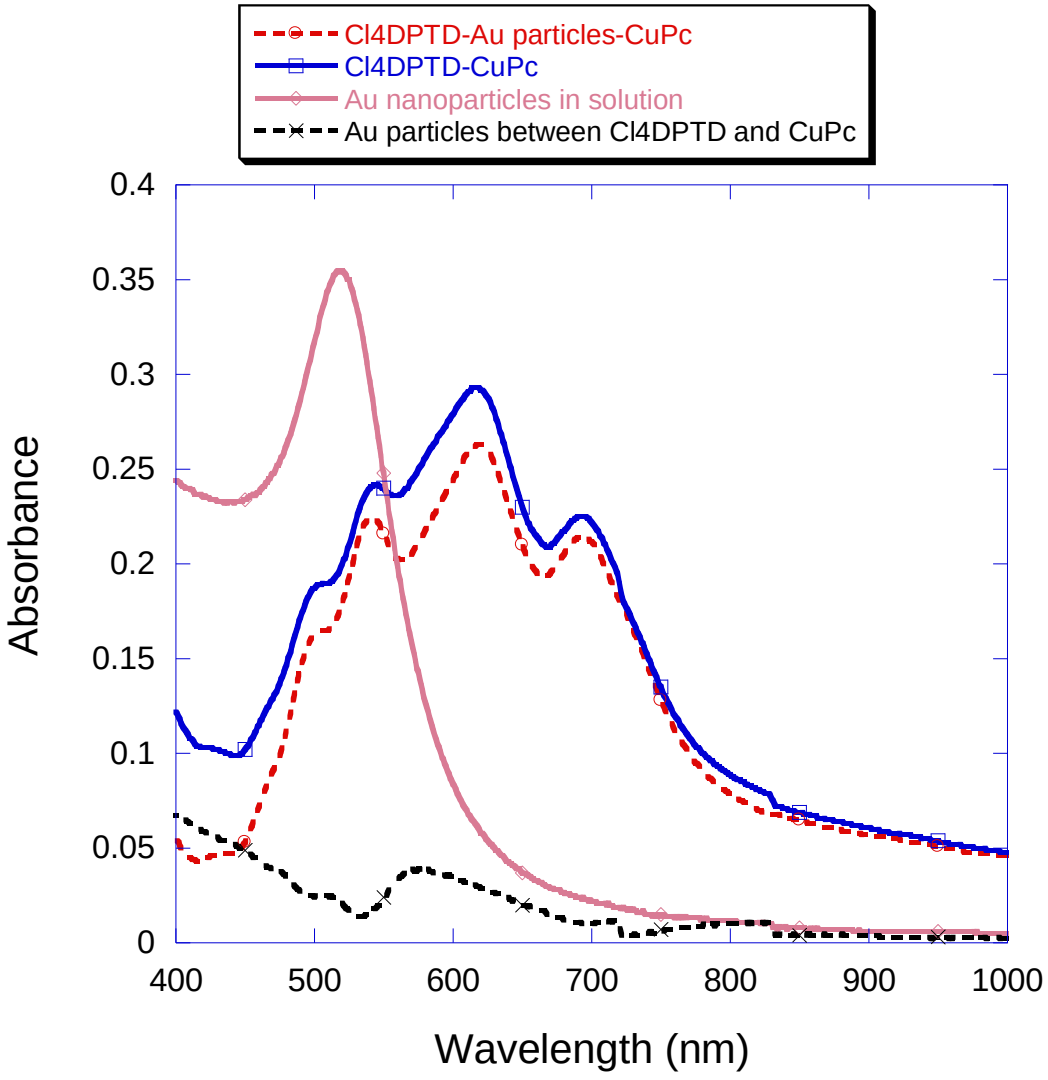

Figure 4-14 UV-Visible Spectra of different polymer Cl_4DPTD-CuPc bilayers with and without gold nanoparticles sandwiched between the p-n heterojunction.

Surface plasmon resonance band.

Figure 4-15 depicts the *J-V* curve of poly(Cl_4DPTD) (Γ=2.56×10^{-9} mol/cm^2)-CuPc (35 nm) with and without Au nanoparticles measured in the dark. Here, the cell resistance is not significantly different in the forward bias with 50-60 Ωcm^2; the R_sA for the cell without Au nanoparticles is 10 Ωcm^2 higher than the one without Au nanopartcles. Figure 4-16 shows the cell performance of ITO|Cl_4DPTD|CuPc|Ag with and without gold nanoparticles on an ITO substrate. The *J-V* curve shows that the short circuit current, J_{sc} for the cell with Au nanoparticles increases by a factor of 2. The V_{oc} for both cells are comparable as shown in Table 4-6, which also summarizes other characteristics of the OPVs with and without Au nanoparticles. The cell performance is improved by ~ 35% from an efficiency of 0.42% to 0.58% when incorporating Au nanoparticles. The series resistance is close to the one measured in the dark. The sheet resistance is 313 Ωcm^2 and 1429 Ωcm^2 with and without Au nanoparticles, respectively. And the fill factor for both cells is close to 50%.

Table 4-6 Photovoltaic cell performance for ITO|Cl_4DPTD|CuPc|Ag devices with and without Au nanoparticles and 35 nm CuPc

Structure	$\Gamma_{\text{n-type}}$ /(mol/cm^2)	J_{sc} /mA.cm^{-2}	V_{oc} /V	R_{series}A (Ωcm^2)	R_{sheet} (Ωcm^2)	FF (%)	PCE (%)	η(%) =PCE/$P_{\text{light absorbed}}$
W/O Au	2.56×10^{-9}	1.47	0.46	51.4	1429	52.8	0.42	1.19
With Au	2.56×10^{-9}	2.66	0.48	64.6	313	48	0.58	1.53

By integrating the transmittance spectra of these devices with and without Au nanoparticles, the absorption spectra has increased about 11% in the wavelength region between (500-800 nm) as compared to the one without Au particles. However, J_{sc} increased by 80% and the cell efficiency was improved by about 35%. In principle, the Au particles can affect the behavior of the solar cells in several ways. The Au nanoparticles sandwiched between poly(Cl_4DPTD) and CuPc layers induce light scattering along the organic active layers and increase the absorption pathlength. As mentioned in Chapter 1, the efficency of an OPV generally depends on several steps: light absorption, exciton diffusion, charge separation, and charge collection. Among these steps, the exciton diffusion and charge separation are the limiting steps.[89] Nanoparticles can not improve exciton diffusion in a solar cell, which is determined by the properties of bulk organic materials. Therefore we postulate that the Au nanoparticles plasmon resonance increasedthe local electric field for facilitating charge separation.[43] Different mechanism of local surface plasmonic resonance (LSPR) on cell performance have been proposed. Shen et al. concluded that the maximum enhanced electric field exists in the vicinity of those metal nanoparticles and absorption enhancement is mainly due to the enhanced near field rather than the scattering.[90] Kim et al. believed that LSPR might induce more photogenerated charge carriers by strong absorption of an active layer.[91]

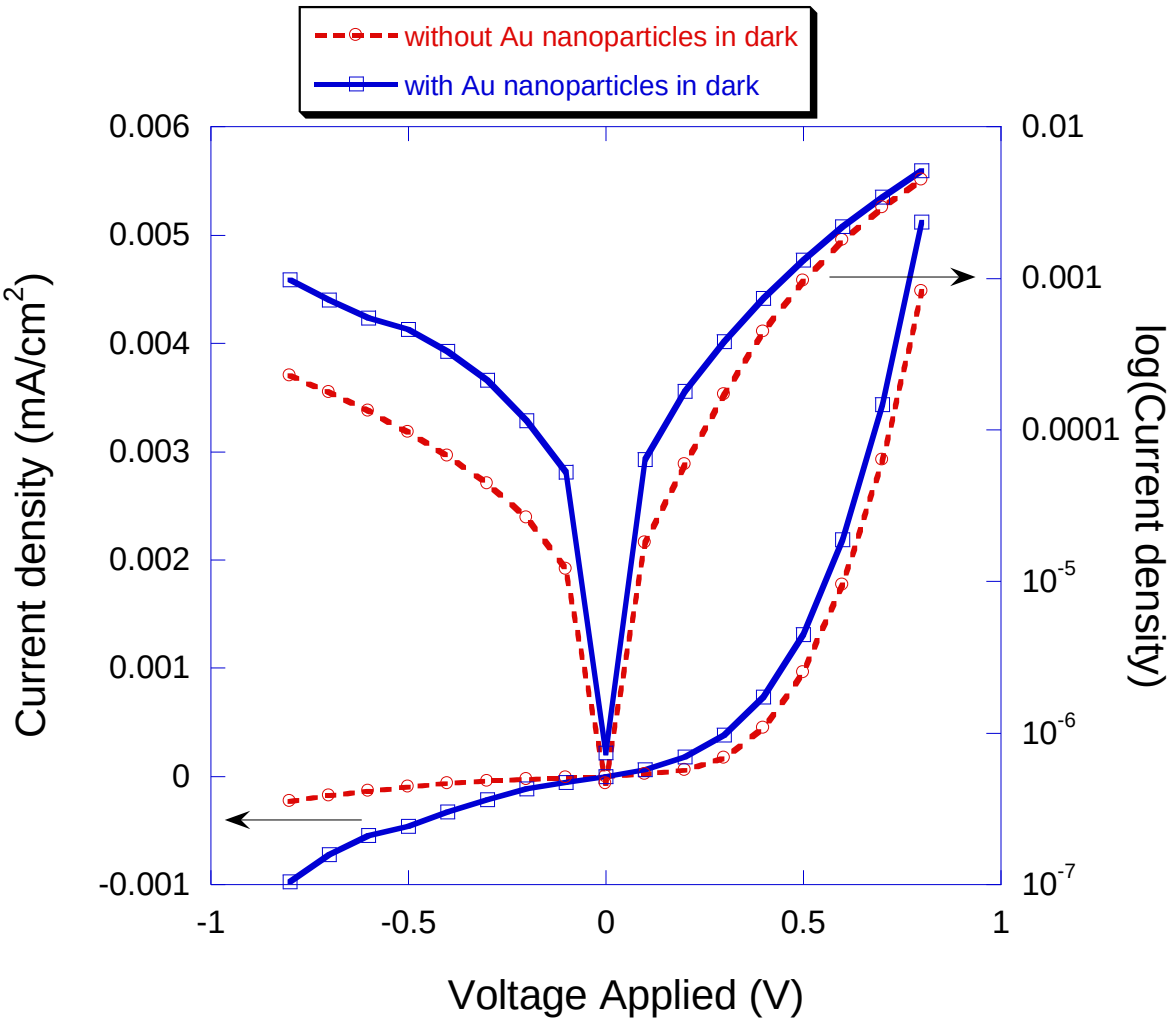

Figure 4-15 The I-V characteristics of PV devices based on Cl_4DPTD polymer and CuPc with or without Au nanoparticles in the dark.

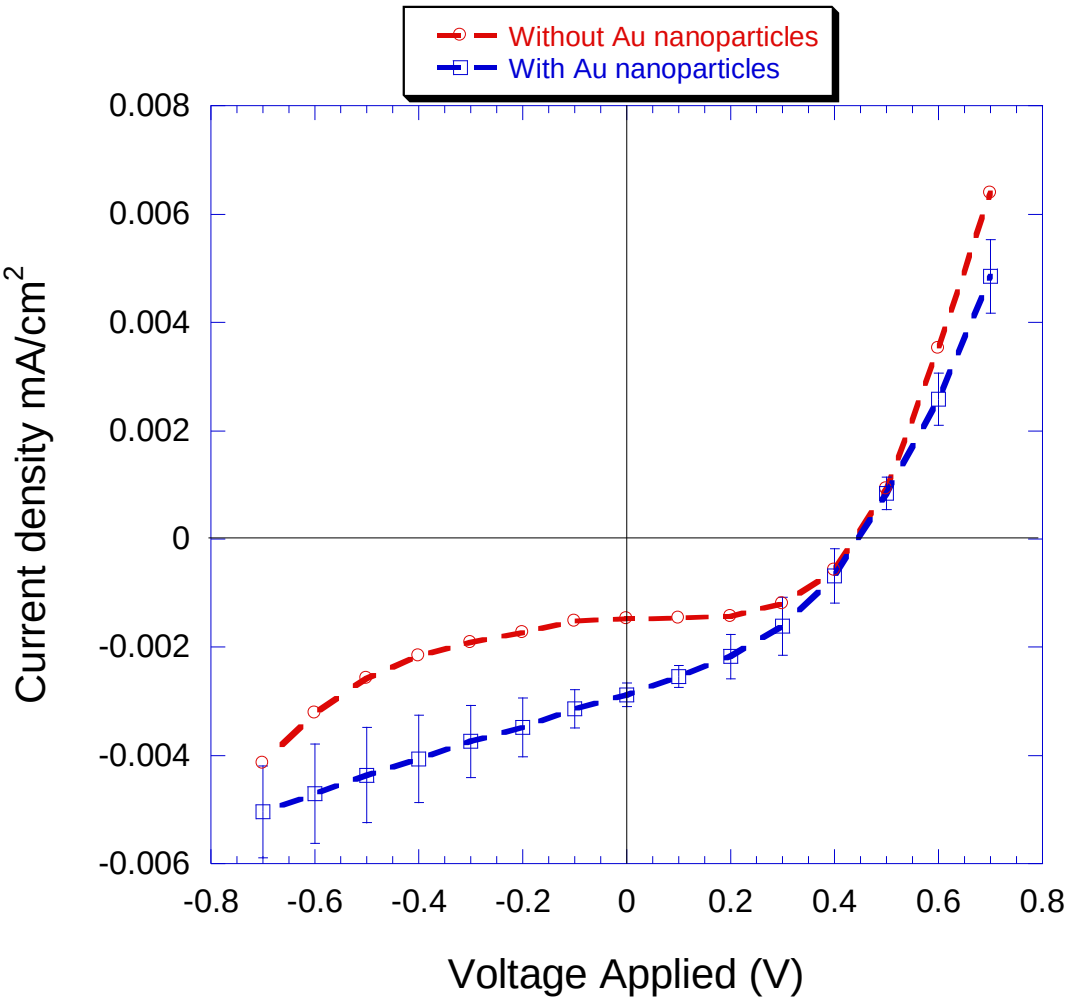

Figure 4-16 The I-V characteristics of PV devices based on Cl_4DPTD polymer and CuPc under illumination.

4.4 CONCLUSIONS

Perylene bay area substitution with different groups can change the perylene core HOMO-LUMO energy level and show different spectral characteristics depending on the incorporated groups. Polymer films made from perylene core monomer solutions via electropolymerization on ITO can work as n-type materials in organic photovoltaic cells. The perylene diimides that are substituted with Cl at bay positions showed a lower HOMO-LUMO gap and provided no significant steric hindrance that twists the conjugated core as compared to its counterpart containing phenoxy groups. This material exhibits similar spectral properties as perylene diimide but possesses higher electron affinity and mobility. Chlorination of the compound is a general route for improving electron transport and cell performance in organic photovoltaic cells. The highest cell efficiency of the organic solar cell is 0.515% and theoretical efficiency of 1.9% based on poly(Cl_4DPTD)-CuPc. Gold nanoparticles incorporated between p-n junction of an OPV can transfer absorbed incident light to the polymer components and may also enhance charge separation, which can boost cell performance.

REFERENCES

1. Tang, C. W. *Appl. Phys. Lett.* **1986**, *48*, 183-5.

2. Xue, J.; Uchida, S.; Rand, B. P.; Forrest, S. R. *Appl. Phys. Lett.* **2004**, *84*, 3013-3015.

3. Yu, G.; Gao, J.; Hummelen, J. C.; Wudl, F.; Heeger, A. J. *Science (Washington, D. C.)* **1995**, *270*, 1789-91.

4. Chen, H.-Y.; Hou, J.; Zhang, S.; Liang, Y.; Yang, G.; Yang, Y.; Yu, L.; Wu, Y.; Li, G. *Nat. Photonics* **2009**, *3*, 649-653.

5. Breeze, A. J.; Salomon, A.; Ginley, D. S.; Gregg, B. A.; Tillmann, H.; Horhold, H. H. *Appl. Phys. Lett.* **2002**, *81*, 3085-3087.

6. Nakamura, J.-I.; Yokoe, C.; Murata, K.; Takahashi, K. *J. Appl. Phys.* **2004**, *96*, 6878-6883.

7. Liang, Y.; Xu, Z.; Xia, J.; Tsai, S.-T.; Wu, Y.; Li, G.; Ray, C.; Yu, L. *Adv. Mater. (Weinheim, Ger.)* **2010**, *22*, E135-E138.

8. Liang, Y.; Feng, D.; Wu, Y.; Tsai, S.-T.; Li, G.; Ray, C.; Yu, L. *J. Am. Chem. Soc.* **2009**, *131*, 7792-7799.

9. Tang, C. W.; Albrecht, A. C. *J. Chem. Phys.* **1975**, *62*, 2139-49.

10. Hiramoto, M.; Suezaki, M.; Yokoyama, M. *Chem. Lett.* **1990**, 327-30.

11. Xue, J.; Uchida, S.; Rand, B. P.; Forrest, S. R. *Appl. Phys. Lett.* **2004**, *85*, 5757-5759.

12. Kim, J. Y.; Lee, K.; Coates Nelson, E.; Moses, D.; Nguyen, T.-Q.; Dante, M.; Heeger Alan, J. *Science (Washington, D. C.)* **2007**, *317*, 222-5.

13. Hiramoto, M.; Fujiwara, H.; Yokoyama, M. *J. Appl. Phys.* **1992**, *72*, 3781-7.

14. Langhals, H. *Heterocycles* **1995**, *40*, 477-500.

15. Kardos, M. *Ber. Dtsch. Chem. Ges.* **1913**, *46*, 2086-2091.

16. Weitzenbock, R.; Seer, C. *Ber. Dtsch. Chem. Ges.* **1913**, *46*, 1994-2000.

17. Herbst, W.; Hunger, K. *Industrial Organic Pigments: Production, Properties and Applications*; 3rd ed.; Wiley-VCH: Weinheim, 2004.

18. Loehmannsroeben, H. G.; Langhals, H. *Appl. Phys. B* **1989**, *B48*, 449-52.

19. Horowitz, G.; Kouki, F.; Spearman, P.; Fichou, D.; Nogues, C.; Pan, X.; Garnier, F. *Adv. Mater. (Weinheim, Ger.)* **1996**, *8*, 242-5.

20. Peumans, P.; Uchida, S.; Forrest, S. R. *Nature (London, U. K.)* **2003**, *425*, 158-162.

21. Dharmadhikari, A. K.; Thakur, M.; Wang, L.; Cammarata, V. *Appl. Phys. Lett.* **2003**, *83*, 1066-1067.

22. Zang, L.; Liu, R.; Holman, M. W.; Nguyen, K. T.; Adams, D. M. *J. Am. Chem. Soc.* **2002**, *124*, 10640-10641.

23. Rahn, M. D.; King, T. A.; Gorman, A. A.; Hamblett, I. *Appl. Opt.* **1997**, *36*, 5862-5871.

24. Peneva, K.; Mihov, G.; Herrmann, A.; Zarrabi, N.; Boersch, M.; Duncan, T. M.; Muellen, K. *J. Am. Chem. Soc.* **2008**, *130*, 5398-5399.

25. Garcia-Moreno, I.; Costela, A.; Pintado-Sierra, M.; Martin, V.; Sastre, R. *Opt. Express* **2009**, *17*, 12777-12784.

26. Häedicke, E.; Graser, F. *Acta Crystallogr., Sect. C: Cryst. Struct. Commun.* **1986**, *C42*, 189-95.

27. Häedicke, E.; Graser, F. *Acta Crystallogr., Sect. C: Cryst. Struct. Commun.* **1986**, *C42*, 195-8.

28. Klebe, G.; Graser, F.; Häedicke, E.; Berndt, J. *Acta Crystallogr., Sect. B: Struct. Sci.* **1989**, *B45*, 69-77.

29. Zugenmaier, P.; Duff, J.; Bluhm, T. L. *Cryst. Res. Technol.* **2000**, *35*, 1095-1115.

30. Wuerthner, F. *Chem. Commun. (Cambridge, U. K.)* **2004**, 1564-1579.

31. Langhals, H.; Demmig, S.; Huber, H. *Spectrochim. Acta, Part A* **1988**, *44A*, 1189-93.

32. Wurthner, F.; Thalacker, C.; Diele, S.; Tschierske, C. *Chem.--Eur. J.* **2001**, *7*, 2245-2253.

33. Chen, Z.; Debije, M. G.; Debaerdemaeker, T.; Osswald, P.; Wuerthner, F. *ChemPhysChem* **2004**, *5*, 137-140.

34. Shin, W. S.; Jeong, H.-H.; Kim, M.-K.; Jin, S.-H.; Kim, M.-R.; Lee, J.-K.; Lee, J. W.; Gal, Y.-S. *J. Mater. Chem.* **2006**, *16*, 384-390.

35. Schmidt, R.; Oh, J. H.; Sun, Y.-S.; Deppisch, M.; Krause, A.-M.; Radacki, K.; Braunschweig, H.; Koenemann, M.; Erk, P.; Bao, Z.; Wuerthner, F. *J. Am. Chem. Soc.* **2009**, *131*, 6215-6228.

36. Malenfant, P. R. L.; Dimitrakopoulos, C. D.; Gelorme, J. D.; Kosbar, L. L.; Graham, T. O.; Curioni, A.; Andreoni, W. *Appl. Phys. Lett.* **2002**, *80*, 2517-2519.

37. van der Boom, T.; Hayes, R. T.; Zhao, Y.; Bushard, P. J.; Weiss, E. A.; Wasielewski, M. R. *J. Am. Chem. Soc.* **2002**, *124*, 9582-9590.

38. Ahrens, M. J.; Kelley, R. F.; Dance, Z. E. X.; Wasielewski, M. R. *Phys. Chem. Chem. Phys.* **2007**, *9*, 1469-1478.

39. Hayes, R. T.; Wasielewski, M. R.; Gosztola, D. *J. Am. Chem. Soc.* **2000**, *122*, 5563-5567.

40. Peumans, P.; Bulovic, V.; Forrest, S. R. *Appl. Phys. Lett.* **2000**, *76*, 2650-2652.

41. Yang, F.; Shtein, M.; Forrest, S. R. *Nat. Mater.* **2005**, *4*, 37-41.

42. Yang, F.; Shtein, M.; Forrest, S. R. *J. Appl. Phys.* **2005**, *98*, 014906/1-014906/10.

43. Prasad, P. N. *Nanophotonics*; John Wiley & Sons: New Jersey, 2004.

44. Duche, D.; Torchio, P.; Escoubas, L.; Monestier, F.; Simon, J.-J.; Flory, F.; Mathian, G. *Sol. Energy Mater. Sol. Cells* **2009**, *93*, 1377-1382.

45. Min, C.; Li, J.; Veronis, G.; Lee, J.-Y.; Fan, S.; Peumans, P. *Appl. Phys. Lett.* **2010**, *96*, 133302/1-133302/3.

46. Kulkarni, A. P.; Noone, K. M.; Munechika, K.; Guyer, S. R.; Ginger, D. S. *Nano Lett.* **2010**, *10*, 1501-1505.

47. Chang, Y. C.; Chou, F. Y.; Yeh, P. H.; Chen, H. W.; Chang, S. H.; Lan, Y. C.; Guo, T. F.; Tsai, T. C.; Lee, C. T. *J. Vac. Sci. Technol., B: Microelectron. Nanometer Struct.--Process., Meas., Phenom.* **2007**, *25*, 1899-1902.

48. Sue, C.-W.; Hsieh, H.-T.; Su, G.-D. J. *Proc. SPIE-Int. Soc. Opt. Eng.* **2007**, *6656*, 66561L/1-66561L/9.

49. Lai, W.-C.; Su, G.-D. J. *Proc. SPIE* **2009**, *7416*, 74161J/1-74161J/10.

50. Yoon, W.-J.; Jung, K.-Y.; Liu, J.; Duraisamy, T.; Revur, R.; Teixeira, F. L.; Sengupta, S.; Berger, P. R. *Sol. Energy Mater. Sol. Cells* **2010**, *94*, 128-132.

51. Zafer, C.; Kus, M.; Turkmen, G.; Dincalp, H.; Demic, S.; Kuban, B.; Teoman, Y.; Icli, S. *Sol. Energy Mater. Sol. Cells* **2007**, *91*, 427-431.

52. Zafer, C.; Karapire, C.; Serdar Sariciftci, N.; Icli, S. *Sol. Energy Mater. Sol. Cells* **2005**, *88*, 11-21.

53. Hiramoto, M.; Fukusumi, H.; Yokoyama, M. *Appl. Phys. Lett.* **1992**, *61*, 2580-2.

54. Tsuzuki, T.; Hirota, N.; Noma, N.; Shirota, Y. *Thin Solid Films FIELD* **1996**, *273*, 177-80.

55. Tsuzuki, T.; Shirota, Y.; Rostalski, J.; Meissner, D. *Sol. Energy Mater. Sol. Cells* **2000**, *61*, 1-8.

56. Breeze, A. J.; Salomon, A.; Ginley, D. S.; Tillmann, H.; Horhold, H.-H.; Gregg, B. A. *Proc. SPIE-Int. Soc. Opt. Eng.* **2003**, *4801*, 34-39.

57. Whitlock, J. B.; Panayotatos, P.; Sharma, G. D.; Cox, M. D.; Sauers, R. R.; Bird, G. R. *Opt. Eng. (Bellingham, Wash.)* **1993**, *32*, 1921-34.

58. Meinhardt, G.; Graupner, W.; Feistritzer, G.; Schroeder, R.; List, E. J. W.; Pogantsch, A.; Dicker, G.; Schlicke, B.; Schulte, N.; Schluter, A. D.; Winter, G.; Hanack, M.; Scherf, U.; Mullen, K.; Leising, G. *Proc. SPIE-Int. Soc. Opt. Eng.* **1999**, *3623*, 46-57.

59. Meinhardt, G.; Moderegger, E.; Schroder, R.; Winter, G.; Hanack, M.; Quante, H.; Geerts, Y.; Mullen, K.; Tillmann, H.; Horhold, H. H.; Leising, G. *Mater. Res. Soc. Symp. Proc.* **2000**, *598*, BB9 2/1-BB9 2/7.

60. Wang, Q., M.S. Thesis, Auburn University, 1999.

61. Liang, J., Ph.D. Dissertation, Auburn University, 2003.

62. Singh, V. P.; Singh, R. S.; Parthasarathy, B.; Aguilera, A.; Anthony, J.; Payne, M. *Appl. Phys. Lett.* **2005**, *86*, 082106/1-082106/3.

63. Chu, C.-W.; Shrotriya, V.; Li, G.; Yang, Y. *Appl. Phys. Lett.* **2006**, *88*, 153504/1-153504/3.

64. Tripathi, V.; Datta, D.; Samal, G. S.; Awasthi, A.; Kumar, S. *J. Non-Cryst. Solids* **2008**, *354*, 2901-2904.

65. Kim, I.; Haverinen, H. M.; Wang, Z.; Madakuni, S.; Kim, Y.; Li, J.; Jabbour, G. E. *Chem.*

Mater. **2009**, *21*, 4256-4260.

66. Sapagovas, V. J.; Kadziauskas, P.; Undzenas, A.; Purlys, R. *Environ. Chem. Phys.* **2001**, *23*, 30-37.

67. Ebina, W.; Rowat, A. C.; Weitz, D. A. *Biomicrofluidics* **2009**, *3*, 034104/1-034104/6.

68. Salbeck, J.; Kunkely, H.; Langhals, H.; Saalfrank, R. W.; Daub, J. *Chimia* **1989**, *43*, 6-9.

69. Pommerehne, J.; Vestweber, H.; Guss, W.; Mahrt, R. F.; Baessler, H.; Porsch, M.; Daub, J. *Adv. Mater. (Weinheim, Ger.)* **1995**, *7*, 551-4.

70. Djurovich, P. I.; Mayo, E. I.; Forrest, S. R.; Thompson, M. E. *Org. Electron.* **2009**, *10*, 515-520.

71. Löhmannsröben, H. G.; Langhals, H. *Appl. Phys. B* **1989**, *B48*, 449-52.

72. Gvishi, R.; Reisfeld, R.; Burshtein, Z. *Chem. Phys. Lett.* **1993**, *213*, 338-344.

73. Böhm, A.; Arms, H.; Henning, G.; Blaschka, P. B. A. *Ger. Pat. Appl.* **1997**, DE 19547209 A1 (*Chem. Abstr.*, **1997**, 127, 96569g).

74. Park, Y.; Choong, V.; Gao, Y.; Hsieh, B. R.; Tang, C. W. *Appl. Phys. Lett. FIELD Full Journal Title:Applied Physics Letters* **1996**, *68*, 2699-2701.

75. Uda, M.; Nakamura, A.; Yamamoto, T.; Fujimoto, Y. *J. Electron Spectrosc. Relat. Phenom.* **1998**, *88-91*, 643-648.

76. Heutz, S.; Nogueira, A. F.; Durrant, J. R.; Jones, T. S. *J. Phys. Chem. B* **2005**, *109*, 11693-6.

77. Yoshida, Y.; Tanaka, S.; Hiromitsu, I.; Fujita, Y.; Yoshino, K. *Jpn. J. Appl. Phys.* **2008**, *47*, 867-871.

78. Abe, T.; Miyakushi, S.; Nagai, K.; Norimatsu, T. *Phys. Chem. Chem. Phys.* **2008**, *10*,

1562-1568.

79. Osasa, T.; Yamamoto, S.; Matsumura, M. *Jpn. J. Appl. Phys., Part 1* **2006**, *45*, 3762-3765.

80. Nakamura, J.-i.; Suzuki, S.; Takahashi, K.; Yokoe, C.; Murata, K. *Bull. Chem. Soc. Jpn.* **2004**, *77*, 2185-2188.

81. Moliton, A.; Nunzi, J.-M. *Polym. Int.* **2006**, *55*, 583-600.

82. Scharber, M. C.; Muehlbacher, D.; Koppe, M.; Denk, P.; Waldauf, C.; Heeger, A. J.; Brabec, C. J. *Adv. Mater. (Weinheim, Ger.)* **2006**, *18*, 789-794.

83. Yamanari, T.; Taima, T.; Sakai, J.; Saito, K. *Sol. Energy Mater. Sol. Cells* **2009**, *93*, 759-761.

84. Zhou, Y.; Riehle, F. S.; Yuan, Y.; Schleiermacher, H.-F.; Niggemann, M.; Urban, G. A.; Krueger, M. *Appl. Phys. Lett.* **2010**, *96*, 013304/1-013304/3.

85. Yakimov, A.; Forrest, S. R. *Appl. Phys. Lett.* **2002**, *80*, 1667-1669.

86. Link, S.; Wang, Z. L.; El-Sayed, M. A. *J. Phys. Chem. B* **1999**, *103*, 3529-3533.

87. Link, S.; Mohamed, M. B.; El-Sayed, M. A. *J. Phys. Chem. B* **1999**, *103*, 3073-3077.

88. Link, S.; El-Sayed, M. A. *J. Phys. Chem. B* **1999**, *103*, 8410-8426.

89. Forrest, S. R. *MRS Bull.* **2005**, *30*, 28-32.

90. Shen, H.; Bienstman, P.; Maes, B. *J. Appl. Phys.* **2009**, *106*, 073109/1-073109/5.

91. Kim, S.-S.; Na, S.-I.; Jo, J.; Kim, D.-Y.; Nah, Y.-C. *Appl. Phys. Lett.* **2008**, *93*, 073307/1-073307/3.

CHAPTER 5

SURFACE METALLIZATION AND ITS MECHANICAL STRENGTH EFFECTS ON KEVLAR® AND ZYLON® HIGH PERFORMANCE FIBERS

5.1 INTRODUCTION

The research described in this chapter is based on proposed lightweight, high-strength, and flexible tethers equipped with electrically conductive elements for maneuvering satellites enabling in-space propulsion. This work aims at establishing methods for the deposition of thin metallic coatings that will protect high performance fibers (in the form of tethers) from degradation in the harsh environment (typified by the presence of atomic oxygen (AO), UV photons and hard radiation) encountered at low Earth orbits (LEO). Such coatings are also anticipated to provide electrical conductivity to the polymeric materials.

Poly-paraphenylene terephthalamide (Kevlar®) and polybenzobisoxazole (Zylon®) yarns were selected as high performance substrates based on their tensile strength/weight ratios and their commercial availability, widely used in space for ultra long duration balloon[1,2] and separation technologies.[3] Their chemical structures are shown in Scheme 5-1. Due to their inherent insulating properties and their susceptibility to chemical degradation in the space environment, application of conductive, protective coatings is needed to preserve the integrity of the yarns. An important requirement is that the coating procedures must result in crack-free coverage both on the exterior and interior of the yarns. To this end, adherent thin layers of Ni, Al, and Au were deposited onto the fibers. Samples of the coated yarns were then selected for testing

under conditions (AO together with UV photons) that simulate those found in the corrosive environment of LEO.

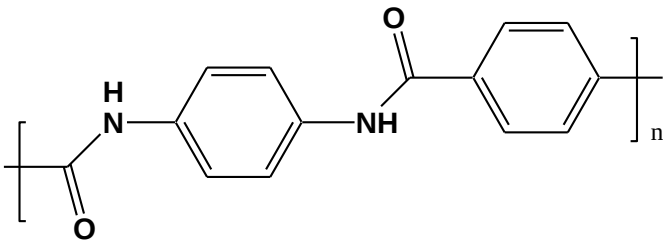

Kevlar

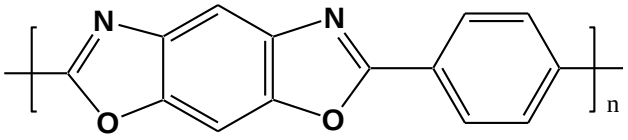

Zylon

Scheme 5-1 Chemical structures of Kevlar® and Zylon®

Kevlar® and Zylon® were selected based on their superior strength to weight ratios and their surface chemical functionalities. These polymers form strong bonds with Lewis acidic metals making adherent metal-based films realistic goals.

5.2 EXPERIMENTAL

Two metallic coatings are proposed to protect the fibers in the harsh environment.

Au deposition:

In order to achieve strongly adherent metal coatings on macromolecular surfaces, a multi-step procedure is required.[4] Clean fiber surfaces are treated first with Sn^{2+} ions, which bind irreversibly to the polymeric substrates. Addition of Pd^{2+} ions yields deposition of Pd particles strongly bound to the fiber surface. The Pd particles act as catalysts for the reduction of Ni^{2+} on

the fiber surface, forming nickel islands.[4] Gold ions are then reduced from aqueous solutions onto the Ni metal, generating Au deposits that grow along the fiber surface electrochemically.

Al deposition:

The coating methods are based on Al deposition technology using both electroless and electrolytic baths to form smooth hard coatings on the outside of polymer fibers. Electroless Al plating was accomplished from solutions of $LiAlH_4$ and $AlCl_3$ in tetrahydrofuran (THF, Fisher) at room temperature.[5,6] Alternatively, Al was electroplated using a bath composed of an ionic liquid.[7] Because successful deposition of Al coatings requires rigorous exclusion of air and water, all experiments with aluminum were performed inside a glove box filled with nitrogen.

5.2.1. Fiber cleaning procedure

Kevlar 49® was obtained from DuPont, whereas Zylon® (273 dtex HM) was provided by Toyobo Corporation, Japan. Kevlar® and Zylon® fibers were cleaned with organic solvents in an ultrasonic bath via the following steps:

(1) Immersion in methanol (Aater), exposure to ultrasonic clean for 10 minutes, then air-dried.

(2) Immersion in hexane (Sigma Aldrich), exposure to ultrasonic clean for 10 minutes, then dried in air.

(3) Immersion in chloroform (Fisher), exposure to ultrasonic clean for 10 minutes, then vacuum dried.

5.2.2 Surface sensitization

Electroless deposition was carried out on cleaned Kevlar and Zylon fibers by first seeding the fiber surface with Sn^{2+} ions, which then are oxidized by Pd^{2+} ions producing palladium metal

particles anchored to the surface of polymers. This process yields nucleation sites for the electroless deposition of metals such as Ni or Au on the surface of the polymeric materials.

$Sn^{2+} + Pd^{2+} \rightarrow \quad Sn^{4+} + Pd^{0}$

Sensitizing and activation of fibers consist of two immersion steps.[8] Immersion times for $SnCl_2$ (Fisher) then K_2PdCl_4 (Aldrich Chemicals) varied depending on the bath type. Fibers were immersed in the $SnCl_2$ solution for 40-60 seconds and then washed with deionized water. This was followed by immediate immersion in the K_2PdCl_4 solution and gently washing with de-ionized water. The concentrations of the sensitizing agents are listed in Table 5-1.

5.2.3. Nickel electroless deposition

Kevlar® and Zylon® fibers were first pretreated via surface sensitizing procedure as described previously with 30 second immersions in each sensitizing agent (i.e. Sn^{2+} then Pd^{2+}). The fibers were kept in the Ni electroless bath at 60 °C for 2-3 minutes, numerous bubbles emerge from the solution, this being a sign that the chemical reaction occurs on the substrate surfaces. To promote the deposition process, a glass rod was used to remove the bubbles from the fiber surface. Table 5-2 summarizes the composition of the electroless Ni bath.

Table 5-1 Sensitizing agents for cleaned fibers

Sn^{2+} sensitizing solution	0.1g of $SnCl_2 \cdot 2H_2O$ in 100ml DI water
Pd^{2+} sensitizing solution	0.2g of $PdCl_2$+KCl (molar ratio 1:1) in 100ml DI water

Table 5-2 Nickel electroless bath composition

Chemical	Concentration (g/L)
$NiCl_2$ $6H_2O$ (Fisher)	30
Citric Acid (Alfa Aesar)	60
NaH_2PO_2 H_2O (Aldrich)	10
NH_4Cl (Fisher, 37%)	50
pH	9.0~9.4

*pH was adjusted with NH_4OH

5.2.4. Aluminum electroless deposition

Several plating methods, described in references,[5,6] were explored. The most successful procedure involved immersion of the fibers into a diethyl ether (Fisher) solution containing 0.87 g/L (0.0046M) $TiCl_4$ (Aldrich) for 1 min. After rinsing gently with THF, the resulting fibers were placed into a solution containing $LiAlH_4$ + $AlCl_3$ (anhydrous, Alfar Aesar) for 5 min. The composition of the solution is described in the Table 5-3 shown below. Al deposition occurred concurrently with bubble formation on the surface of the fibers. The coated materials cleaned and dried in a vacuum oven for 30 min at 98 °C.

Table 5-3 Al electroless bath composition

Chemical	Concentration (g/L)
$AlCl_3$	53.4
$LiAlH_4$	15.2
Diethyl ether	solvent

Note: All experiments were performed in a glove box.

5.2.5 Aluminum electrochemical deposition

The plating procedure was adapted from somewhere else,[7] employing an ionic liquid bath

at room temperature for depositing Al on nickel coated fibers in a glove box. Highest Al depositing rates were obtained in a solution with a molar ratio of $AlCl_3$ (Anhydrous, Alfa Aesar): Benzyl Tri-Methyl Ammonium Chloride (BTMAC, Alfa Aesar, 97%) = 2:1; the bath composition is described in Table 5-4. An Al wire served as the anode and Ni-coated fibers operated as the working electrodes. Plating conditions: T = 50 °C, Voltage = -0.40 V and I = 1.60-2.0 μA.

Table 5-4 Al ionic liquid electrodeposition bath composition

Chemical	Mass (g)
$AlCl_3$	10.2
BTMAC	14.3

Note: All experiments were performed in a glove box.

5.2.6. Gold electrochemical deposition in Au-cyanide solution

A commercial gold cyanide bath from SMC Inc. was employed (bath composition is proprietary information), which was diluted by a factor of 10 times with deionized water. Operating conditions were: Voltage =-1.09 V and I = -2.5 mA. As anticipated, the net current output increased during the coating process because the deposited Au decreases the resistance of the fibrous material and facilitates further metal deposition. An Au wire served as the anode and Ni-coated fibers operated as the working electrodes.

5.2.7 Instrumental analysis

Zylon and Kevlar fibers coated with Ni, Al, Au were characterized in terms of mass gain, conductivity, tensile strength and adhesion of the deposited layers. Mass changes were monitored

throughout the coating steps with analytical balances. Alterations in the resistance of the fibers after metallization were followed by means of a two point method using an ohm-meter. Adhesion of the deposited coatings was tested via exposing fibers immersed in purified water to ultrasound waves, which dislodge any material not firmly bonded to the surface of the polymeric materials. Exposure to ultrasound lasted for 10 min; the samples were then air-dried and weighed to determine mass losses.

Surface morphology was examined with optical microscopy, scanning electron microscopy (SEM) together with energy dispersive x-ray spectroscopy (EDS), and transmission electron microscopy (TEM). SEM measurements were performed on a Zeiss DSM 940 microscope equipped with an EDS detection system and Zeiss EVO 50 Variable Pressure Scanning Electron Microscope. TEM analysis was carried out on a Zeiss EM 10CR instrument using thin slices of fibers prepared via microtoming. X-ray diffraction (XRD) studies, conducted to confirm that metallization of the fibers occurred, employed a Brucker Smart APEX CCD diffractometer using Mo Kα radiation. The tensile strength of the coated fibers was determined on an Instron 1122-4400R test machine.

5.3. RESULTS AND DISCUSSION

Conductive modified surface polyimide fibers have been studied for the use of circuit patterns.[9] Controlled nanoparticle deposition onto heterocyclic-aromatic fibers for electrical conduction has also been tried in the literature.[10] However, neither application requires uniformed surface electroless deposition. Here, we have to make the metallic coating layer with a minimum of defects as possible. Also, Nickel and its alloy electroless deposition have been

widely investigated in the past decades.[11-14] In order to get smooth, uniformed Ni layer, the sensitization of the surface needs to be uniform, so the fiber cleaning treatment is critical.

5.3.1 Fiber cleaning treatment

Depicted in Figure 5-1 is a SEM image of Kevlar fibers, "as received". An image obtained after cleaning the fibers as described in section 5.2.1 is shown in Figure 5-2 for Kevlar, and in Figure 5-3 for Zylon. Comparison of Figures 5-1 and 5-2 reveals that the cleaning process eliminated most of the material adsorbed on the Kevlar surface, which is clearly observed in Figure 5-1. In contrast, Figure 5-3 shows that the cleaning procedure is not as effective in the case of Zylon.

5.3.2 Mass change of metallized fibers

The results of mass increases obtained from coating experiments are compiled in Table 5-5. For the Au-cyanide electroplating method the deposition time was 60 min (Kevlar-Ni fiber samples were coated for 120 min). Not satisfactory means that the deposits exhibited deficiencies detected upon visual inspection (see section 5.3.7). Deficient or non uniform coatings were obtained when the fiber surfaces were not fully exposed to the plating solutions. All efforts to generate Al coatings using the electrochemical method failed, electroless deposition of aluminum produced metal films but their quality was poor.

5.3.3 Conductivity of treated fibers

Table 5-6 depicts values of resistance for metallized fibers. The data shows that metallization with Ni and Au increases the conductivity of the fibers significantly. Ni coating increase the conductivity of the fibers; further decreases in the resistance of Ni-coated fibers can

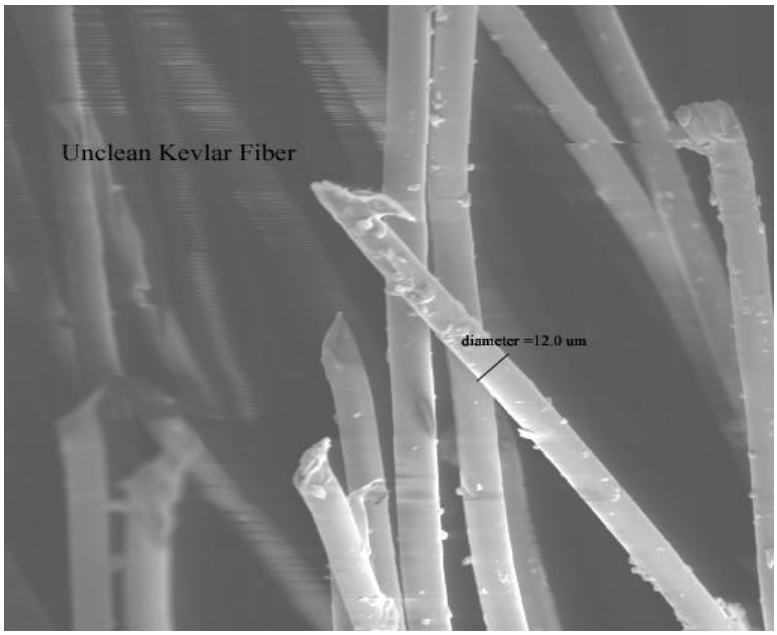

Figure 5-1. SEM image of "as received" Kevlar fibers with 500X

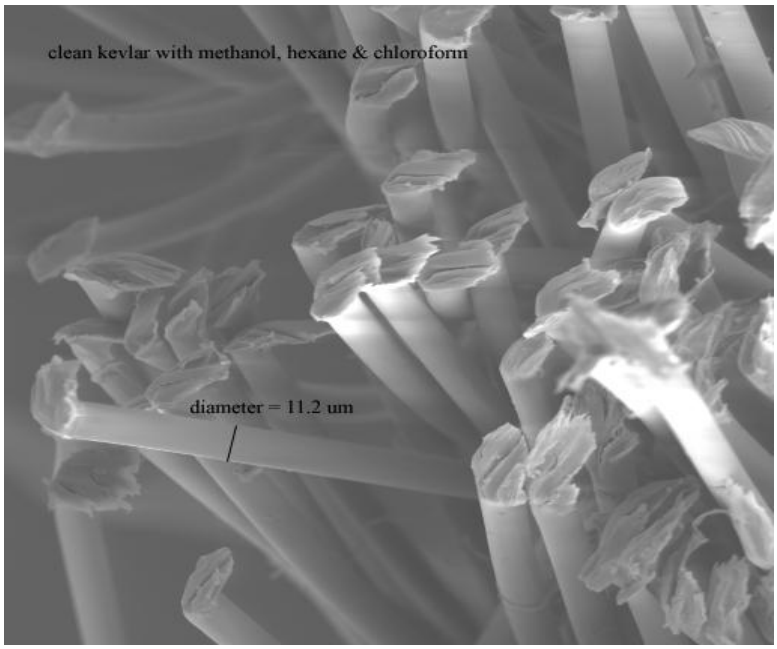

Figure 5-2. SEM image of cleaned Kevlar fibers with 500X.

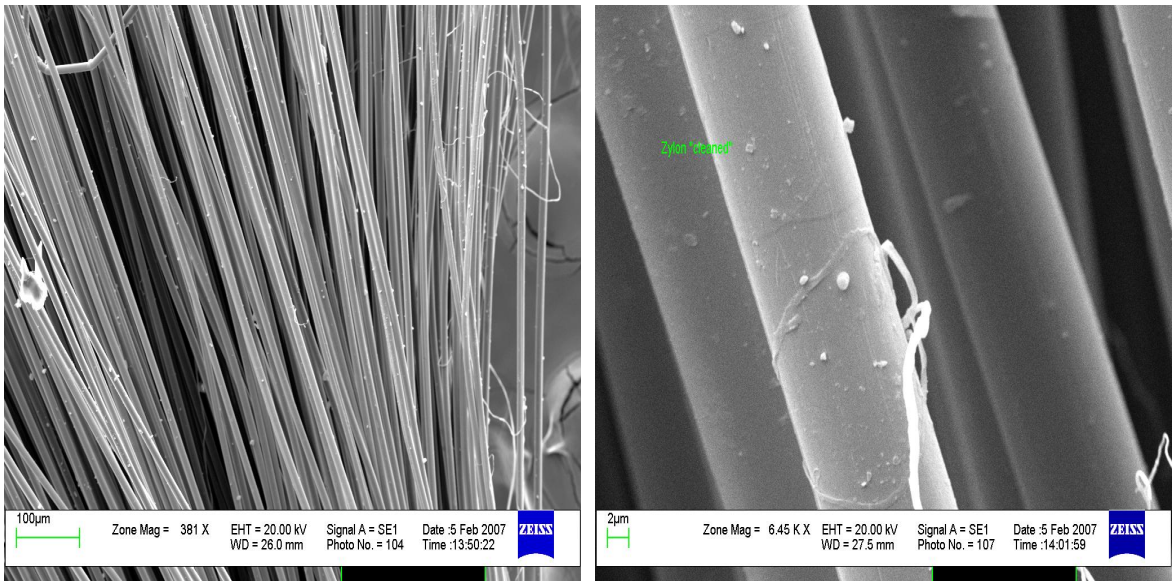

Figure 5-3. SEM images of “cleaned” Zylon fibers.

be achieved via gold deposition. Lower concentrations of the Au-cyanide deposition solution yields better electro-conductivity. In contrast, deposition of Al onto Ni-coated fibers increases the resistance most probably due to oxidation of aluminum by air forming insulating Al_2O_3 layers. An important observation is that electroless and electrolytic formation of Au layers is not possible in the absence of the Ni deposits.

Table 5-5. Mass change of different fiber treatment processes

Fiber	Treatment	Mass change	Results
Blank Kevlar	Ni-electroless coating	13.9%	S
Blank Zylon	Ni-electroless coating	14.8 %	S
Kevlar-Ni-Al	Al-electroless	38.5%	NS
Zylon-Ni-Al	Al-electroless	40.5%	NS
Kevlar-Ni[a]	for: Al-electroless	38.7%	Not uniform
Zylon-Ni [a]	for: Al-electroless		NS
Kevlar-Ni [a]	for: Al-ionic liquid bath		NS
Zylon-Ni [a]	for: Al-ionic liquid bath	39.8%	Not uniform
Kevlar-Ni [a]	for: Au-Cyanide electrodep.	113.23%	S
Zylon-Ni [a]	for: Au-Cyanide electrodep.	21.13%	S
Zylon-Ni (1:3)[a,b]	for: Au-Cyanide electrodep.	37.12%	S

* NS = not satisfactory; S = Satisfactory.

a) Ni deposition to prepare precursors for subsequent Al or Au coating; electrodep. = electrodeposition. b) plating employed the commercial gold cyanide bath diluted 3 times with DI water.

Table 5-6 Fiber resistance of different fiber treatment processes

Fiber	Treatment	Resistance (ohm/cm)
Kevlar-Ni	Ni-electroless coating	31.0
Zylon-Ni	Ni-electroless coating	5.0
Kevlar-Ni-Al	Al-electroless	High: 1.35~14.6 KΩ
Zylon-Ni-Al	Al-electroless	High: ~ 1 KΩ
Kevlar-Ni-Au	Au-Cyanide electrodeposition	0.93
Zylon-Ni-Au	Au-Cyanide electrodeposition	0.92
Zylon-Ni-Au (1:3)[a]	Au-Cyanide electrodeposition	0.24

a) the Au content of the cyanide bath was diluted by a factor of 3.

5.3.5 SEM analysis of metallized fibers

The SEM images presented in Figure 5-4 demonstrate that electroless deposition of Ni on Kevlar fibers yields uniform coatings. Also, presented in Figure 5-5 are SEM images of Ni-coated Zylon fibers obtained via electroless deposition. As in the case of Kevlar fibers, uniform coatings were obtained. Figures 5-6 and 5-7 depict SEM images of Ni-coated Kevlar and Zylon fibers metallized with Al using the electroless metallization procedure. In all cases, the resulting coatings appeared to be non-uniform, and also exhibited fractures.

SEM samples were prepared by sectioning the fibers with a sharp knife, which induced significant damage to the coating including the formation of fractures. Presented in Figure 5-8 are images of Ni-Al coated Zylon fibers depicting sectioned polymeric material, which illustrates the damage induced by the sectioning process. However, a comparison with the images shown in Figures 5-6 and 5-7 reveals that the morphological features noticed in the case of Al coated fibers are not a result of the sectioning procedure. The non-uniform coatings depicted in Figures 5-6 and 5-7 are attributed to the oxidation of the Al layers upon exposure to air. Support for this interpretation is provided by the increases in resistance that occurred when Ni-coated fibers were metallized with Al (see Table 5-6).

Presented in Figure 5-9 and Figure 5-10, are the SEM images of Au-plated Kevlar and Zylon fibers with Nickel treated with the gold cyanide procedure. Some cracks can be found in both fibers due to the imperfection of Ni coating layer. In general, the reproducibility of the coatings in terms uniformity and surface coverage was higher in the case of the electrodeposition methods. Both fibers in this electrochemical procedure yielded similar coatings. The

reproducibility of the coatings in terms of uniformity was high for electrodeposition by means of the gold-cyanide system.

5.3.6 Tensile strength testing

In table 5-7 are summarized the tensile strength data (given as maximum load) collected for untwisted fibers. The values are plotted for the different samples in Figure 5-11. Preliminary data obtained with fibers coated with Ni and Au yielded tensile strength values similar to those obtained for samples coated only with Ni. These results indicated that coating of Zylon fibers with Ni (or Au) decreases the tensile strength by a factor of two. A further decrease in tensile strength by the same factor resulted after Al was deposited on top of the Ni coating. In contrast, only slight decreases in the tensile strength of Kevlar fibers were noticed after surface metallization; the largest drop was again observed after depositing Al. Overall, these results suggest that either metal or unreduced metal ions are able to penetrate the surface of the Zylon fibers, decreasing their strength.

Table 5-7 Maximum loads of different modified fibers

sample	Maximum loads (lbf)	Sample names
1	141.5	blank zylon
2	77.96	Zylon-Ni
3	35.09	Al-Ni-zylon
4	18.67	blank Kevlar
5	16.33	Kevlar-Ni
6	15.97	Kevlar-Ni-Al

Note: Maximum load number is an average of four data points per sample number.

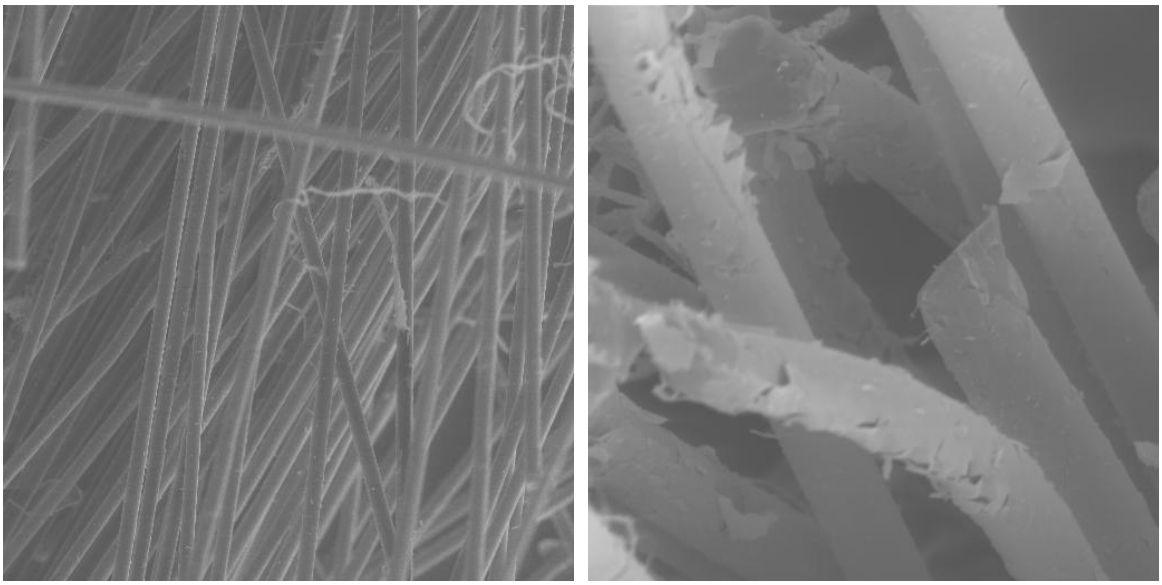

Figure 5-4. Kevlar fibers coated with Ni after electroless treatment; magnification:200x for left image, 1000x for right image.

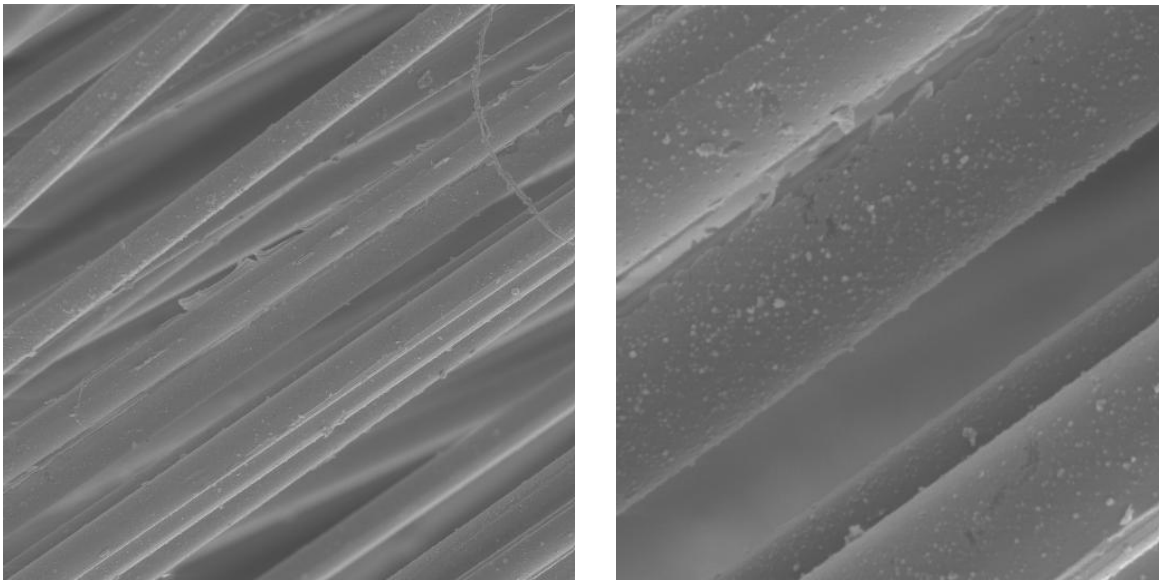

Figure 5-5. SEM images of Zylon fibers coated with Ni using electroless metallization; magnification: 500x for left image, 2300x for right image.

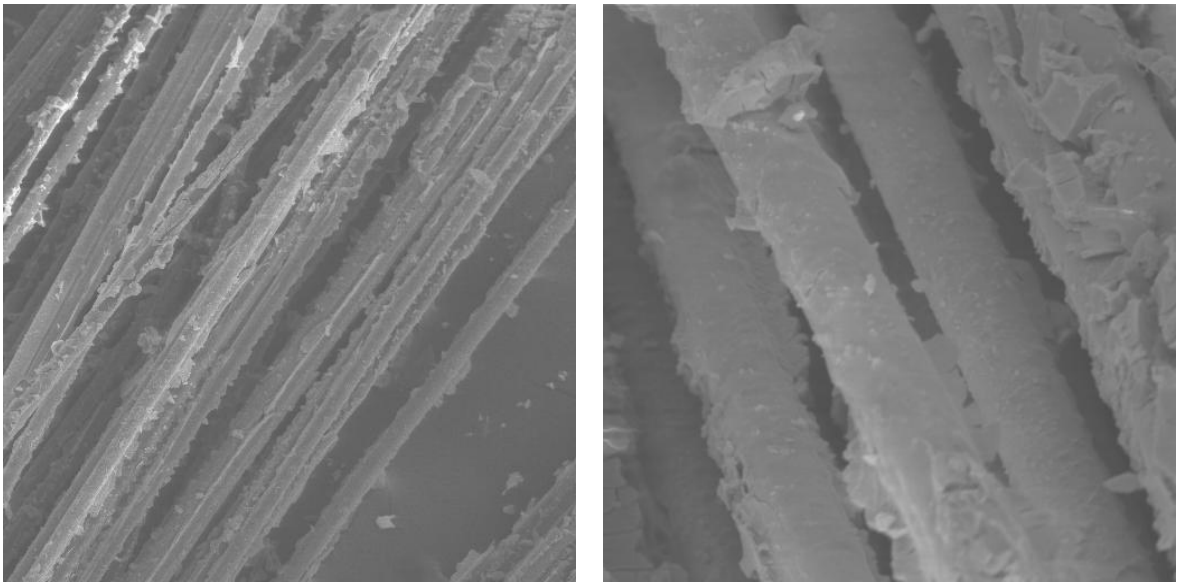

Figure 5-6. SEM images of Ni-coated Kevlar fibers metallized with Al via electroless deposition; magification: 200x for left image, 1000x for right image.

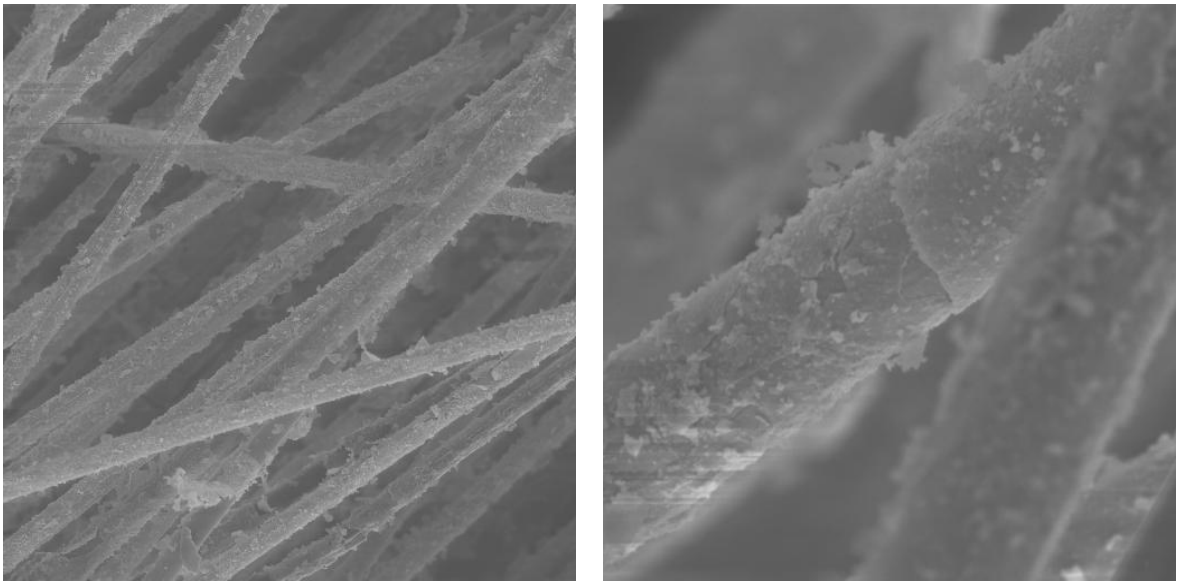

Figure 5-7. SEM images of Ni-coated Zylon fibers metallized with Al using the electroless method (magification: 300x for left image, 2000x for right image).

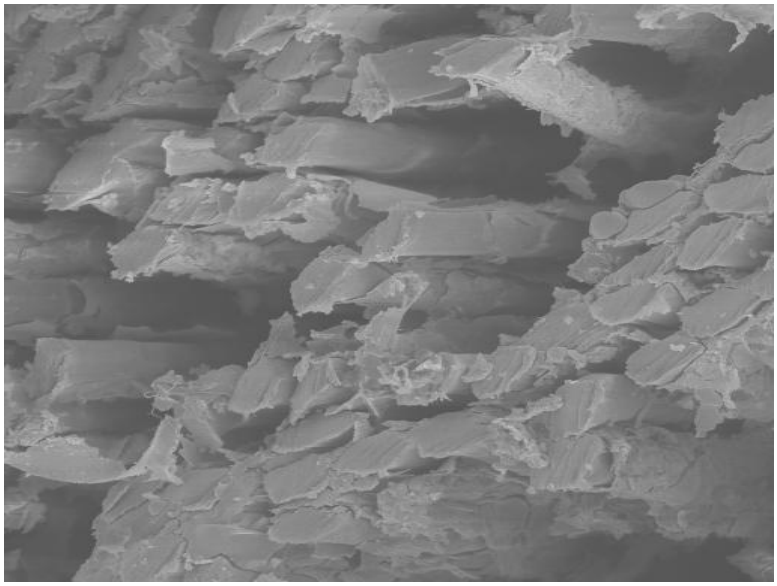

Figure 5-8. SEM image of Ni then Al coated Zylon fibers showing the region where sectioning took place (magnification = 550X).

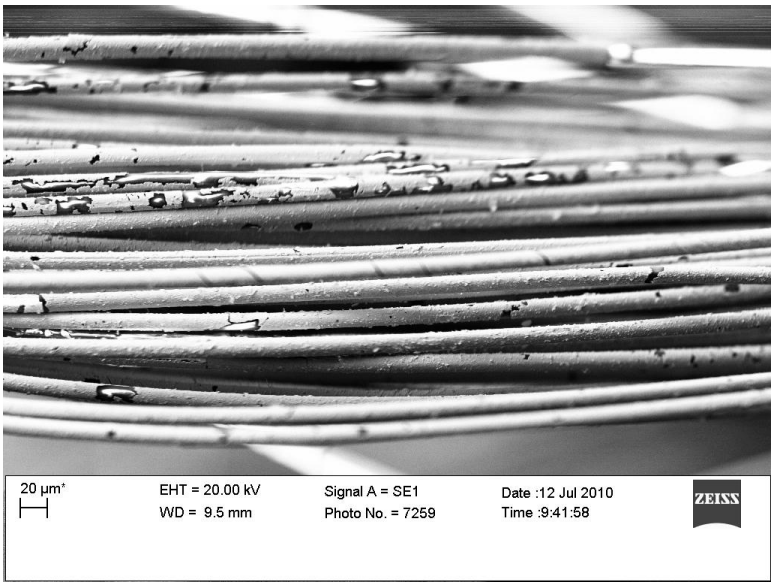

Figure 5-9 Surface image of Kevlar coated with Ni then electrodeposited gold

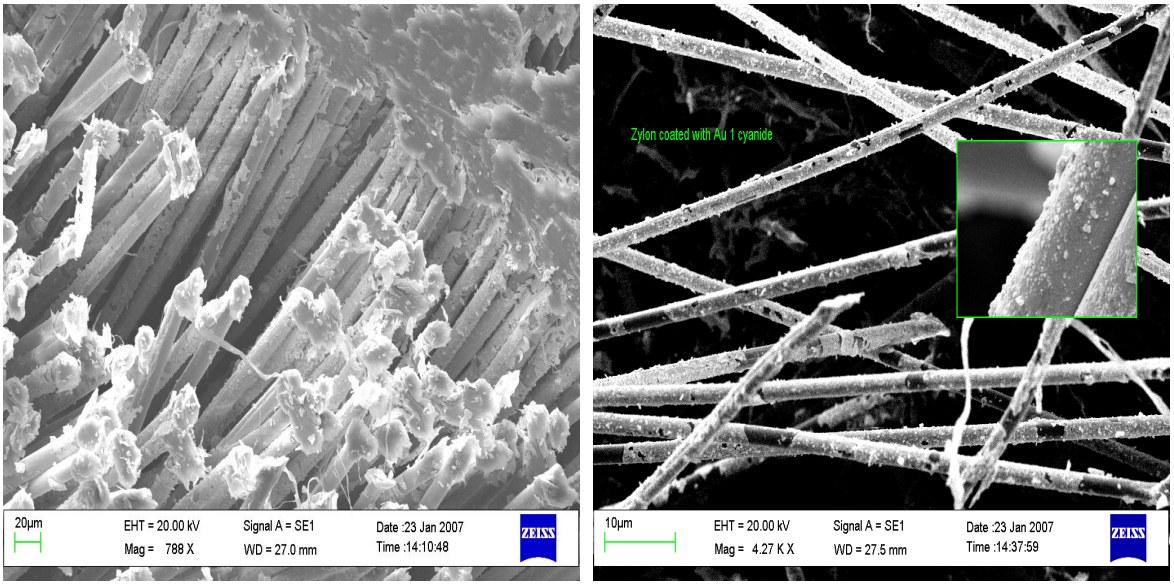

Figure 5-10. SEM image of Ni-coated Zylon fibers coated with gold using the Au-cyanide electrochemical deposition method.

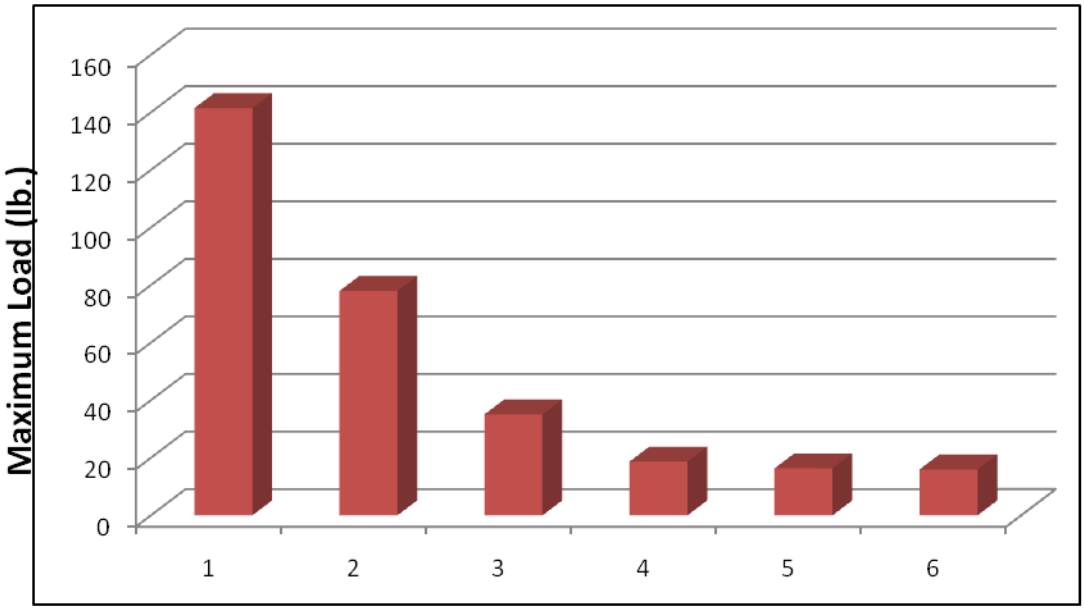

Figure 5-11. Plot of maximum load as a function of sample number in Table 5-7.

5.3.7 EDX, XRD and TEM results

EDX experiments performed using coated fibers confirmed that the deposited elements (Ni, Al, Au or Ti) were present on the substrate surface. No diffraction signals were obtained for Al-coated fibers, supporting the assumption that the deposited aluminum is oxidized to amorphous Al_2O_3 by air. XRD data of the Ni powder coated on Zylon fibers shows that the coating materials have a broad peak at 45 ºin Figure 5-12. The most probable explanation for such findings is that the electroless Ni bath yielded amorphous nickel phosphides instead of the pure metallic phase. Efforts to characterize the Ni-coated Zylon and Ni-Au coated Kevlar fibers by means of TEM were depicted in Figure 5-13 and 5-14. Microtoming induced separation of the coatings from the polymeric substrates. In the case of nickel coating, dark spots can be found, showing nickel was non-uniformly distributed in the amorphous Ni-P compounds. However, the coating obtained via Au electrodeposition onto Ni treated Kevlar is relatively uniform, which also decreases the resistance as compared to the fibers only via electroless Ni deposition. Surprisingly, only reflections corresponding to metallic Au were detected, but signals due to fcc Ni were missing when Ni-Au-coated fibers were analyzed. This was unexpected given that the employed coating procedure is widely used for Ni deposition.[4]

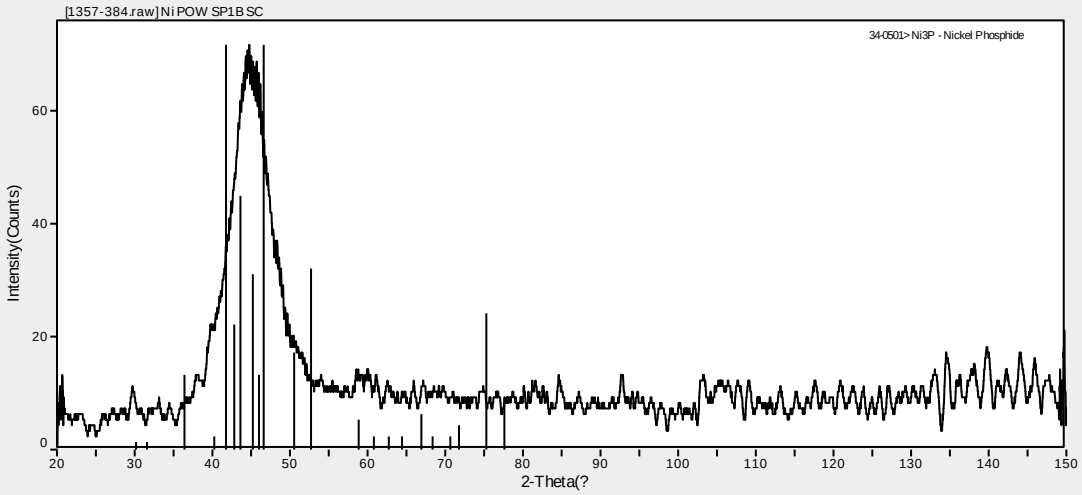

Figure 5-12 XRD of the Ni powder coated on Zylon fibers

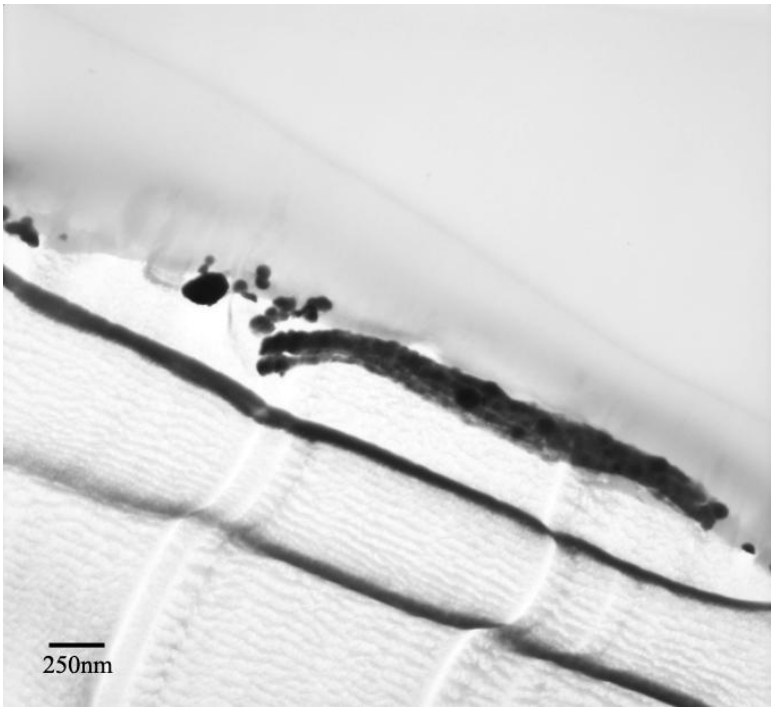

Figure 5-13 TEM of Ni coated on Zylon

Figure 5-14 TEM of Ni-Au coated on Kevlar

5.4. CONCLUSIONS

Ni deposition using electroless method is both successful for Kevlar and Zylon and it shows uniform and good adhesion on fiber surface, which results in relatively low resistance values. However, the use of sodium hypophosphite as reducing agent inevitably forms Ni-P mixtures or compounds (probably amorphous Ni-phosphides) and such deposits on the fibers surfaces may inherently yield non-uniform coatings, affecting in an adverse way the uniformity of the subsequent Au (and Al) coating. Further efforts should be devoted to achieving uniform metallic Ni coatings by means of electroless processes free of reducing agents based on phosphorus compounds.

All efforts to produce uniform Al coatings on Kevlar and Zylon fibers were unsuccessful. Although electroless deposition yielded Al coatings, oxidation of the metal films by air resulted in alumina, which exhibited poor adhesion to the substrates and decreased substantially the tensile strength of Zylon fibers. The conversion of Al into an alumina with enhanced adhesion may be possible via controlled oxidation of the metal surface under low oxygen pressures.

Gold electrodeposition procedures were superior as compared to electroless methods in terms of reproducibility, and yielded higher mass gains, better adhesion and lower resistance. Further analysis should be carried out on the two Au electrodeposition methods with SEM/EDX to compare surface morphology. Also, tensile strength measurements should be completed to quantify the effect of the two gold treatment processes on the fiber strength. Inconsistencies encountered during Au electrodeposition onto the surface of long fiber samples (1 m and longer) is a system design problem that needs to be addressed in order to improve the uniformity of the

coatings. Improved design of the coating procedures should be addressed for treating larger fibers if this project is to be continued in the near future.

REFERENCES

1. Kerzhanovich, V. V., Cutts, J.A., Cooper, H.W., Hall, J.L, McDonald, B.A., et. al. *Adv. Space Res.* **2004**, *33*, 1836-1841.

2. Seely, L.; Zimmerman, M.; McLaughlin, J. *Adv. Space Res.* **2004**, *33*, 1736-1740.

3. Abe, A.; Saito, Y.; Imaizumi, M.; Ogawa, M.; Takeichi, T.; Jinno, K. *J. Sep. Sci.* **2005**, *28*, 2413-2418.

4. *Electroless Plating: Fundamentals and Applications*; Mallory, G. O.; Hajdu, J. B., Eds.; AESF: Orlando, 1990.

5. Schmidt, D. L.; Hellmann, R. US Patent 3462288, 1969.

6. Birkle, S.; Dötzer, R.; Rissel, E.; Siemens Aktiengensellschaft: US Patent 4144360, 1979.

7. Abbott, A. P.; Eardley, C. A.; Farley, N. R. S.; Griffith, G. A.; Pratt, A. *J. Appl. Electrochem.* **2001**, *31*, 1345-1350.

8. Pinto, N. J.; da Silva, A. N. R.; Fachini, E.; Carrion, P.; Furlan, R.; Ramos, I. *Polym. Prepr. (Am. Chem. Soc., Div. Polym. Chem.)* **2003**, *44*, 138-139.

9. Akamatsu, K.; Ikeda, S.; Nawafune, H. *Langmuir* **2003**, *19*, 10366-10371.

10. Vaia, R. A.; Lee, J. W.; Wang, C. S.; Click, B.; Price, G. *Chem. Mater.* **1998**, *10*, 2030-2032.

11. Goldenstein, A. W.; Rostoker, W.; Schossberger, F.; Gutzeit, G. *J. Electrochem. Soc.* **1957**, *104*, 104-10.

12. Abrantes, L. M.; Fundo, A.; Jin, G. *J. Mater. Chem.* **2001**, *11*, 200-203.

13. Kim, D.-G.; Kim, J.-W.; Yoon, J.-W.; Lee, W.-B.; Jung, S.-B. *Surf. Interface Anal.* **2006**, *38*,

440-443.

14. Valova, E.; Armyanov, S.; Dille, J.; Van Ingelgem, Y.; Hubin, A.; Steenhaut, O. *J. Electrochem. Soc.* **2008**, *155*, D449-D458.